Mendel University in Brno

Faculty of Forestry and Wood Technology

Department of Wood Science

Lignocellulosic Nanomaterials: Preparation, Characterization and Applications

Doctoral Thesis

Author: Ing. Pawan Kumar Mishra

Supervisor: Univ. Prof. Dipl.Ing.Dr. Rupert Wimmer

2016

Declaration

I declare that I have written the presented doctoral thesis titled “Lignocellulosic Nanomaterials: Preparation, Characterization and Applications” independently and I have listed all references. I agree that my thesis will be published in accordance with Section 47b of Act no. 111/1998 Coll. On Higher Education, as amended thereafter and in accordance with the Guidelines on the Publishing of University Student Theses.

I am aware of the fact that my thesis is subject to Act. No. 121/2000 Coll., the Copyright Act and that the Mendel University in Brno is entitled to close a licence agreement and use the results of my thesis as the “School Work” under the terms of Section 60 para. 1 of the Copyright Act.

Before closing a licence agreement on the use of my thesis with another person (subject) I undertake to request for a written statement of the university that the licence agreement in question is not in conflict with the legitimate interests of the university, and undertake to pay any contribution, if eligible, to the costs associated with the creation of the thesis, up to their actual amount.

Brno 18.7.2016 Pawan Kumar Mishra

Abstract

Mishra, P.K. (2016) "Lignocellulosic Nanomaterials: Preparation, Characterization and Applications, Doctoral thesis, Mendel University in Brno, 227p.

Cellulose and lignin are two most occurring biopolymers on earth. Wood has been a traditional source of cellulose for the paper-based industry. Lignin, which is a by-product, has been investigated for its value-added utilization. Increasing demand for timber and rise in prices of wood gives an impetus to look for alternative sources of lignocellulosic materials. Crop-based biomass offers a sustainable alternative especially for the preparation of Nano-cellulosic and lignin-based products. Although a wide range traditional applications have been reported for lignocellulosic nanomaterial, but for this work we focus mainly on nanocomposites and biomedical applications.

This thesis has been divided into two parts. The first part which has two subunits, first subunit is preparation and characterization cellulosic nanomaterials viz. cellulosic nanofibres (CNF). Brewers Spent Grains (BSG), which is commonly available by-product from brewing industry was used to prepare CNF and characterized for morphological, chemical and thermal characteristics. In the second subunit, Kraft lignin was used to synthesize lignin-based solid and hollow colloids and characterized, an application in UV protection was studied. In second part which also has two subunits, applications in drug delivery and nanobiocomposites were studied. To study application in drug delivery review of metal and ceramic nanoparticles were made and the anticancer drug was loaded on CNF and tested for drug release studies (our contribution was to prepare nanocellulose based scaffold and help in the morphological evaluation, rest of the work was done by a collaborating group). In nanocomposites, a book chapter was written enlisting biopolymers including nanocellulose with title smart nanocomposites in food packaging.

For the preparation of CNF from BSG, the raw material was procured from the in-house brewery at Mendel University, Department of food science. Separation of protein followed by bleaching was used to obtain cellulose material. Thus obtained cellulosic material was passed through a high-pressure homogenizer to obtain CNF. Change in colour and morphology was observed by taking photographs. Morphological characterization was done using scanning electron Microscope (SEM) and atomic force microscopy (AFM). Thermal characterization was done using DSC (Differential Scanning Calorimetry) and TGA (Thermogravimetric analysis). Chemical

characterization by HPLC (high-pressure liquid chromatography) and crystallinity by XRD (X-ray diffraction) was done.

Lignin colloids were prepared from Kraft Lignin using Ultrasonic spray freezing. Dioxane soluble fraction of lignin was used and dissolved in DMSO and sprayed over copper plate cooled by liquid Nitrogen. Solid and hollow colloids were obtained depending on the concentration of sprayed solution. Obtained colloids were studied for their size by DLS (dynamic light scattering) followed by comparison with theoretically expected values and size obtained by image analysis technique. SEM and TEM images were also taken to study the morphology of particles. In addition, the obtained lignin particles were deposited on a quartz plate with layer-by-layer deposition. A higher UV absorbance was observed, as the number of layers increased

In the application part, the literature on metal nanoparticles and ceramic nanoparticles were comprehensively surveyed with two separate review articles with respect to applications for drug delivery. This is followed by the preparation of CNF aerogels through freeze drying technique. An anticancer drug was loaded and its morphology characterized by SEM and AFM. The difference between the loaded and the unloaded aerogel could be clearly seen. Further, the characterization was done for tensile strength, swelling tendency at different pH, floating behaviour, and mucoadhesive detachment force and drug release profile in different pH conditions. The results showed a matrix type, a porous and a woven type of aerogel, with the formulations having excellent mechanical properties. The drug release was assessed by the dissolution tests.

In the composites section nanocomposites and their classification, methods of preparation, biopolymers used (including nanocellulose), and reinforcement strategies for food packaging were reviewed. Smart packaging techniques and marketed products were also studied. It was accepted as book chapter “smart nanocomposites for food packaging” published by Elsevier publications.

Keywords: Nanocellulose, Lignin colloids, Drug Delivery, Nanobiocomposites, hollow colloids of lignin, Mucoadhesive, Brewers spent grains.

Abstrakt

Mishra, P.K. (2016) Lignocellulosic Nanomaterials: Preparation, Characterization and Applications, DISERTAČNÍ PRÁCE, MENDELOVA UNIVERZITA V BRNĚ, 227P.

Celulóza a lignin jsou dva nejvíce se vyskytující biopolymery na zemi. Dřevo je tradičním zdrojem celulózy pro papírenský průmysl. Lignin, který je vedlejším produktem, byl zkoumán z hlediska dalšího využití jako hodnotný materiál. Zvyšující se poptávka po dřevu a nárůst cen dřeva dává podnět k hledání alternativních zdrojů lignocelulózových materiálů. Zemědělsky pěstovaná biomasa nabízí udržitelnou alternativu především pro přípravu výrobků na bázi nanocelulózy a ligninu. Ačkoli už bylo publikováno široké spektrum tradičního využití lignocelulózového nanomateriálu, tato práce se zaměřuje hlavně na nanokompozity a cílený transport léčiv. Tato práce byla rozdělena do dvou částí. První část je rozdělena na dvě témata, z nichž první je příprava a charakterizace celulózových nanomateriálů a to (CNF). Pro přípravu CNF bylo použito pivovarské mláto (BSG), které je běžně dostupný vedlejší produkt pivovarnictví. Byly popsány morfologické, chemické a tepelné vlastnosti připravených celulózových nanovláken. Druhé téma se zabývá Kraft ligninem (z výroby sulfátové buničiny) který byl použit pro syntézu plných a dutých koloidů na bázi ligninu. Tyto koloidy byly následně charakterizovány. Bylo zkoumáno využití jako ochrana proti UV záření. Ve druhé části, která je rozdělena na dvě témata, bylo zkoumáno využití pro transport léčiv a přípravu kompozitů. Při studiu využití pro transport léčiv bylo zpracováno review o kovových a keramických nanočásticích. Lék proti rakovině byl nanesen na CNF a testován pro potřeby studie uvolňování léku. Téma o nanokompozitech, které je zaměřeno na biopolymery včetně nanocelulózy, je zpracováno jako kapitola v knize s názvem chytré nanokompozity na balení potravin. Surový materiál pro přípravu CNF z BSG byl získán z malého pivovaru na ústavu technologie potravin na Mendelově univerzitě. Celulózový materiál byl získán po separaci proteinů a následném procesu bělení. Takto připravený celulózový materiál byl zpracován na CNF pomocí vysokotlakého homogenizátoru. Změna barvy a morfologie byla pozorována na pořízených snímcích. Morfologická charakteristika byla provedena pomocí SEM (rastrovacího elektronového mikroskopu) a AFM (mikroskopie atomárních sil). Teplotní charakteristika byla provedena pomocí DSC (diferenciální skenovací kalorimetrie) a TGA (termogravimetrie). Chemická charakteristika byla provedena pomocí HPLC (vysokotlaké kapalinové chromatografie) a krystalinita byla

změřena pomocí XRD (rentgenové difrakce). Koloidy ligninu byly připraveny z Kraft ligninu pomocí ultrazvukového rozprašování s následným zmrazením. Byla použita frakce ligninu rozpustná v dioxanu, která byla rozpuštěna v DMSO (dimethylsulfoxidu) a nastříkána na měděnou desku chlazenou tekutým dusíkem. Plné a duté koloidy byly získány v závislosti na koncentraci rozprašovaného roztoku. Velikost získaných koloidů byla měřena pomocí DLS (dynamický rozptyl světla) a pomocí techniky analýzy obrazu. Výsledky byly následně porovnány s očekávanými teoretickými hodnotami. Ke studiu morfologie částic byly také využity obrazy pořízené pomocí SEM a AFM. Kromě toho získané částice ligninu byly nanášeny na křemennou desku vrstvu po vrstvě a bylo pozorováno zvyšování UV absorbance se zvyšováním počtu vrstev.

V aplikační části byly popsány kovové a keramické nanočástice ve dvou oddělených review článcích z hlediska jejich využití na transport léčiv. Následovala příprava CNF aerogelů lyofilizační technikou. Protinádorový lék byl aplikován na aerogel a jeho morfologie byla charakterizována pomocí SEM a AFM. Rozdíl v aerogelu s lékem a bez léku byl jasně viditelný. Další charakterizace byla provedena na pevnost v tahu, tendenci k bobtnání při různých hodnotách pH, plovoucí chování, mukoadhezivní uvolňovací síla a profil uvolňování léku při různých podmínkách pH. Výsledky ukázaly mřížkové, porézní a tkané typy aerogelů s vynikajícími mechanickými vlastnostmi. Uvolňování léku bylo hodnoceno testem rozpouštění, který byl podložen vhodnými matematickými modely. V sekci kompozitů byly popsány nanokompozity a jejich klasifikace, metody přípravy, používané biopolymery (včetně nanocelulózy), a strategie zpevňování obalů na potraviny. Byly také studovány chytré obalové technologie a výrobky uváděné na trh. To vše bylo publikováno jako kapitola v knize s názvem "Chytré nanokompozity pro balení potravin", kterou vydalo nakladatelství Elsevier.

Klíčová slova: Nanocelulóza, koloidy ligninu, cílený transport léčiv, nanokompozity, duté koloidy ligninu, mukoadheze, pivovarské mláto

Preface

The present study was carried out at the Department of Wood Science at Faculty of Forestry and Wood Technology, Mendel University in Brno (Czech Republic).

This work was supported by the European Social Fund and the state budget of the Czech Republic, (project "The Establishment of an International Research Team for the Development of New Wood-based Materials", reg. no. CZ.1.07/2.3.00/20.0269–Inwood) as well as the Internal Grant Agency (IGA) of the Faculty of Forestry and Wood Technology, Mendel University in Brno – projects LDF_VT_2015_018, LDF_VP_2015003 and IGA V 79/2013 (Combined processes of beech wood modification for floorings).

I would like to express my gratitude to all those who supported me during my research studies and made this thesis possible. First, to my supervisor Prof. Rupert Wimmer for keeping me buoyed throughout the period of study. Special thanks to Prof. Ingo Burgert for his support and guidance during my stay at ETH Zurich and to Associate Prof. Vladimir Gryc (former Head of department) for his administrative support.

Furthermore, I would like to thank my colleagues of the Department of Wood Science (Mendel University in Brno), ETH Zurich and EMPA laboratories for valuable support and suggestions.

Finally, I would like to express my deepest gratitude to my parents and family for their incessant support during my study.

Brno

Pawan Kumar Mishra

List of Papers

This doctoral thesis is a summary of the following papers, which are referred in the text by Roman numerals I–VI.

I. Mishra P.K., Wimmer R., Gregor T., Utilising Brewer's Spent Grain as a Source of Cellulose Nanofibres Following Separation of Protein-based Biomass. (Under review- Bioresources).

II. Mishra P.K., Wimmer R., Aerosol assisted self-assembly as a route to solid and hollow spherical lignin colloids and its utilization in layer by layer deposition. (Accepted- Ultrasonics Sonochemistry).

III. Bhandari J., Sharma H., Mishra P.K., Wimmer R., Talegaonkar S., Cellulose nanofibre aerogel as a promising biomaterial for customized oral drug delivery (Under review- International Journal of Nanomedicine).

IV. Talegaonkar S., Sharma H., Pandey S., Mishra P.K., Wimmer R., "Bionanocomposites: Smart biodegradable packaging Material for food preservation", In: A. M. Grumezescu, Food Packaging in Agri-food industry, Elsevier, ISBN: 978-0-12-804302-8.(Accepted –book chapter)

V. Thomas S.C., Harshita, Mishra P.K., Talegaonkar S., 2015. Ceramic Nanoparticles: Fabrication Methods and Applications in Drug Delivery. Current Pharmaceutical Design. 21, 6165–6188.(Accepted and Printed)

VI. Sharma H., Mishra P.K., Talegaonkar S., Vaidya B., 2015. Metal nanoparticles: a theranostic nanotool against cancer. Drug Discovery Today 20, 1143–1151. doi:10.1016/j.drudis.2015.05.009(Accepted and Printed)

Table of Contents

List of Figures

List of Tables

List of Abbreviations

CNF	Cellulose Nano-fibre
NCC	Nanocrystalline cellulose
UV	Ultraviolet
SPF	Sun protection factor
LNP	Lignin Nanoparticle
HPMC	Hydroxyl propyl methyl Cellulose
CNC	Cellulose Nanocrystal
HPH	High-pressure Homogenisation
SEM	Scanning electron Microscope
TEM	Tunnelling electron microscope
AFM	Atomic Force Microscopy
FESEM	Field emission scanning electron microscopy
WAXS	Wide angle X-ray scattering
CAMAS	solid state 13C cross polarization magic angle spinning
NMR	Nucleo-magnetic resonance
TGA	Thermo-gravimetric analysis
DSC	Differential Scanning Calorimetry
XRD	X-ray diffraction studies
DP	Degree of polymerization
PDADMAC	[poly(diallyl dimethyl) ammonium chloride]
SPIONS	Superparamagnetic iron oxide nanoparticles
USPIONS	Ultra-small paramagnetic iron oxide nanoparticles
MFC	Micro fibrillated cellulose
GIT	Gastrointestinal Tract
FTIR	Fourier transformed infrared spectroscopy
NIR	Near infrared
XPS	X-ray photoelectron spectroscopy
AFEX	Ammonia fibre explosion
ACL	Acylated lignin
THF	Tetra hydro furan

Symbols

π - pi,

θ - Surface Tension (theta) $mN.m^{-1}$

ρ - Density, gcm^{-3}, (rho)

f - Frequency

$D_{N,\,0.5}$ - Number Median Diameter of Droplet

λ_L - Wavelength in the liquid (lambda)

Tsf - Characteristic time for solvent freezing

T_{ld} - Characteristic time for diffusion of lignin

M_w - The weight of swollen nanofibre sample

M_d - The weight of dried nanofibre.

DL% - Drug loading

D_i - Initial amount of drug added

D_f - Amount of free drug in the supernatant

C - Total amount of Nanofibres recovered

EE %- Entrapment efficiency

1. INTRODUCTION

1.1 Background

Cellulose and lignin are two most occurring forms of fixed carbon in the biosphere. Effective utilization and value-added applications of them have been always aimed at. This lignocellulosic biomass could either be wood, agriculture residue and byproducts of the food industry. Nanotechnology adds a wide range of interesting properties and applications to lignocellulosic materials. For the purpose of this thesis, we have considered nanomaterials derived from cellulose and lignin separately. The first patents on CNF production by homogenisation dates back to 1984 (JP 59120638A), since then a number of methods have been reported. These other methods to produce cellulose nanoparticles include enzymatic hydrolysis (Engelhardt et al., 2010), oxidation (Miyawaki et al., 2009), electrospinning (Frey and Joo, 2005) and steam explosion. The CNFs (cellulose nanofibres) have been applied in biomedical applications, composite materials, barriers, antimicrobial and transparent films, drug delivery, fabrics, textiles and many other fields. In addition to wood, a wider range of other sources have also been reported for CNF and NCC (nanocrystalline cellulose) production. Lignin (technical lignin) varies in their properties based on source that they are derived from and pulping method. Lignin has been studied for its value-added applications but the majority is still utilized for the heating purpose. Lignin-based nanomaterials add many new dimensions to its utilization. A facile and effective method with good control on morphology and particle size for preparation of lignin nanoparticles has been always aimed at. The presence of hydroxyl groups and H-bonding make it really difficult for lignin to assemble into nanoparticle in an aqueous environment. The reported methods include ultrasonication, mechanical grinding, chemical methods and ultrasonic spray freezing. The self-assembling tendency of modified lignin into nanoparticles has also been recently reported. Due to their specific properties, these new materials could be effectively used for drug delivery and nanobiocomposites for a wide range of applications. Properties of lignocellulosic nanomaterials support an extended range but this work mainly focuses on drug delivery and smart composites. The first problem for application in drug delivery arose from biocompatibility and toxicity challenges. Many studies have reported positive results in that direction and a lot also needs to be investigated before the commercial application is achieved. Nanocellulose based

aerogels, hydrogels, and films have already been reported for drug delivery studies, this is in additions to the traditional utilization of micro-sized cellulose in tablets, sustained release, and targeted delivery dosage forms. Lignin nanorods and particles have already been reported for its drug delivery utilities. Its UV absorbance properties have been reported to improve the SPF of cosmetics. A recent report of synthesis techniques for capsules, hollow colloids and facile methods to prepare LNP adds impetus to its new applications. Utilization of CNF in nanocomposites is not new, first, because of the smaller size of nanofibres; surface area-volume ratio is relatively higher than micro-particles. These nanosized fibres cause improvement of barrier properties by forming a dense network in combination with sufficiently strong particle- polymer bonds. One of the ways to improve moisture resistance of inherently hydrophilic cellulose can be pre-treatment before homogenization, post treatment and chemical grafting (Dufresne, 2013). Gas permeability can also be improved by forming nanocomposites with other fillers (clay) or chemical modification of cellulose especially for utilization in moist conditions, which has been a major limitation of cellulose. Utilization of nanocellulose in smart composites has been covered in detailed in book chapter enclosed in the thesis.

1.2 Aims of the thesis

The main aim of the presented doctoral thesis was to enhance the knowledge about lignocellulosic nanomaterials and their interdisciplinary applications. The derived aims were to: (a) to prepare and characterize nanomaterials based on cellulose (CNF) and lignin, and (b) to review and apply these materials in interdisciplinary fields like biomedicine, or as nanocomposites to be used in e.g. food packaging. This thesis with the associated publications should provide a better understanding of lignocellulosic nanomaterials and their interdisciplinary applications, which will potentially contribute to value-added and high-end utilizations of crop-based biomass. The thesis pursues the following objectives:

Part a: Preparation and characterization of CNF and lignin colloids.

I. To prepare and purify cellulose, i.e. CNF from brewers spent grains.
II. Characterize the obtained material for its chemistry, morphology, and thermal properties.
III. Ultrasonic spray freezing of lignin to obtain lignin colloids.
IV. Characterization and application of lignin colloids in UV protection.

Part b: Interdisciplinary application of lignocellulosic nanomaterials.

V. Review the nanoparticles used in drug delivery (metal and ceramic nanoparticles).
VI. Fabrication of nanocellulose aerogels in drug delivery and characterization of obtained product.
VII. Review and reporting of nanobiocomposites used in smart packaging (Including nanocellulose based packaging).

1.3 Outline of the thesis

This doctoral thesis summarizes lignocellulosic nanomaterials prepared, characterized and their interdisciplinary application reported together with review and research articles published in scientific journals and a book chapter that were co-authored during the years 2014 to 2016. The work done during this time includes review and research on lignocellulosic biomass and its application interdisciplinary fields and consists of theoretical background, materials and methods and results together with a discussion and the conclusions drawn from this work. An introductory chapter presents the general background, the state-of-the-art and itemizes the aims of the thesis. The literature chapter reports and discusses sources and types of nanocellulose, methods of production and characterizations techniques used. For lignin, an overview of technical lignin and their characteristics features are reported. Additionally, the method used for the preparation of lignin nanoparticles and application reported are enlisted. In the application part, a general overview of nanoparticles types and nanocellulose-based patents with reference to biomedical applications has been tabulated. The advantage of lignocellulosic biomass in the light of drug delivery and the composite application is also discussed. This is followed by a brief description of possible risks in connection with the use of nanoparticles.

2. LITERATURE REVIEW

2.1 Nanocellulose

2.1.1 Chemistry and classification

Cellulose is one of the major components of plant cell wall. It is a linear polymer of D-Glucose linked by β (1→4) glycosidic bond. A number of monomer units per chain (degree of polymerization); can vary depending on the source of cellulose. Linear chain and no branching aids the formation of hydrogen bonds between the hydroxyl group and hence the formation of microfibrils. Extensive presence of hydroxyl groups on the surface dictates surface and chemical properties of cellulose (Figure 1-1).Microfibrils meshed into polysaccharide matrix provide tensile strength to the cell wall.

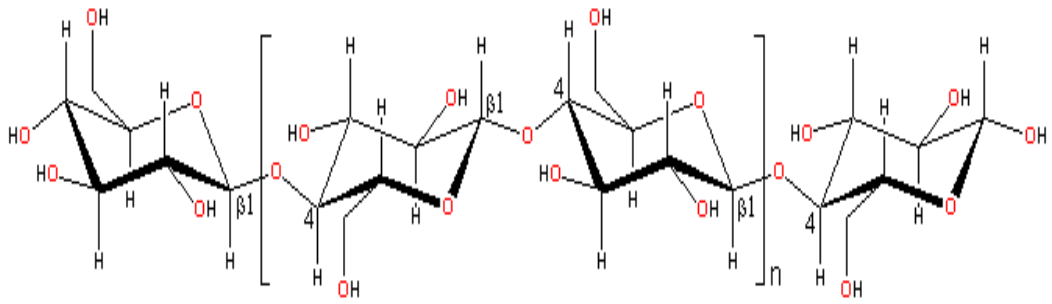

Figure 1-1 Structure of cellulose (red coloured oxygen highlights reactive positions)

Cellulose has been traditionally used in tablet formulations as an important excipient such as a binder (hydroxypropyl cellulose, methyl cellulose) and a disintegrant (croscarmellose sodium). In addition to tablet coating (hydroxypropyl methylcellulose (HPMC) and pH, responsive drug release (phthalate derivative of HPMC) are few other uses (Kamel et al., 2008). Nanocellulose is mechanically produced by high-pressure homogenization of cellulose fibres. Cellulose thus processed is called CNF (cellulose nanofibre) or nano-fibrillated cellulose. This CNF has amorphous and crystalline both parts, out of that amorphous part get dissolved by acid hydrolysis leaving CNC (cellulose nanocrystals) or cellulose nanowhiskers. Bacterial cellulose (produced by bacteria) has been widely studied for its biomedical applications due to its high purity.

Table 1-1 Family of nanocellulose (Klemm et al., 2005)

Terminology for nanocellulose	Selected references and synonyms	Typical sources	Formation and average size
Microfibrillated cellulose (MFC)	Microfibrillated cellulose, nanofibrils, and microfibrils nano-fibrillated cellulose	wood, sugar beet, potato tuber, hemp, flax	Delamination of wood pulp by mechanical pressure before and/ or after chemical or enzymatic treatment diameter: 5–60 nm length: several micrometres
Nanocrystalline cellulose (NCC)	cellulose nanocrystals, crystallites, whiskers, rod-like cellulose microcrystals	wood, cotton, hemp, flax, wheat straw, mulberry bark, ramie, Avicel, tunicin, cellulose from algae and bacteria	Acid hydrolysis of cellulose from many sources diameter: 5–70 nm length: 100–250 nm (from plant celluloses); 100 nm to several micrometres (from celluloses of tunicates, algae, bacteria)
Bacterial Nanocellulose (BNC)	bacterial cellulose, microbial cellulose, biocellulose	low-molecular weight sugars and alcohols	Bacterial synthesis diameter: 20–100 nm; different types of nanofibre networks

Nanocellulose has been produced from wide range of lignocellulosic sources that includes wood, the lignocellulosic biomass of different origins and even some byproducts of food processing industry. Chemically, the ability of the hydroxyl groups to form hydrogen bonds plays a major role in the formation of fibrillar and semicrystalline packing, which governs the important physical properties of this highly cohesive material. One of the most specific characteristics of cellulose is that each of its glucose units bears three hydroxyl groups, which endows Nanocellulose a reactive surface covered with numerous active hydroxyl groups. Nanocellulose based composites in comparison in traditional composites show improved and tunable barrier properties while keeping biodegradability property intact. Due to the smaller size of nanofibres, surface area-volume ratio is relatively higher than micro-sized particles. These nanosized fibres cause improvement of barrier properties by forming a dense network in combination with sufficiently strong particle - polymer bonds. The other ways to improve moisture resistance of inherently hydrophilic cellulose can be pretreatment before homogenization, post treatment and chemical grafting (Dufresne, 2013). Gas permeability can be improved by forming nanocomposites with other fillers

(clay) or chemical modification of cellulose especially for utilization in moist conditions, which has been a major limitation of cellulose.

2.1.2 Method of preparation

Many methods have been reported for the production of cellulose nanofibres. Processing steps to obtain cellulose nanofibres depends upon the source of cellulose. Generally followed technique involves mechanical treatment and chemical treatment method which is accompanied by High Pressure Homogenization, Cryocrushing, Super Grinding, Microfluidization and others include ultrasonic and enzymatic methods. However, the fibrils obtained by these methods are aggregated with wide distribution in width because of the complicated multi-layered structure of plant fibres and the interfibrillar hydrogen bond. Different parameters like opacity, roughness, density, water interaction properties tensile strength are affected by different methods of processing nanofibres.

Homogenization is the considered as an efficient technique for refining cellulose. Here, the slurry of cellulose is passed through the small nozzle at high pressure. Due to the high velocity, pressure, shear force and collision, there is the generation of high shear in the cellulose stream and thus the fibres of cellulose in nanoscale is generated (Frone et al., 2011). It was introduced in 1983 to produce NFC from wood pulp. NFC was isolated from the sugar beet by 10–15 cycles at 30 MPa (Leitner et al., 2007). Similarly, NFC was extracted from the skin of pear. NFC produced were of 2–5 nm after passing the cellulose fibres from the pear in HPH (high pressure homogenisation) at 15 cycles at 50 MPa with temperature below 95 °C. It has high efficiency, simplicity and there is no need of organic solvent. Supports green technique for nanofibre production. The homogenizer can easily be scaled to industrial production and can be operated continuously. Nevertheless, there is clogging of the HPH due to the microfibrillated cellulose residue in the moving parts of HPH. However, this can be overcome by reducing the size of the fibres before passing through HPH. It can be stated that homogenization is an energy-intensive process.

Microfluidization technique is similar to HPH. This process is commonly used in the cosmetic, biotechnology, and pharmaceutical industries. In this technique, cellulose pulp is passed through an intensifier pump, interaction chamber. Intensifier pump (pump used to amplify pressure) increases the pressure to 276 MPa (40.000 psi) and the shear

force and impact against the channel wall and colliding streams in interaction chamber defibrillates the fibres (Spence et al., 2011). Here, isolated cellulose nanofibre suspension was passed through high-pressure microfluidizer for 5 times through the intensifier pump. High pressure and high shear forces and impacts inside the microfluidizer; the nanofibres are broken into Nano-sized structure forming slurries of NFC. The pressure was maintained at 55 MPa and temperature, not more than 90 °C (Ferrer et al., 2012). One of the advantages of microfluidization is that, the microfluidizer reduces the chances of clogs compared to HPH because of no moving parts. Also, the interaction chamber can be designed with different geometries to produce different sized materials.

Grinding is a mechanical technique of disintegration, where cellulose slurry is forced through the gap between a rotary and a stator grinding stones. There is a generation of shear forces between the stones, which leads to delamination of cellulose fibres and hence individualization of nanofibrils. Taniguchi et al., (1998) produced NFC with diameter 20–90 nm by passing the 5–10 % fibre suspension for 10 times through the grinder (Nechyporchuk et al., 2014). The mechanism of fibrillation in grinder is to break down of hydrogen bond and cell wall structure by shear forces and individualization of pulp to nanoscale fibres. One of the advantage with microfluidization is the pre-treatment process used for other mechanical technique may not be required for fibre shortening. It is a powerful yet quite simple method for the production of the nanocellulose from plant fibres. However, disk maintenance and replacement are necessary because of the wearing of the gloves and grit on the disk with use.

In Cryocrushing, by mechanical fibrillation cellulose fibres are disintegrated into Nano-size by crushing. Because of crushing, there is the change in conformation and modification in configuration thus decreasing crystallinity and increasing polymer solubility. Cellulose polymers are grounded up to 1–3 μm in diameter by crushing. Crushing process is influenced by factors like the origin of cellulose, technological factors like processing time and equipment depending factors. Crushing time of 8 h is needed to achieve 1–20 μm diameters for 25% cellulose material. Cryocrushing is the subclass of crushing in which water-swollen cellulose material is immersed in liquid nitrogen and then is crushed using mortar and pestle (Frone et al., 2011) or in combination with high-pressure defibrillation process. Production of nanofibres by

combination method using cryocrushing and high-pressure defibrillation, TEM analysis showed nanofibres of 50–100 nm were produced (Abdul Khalil et al., 2014)

Electrospinning technique has gained a lot of attention recently, being a very simple and versatile technique and an effective top down the fabricating process in the production of nanofibres. Electrospun nanofibres special attributes like high surface-to-volume ratio and high surface roughness, cost effectiveness thus is thought to be a promising carrier for novel drug delivery systems. By this technique, nanofibres having a diameter from few nm to several micrometers is produced (Frey and Joo, 2005). This technique mainly consists of three components: a high voltage supplier, a capillary tube with a pipette or needle and a metal collecting screen. A high voltage creates an electrically charged jet of polymer solution or polymer melt out of the needle or pipette. The solution jet evaporates and solidifies before reaching the collecting screen which is then collected as an interconnected web of small fibres. There is one electrode into the spinning solution/ melt and the other one attached to the collector.

In this method, there is a capillary tube containing the polymer solution fluid which is held by the surface tension. The electric field is applied across the end of the capillary tube which induces a charge on the surface of the liquid. There are mutual charge repulsion and the contraction of the surface charges developing a force directly opposite to the surface tension. With the increase in the intensity of electric field the hemispherical surface of the fluid at the tip of the capillary tube elongates to form a conical shape which is known as the Taylor cone and a critical value is attained. After attaining critical value, the surface tension is overcome by repulsive electrostatic force ejecting the charged jet of the fluid from the tip of the Taylor cone. There is internal instability in the discharged polymer solution jet and undergoes elongation process which makes the discharge very long and thin. During this process, the solvent dissolving the polymer evaporates forming a charged polymer fibre while for the polymer melt; the discharge solidifies when it travels in the air stream forming the polymer fibre.

2.1.3 Characterization

Some characteristics of CNF depends on its physical state (powder or suspension), for example, spray dried can be tested for its powder characteristics, e.g. NFC powder can be checked for bulk density, tapped density, compressibility index,

Hauser's ratio, flow properties- the angle of repose. NFC suspension requires additional rheological evaluation. In addition, some features are common to a common to all forms.

Morphological parameters such as length, microfibril angles, residues of lignin and hemicelluloses, particularly depend on the source from which the native cellulose fibres are extracted, on the production process and on the pre-treatment method. Only the diameter of the NFC is possible for measurement because NFC is entangled among themselves due to the presence of the hydroxyl groups on the surface of the microfibrils, which makes the length measurement difficult. Techniques to characterize morphology include SEM (Scanning electron microscopy), TEM (Transmission electron microscopy), AFM (Atomic force microscopy), field emission scanning electron microscopy (FE-SEM), WAXS (Wide angle X-ray scattering), CPMAS (Solid state 13C cross- polarization magic angle spinning NMR spectroscopy.

Techniques to characterize thermal properties of cellulose include DSC (differential scanning calorimetry) and TGA (Thermogravimetric analysis). Tensile strength can be measured by the degree of polymerization. The degree of cellulose polymerization (DP) is reported to correlate strongly with the aspect ratio of the nanofibres; longer fibrils are associated with higher cellulose DP. DP is generally measured through the intrinsic viscosity. The degree of polymerization is related to the raw material used and the mechanical and the chemical fibrillation parameters.

The degree of swelling represents the relative measure of the cross-linking between the nanofibres and the hygroscopicity of cellulose nanofibre. Water absorption and swelling of MFC is a complex phenomenon, which is thought to be influenced by both, the molecular structure of cellulose and the mesostructure of the films. It can be determined by the conventional method or can be also determined through SEM. By the conventional method, to check the swelling behaviour, which could originate at the physiological condition (when administered orally), the cellulose nanofibres of known weight (denoted as M_d) are to be put in test tubes containing 10 ml SGF (simulated gastric fluid, pH 1.2) and SIF (simulated intestinal fluid) (pH 7.4) and at different pH of GIT (gastrointestinal tract) 6.8 is incubated for 24 h at 37 °C. Then the water on the specimen surfaces is removed with filter paper and the specimens are weighed in wet condition (denoted as M_w). The swelling ratio was calculated according to the following equation for each sample:

Swelling ratio (%) = $(M_w - M_d)/M_d$

Where, M_w is the weight of swollen nanofibre sample and M_d is the weight of dried nanofibre. Also, swelling property can be determined by saturating the cellulose material with water, followed by dipping in water and then centrifuging for minutes in a centrifugal drier. The index of swelling is the weight of the water retained by the centrifuged material compared with the original dry material (Kirillov et al.,1987). It can be also determined through SEM by checking the increase in diameter of the NFC after allowing it to swell for the specified time interval (Agarwal and Mishra, 1999).

Surface charge and crystallinity can be measured confocal microscopy (CSLM), Electron Microscopy (TEM, SEM, ESEM), X-ray diffraction, NMR (solid state), Atomic Force Microscopy (scanning/ AFM) and porosimetry.

Surface chemistry can be measured by FTIR, NIR, and Raman-spectroscopy, titrations, and adsorption (ionisable groups in bulk and surface), Secondary Ion Mass Spectroscopy (SIMS), X-ray Photoelectron Spectroscopy/ Electron Spectroscopy for Chemical Analysis (XPS/ ESCA), Surface energy can be measured by Adsorption (from gas or solution), Contact angles (fibres and sheets), Surface force measurements (model surfaces/ surface force apparatus, and AFM) Chemistry.

2.2 Lignin colloids and nanoparticles

2.2.1 Introduction and overview of technical lignins

Lignin is second most abundant natural polymer after cellulose to exist on earth. It exists mainly in plant cell wall as a binder to wall components. A major portion of it is burnt as fuel, which is underutilization of the resource. So, it has been widely studied and reported for its value-added applications.

Chemically lignin is composed of three monomers viz. syringyl, guaiacyl, and p-hydroxyphenyl alcohols (Figure 1-2). The basic ring structure is para- hydroxyphenyl, methoxy or dimethoxy substitution names them guaiacyl and syringyl groups.

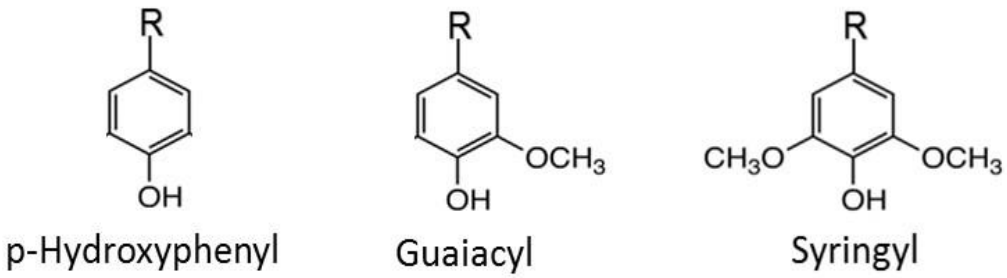

Figure 1-2 Monomers of lignin.

Lignin loses its chemical structure during the lignification process and resultant properties of lignin are dictated by its structure and chemical nature. The source based difference also exists in lignin, for ex. G: S ratio impacts properties and G: S ratio changes within cell wall based on location.

Table 1-2 Lignin monomers and their percentage quantity.

Lignin Sources	Grasses	Softwood	Hardwood
p-Hydroxyphenyl	10-25%	0.5-3.5%	Trace
Guaiacyl	25-50%	90-95%	25-50%
Syringyl	25-50%	0-1%	50-75%

For specific applications and optimal utilization of technical lignins, it is required that they should be characterized by their structure, composition and specific feature. Individual consideration is needed for each type of lignin due to their difference in processing parameters and methods. The following table enlists some of the technical lignin, their sulfur content and other parameters.

Table 1-3 Different types of technical lignin

Type	Scale	Chemistry	Sulphur content	Purity
Kraft	Industrial	Alkaline	Moderate	Moderate
Soda	Industrial	Alkaline	Free	Moderate-Low
Lignosulphate	Industrial	Acidic	High	Low
Organosolve	Pilot	Acidic	Free	High
Hydrolysis	Industrial/pilot	Acidic	Low-free	Moderate-Low
Steam explosion	Demo/Pilot	Acidic	Low-free	Moderate-Low
AFEX(ammonia fibre expansion lignin)	Pilot	Alkaline	Free	Moderate-Low

Kraft lignin is produced by sulfate cooking and contributes maximum to global lignin production (Tejado et al., 2007). During cooking, a major portion of lignin dissolves in an aqueous solution of sodium hydroxide and sodium sulfide. During the dissolution process, lignin also generates low molecular weight fragments, which ultimately contribute to the brown color of lignin. The signature feature of kraft lignin is the increased number of phenolic hydroxyl groups due to extensive cleavage of beta-aryl bonds due to extensive cooking. The molecular weight varies in the range of 200–200.000 g $mole^{-1}$.

A byproduct of soda or soda-anthraquinone process, it is mainly used for cooking crop-based biomass. Being free of sulphur, its application in the production of phenolic resins, dispersants, and animal nutrition have been reported. Soda lignins from non-wood plants contain more p-hydroxyl units and carboxyl groups. Other characters of non-wood lignin are high silicate and nitrogen contents (Belgacem and Gandini, 2011).

Lignosulphonate lignin is the byproduct of sulphite cooking, in which lignin gets suphonated and solubilized (Fan and Zhan, 2008). The anionic polyelectrolyte nature and presence of phenolic hydroxyl, carboxylic and sulphur containing groups give them unique colloidal properties. Water solubility, high molecular weight, and high ash content are some other features of lignosulphonates.

Organosolv process utilizes organic solvent/ solvents (acetic acid, formic acid, ethanol and peroxy organic acid) with water for pulping (Xu et al., 2006). They are more homogenous than alkali and lignosulphonates (separation via solubilization). It has low molecular weight, high purity, poor water solubility and availability of side chains for chemical reactions.

Hydrolysis can be done either chemically or enzymatically. Chemical hydrolysis (dilute acid hydrolysis) is outdated due to high water consumption and low recovery rates (Chandra et al., 2007). Enzyme-mediated processes are more accepted and utilized. They contain a high amount of condensed structures and high ability to sorb, hence used for the synthesis of sorbents.

Steam explosion is a pretreatment method to facilitate enzymatic or chemical pulping. Ammonia Expansion is a more novel approach to low cost and efficient pre-treatment of cellulosic biomass. Also known as AFEX, this pre-treatment process operates at relatively mild conditions at ~100 °C and is concentrated with ammonia. At high pressures, this process depolymerizes hemicellulose and removes lignin from

cellulose and hemicellulose. The AFEX pretreatment process minimizes degradation of the sugar in the biomass and is relatively cost effective. A high recycle ratio is also used for ammonia where 99% of the ammonia is recovered and reused, which helps reduce operating costs.

2.2.2 Nanomaterials derived from lignin

Lignin, a molecular mess poses different problems while being assembled into nano-size materials. Due to the presence of hydroxy groups, it is nearly impossible to assemble the nanoparticle in an aqueous environment (Qian et al., 2014a). Many attempts have been made to synthesize lignin colloids and nanoparticles.

The first method was based on precipitation of low-sulfonated lignin from an ethylene glycol solution by using diluted acidic aqueous solutions, which yields lignin NPs that are stable over a wide range of pH (Qian et al., 2014c). The second approach was based on the acidic precipitation of lignin from a high-pH aqueous solution which produces Nanoparticles stable only at low pH. This study revealed that lignin NPs from the ethylene glycol-based precipitation contain densely packed lignin domains which explain the stability of the NPs even at high pH.

Nanotechnology allows using chemical, physical and biological effects that do not occur outside the nanoscale world. In a reported method, a glass reactor equipped with a mechanical stirrer was immersed in a water bath. A quantity of 10 g of lignin (absolutely dry) was suspended in 47 mL of distilled water and stirred for 2 h at room temperature. After that, the heating was started to the set temperature. The reaction time was kept constant at 4 h and the temperature was varied between 50 and 95 °C. After the lignin suspension reached the desired temperature, a 50 % sodium hydroxide solution and an ammonia hydroxide (25%) solution (depending on pH) were added and stirred for another 2 h. The pH of the mixture was varied in the range of 7.5–12.0 during the experiments. After 2 h of stirring, a formaldehyde solution (37%) (Depending on lignin/formaldehyde mass ratio) was added to the reaction mixture. The obtained product was recovered by precipitation at pH 2 with a solution of hydrochloric acid (2%), separated by centrifugation, washed and dried.

A physical method to modify lignin by ultrasonic irradiation in order to obtain nanoparticles was also reported (Gilca et al., 2015).

In another method, emulsification was followed by the internal lignin-rich phase cross-linking to produce the solid particles that could be easily separated by removal of the organic, continuous phase. The ability of the fractionated lignin particles to stabilize hexadecane-in-water Pickering emulsions was shown and their properties were compared against those obtained by using traditional inorganic particles (Nypeloe et al., 2015). In a method reported by Qian et al in 2014, lignin recovered from the pulping black liquor was chemically modified by acetylating and then used as a biomass resource to prepare uniform colloidal spheres via self-assembly (Qian et al., 2014a). In this method, ACL (acetylated lignin) molecules start to form colloidal spheres at a critical water content of 44 vol% when the initial concentration of ACL in THF is 1.0 mg mL(-1), and the colloidization process is completed at a water content of 67 vol%. An excessive amount of water is added to the dispersions to "quench" the structures formed and then the ACL dispersion is treated by rotary evaporation for recycling THF and acquiring colloidal spheres. Water-dispersive lignin nanoparticles open up a green and valuable pathway for value-added utilization of lignin biomass recovered from pulping spent liquor, which is of great significance for both the utilization of renewable resources and environmental protection.

In a recent work, straightforward method to produce lignin nanoparticles from waste lignin obtained from kraft pulping is introduced (Lievonen et al., 2016). Spherical lignin nanoparticles were obtained by dissolving softwood kraft lignin in tetrahydrofuran (THF) and subsequently introducing water into the system through dialysis. No chemical modification of lignin was needed. Water acted as a non-solvent reducing lignin's degrees of freedom causing the segregation of hydrophobic regions to compartments within the forming nanoparticles. The final size of the nanoparticles depended on the pre-dialysis concentration of dissolved lignin. The stability of the nanoparticle dispersion as a function of time, salt concentration and pH was studied. In pure water and at room temperature the lignin nanoparticle dispersion was stable for over two months, but a very low pH or high salt concentration induced aggregation. It was further demonstrated that the surface charge of the particles could be reversed and stable cationic lignin nanoparticles were produced by adsorption of poly(diallyl dimethyl ammonium chloride) (PDADMAC).

2.2.3 Applications of lignin

Lignin has been reported for a wide range of applications. Depending on nature and property utilized they can be classified in five categories viz. dispersion, materials, agricultural application, high-value application, and miscellaneous applications. Lignin-based dispersions can be utilized in ceramics, oilwell drilling, clay bricks and tiles, cement, concrete, gypsum board, dyestuff, electrolytes, paper sizing, emulsions wax, asphalt, bitumen, vitamins, micronutrients, complexing agents, flocculating, heavy metal binders, ion exchange, water softening, protein coagulants, destabilizing, oil emulsion, corrosion protection, anti-scaling, metal cleaners, grinding aids (Lin et al., 2014). Materials utilization of lignin includes phenolic, polyurethanes, epoxides, particle boards, resin boards, rubber re-enforcing, block copolymers, polyesters, composites, polyolefin, biodegradable, carbon sieves, activated carbons, carbon fibres, heat resistance, antioxidants, anti-inflammatory and paper bounding (Upton and Kasko, 2016).

In the field of agriculture soil rehabilitation, slow release fertilizers, artificial humus, fertilizer encapsulation, composting aid, manure treatment, humus improvement, soil stabilization, insecticides, granulation, pelletising, chelates are few applications of lignin (Frei and Frei, 2013). High-purity and high-end application are based upon antibacterial effects, HIV inhibition, digestion regulation, antibiotics, plant immunology, growth stimulators, oxygen scavengers and hydrogels. Energy production, diesel fuel, foam stabilizers, binders, tanning agents, hydrophobization, and absorbents can be classified as miscellaneous applications (Purkiss, n.d.)

2.3 Interdisciplinary applications

2.3.1 Nanoparticles and biomedical applications

Nanomaterials cannot be assumed as same materials in very small quantity and their effects cannot be extrapolated. Due to the very small size, they open several pathways and route of interaction which will otherwise be not accessible. The nanomaterials can be classified in six categories for application drug delivery, which includes Natural based material, Dendrimers, fullerenes, Polymeric materials, ferrofluids, Quantum Dots, and Miscellaneous. Nature-based materials can be chitosan,

dextran, gelatins, alginates, liposomes, starch, cellulose and lignin based nanomaterials. Dendrimers are mainly branched chain polymers and fullerenes are carbon based carriers. Polymer carriers can be polylactic acid, polycyanoacrylates, polyethyleneimine, block copolymers and polycaprolactone. Ferrofluids SPIONS and USPIONS are used in imaging (MRI). In additions to that metal and ceramic nanoparticles are also being investigated (De Jong and Borm, 2008).

Cellulose and Lignin-derived nanoparticles have also been reported in drug delivery. Few patents on nanocellulose in the biomedical application have been discussed in the following table 1-4.

Table 1-4 Patented application of nanocellulose (Duran et al., 2012)

Patent number	Title	Year of publication
WO 2009063508A2	Nanoparticle composition, useful for manufacturing antibacterial medicament, which is useful in e.g. medical applications e.g. wound dressing, comprises cellulose nanofibres embedded with nanosized material e.g. silver	2009
US 2010233245A1	Nanoparticle composition and process thereof	2010
WO 2008100163A	Method of manufacturing silver nanoparticles, cellulosic fibres and nanofibres containing silver nanoparticles, fibres and nanofibres containing silver nanoparticles, use of silver nanoparticles to the manufacture of cellulosic fibres and nanofibres	2008
US 2009192264A1	Method of in situ bioproduction and composition of bacterial cellulose nanocomposite	2009
WO 2010042647A2	High flux high-efficiency nanofibre membranes and methods of production thereof	2010
WO 2010115426A1	Skin care compositions for the delivery of agents	2010
WO 2011030170A1	Cellulose nanoparticle aerogels, hydrogels, and organogels	2011

2.3.2 Bionanocomposites

The interdisciplinary application of cellulose is mainly determined by its chemistry. The ability of these hydroxyl groups to form hydrogen bonds plays a major role in the formation of fibrillar and semicrystalline packing, which governs the

important physical properties of this highly cohesive material. One of the most specific characteristics of cellulose is that each of its glucose units bears three hydroxyl groups, which endows nano-cellulose a reactive surface covered with numerous active hydroxyl groups nano-cellulose based composites in comparison in traditional composites show improved and tunable barrier properties while keeping biodegradability property intact. First, because of the smaller size of nanofibres, surface area-volume ratio is relatively higher than microparticles. These nanosized fibres cause improvement of barrier properties by forming a dense network in combination with sufficiently strong particle-polymer bonds. The other ways to improve moisture resistance of inherently hydrophilic cellulose can be pretreatment before homogenization, post treatment and chemical grafting (Dufresne, 2013). Gas permeability can also be improved by forming nanocomposites with other fillers (clay) or chemical modification of cellulose especially for utilization in moist conditions, which has been a major limitation of cellulose. A detailed account of bionanocomposites has been covered in book chapter attached.

2.3.3 Risk and opportunity offered by nanoparticles

Challenges posed by nanoparticles can be explained by following points. First, nanomaterials are designed to target specific surface characteristics. So the estimation of risk cannot be done by the traditional method, new methods should be established. Particle size has shown to alter qualitative characteristics when particle size moves from macro to micro to nano scale (De Jong and Borm, 2008). Small size particles interact physiological differently as new channels get accessible due to a smaller size. The high surface area somehow changes the potency of material inside a human body, which also means new unreported effect could also be expected. The challenge to extrapolate data from macroscopic observations is the biggest. An additional legal system reform is also an issue to address the issue of material with unknown long term effect. The challenge of the unknown is the level playing field for newly developed and traditionally used nanomaterials. Details of toxicity and regulation issues for utilization of metal nanoparticles have been covered in attached review article.

3. PAPER I

Utilising brewer's spent grains as a source of cellulose nanofibres following separation of protein-based biomass

Pawan Kumar Mishra, Tomas Gregor, and Rupert Wimmer

(Under Review- Bioresources)

Abstract

In this work, a multistage process was employed to obtain value-added products from brewer's spent grain (BSG). This paper is focused on the production and characterisation of cellulose nanofibres (CNF) as one of the products obtained during the complete process. In the first stage, protein-rich liquor was separated via the alkaline (NaOH) treatment of dried BSG and stored for further utilisation. In the second stage, bleaching treatments were conducted to separate cellulose, which was later converted to CNF by high-pressure homogenisation. The lignocellulosic product from each step was analysed for its chemical composition by means of alkaline hydrolysis combined with the HPEAC method. The thermal properties were measured using thermogravimetric analysis (TGA). The morphology was studied using scanning electron microscopy (SEM) and atomic force microscopy (AFM). X-ray diffraction (XRD) was done to observe changes in crystallinity. The nanocellulose produced was one of the value-added materials from the bio-refinery of BSG along with numerous already-reported products.

Keywords: Nanocellulose; Cellulose nanofibres; Brewer‘s spent grain, Bio-refinery

Contact information: Faculty of Forestry and Wood Technology, Mendel University in Brno, Zemědělská 3, 613 00 Brno, Czech Republic; *Corresponding author: xmishra@mendelu.cz

INTRODUCTION

The brewing industry generates spent grains, hops, and yeasts from the fermentation process as its major wastes and byproducts. Spent grains constitute 85% of the total waste generated by a given brewery, with a composition of cellulose (16 to 25%), protein (15 to 24%), lignin (11 to 27%), and other components (Mussatto et al. 2006a). It has also been widely used as an ingredient for human and animal food products (Ozturk et al. 2002), energy production (Ezeonu and Okaka 1996), charcoal manufacture (Okamoto et al. 2002), brick manufacture (Okamoto et al. 2002), paper production (Ishiwaki et al. 2000), and adsorbent production (Low et al. 2000). The bio-refining of BSG and techno-economic analysis is reported by Mussatto et al. (2006b).
Nanocellulose has been reported to be prepared from a wide range of sources, including raw cotton linter (Morais et al. 2013), sisal fibres (Morán et al. 2008), sugarcane bagasse (Mandal and Chakrabarty 2011), oil palm empty-fruit-brunch (Fahma et al. 2010), rice husk, (Ludueña et al. 2011), wood (Abe et al. 2007), bamboo (Abe and Yano, 2009), cotton (Morais et al. 2013), soy hulls (Alemdar and Sain 2008), hemp (Wang et al. 2007), branch-barks of mulberry (Li et al. 2009), pineapple leaf fibres (Cherian et al. 2010), pea hull fibre (Chen et al. 2009), coconut husk fibres (Rosa et al. 2010), banana rachis (Zuluaga et al. 2009) and sugar beet (Dufresne et al. 1997; Dinand et al. 1999). The production and characterisation of nanocellulose derived from BSG were not shown before and needs to be explored. In this research, the aim was to prepare cellulose nanofibres without destroying the protein content of the material, which can be later utilised for other various purposes. First, the protein-based material was separated using alkaline dissolution and acidic precipitation without affecting other contents significantly. Lignocellulosic biomass obtained in the first step of alkaline treatment was bleached to obtain cellulose fibres. Cellulose fibres thus obtained were processed in a high-pressure homogeniser to obtain cellulose nanofibres. This postulated a method to complete utilisation of BSG including reclaimed lignin and denaturated protein (reported as a wood adhesive (Hettiarachchy et al. 1995) along with CNF as products.

EXPERIMENTAL

Materials

The BSG used in this research was obtained from a microbrewery of the Department of Food Science, Mendel University in Brno, Czech Republic. As soon as it had been obtained, the material was washed with distilled water until a neutral pH was reached, after which it was stored at -5 °C until further utilization. The stored material was then dried at 50 ± 5 °C for 24 hrs to attain 10% moisture content (untreated material). The dried material was further stored in a hermetic container at -5 °C to prevent any microbial growth. The reagents used in chemical treatment were: sodium hydroxide (NaOH), sodium chlorite ($NaClO_2$), sodium sulphite (Na_2SO_4), and hydrochloric acid (HCl). All chemical were purchased from Sigma-Aldrich and used without any further purification.

Methods

The alkali treatment, first milder (for a shorter time) to dissolve the protein-based biomass followed by bleaching process and second alkali treatment (for complete removal of lignin) was done to obtain cellulose. This resulted in reclaimed lignin from bleaching liquor and protein-based biomass as potentially usable products. We characterised mainly lignocellulosic biomass and cellulose for morphology, thermal properties, and CNF for obtained diameter.

Treatment of BSG

Dried BSG (P0) was extracted with (17% w/v) with 0.1 M NaOH at 60 °C for 60 min with continuous stirring at 30 rpm. To separate the protein extract from the lignocellulosic part, centrifugation was done at 2000 rpm for 10 min at 4 °C, protein rich supernatant was collected, and the lignocellulosic residue (washed with distilled water) was used for the further experiment. The lignocellulosic residue (P1) obtained in the previous step was boiled with 0.7% (w/v) sodium chlorite (1:50 g/ml), for 2 h at pH 4. The residue from the previous step was treated with 5% (w/v) sodium bisulphite (1:50 g/mL) at room temperature for 1 h, washed with distilled water, and dried. This was followed by treatment with 17.5% NaOH (1:50 g/mL) at room temperature for 8 h, washed, and dried again (P2), the scheme of treatment is shown in Figure 2-1

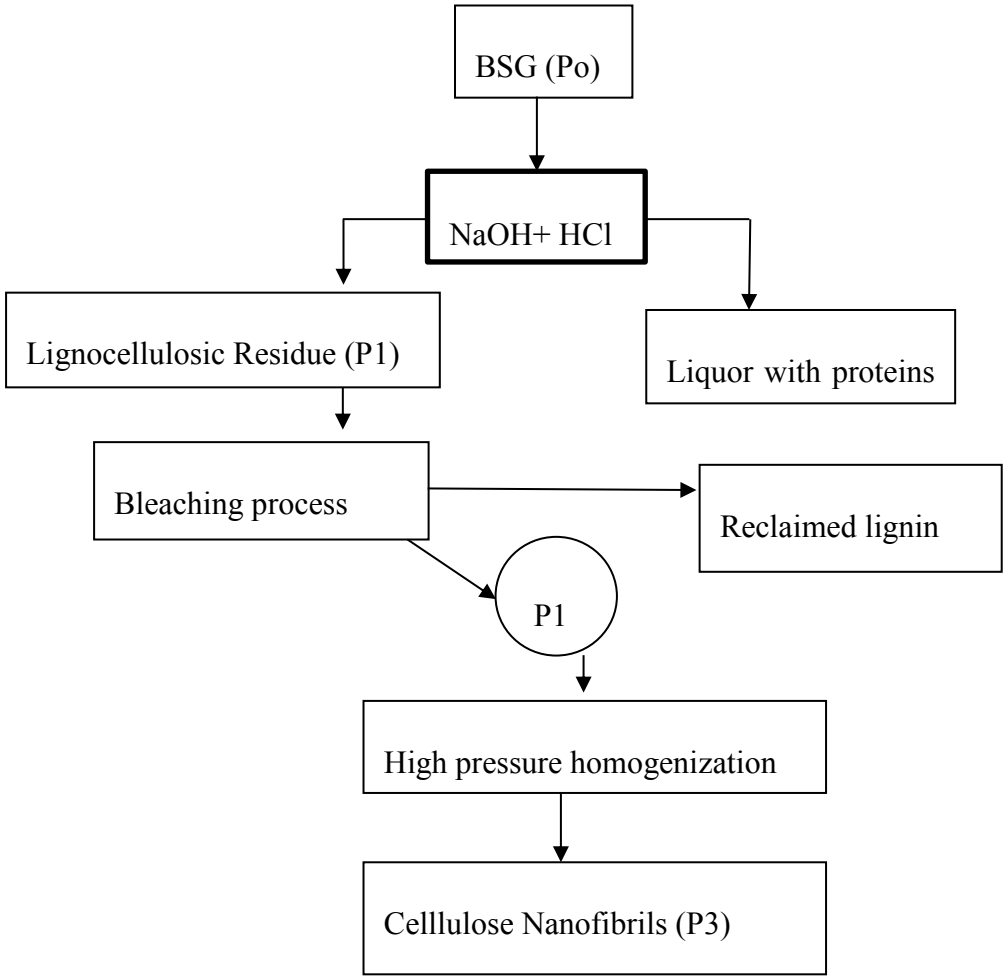

Figure 2-1 Scheme of different steps of mechanochemical treatment of BSG.

Nanocellulose production

The cellulose-based product (P2) obtained in the previous step was collected, and a 1.5% dispersion was prepared in water. This dispersion was processed by IKA-T10 (Ultra-Turrax supplied IKA, Germany) to disperse the fibres. The resultant dispersion was homogenized in a high-pressure homogenizer (APV 1000 from SPX Corporation, USA) at 700 to 800 atm for 20 cycles.

Chemical composition

The chemical composition of BSG was analysed at every stage (P0, P1, and P2) according to the following method. Approximately 200 mg of each sample was pre-hydrolysed with 2 mL of 72% H_2SO_4 at 30 °C for 1 h), followed by hydrolysis in an autoclave using 56 mL of ultra-pure water at 120 °C for 30 min. For the borate complex anion exchange chromatography HPAEC-Borate analysis (Willför et al., 2009), Sinner

et al. 1975), the wood sugars were separated on a 5.6 mm bore column 115 mm in length (omnifit) that was filled with a strong anion exchange resin (MCL gel CA08F (Mitsubishi chemicals, Japan) at 60 °C). The mobile phase (0.7 mL/min) was composed of A (0.3 potassium borate buffer with pH 9.2) and B (0.9 M potassium borate buffer with pH 9.5). After the sample injection separation was started with 90% A and 10% B. A linear gradient was run within 35 min to 10% A and 90% B. The data acquisition was stopped after 50 min. The sugar quantification was performed after the column derivatisation with Cu-bichincininate (0.35 mL/min) at 105 °C in a 30 m crocheted teflon coil with a 0.3 mm inner diameter and detection at 560 nm (Sinner *et al*. 1975; Sinner and Puls 1978). Data were processed with Dionex Chromeleon software (Thermo Scientific, USA).

Thermo-gravimetric analysis (TG)

The thermo-gravimetric analysis was performed to compare the degradation characteristics of the raw BSG, bleached cellulose fibres, and cellulose fibres. The thermal stability of reinforcing fibres is very important for their greater application in reinforced-biocomposite materials because typical processing temperature for many thermoplastics exceeds 200 °C (Tadmor and Gogos 1979). The thermal stability of the different samples was determined by TGA measurements performed using a Netzch thermo-gravimetric analyser (TG 209 F1, Netzch, Germany). The amount of sample used for each measurement was 5 to 7 mg. All measurements were performed under a nitrogen atmosphere with a gas flow of 10 mL/min while the material was heated from room temperature to 300 °C at a heating rate of 10 °C/min.

Scanning electron microscopy

SEM images were taken using a Hitachi TM3030 tabletop model (Hitachi, Japan) to observe the surface morphology of BSG based CNF. The SEM images were used to assess the effect of chemical treatment on untreated, alkali-treated, and bleached fibres. Samples were observed at an accelerating voltage of 15 kV. No sputtering was required; samples were placed on sampling pads procured from Christine-Gropl Company, Tulln, Austria.

X-ray diffractometry (XRD)

Cellulose crystallinity is a key factor in determining the mechanical and thermal properties of cellulose nanofibres. XRD studies on P0, P1, and P2 stages of cellulose fibres were conducted to investigate the crystalline behavior of the fibres. XRD was performed using a PANalytical Empyrean diffractometer system (PANalytical, Netherlands) using copper Kα-radiation. Scans were collected from 10 to 40° with a scan step size of 0.026° and a time per step of 96.39 s. The Segal crystallinity index (CI (%) was calculated by the following equation:

$$CI\ (\%) = ((Ia-Ib)/Ia) * 100 \quad (1)$$

where Ia is the total intensity of the (2 0 0) peak for cellulose representing amorphous and crystalline both regions at 22° 2θ and Ia is the amorphous region intensity at 18° 2θ (Segal et al. 1959).

Atomic force microscopy (AFM)

AFM imaging was done using a Bruker (Bruker Corporation) Dimension Icon. Measurements were performed in tapping mode with an OTESPA (Bruker Corporation) cantilever (rectangular shape, resonance frequency 300 (range 200 to 400), spring constant 42 (range 12 to 103), length 160 µm (range 140 to 180 µm), and width 50 µm (range 48 to 52 µm)). The scanning frequency varied between 0.5 and 1 Hz. The sample, as a suspension, was diluted to a dry content of 0.001%. A drop of the obtained solution was given on mica and placed to dry in an oven at 103 °C for a few minutes.

RESULTS AND DISCUSSION

Chemical Composition of BSG at Different Steps of Processing

Materials from stages P0, P1, and P2 were analysed for their chemical compositions, as shown in Table 2-1. The composition of the original material included cellulose (24.5%), hemicellulose (9.8%), and lignin (15.8%). The cellulose and lignin percentages agreed closely with 25.4% and 11.8%, respectively (Kanauchi et al. 2001). The quantity of cellulose and lignin was in agreement with the reported composition of BSG, that is, 16% to 25% cellulose and 11% to 27% lignin (Mussatto et al. 2006b). The composition of BSG depended on the type of malting barley, the process and conditions of malting, sample preparation, and method of chemical characterisation. Upon chemical treatment, the cellulose content increased as expected. Bleaching almost removed the lignin and hemicellulose.

Table 2-1 Chemical composition of BSG at different stages of processing.

Material	P0	P1	P2	Russ et al. (2005)	Mussato et al. (2008a)
Cellulose (w/w%)	24.5	43.2	94	23-25	16.8±0.8
Hemicellulose (w/w%)	23.8	14.2	-	30-35	8.4±2.0
Lignin (w/w%)	13.5	12.2	-	7-8	27.8±0.3

Morphological evaluations

The visual morphology of the P0, P1, and P2 stages are shown in Figure 2-2. The colour changed from brownish to slightly brownish-orange after the first treatment. The bleached material was clearly different and white in colour, which was due to the removal of non-cellulosic material like lignin, hemicellulose, and pectin. The White colour is an indication of cellulose. The chemical treatment also induced some morphological changes. After the first treatment, the surface became much rougher, mainly because of some materials like waxes, pectin, some sugars, and proteins.

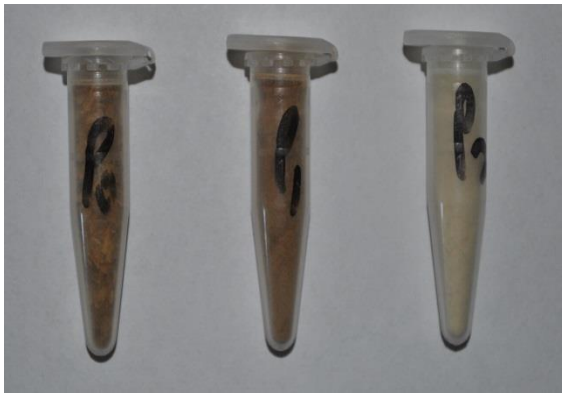

Figure 2-2 Change in colours of BSG with processing steps (P0, P1, P2, left to right)

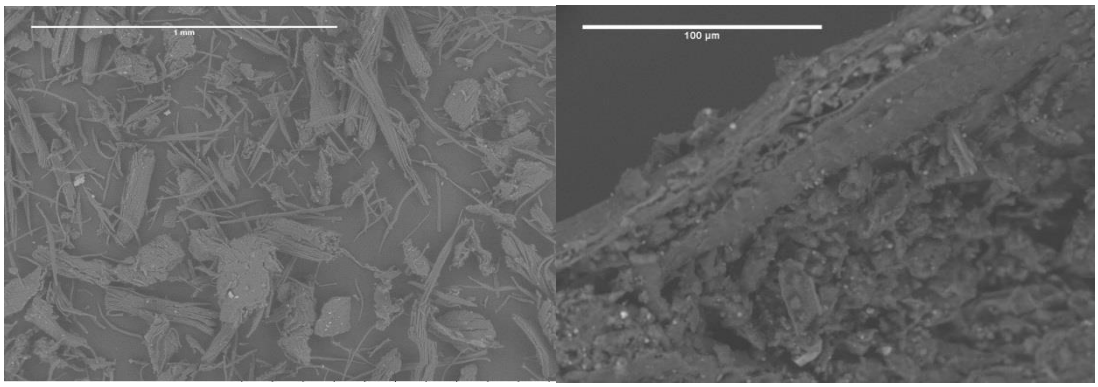

Figure 2-3 Cellulose fibres visible in bundles and raw BSG (right side, P0)

The fibres could easily be recognised in the optical microscope coupled to the AFM, which allowed a quick selection of the area to scan. As seen in Figure 2-3 the presence of nanofibrils is obvious. The height profiles shown in Figure 2-3 and corresponding to the positions marked with a 3 in Figure 2-4 revealed the fibre diameters to be about 5 nm. A statistical analysis of 20 nano-fibrils depicted in Figure 2-4 indicated a mean diameter of 4.578 nm, the median value being 4.250 nm. Some fibrils had a diameter smaller than 3 nm, which corresponded to elementary fibrils.

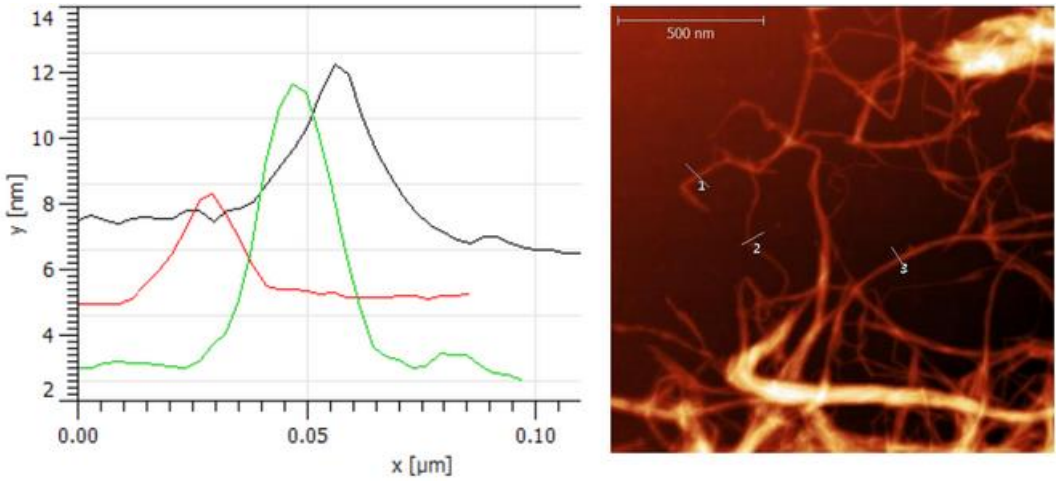

Figure 2-4 BSG nanocellulose picture obtained with the AFM and example of extracted height profiles.

Thermal stability:

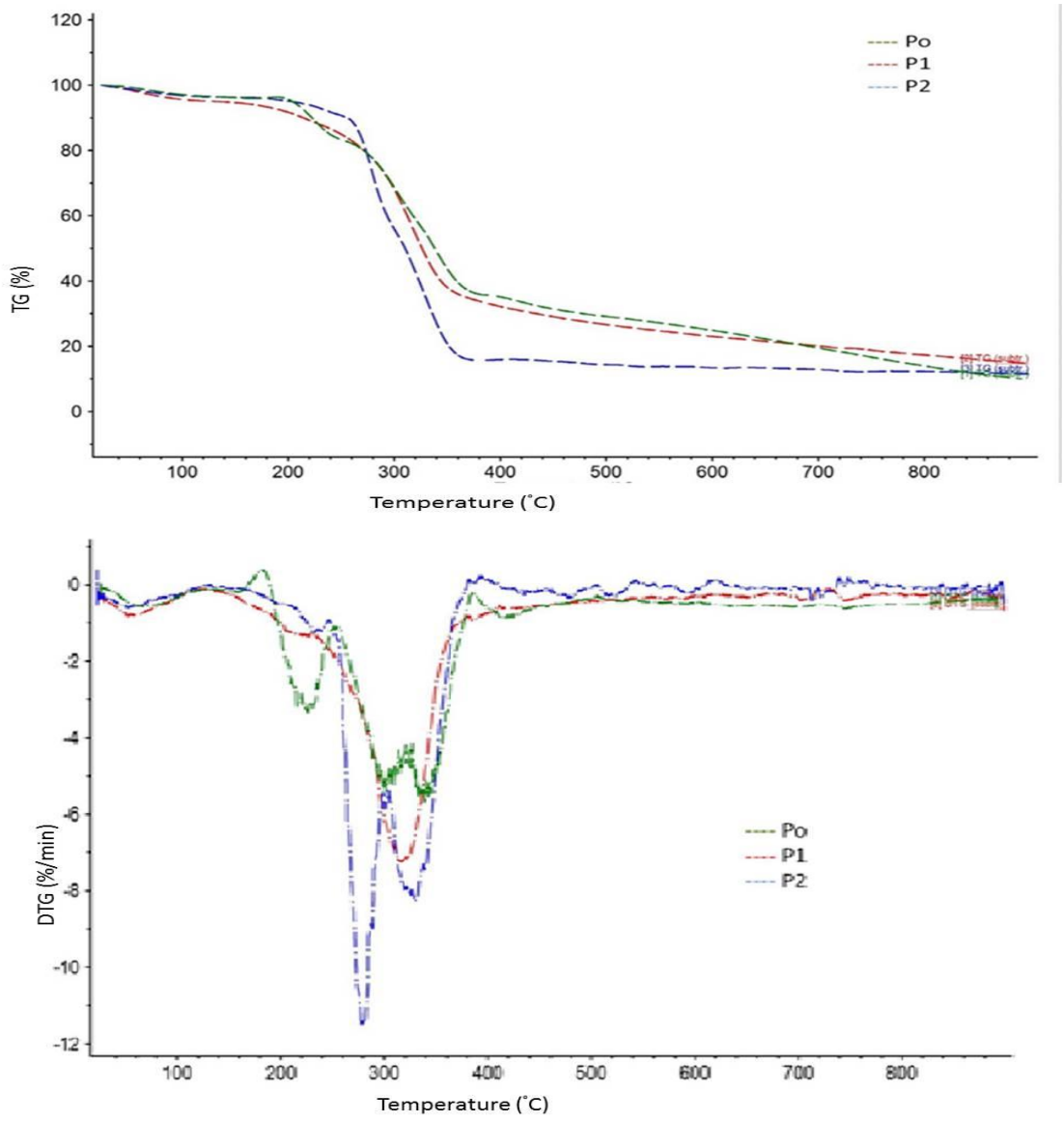

Figure 2-5 TG and DTG curves of BSG at Po, P1, and P2 stages of processing

The initial weight losses starting at ~25 °C for P0, P1, and P2 could be attributed to the evaporation of loosely bound moisture on the surfaces of the materials. The chemisorbed water was found to be given off near 100 °C for almost all the three materials. The degradation of P0 began at approximately 200 °C, and the rate of degradation reached two different peaks, at 300 and 340 °C. The early degradation could be explained by the presence of proteins and sugars in P0, which was followed by

P1 and P2 because of the presence of hemicelluloses and lignin in P1 and the removal of the same during the bleaching process. In the range of 400 to 640 °C, the residual weight decreased with the number of processing steps, which might have been due to char-forming substances (sugars, proteins, lignin, and hemicelluloses) and their subsequent removal during the different processing steps.

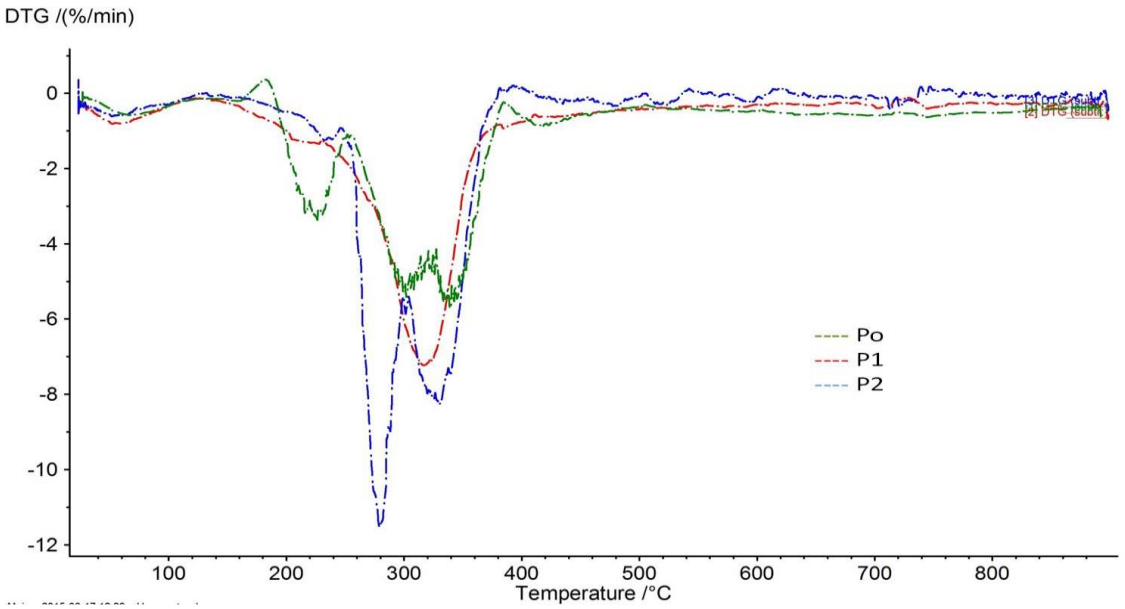

Figure 2-6 XRD curves of P0, P1, and P2

In the XRD (Figure 2-6), P2 showed a clear doublet at and asymmetric peak around 21.27 and 19.8, with a small shoulder around 12.05 degrees. In the raw BSG cellulose is mixed with hemicellulose, lignin, and protein. As these components are removed with increase in processing steps the crystallinity is expected to increase, seen by XRD curve (sharpening of curve) and increasing values of 17.4% (P0), 18.1% (P1), and 48.8% (P2) crystallinity index. This marked the presence of cellulose II (Cheng *et al*. 2011). The conversion of cellulose I to cellulose II could have happened because of alkaline treatment, but the change was visible only after the bleaching process (P2 stage) (Klemm *et al.* 2005).

CONCLUSIONS

1. BSG can be used as a potential source of CNF especially in the countries like Czech Republic (with significant size of brewing industry).
2. Wastage can be minimised by potential utilisation of protein-based biomass (degenerated protein based adhesive reported elsewhere and reclaimed lignin).
3. Reported work can be a useful part of the multistep process for producing value-added products from BSG.

ACKNOWLEDGEMENT

This work was funded by the Internal Grant Agency of the Faculty of Forestry and Wood Technology, Mendel University in Brno, Grant number LDF_VP_2015003.

REFERENCES CITED

- Cheng, G., Varanasi, P., Li, C., Liu, H., Melnichenko, Y. B., Simmons, B. A., Kent, M. S., and Singh, S. (2011). "Transition of cellulose crystalline structure and surface morphology of biomass as a function of ionic liquid pretreatment and its relation to enzymatic hydrolysis," Biomacromolecules 12(4), 933-941. DOI: 10.1021/bm101240z
- Ezeonu, F. C., and Okaka, A. N. C. (1996). “Process kinetics and digestion efficiency of anaerobic batch fermentation of brewer’s spent grains (BSG),” Process Biochem. 31(1), 7-12. DOI: 10.1016/0032-9592(94)00064-6
- Klemm, D., Heublein, B., Fink, H.-P., and Bohn, A. (2005). "Cellulose: Fascinating
- Biopolymer and sustainable raw material," Angew. Chem. Int. Ed. 44(22), 3358-3393. DOI: 10.1002/anie.200460587
- Mussatto, S. I., Dragone, G., and Roberto, I. C. (2006). “Brewers’ spent grain:
- Generation, characteristics and potential applications,” J. Cereal Sci. 43(1), 1-14. DOI: 10.1016/j.jcs.2005.06.001
- Morais, J. P. S., Rosa, M. de F., de Souza Filho, M. de sá M., Nascimento, L. D., do Nascimento, D. M., and Cassales, A. R. (2013). “Extraction and characterization of Nanocellulose structures from raw cotton linter,” Carbohyd. Polym. 91, 229-235. DOI: 10.1016/j.carbpol.2012.08.010

- Morán, J. I., Alvarez, V. A., Cyras, V. P., and Vázquez, A. (2008). “Extraction of
- Cellulose and preparation of Nanocellulose from sisal fibres,” Cellulose 15(1), 149-159. DOI: 10.1007/s10570-007-9145-9
- Mandal, A., and Chakrabarty, D. (2011). “Isolation of Nanocellulose from waste sugarcane bagasse (SCB) and its characterization,” Carbohyd. Polym. 86(3), 1291-1299. DOI: 10.1016/j.carbpol.2011.06.030.
- Fahma, F., Iwamoto, S., Hori, N., Iwata, T., and Takemura, A. (2010). “Isolation,
- Preparation, and characterization of nanofibres from oil palm empty-fruit-bunch (OPEFB),” Cellulose 17(5), 977-985. DOI: 10.1007/s10570-010-9436-4.
- Ludueña, L., Fasce, D., Alvarez, V. A., Stefani, P. M. (2011). “Nanocellulose from rice husk following alkaline treatment to remove silica,” BioResources 6(2), 1440-1453. DOI: 10.15376/biores.6.2.1440-1453
- Öztürk, S., Özboy, Ö., Cavidoğlu, İ., and Köksel, H. (2002). “Effects of brewer’s spent grain on the quality and dietary fibre content of cookies,” Journal of the Institute of Brewing 108(1), 23-27. DOI: 10.1002/j.2050-0416.2002.tb00116.

4. PAPER II

Aerosol assisted self-assembly as a route to synthesize solid and hollow spherical lignin colloids and its utilization in layer by layer deposition.

Pawan Kumar Mishra, Rupert Wimmer

(Accepted Article- Ultrasonic Sonochemistry)

Keywords: hollow and solid lignin colloids, layer by layer deposition, UV absorbance by lignin.

Abstract

Lignin, a major constituent of plant cell-wall and a by-product of paper-based industries is traditionally used for low-value applications (heat or electricity generation), but its potential in high-value utilization has also been widely reported. In this work, we synthesized lignin colloidal particles using ultrasonic spray-freezing route without any chemical functionalization of material and stabilized it by electrostatic route. As per our knowledge, this technique is the first reported method which yields hollow/solid lignin colloids having good particle size control without any chemical functionalization of material. Dioxane soluble fraction of Alkali lignin (D-lignin) was used without any further chemical functionalization. D-lignin dissolved in DMSO was sprayed upon liquid nitrogen cooled copper plate using an ultrasonic nebulizer. The resulting frozen droplets were collected and found to possess hollow and solid morphology. Particles thus obtained were characterized by their size distribution and morphology, and compared to theoretically anticipated values. Size tunability of particles in relation to the concentration of sprayed lignin solution was also studied. In addition to that, six layers of lignin colloids were deposited on quartz slide with the aid of negligible UV absorbing polyelectrolyte aqueous solution PDADMAC [Poly(diallyl dimethyl ammonium chloride)]. Gradation in UV absorbing ability of lignin with increase in a number of layers could be clearly observed. Hollow and solid lignin colloids, apart from their application in sunscreen cosmetics owing to their UV-absorbing ability, show potential applications in drug delivery also.

Introduction

Lignin is one of the most abundant biopolymers available on earth which has been traditionally treated as a waste product and burned to generate heat or electricity (Ten and Vermerris, 2015). It has also been widely studied for its potential applications. Lignin nano/micro particles add a new dimension to its applicability. They can be used as surfactants (Qian et al., 2014c), drug delivery vehicles (Frangville et al., 2012) and in formulation stabilization (Coccia et al., 2013). In addition to these, lignin granules in pesticide delivery (Garrido-Herrera et al., 2009), sun blocking (Qian et al., 2014b) and lignin-based carbon for hydrogen sorption (Babeł and Jurewicz, 2008) have also been reported. Several different approaches have been reported for lignin nanoparticles and colloid synthesis. Physical approaches like ultrasonic irradiation and ball milling (Snowdon et al., 2014) limit the control on particle shape, whereas chemical approaches like self-assembled colloidal spheres (Qian et al., 2014a) and chemical precipitation (Frangville et al., 2012) require pre-functionalization and use of ethylene glycol for particle formation respectively.

Self-assembly of lignin in an aqueous environment is infeasible due to hydrogen bonding and its unfavourable energetics (Qian et al., 2014a). On the contrary, it is favoured in an organic solvent by fall in temperature in addition to its self-associative properties (Guerra et al., 2007). Ultrasonic spray freezing for lignin colloid synthesis does not require any pre-functionalization of molecule and particles formed can be stabilized electrostatically without any surfactant utilization. Self-assembly and stabilization in lignin chains are reportedly explained by protonation of phenolic hydroxyl groups of lignin resulting in highest occupied molecular orbital-lowest occupied molecular orbital (HOMO-LUMO) interactions of the π-orbitals of the benzene ring (Achyuthan et al., 2010). In this work, we could successfully induce self-aggregation of unmodified-lignin by temperature reduction of an organic solvent (aerosol droplet) leading to solid and hollow spherical particle formation. To our knowledge, this is the first work in which solid and hollow spherical-colloid of lignin could be formed without any prior chemical modification of the material. Utilizing the negative charge on lignin in alkaline pH, six-layered layer by layer deposition was done with the aid of PDADMAC and a clear increase in UV absorbance with an increase in a number of layers was observed.

Experimental

Materials

Chemicals used in this study were Alkali lignin (Sigma-Aldrich); Dioxane (99.9%, Sigma-Aldrich); DMSO (analytical grade, Sigma-Aldrich); 0.1M sodium hydroxide (Sigma-Aldrich, ACS grade); PDADMAC 20 wt % in water (Poly(diallyl dimethyl ammonium chloride) solution, Sigma-Aldrich). All chemicals were purchased and utilized without any further modification. Water used was of Milli-Q quality for suspending the particles. Tubes used for dialysis made of regenerated cellulose were supplied by Carl Roth Company, Switzerland with a molecular weight cut-off 14000 D and nominal thickness 20.32 microns.

Methods

Lignin colloid synthesis

Lignin was dissolved in Dioxane and insoluble fraction was separated using vacuum filtration. This solution was dried using Buchi, Rotavapor R-215 at 40^0 C and 107 mBar pressures and called as D-Lignin. This D-lignin was dissolved in DMSO at four different concentrations (0.02, 0.07, 0.1 and 0.5w/v% (Weight of solute per 100 ml of solution)). These solutions were sprayed using an ultrasonic nebulizer (1.7MHz, 29^oC) and carrier gas N_2 (25l/min) upon a Cu-plate pre-cooled with liquid nitrogen and collected as frozen droplets. These droplets were dispersed in liquid nitrogen and transferred to a beaker containing water at $10^{\circ}C$ and pH 10.5. This beaker was left overnight at room temperature, thus obtained particle-suspension was dialysed against 1000ml of MilliQ water adjusted to pH=10.5 for 72 hours. Water was exchanged every 12 hours and the membrane once at 36 hours.

Characterization

Surface tension

Surface tension was measured with the instrument supplied by Dataphysics, contact angle system 20, with user interface SCA20, using pendant drop method at 70% R.H. and 20^0C in ambient air atmosphere.

Dynamic light scattering

DLS measurements were done using Malvern Nano ZS instrument by Malvern Instruments (UK) Company. The average size and polydispersity were determined by

dynamic light scattering at a scattering angle of 173° for 60 s. A minimum of 3 measurements were averaged to compute the correlation function.

Transmission electron microscopy

TEM images were obtained using FEI F30 electron microscope with an accelerating voltage of 300kV. The TEM samples were prepared by dropping diluted particle suspension onto copper grids coated with a thin carbon film and then dried at room temperature for 24 hours. No staining treatment was performed for the measurements.

Scanning electron microscopy

Surface morphologies were analysed using a field-emission scanning electron microscopy (SEM) (FEI, Quantum 200) working at an acceleration voltage of 15 kV. Few drops of colloid suspension at were placed on a specimen holder, sputter-coated directly with a platinum layer of about 7.5 nm (BAL-TEC MED 020 Modular High Vacuum Coating Systems, BAL-TEC AG, Liechtenstein) in Ar as a carrier gas at 0.05 mbar.

UV-vis absorbance spectrum

Absorbance was measured by Lambda 650(650L1501203), PerkinElmer instrument with an integrating sphere and UV Win Lab 6.0.4.0738 interface.

Layer by layer deposition on Quartz slides

Quartz slides were washed with pirhana solution for 30 min. These slides were dipped in 10mg/ml solution of PDADMAC in deionized water for 15 minutes, followed by washing with deionized water (3 times, 1 minute each in three different beakers). This PDADMAC layered slide was then transferred into lignin colloid suspension for 15 minutes and washed in the same way as in the previous step. This created a single layer lignin colloid on quartz slide with the aid of polyelectrolyte PDADMAC. This process was repeated for 6 times and UV absorbance was measured with 1, 2, 4, 6 layers.

Results and Discussion

Proposed mechanism of particle formation

The mechanism of particle formation can be divided into two steps. The first step is droplet formation and second is particle formation based on conservation of mass theory. Aerosol droplet size is decided by the operational frequency of nebulizer, surface tension and density of solution to be sprayed (Lang, 1962). Apart from it, effects of viscosity and empirical relations involving all these parameters have also been reported (Rajan and Pandit, 2001). For this work, we calculated droplet diameter based on

equation 1 & 2 and assumed it to be constant and unaffected by variation in precursor solution parameters. Furthermore, particle size was estimated on the basis of mass conservation and density of lignin, which is 1.33 g cm^{-3}, as reported elsewhere.

$\mathbf{D_{N,0.5}=0.34*\lambda_L}$(Lang,1962)……………………………………………*(Eq.1)*
$\mathbf{\lambda_L=((8*\pi*\theta)/(\rho*f2))^{1/3}}$*(*Rayleigh,1898*)*………………………………*(Eq.2)*

Using the above equation and π = pi, θ = Surface Tension of DMSO as 43.54 $mN.m^{-1}$ at 20°C, ρ =Density of DMSO as 1.10 g/cm^3, f = Frequency of nebulizer as 1.7 MHz, $D_{N,\ 0.5}$ = Number Median Diameter of Droplet, λ_L =Wavelength in the liquid, theoretical expected values (approximate) can be obtained. Based on above-mentioned equations and assumption, calculated droplet size was 1.18 microns for pure solvent. On the basis of different values of surface tension and density of different solutions, theoretically expected droplet size and thereof particle size are reported in table 3-1.
The diffusional nature of the material (represented by Peclet number) decides the mechanism of particle formation. The material with Peclet number less than one (e.g. solid saccharides) show higher diffusional motion than the radial velocity of diffusional motion mainly lead to solid particles. While materials with Peclet number more than one (polymers including lignin and proteins) can lead to hollow, wrinkled or solid particle depending on other properties of sprayed solution (Vehring, 2008). Based on one drop-one particle mechanism, every aerosol droplet acts as a reactor while travelling from the nebulizer to copper plate. At this stage two different processes occur simultaneously, first freezing of solvent (represented by the time is taken in solvent freezing, Tsf) and second diffusion of lignin (represented by the time is taken in lignin diffusion, Tld). If Tsf is enough for the solute to diffuse, a solid particle should be expected; else a hollow or porous particle should be expected (Okuyama and Wuled Lenggoro, 2003). In addition to that, various other parameters like droplet size, nature of polymers and concentration of solute (higher concentration favours solid particle formation) also play a major role in deciding particle morphology (Jayanthi et al., 1993). For a particle formation, lignin has to undergo self-assembly and precipitate to the formation of a particle (Figure 3-1). Alkali Lignin has been reported to have the propensity to self-aggregate in an organic solvent (Contreras et al., 2008; Norgren et al., 2002, 2001). In addition to that, fall in temperature and increase in concentration due to

solvent freezing from outside to inside, induce the further aggregation and particle formation. This is in agreement to low temperature induced and concentration dependent aggregation reported by Guerra et. al, 2007 and Deng et al., 2011. Once the molecular aggregation starts to happen, stabilization of particles can be explained by non-covalent pi-pi interaction (Achyuthan et al., 2010; Sarkanen et al., 1984), long range wander val forces (Guerra et al., 2007) and chain entanglement (Guerra et al., 2007). This mechanism of self-assembly and solid particle formation is indirectly supported by agreement of theoretically expected particle size and experimentally obtained one (table 3-1). After being transferred to water (MilliQ water adjusted to pH 10.5) with the rise in temperature, DMSO diffuses into the water and water forms a hydration shell thereby stabilizing the particle by electrostatic forces. The solvent is later removed by dialysis of the suspension against MilliQ water. Stabilization in alkaline pH can be attributed to the ionization of functional group at alkaline pH which facilitates electrostatic stabilization of suspension.

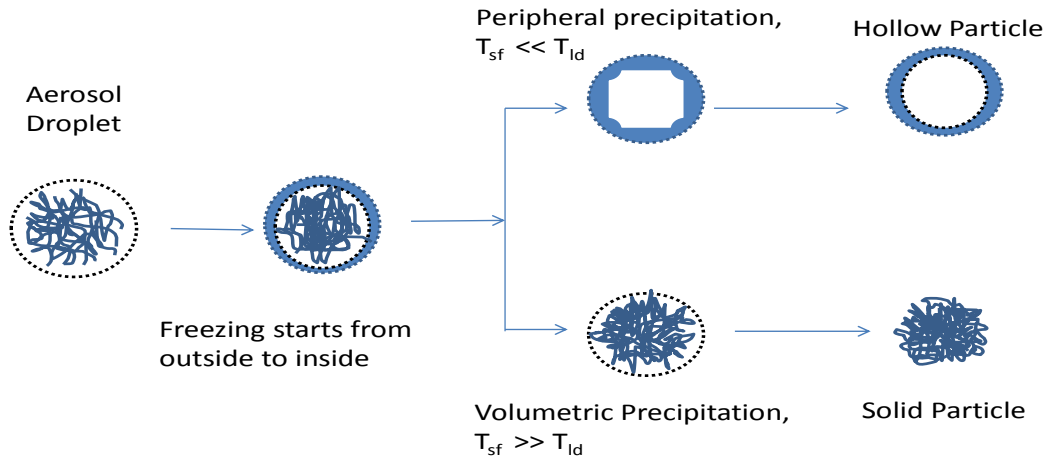

Figure 3-1 Morphology of particle based on mechanism followed, Tsf- characteristic time for solvent freezing, Tld- characteristic time for diffusion of lignin.

Comparison of particle size distribution

In one drop – one particle mechanism of spray freezing, each droplet acts as a micro-reactor and leads to the formation of a particle. Based on the weight percentage of lignin in precursor solution and droplet size from Eq.1 and Eq. 2, we calculated expected particle size and compared it with obtained particle size from DLS. Experimental particle sizes as obtained by DLS and SEM image analysis are shown in

Figure 3-2(a), These figures clearly show a decrease in particle size with increase in sprayed solution concentration from 0.02% to 0.07%, followed by an increase in particle size with increase in sprayed solution concentration. This can be explained by the difference in particle formation mechanism and change in particle morphology (hollow). However, experimentally obtained particle size was either higher or lower than predicted by one drop-one particle mechanism, which can be explained by the difference in packing efficiency of chains and density of final product. Curves in Figure 3-2(b) depict the particle size distribution of obtained particles with respect to the concentration of precursor solution, showing the clear unimodal distribution. SEM images were analyzed using ImageJ software. Minimum 120 particles were analyzed for particle size (manual method) and later converted in percentage frequency in the histogram.

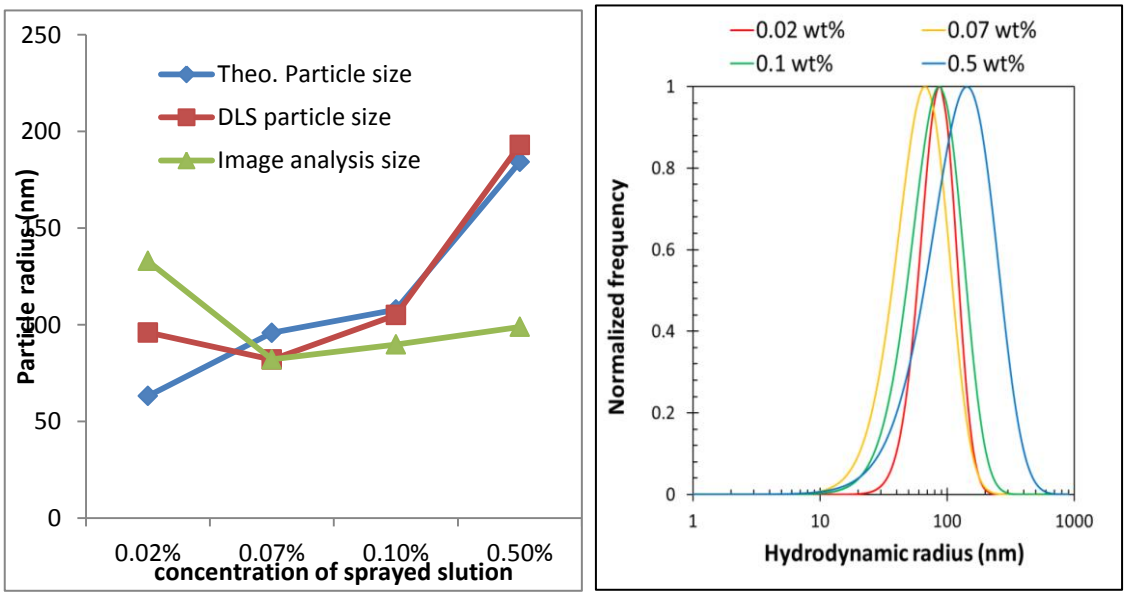

Figure 3-2 (a)Comparative particle size as calculated by theory, DLS and SEM images (left side). Figure 2(b) Particle size distribution of different particles obtained using different concentrations of precursor solution (right side).

Table 3-1 Theoretically predicted droplet size, particle size and obtained particle size.

	Concentration of sprayed solution (wt %)			
	0.02%	0.07%	0.1%	0.5%
Density of solution(g/cm³)	1.1018	1.1042	1.1805	1.1984
Surface tension(mN·m^{-1})	49.12	49.54	51.46	51.67
Predicted particle rad.(nm)	63.1	95.8	107.8	184.2
Measured particle rad. by DLS(nm)	96	82	105	193
Polydispersity	0.42	0.31	0.42	0.51
Measured particle rad. SEM image analysis	133	82.11	89.8	98.9

Morphological evaluation

Through SEM, clear images of solid and hollow particles could be observed, which were in agreement to an anomaly in particle size distribution and mechanism of particle formation. As seen in Figure 3-3 (part A, B, and C), hollow colloids were formed. Representative TEM images of the solid colloid can also be clearly seen in Figure 3-4. TEM image of an intact hollow particle could not be obtained, which might be because of shell thickness or nature of material.

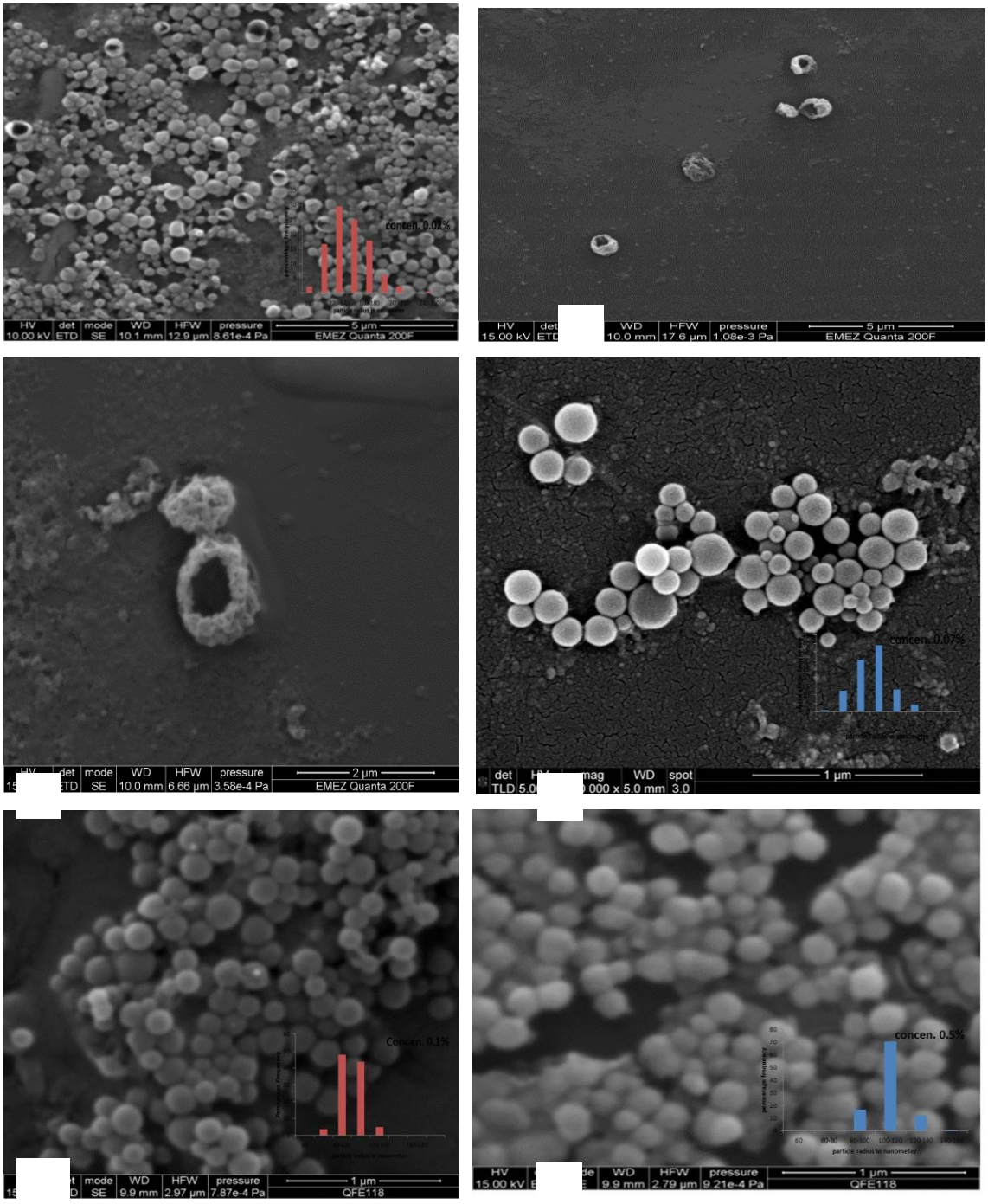

Figure 3-3 Representative SEM images of particles obtained using 0.02% (A,B,C), 0.07% (D), 0.1% (E) and 0.5% (F) concentration of spray solution.

TEM images

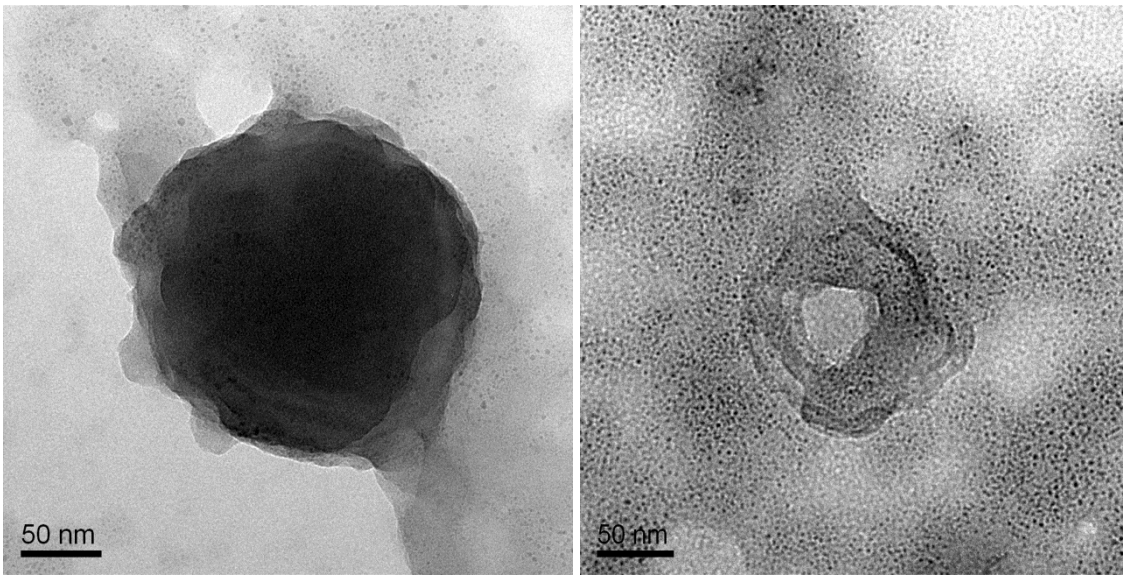

Figure 3-4 Representative TEM images of a solid and hollow colloid (broken).

Layer by layer deposition and UV absorbance

In UV spectrum of deposited layer of colloids, characteristic peaks of lignin were observed around 202 and 280 nm, and a shoulder was observed around 230 nm. Peak around 202 nm corresponds to the portions of unsaturated chain (Bentivenga et al., 2003; Tonucci et al., 2011). Whereas, peak at 280 nm can be attributed to unconjugated phenolic hydroxyl groups and aromatic rings of lignin (Awungacha Lekelefac et al., 2014; Ohnishi et al., 1989). A clear linear increase in absorbance with an increase in a number of layers can be clearly seen in Figure 3-5, which is an anticipated trend from the layer by layer deposition of colloids.

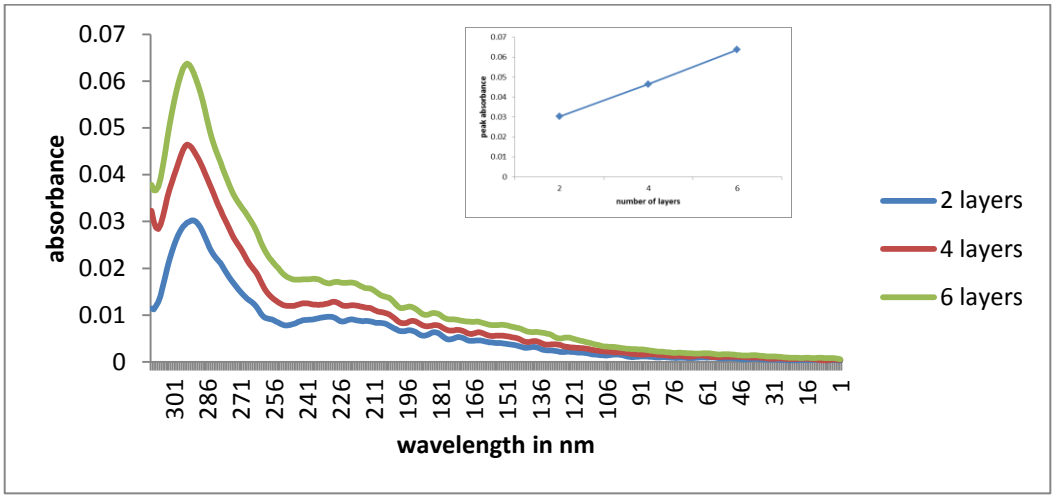

Figure 3-5 UV absorbance with an increase in a number of layers deposited by layer by layer deposition.

Conclusions

1. Lignin colloid particles were synthesized without any pre-chemical modification and the stable aqueous suspension was obtained in alkaline pH (10.5).
2. In particle formation, peripheral and volumetric precipitation was observed to be the dominant mechanism at low concentration and high concentrations respectively.
3. Lignin colloids were successfully used in six layered coating by layer by layer deposition on quartz slide with the aid of polyelectrolyte PDADMAC (negligible UV absorbance) and increase in absorbance with an increase in a number of layers was observed.
4. Thus, this work presented a unique and novel method for preparation of hollow/ solid lignin colloids which is supposed to be a better technique than other existing methods in terms of control of structure (solid/ hollow), pre-functionalization of lignin and use of electrostatic stabilization.

References

- Achyuthan, K.E., Achyuthan, A.M., Adams, P.D., Dirk, S.M., Harper, J.C., Simmons, B.A., Singh, A.K., 2010. Supramolecular Self-Assembled Chaos:

Polyphenolic Lignin's Barrier to Cost-Effective Lignocellulosic Biofuels. Molecules 15, 8641–8688. doi:10.3390/molecules15118641

- Awungacha Lekelefac, C., Hild, J., Czermak, P., Herrenbauer, M., 2014. Photocatalytic Active Coatings for Lignin Degradation in a Continuous Packed Bed Reactor. Int. J. Photoenergy 2014, e502326. doi:10.1155/2014/502326
- Babeł, K., Jurewicz, K., 2008. KOH activated lignin based nanostructured carbon exhibiting high hydrogen electrosorption. Carbon 46, 1948–1956. doi:10.1016/j.carbon.2008.08.005
- Bentivenga, G., Bonini, C., D'Auria, M., De Bona, A., 2003. Degradation of steam-exploded lignin from beech by using Fenton's reagent. Biomass Bioenergy 24, 233–238. doi:10.1016/S0961-9534(02)00135-6
- Boyer, B., Rudie, A., 2007. Single fibre lignin distributions based on the density gradient column method. Presented at the Proceedings of TAPPI engineering, pulping and environmental conference, Jacksonville, FL. Atlanta, GA, TAPPI Press (October 2007), Citeseer.
- Coccia, F., Tonucci, L., d'Alessandro, N., D'Ambrosio, P., Bressan, M., 2013. Palladium nanoparticles, stabilized by lignin, as catalyst for cross-coupling reactions in water. Inorganica Chim. Acta 399, 12–18. doi:10.1016/j.ica.2012.12.035
- Contreras, S., Gaspar, A.R., Guerra, A., Lucia, L.A., Argyropoulos, D.S., 2008. Propensity of Lignin to Associate: Light Scattering Photometry Study with Native Lignins. Biomacromolecules 9, 3362–3369. doi:10.1021/bm800673a
- Deng, Y., Feng, X., Zhou, M., Qian, Y., Yu, H., Qiu, X., 2011. Investigation of Aggregation and Assembly of Alkali Lignin Using Iodine as a Probe. Biomacromolecules 12, 1116–1125. doi:10.1021/bm101449b
- Dong, F., Huang, Y., Zou, S., Liu, J., Lee, S.C., 2011. Ultrasonic Spray Pyrolysis Fabrication of Solid and Hollow PbWO4 Spheres with Structure-Directed Photocatalytic Activity. J. Phys. Chem. C 115, 241–247. doi:10.1021/jp108221v
- Frangville, C., Rutkevičius, M., Richter, A.P., Velev, O.D., Stoyanov, S.D., Paunov, V.N., 2012. Fabrication of Environmentally Biodegradable Lignin Nanoparticles. ChemPhysChem 13, 4235–4243. doi:10.1002/cphc.201200537

- Garrido-Herrera, F.J., Daza-Fernández, I., González-Pradas, E., Fernández-Pérez, M., 2009. Lignin-based formulations to prevent pesticides pollution. J. Hazard. Mater. 168, 220–225. doi:10.1016/j.jhazmat.2009.02.019
- Gilca, I.A., Popa, V.I., Crestini, C., 2015. Obtaining lignin nanoparticles by sonication. Ultrason. Sonochem. 23, 369–375. doi:10.1016/j.ultsonch.2014.08.021
- Guerra, A., Gaspar, A.R., Contreras, S., Lucia, L.A., Crestini, C., Argyropoulos, D.S., 2007. On the propensity of lignin to associate: A size exclusion chromatography study with lignin derivatives isolated from different plant species. Phytochemistry 68, 2570–2583. doi:10.1016/j.phytochem.2007.05.026
- Jayanthi, G.V., Zhang, S.C., Messing, G.L., 1993. Modeling of Solid Particle Formation During Solution Aerosol Thermolysis: The Evaporation Stage. Aerosol Sci. Technol. 19, 478–490. doi:10.1080/02786829308959653
- Lang, R.J., 1962. Ultrasonic Atomization of Liquids. J. Acoust. Soc. Am. 34, 6–8. doi:10.1121/1.1909020
- Norgren, M., Edlund, H., Wågberg, L., 2002. Aggregation of Lignin Derivatives under Alkaline Conditions. Kinetics and Aggregate Structure. Langmuir 18, 2859–2865. doi:10.1021/la011627d
- Norgren, M., Edlund, H., Wågberg, L., Lindström, B., Annergren, G., 2001. Aggregation of kraft lignin derivatives under conditions relevant to the process, part I: phase behaviour. Colloids Surf. Physicochem. Eng. Asp. 194, 85–96. doi:10.1016/S0927-7757(01)00753-1
- Ohnishi, H., Matsumura, M., Tsubomura, H., Iwasaki, M., 1989. Bleaching of lignin solution by a photocatalyzed reaction on semiconductor photocatalysts. Ind. Eng. Chem. Res. 28, 719–724. doi:10.1021/ie00090a012
- Okuyama, K., Wuled Lenggoro, I., 2003. Preparation of nanoparticles via spray route. Chem. Eng. Sci., 17th International Symposium of Chemical Reaction Engineering (IS CRE 17) 58, 537–547. doi:10.1016/S0009-2509(02)00578-X
- Qian, Y., Deng, Y., Qiu, X., Li, H., Yang, D., 2014a. Formation of uniform colloidal spheres from lignin, a renewable resource recovered from pulping spent liquor. Green Chem. 16, 2156–2163. doi:10.1039/C3GC42131G

- Qian, Y., Qiu, X., Zhu, S., 2014b. Lignin: a nature-inspired sun blocker for broad-spectrum sunscreens. Green Chem. 17, 320–324. doi:10.1039/C4GC01333F
- Qian, Y., Zhang, Q., Qiu, X., Zhu, S., 2014c. CO_2 -responsive diethylaminoethyl-modified lignin nanoparticles and their application as surfactants for CO_2 /N_2 -switchable Pickering emulsions. Green Chem 16, 4963–4968. doi:10.1039/C4GC01242A
- Rajan, R., Pandit, A.B., 2001. Correlations to predict droplet size in ultrasonic atomisation. Ultrasonics 39, 235–255. doi:10.1016/S0041-624X(01)00054-3
- Sarkanen, S., Teller, D.C., Stevens, C.R., McCarthy, J.L., 1984. Lignin. 20. Associative interactions between kraft lignin components. Macromolecules 17, 2588–2597. doi:10.1021/ma00142a022
- Snowdon, M.R., Mohanty, A.K., Misra, M., 2014. A Study of Carbonized Lignin as an Alternative to Carbon Black. ACS Sustain. Chem. Eng. 2, 1257–1263. doi:10.1021/sc500086v
- Ten, E., Vermerris, W., 2015. Recent developments in polymers derived from industrial lignin. J. Appl. Polym. Sci. 132, n/a-n/a. doi:10.1002/app.42069
- Tonucci, L., Coccia, F., Bressan, M., d'Alessandro, N., 2011. Mild Photocatalysed and Catalysed Green Oxidation of Lignin: A Useful Pathway to Low-Molecular-Weight Derivatives. Waste Biomass Valorization 3, 165–174. doi:10.1007/s12649-011-9102-6
- Vehring, R., 2008. Pharmaceutical Particle Engineering via Spray Drying. Pharm. Res. 25, 999–1022. doi:10.1007/s11095-007-9475-1

5. PAPER III

Cellulose nanofibre aerogel as a promising bio-material for customized oral drug delivery

Jyoti Bhandari, Harshita Mishra, Pawan Kumar Mishra, Rupert Wimmer, Sushama Talegaonkar

(Under Review –International Journal of Nanomedicine)

ABSTRACT

Cellulose Nanofibre (CNF) aerogels prepared by freeze drying method have been introduced as the new possible carriers for oral controlled drug delivery system with floatability and mucoadhesive properties. Bendamustine Hydrochloride is taken as the model drug. Drug loading was done by physical adsorption method and optimization of drug loaded formulation was done by using Central Composite Design. Very light weight aerogel with matrix system was produced with drug loading of 18.98±1.57%. Produced aerogel film was characterized for morphology, tensile strength, swelling tendency in different pH, floating behavior, mucoadhesive detachment force and drug release profile in different pH conditions. The results showed the matrix type, porous and woven type of aerogel formulation with excellent mechanical properties. The drug release was assessed by dialysismethod which is fitted with suitable mathematical models. Approximately, 69.205 ± 2.5 % of the drug was released in 24 hours in pH medium 1.2 whereas about 78 ± 2.28 % of drug was released in the pH medium 7.4 with floating behavior for approximately 7 hours and 30 minutes. The results of in vivo study showed a 3.25 ± 0.32-fold increase in bioavailability. Thus, we concluded that cellulose nanofibre aerogels offer a great possibility for a gastro retentive drug delivery system with improved bioavailability.

Keywords: Aerogel, controlled release, gastroretentive, floating behavior, swelling behavior, mucoadhesion and bioavailability.

Introduction

Drug delivery systems especially having sustained and targeted release, have received more attention in the last few decades due to potential benefits that they offer, such as decrease in side effects and enhancement in therapeutic efficacy for the prolonged period of time with the possibility for dose reduction(1). Further, Oral controlled drug delivery is always considered as the ideal drug delivery system. Oral route presents the benefits over the i.v. route in the cancer therapy in several ways. Though i.v. route leads to immediate and complete bioavailability and accurate dosing, this route could be hazardous because high concentration of the drug is delivered to normal tissues. Other advantages of oral route include patient compliance, painless delivery, economical advantage, and improvement in daily dosage regime of the patient (2). In order to enhance the gastric residence time of the oral formulations, different approaches have been studied like altered density formulations, floating system, bio-adhesive formulations, swelling systems, ion exchange resins, porous systems, osmo-regulated formulations, and effervescent formulations (3).

Nanofibres urge a huge potential in the biomedicine as a carrier for controlled drug delivery because of its unique attributes like high surface area per unit mass, extensive porosity, strength with flexibility, and being economical (4). Due to these significant physicochemical properties, nanofibres are exploited for wide range of applications. In the field of biotechnology, nanofibres serve for variety of purposes such as in drug delivery, dental applications, wound dressing medicinal implants and tissue engineering (5). They serve as the carrier for the drug delivery like antimicrobials, enzymes, other drugs, antioxidant, flavor and functional group compound. Besides the medicinal purposes they are also used in filtration media as biosensor, military protective clothing and for various other industrial applications like in food industry (6). Nanofibres can also be used for the controlled release of compounds by protecting and stabilizing the compound and are slowly released under suitable conditions (7). Moreover, cellulose Nanofibre is a relatively stable polymer with hydrogen bonding, has a good flexibility and elasticity, possesses low density, is a renewable resource, has relatively reactive surface which can be used for grafting specific groups, and is cheap (8).

Cellulose nanofibre can be broadly classified into two categories. One is plant source and the next is bacterial source. With the plant source cellulose, they are further

classified into wood and non-wood source. The non-wood source contains agricultural crops and the agricultural by- product obtained from corn, wheat rice, barely, sugar cane, pine apple, banana, coconut crops, potato pulp, sweet beet pulp, soy. Bacterial cellulose which is also referred to as microbial cellulose has gained particular attention recently especially in biomedical and tissue engineering. Bacterial Cellulose is mainly produced by Acetobacter xylium (9) which is a gram negative stain of acetic acid producing bacteria. However, other bacteria like Acanthamoeba, Achromobacter, Zoogloea, Agrobacterium, Pseudomonas, Alcaligenes, Sacrina, Rhizobium also secrets cellulose fibres extracellularly. Microbial or bacterial cellulose (BC) is chemically identical to plant cellulose (PC), though they possess different macromolecular structure and different physical properties (10).

Cellulose nanofibres generally convert into aerogel form during drug adsorption and subsequent freeze drying. Aerogel is another form of CNF which is foam like structure with very light weight, highly porous and can be prepared by freeze drying technique. The main aim of our project was to explore the properties of procured CNF in oral drug delivery. Because of the hydrophilic nature of Bendamustine hydrochloride and the ability of cellulose to swell in aqueous media, bendamustine hydrochloride was chosen as a model cancer drug.

MATERIALS AND METHODS

Materials

CNF was procured from University of Maine, USA. Bendamustine Hydrochloride was obtained as a gift sample from Fresenius Kabi Oncology Limited (Gurgaon, India). All the other chemicals used were of analytical grade.

Preparation of plain CNF

The procured CNF was prepared by the spray drying technique with main source of cellulose being US Forest Service's Cellulose Nanomaterials Pilot Plant at the Forest Products Laboratory (FPL). These nanofibres are prepared from wood.

Preparation of Drug loaded cellulose nanofibre (DCNF) aerogels

The method reported by Kolakovic *et al*. (11) was used with slight modification. Saturated solutions of the drug were prepared in HCLbuffer (pH 2.5) with keeping volume constant at 4 ml. Different amounts of cellulose Nanofibres were added to it in order to get the ratios of CNF: drug 1: 0.5, 1:1, 1:2, 1:3, 1:4, 1:5. The solution was magnetically stirred for 1 to 16 hrs. For preliminary test hours at 1500 rpm. The

prepared suspension was transferred to the centrifuge tubes and was centrifuged at 14000 rpm for 15 minutes. Supernatant was decanted and its volume was measured. Absorbance of the supernatant solution was measured after suitable dilution at 233 nm using UV Spectrophotometer. Concentration of the drug in the supernatant was then calculated. The drug loading was further optimized using the two factor Central Composite design as suggested by Design of Experiment (DOE, Stat Ease Design Expert) software for the one dependent attribute- Drug Loading. The independent variables selected for the optimization are: Stirring Time varied from 3 to 8 hours and CNF Ratio varied from 0.6 to 3. The settled DCNF were collected and lyophilized using mannitol (1%) as the cryoprotectant. The primary drying was performed at -30°Cfor 72 h followed by the secondary drying, where the temperature was first increased to -10°C for 4 h, and then to -5°C for 18 h and 0°C for next 2 h. Pressure was maintained at 150–225 mTor (20–30 Pa) according to Valo *et al*. (12).

Characterization of the bendamustine-loaded Cellulose nanofibre (DCNF) aerogel system

The aerogels were characterized on the basis of various parameters such as surface morphology using scanning electron microscopy (SEM) and transmission electron microscopy (TEM), swelling index in different pH media, floating behavior, tensile strength, mucoadhesion, drug content, and in vitro release in different pH media.

Determination of drug loading and drug entrapment efficiency

Drug was loaded onto the particles by physical absorption. Drug content of the cellulose nanofibres was calculated by indirect method (13), where the supernatant collected was analyzed for the amount of drug present in it, and finally the drug loading was calculated using the following formula:

$$\text{Drug loading (DL \%): DL} = \frac{Di-Df}{C}\ X\ 100$$

Where, D_i& D_f represent the initial amount of drug added and the measured amount of free drug in the supernatant, respectively.

C is the total amount of Nanofibres recovered.

For the optimized drug loaded formulation, the entrapment efficiency was calculated by the following formula:

$$\text{Entrapment efficiency (EE \%): } \mathbf{EE\%} = \frac{Di-Df}{Di} X\ 100$$

Where, D_i& D_f represent the initial amount of drug added and the measured amount of free drug in the supernatant, respectively.

Scanning electron microscopy

The surface morphology of aerogel was examined by scanning electron microscopy. The aerogel was mounted on aluminum stubs using double sided carbon adhesive tape and sputter-coated with conductive gold-palladium. They were viewed with an EVO LS 10 (Carl Zeiss, Brighton, Germany) scanning electron microscope operating at an accelerating voltage of 13.52kV under high vacuum. Data analysis was done using Smart SEM software program.

Transmission electron microscopy

TEM study was carried out for the provided CNF and the optimized DCNF. The samples were mounted on copper grids with salt of heavy metal viz. 1% uranyl acetate for negative staining, followed by sample drying. They were then analyzed by TEM at an accelerating voltage of 100kV and data acquisition was done on the AMT Image Capture Engine.

Swelling index

In order to evaluate the swelling behavior, the known weight of CNF and DCNF aerogel were placed in test tubes containing 10 mL of HCL buffer pH 1.2 and phosphate buffer pH 7.4 for 24 h and 48 h at 37°C. Thereafter, samples were collected back and the water on the surfaces of the samples was removed with filter paper. Samples were then weighed in the wet condition (14). The swelling ratio for each sample was calculated according to the following equation.

$$\text{Swelling ratio (\%)} = \frac{Mw-Md}{Md} X\ 100$$

Where, 'M_d' is the initial weight of drug-loaded nanofibres & 'M_w' is the final weight of drug-loaded nanofibres in wet condition.

Mucoadhesion test

Mucoadhesive strength was determined with the help of the texture analyzer (TA. XT Plus, Stable Micro Systems, UK). The aerogel approx. 2 cm^2 was attached to the cylindrical probe by double sided adhesive tape. The goat stomach mucosa (about 20 X 20 mm) was hydrated for 15 minutes at 37 ± 0.5°C and then was placed on the holder stage of mucoadhesive holder (15). The instrument was run at a load of 200 grams, and the weight required to detach the fibre from the mucosa was determined.

Tensile strength

Tensile strength of the CNF and DCNF aerogel formulation was determined using a texture analyzer (TA. XT Plus, Stable Micro Systems, UK). Aerogel was cut into dimensions 6 * 2 cm^2 with thickness of about 1 mm and was placed in a vertical position along the axis of the texture analyzer, using clamps. The instrument was run at a load of 3 gram/cm^2 after necessary adjustments. The force required to break the formulation was determined (16).

Floating time

In order to calculate the Floating Time, DCNF aerogel with dimensions of approximately 3*3 cm^2 was taken and placed into the HCL buffer of pH 1.2, maintained at 37°C. Total Floating Time i.e. the time period for which the formulation remained buoyant was measured (17).

In-vitro drug release

DCNF were evaluated for in vitro drug release by using dialysis membrane. HCL buffer (pH 1.2) was employed as the release media in the studies as the formulation is intended to release the drug in the stomach. The dialysis bags (MW cut off 8-10 kDa; Spectra/Por® Spectrum Laboratories, Inc, USA) were soaked in double-distilled water for 12 h before use. DCNFs and equivalent pure drug bendamustine solution were poured in separate dialysis bags. The bags were suspended in 200 ml of receiving phase i.e. HCL buffer (pH 1.2) and placed into an incubator shaker maintained at 37°C and at 100 rpm. Aliquots were withdrawn at various time points. Sink condition was maintained throughout the experiment. Concentration of Bendamustine Hydrochloride in aliquots was analyzed by UV spectrophotometry at 233 nm and cumulative percent of drug release was determined. In order to compare the difference in release profile from cellulose nanofibre film in different pH media, same study was carried out in phosphate buffer pH 7.4. The obtained results from two different pH media are compared.

Release kinetic study

The kinetics of Bendamustine Hydrochloride release from the DCNF in pH 1.2 media was studied using different kinetics models including: zero order release kinetics, first order release kinetics and Higuchi model and Korsmeyer-Peppas model.

In-vivo studies

HPLC analysis in plasma

For the HPLC analysis, method reported by Xie et al. (18) was used with slight modification. Separation was carried out in isocratic mode with TC-C 18 column (4.6mm X 250mm, 5µm, Walbdrom, Germany). The mobile phase consisted of Acetonitrile (ACN): 10mM potassium dihydrogen phosphate solution in ratio 32:68 (v/v, pH 2.5). The flow rate was 1.0 $mLmin^{-1}$; column temperature was 30°C; and UV detector was set at 235 nm. Calibration curve in plasma was prepared for different concentration ranging from 250 to 5000 $ngmL^{-1}$. Dilution was carried out using mobile phase. For the preparation of sample, precipitation of protein in plasma was carried out using 10% perchloric acid–methanol solution which was then centrifuged at 15000 rpm for 15 minutes. 20µL of supernatant was withdrawn and injected into the chromatographic system.

Animals

The animal study protocol to carry out in vivo studies was duly approved by the Jamia Hamdard, Institutional Animal Ethics Committee (Approval No. 1192, 2015). Wistar rats (200–300 g) of either sex were kept under standard laboratory conditions (temperature 25 ± 2°C and RH 55 ± 5%). They were housed in polypropylene cages (two per cage) with free access to standard laboratory diet (Lipton Feed, Mumbai, India) and water ad libitum.

Method

For the in-vivo pharmacokinetic study the animals were divided into three groups. Group A was given marketed preparation (Bendit) intravenously via tail vein keeping volume 0.5 ml and Group B and C were respectively pure drug solution and DCNF formulation orally by using feeding tube. The dose calculation of the rats was based on bodyweight and was determined to be 27.75 mg/kg.

Human equivalent dose of Bendamustine Hydrochloride → 4.2-5.5 mg/kg (Colledge, 2014).

$$Rat\ Dose\ (mg/kg) = Human\ Equivalent\ Dose\ (mg/kg)\ X\ \frac{Human\ Km}{Rat\ Km}$$

$$= 4.5\ X\ 37/6$$

$$= 27.75\ mg/kg$$

At the time of blood sampling, each animal was anaesthetized with diethyl ether and blood samples (1 ml) were collected from the retro orbital plexus into eppendorf tubes containing EDTA. The blood samples were collected at the following time points: 0 (pre dose), 0.5, 1, 2, 3, 4, 6, 8, 12, and 24 hours. The blood samples were then centrifuged at 5000 rpm for 15 minutes. The plasma (supernatant) was collected in eppendorf tubes and was precipitated with the procedure as stated in section below and the supernatant was stored in freezer at -20 °C which was analyzed by HPLC method, as per analysis.

Statistical analysis

Statistical analysis was done using Statistica11 (statsoft, Inc., a unit of Dell software, California, USA). Results were expressed as mean ± standard deviation. Comparison of marketed preparation, drug solution and formulation suspension data was done by analysis of variance (ANOVA) and p-value less than 0.05 was considered significant.

RESULTS AND DISCUSSION

DCNF was prepared from CNF by physical adsorption method. During the preparation and optimization of DCNF it was observed that after going through the process of freeze drying, DCNF converted into foam like structure, i.e. aerogel. It was also observed that some physical changes took place after freeze drying. Therefore, in-vitro characterization was performed on both CNF and DCNF aerogel.

Optimization of formulation

To identify the optimum levels of different process variables influencing the response, i.e., drug loading of Bendamustine HCl, two factor Central Composite design as suggested by Design of Experiment (DOE, Stat Ease Design Expert) software for the one dependent attribute-was used. The individual and interactive effects of these process variables were studied by conducting the process at different levels of all the factors. The results of the experimental data and simulated values are listed in Table 4-1. According to the software generated data, 13 formulations were prepared with n = 3.

Table 4-1 Drug loading with two factor central composite design

Cellulose-Nanofibre Ratio	Stirring Time (hours)	Drug Loading (%)
	8.0	18.98±1.57
1.8	5.5	11.46 ± 2.63
1.8	5.5	14.51 ± 1.89
1.8	9.04	14.35 ± 3.21
3.5	5.5	20.16 ± 2.64

1.8	5.5	13.33 ± 2.11
0.1	5.5	0.22 ± 1.21
1.8	5.5	12.62 ± 1.66
0.6	3.0	0.46 ± 0.32
3	3.0	6.08 ± 0.86
1.8	1.96	3.12 ± 1.2
1.8	5.5	13.24 ± 1.43
0.6	8.0	0.81 ± 0.43

Effect of different factors on drug loading

According to the 3 D plot (Figure 4-1), it is evident that the drug loading increases with increase in the concentration of fibres, reaches to maximum and then becomes constant. Similarly, the analysis of effect of stirring time showed increase in the drug loading with increase in the stirring time up to a point after which it remains almost constant.

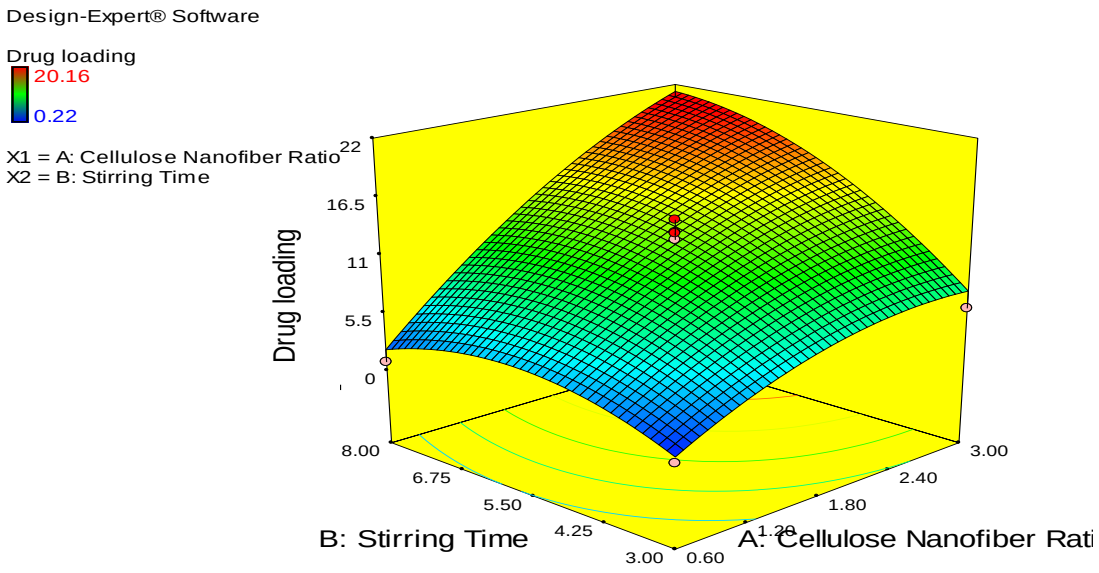

Figure 4-1 3D Response surface plot showing the influence of the polymer ratio and stirring time on drug loading.

The drug loading predicted by design expert software (Table 4-2) was 21.3001 % whereas the obtained value was 18.98 ± 1.57 % with entrapment efficiency of 77.6 ± 1.58%.

Table 4-2 Optimized points for maximum drug loading by Design Expert.

Polymer Ratio	Stirring Time	Drug Loading Predicted	Drug Loading obtained (%)	Entrapment Efficiency (%)
3	8.00	21.3001	18.98±1.57	77.6±2.66

Morphology (Scanning Electron Microscopy)

For the surface characteristics of the formed CNF aerogel, scanning electron microscopy was done. There is the difference in the surface attributes of CNF aerogel and DCNF aerogel. For the plain CNF aerogel (Figure 4-2a), it showed the porous matrix while in DCNF aerogel, pores are much filled with matrix type layered structure due to physical adsorption of drug on fibres (Figure 4-2b).

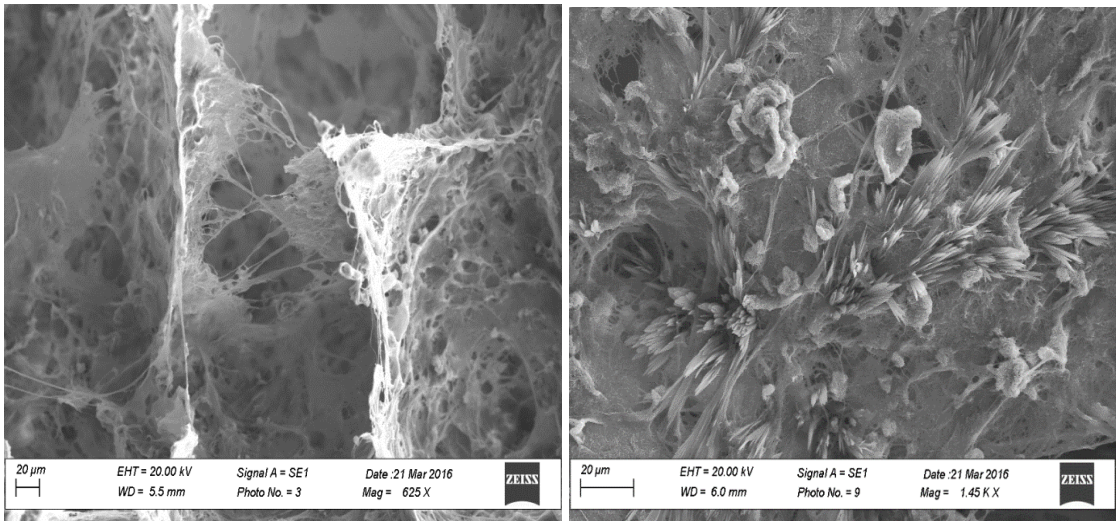

a. **b.**

Figure 4-2 SEM images (a.) CNF aerogel (b.) DCNF aerogel.

Transmission electron Microscopy (TEM)

TEM image (Figure 4-3b) shows the loading of the drug molecules onto the nanofibre by the increase in diameter. The diameter of plain CNF was found to be 7.47 ± 0.82 nm (Figure 4-3a) while in case of DCNF it was recorded to be 39.33 ± 0.56 nm (Figure 4-3b). Several nodes are seen on the nanofibre indicating the attachment of drug molecules.

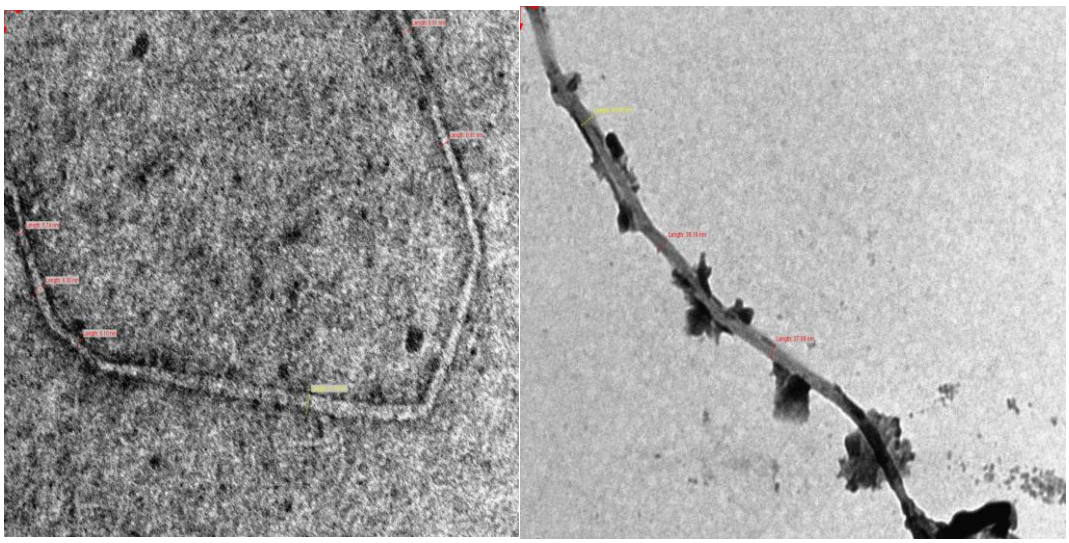

a. b.

Figure 4-3 TEM Image (a.) CNF (b.) DCNF.

Swelling Index in different pH media

Swelling Property of CNF aerogel and DCNF aerogel was studied in different pH medium (1.2 and 7.4) for different time periods (12 and 24 hours). Difference in swelling tendency was observed and results are shown in Figure 4-4. Maximum swelling was seen at 24 hours, with swelling index of 254 ± 19 % and 225 ± 15 % for the CNF aerogel and DCNF aerogel respectively at pH 7.4; and 210 ± 18% and 189 ± 12% respectively at pH 1.2.

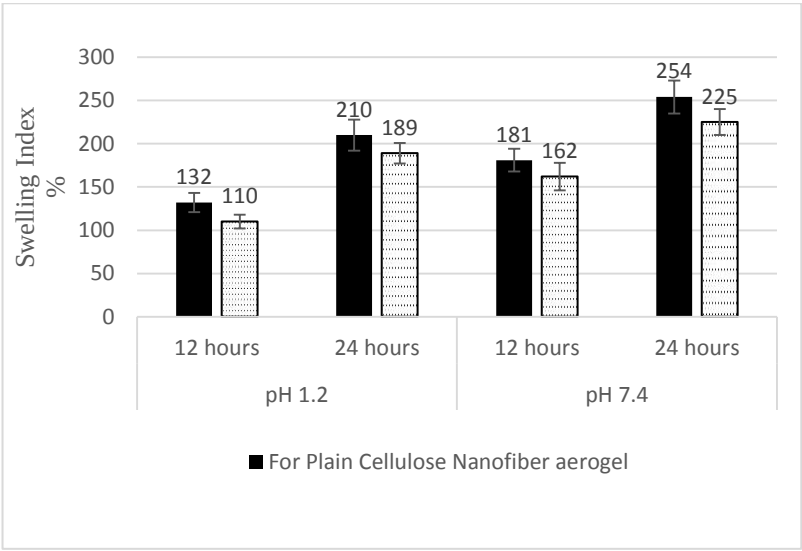

Figure 4-4 Swelling Index of CNF and DCNF aerogel at different time interval at different pH media.

High degree of swelling can be correlated to the water retained in the highly porous interconnected fibres; whereas, the difference in the swelling under different pH conditions is due to the characteristics of the cellulose. The findings are very well corroborated with findings reported by Silvestre *et al*. (19) in which authors reported that for bacterial cellulose the swelling index is less below pH 5 then rises till pH 7, and then again there is a slight decrease till pH 10**.**

Mucoadhesive Strength

Figure 4-5a and 4-5b represent the mucoadhesive strength of the CNF aerogel and the DCNF aerogel. The mucoadhesive strength of the blank nanofibre aerogel was found to be 36.9 ± 3.8 g/cm^2, and that of the drug-loaded nanofibre aerogel was found to be 18.19 ± 3.64 g/cm^2. The decrease in mucoadhesive strength in the case of DCNF aerogel can be attributed to the decrease in the availability of specific surface area of CNF available for adhesion (17).

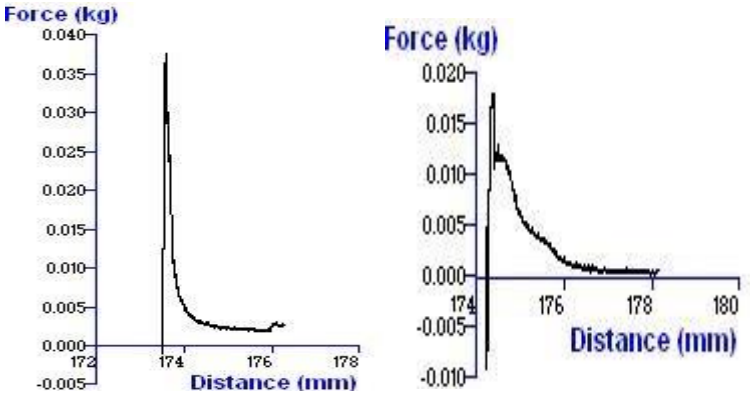

a. b.

Figure 4-5 Mucoadhesive strength (a.) CNF aerogel (b.) DCNF aerogel.

Tensile Strength

Tensile strength of the cellulose nanofibre formulation can be attributed to the fact that when water is removed from the cellulose fibres during drying, hydrogen bonds are formed between neighboring fibres creating a tight fibre network. This process is irreversible and is known as ‘‘hornification’’ which imparts it strength and makes it durable (12).

The Figure 4-6a and 4-6b shows the tensile strength of CNF aerogel and DCNF aerogel. The tensile strength of CNF aerogel was found to be 122.69 ± 17 g/cm^2, and that of the DCNF aerogel was found to be 115.3 ± 11 g/cm^2. The low value of tensile strength for DCNF aerogel may be attributed to the changes in the property of cellulose

nanofibres after drug loading, as the mechanical strength of fibres is inversely proportional to the diameter of the fibres (20). With the increase in the fibre diameter, the fibre density decreases which is related with the decrease in mechanical strength, this explains for lower tensile strength of drug loaded nanofibre formulation. These results are very well correlated with our TEM results, in which DCNF had shown significant increase in diameter.

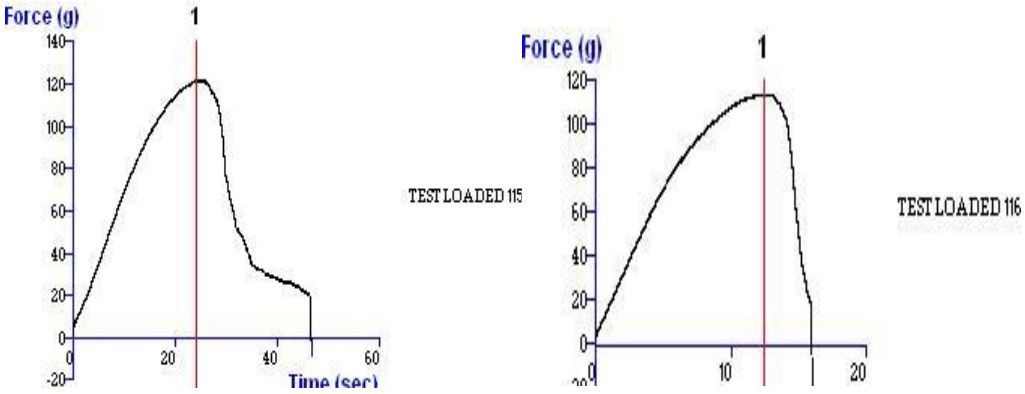

a. b.

Figure 4-6 Tensile strength (a.) CNF aerogel (b.) DCNF aerogel.

Floating Time

The obtained DCNF aerogel floated for approximately 450 ± 30 minutes in dissolution media pH 7.4 and pH 1.2. This property can be attributed to the extremely high surface area. Nanofibres with 100 nm diameter provide a specific area of 1000 sqm/gram. Increased surface area of the nanofibres contributes to the significant reduction of bulk density (17).

In-vitro Drug Release Study

The in-vitro drug release was conducted for 24 hours using dialysis bag filled with pure drug and DCNF formulation. The result is depicted in the Figure 4-7.

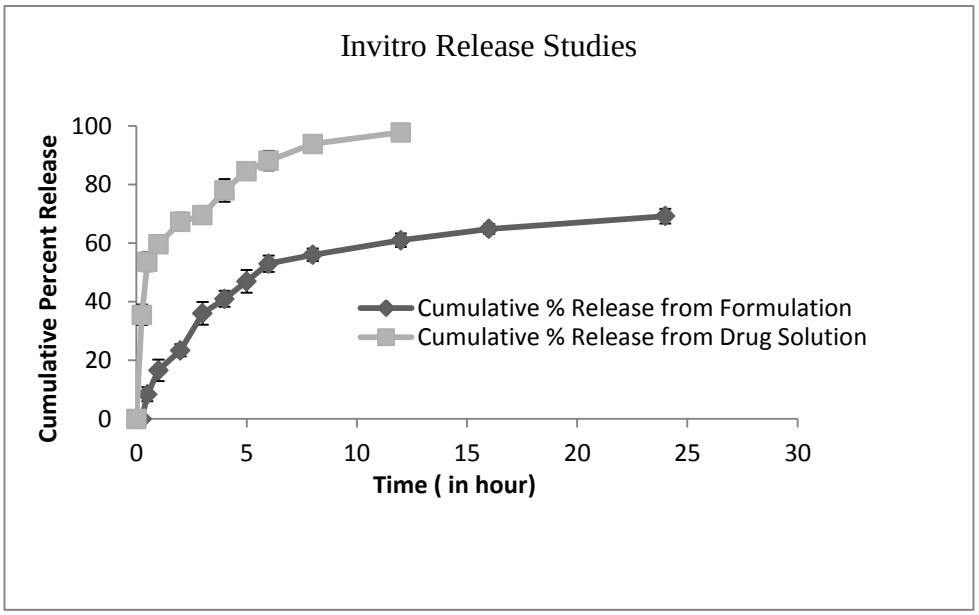

Figure 4-7 In-vitro Drug Release at pH 1.2 at different time interval.

Approximately 88.12 ± 3.33 % of the pure drug is released in the first 6 hours from the drug solution while only 53 ± 2.79 %of drug was released from the nanofibre formulation. The DCNF showed a controlled release behavior with 69.205 ± 2.5 % of the drug was released in 24 hours while almost complete drug release was seen in 12 hours from the drug solution. The dissolution behavior from cellulose film is primarily dependent on the penetration of medium into the matrix and the swelling properties of the porous matrix formed after lyophilization (12), and then the dissolution of the drug from the matrix.

Release Kinetic Study

The data obtained from the release study at pH 1.2 was fitted into various release kinetics model – Zero order, First order, Higuchi model and Peppas model (Figure 4-8).

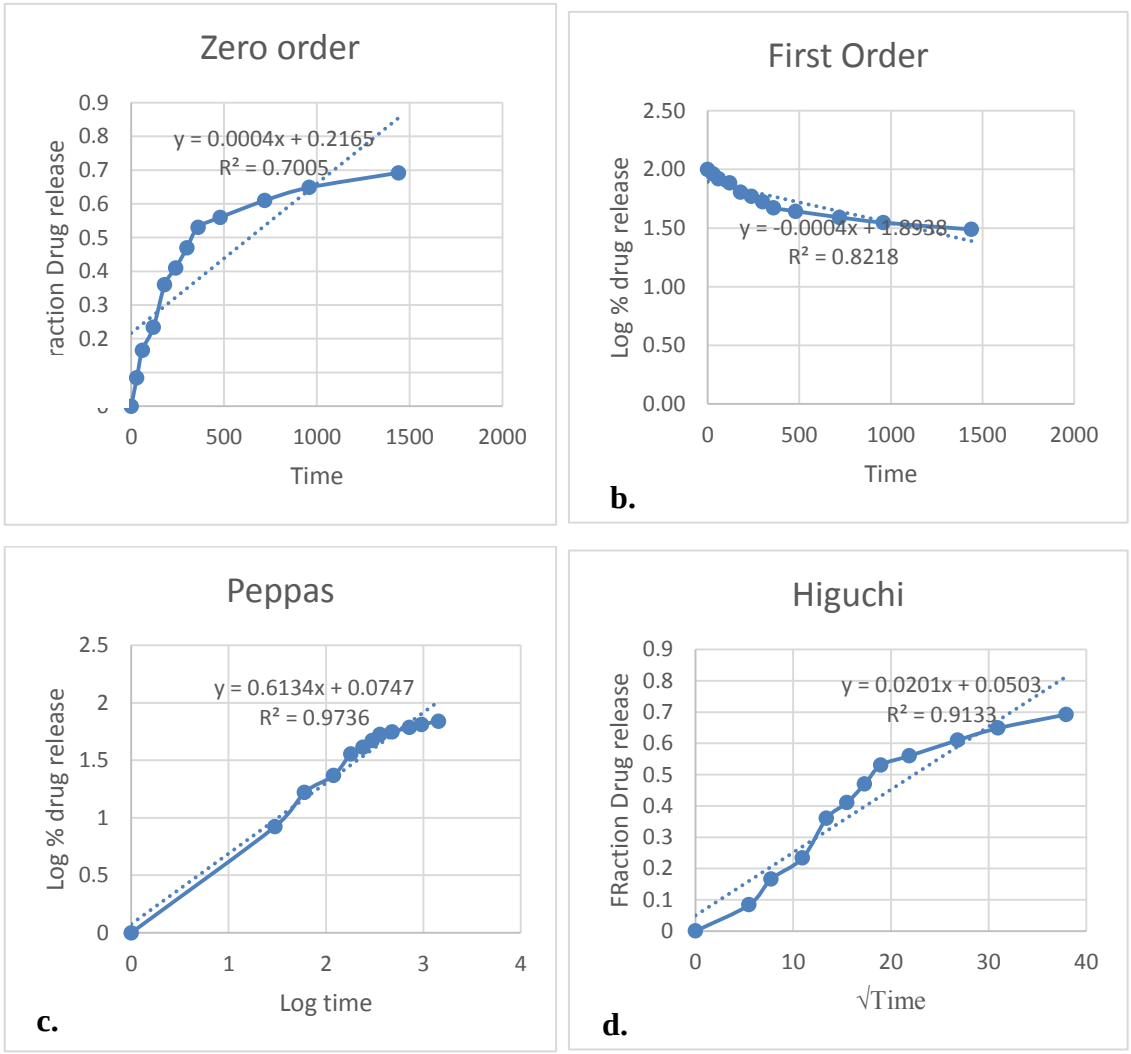

Figure 4-8 Release Kinetic Study Profile. a- Zero order, b- First order, c- Higuchi d- Korsmeyer-Peppas.

The release data best fitted into the Korsymer Pappes Model (Graph between log cumulative percentage of drug released versus log time); the exponent n was calculated through the slope of the straight line. Generally, one of the two conditions exists. In Case I, where the drug transport mechanism from spherical matrices is by Fickian diffusion when $n \leq 0.43$, if $0.435 < n < 0.85$, it is anomalous (non-Fickian) transport and in Case II, for values of $n \geq 0.85$, zero order release kinetics is indicated. Model fitting revealed that nanofibre formulation showed anomalous transport (non-Fickian) mechanism for the release of drug, where the R^2 was found to be 0.9736 and n = 0.613.

However, it does not always confirm that the CNF aerogel film follows the Korsymer Pappes Model. Literature mentions that the release from the CNFs depends on the thickness of the film/ aerogel (21) and also depends on the property of the drug, and type of the cellulose used in the formulation (12).

Comparison of Drug Release in Different pH

Cumulative percentage release was determined in pH 1.2 and pH 7.4. Release study conducted for 24 hours showed the difference in percentage release which is depicted in Figure 4-9.

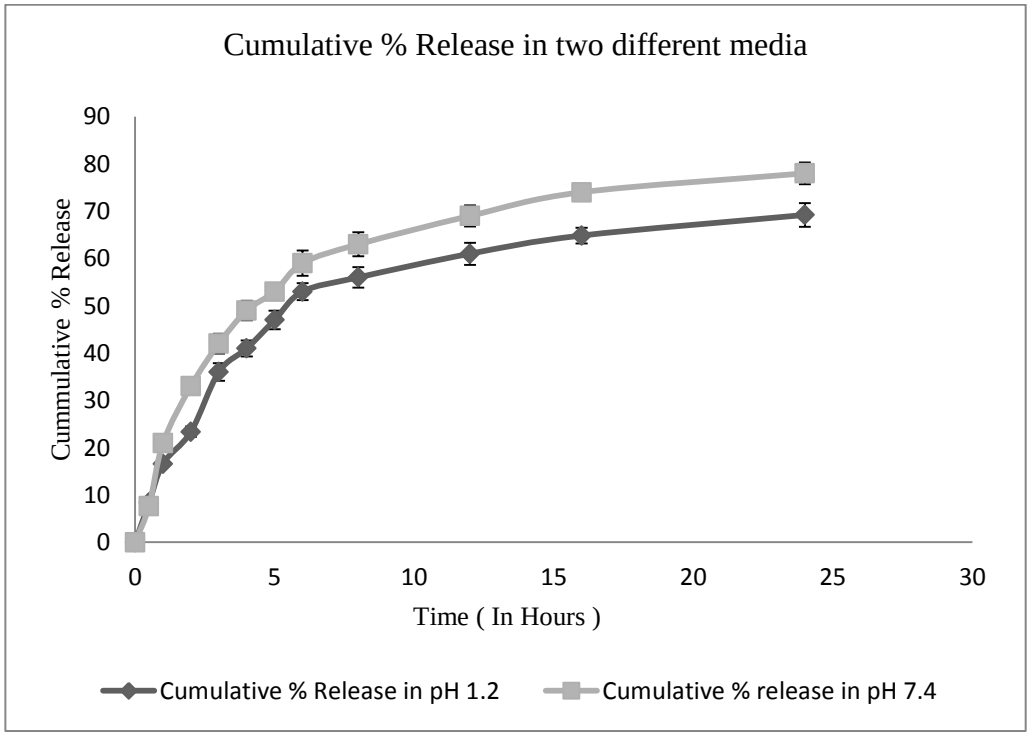

Figure 4-9 Cumulative percentage release at two different pH.

About 69% ± 2.5 % of drug was released in the pH medium 1.2 whereas about 78% ± 2.28 % of drug was released in the pH medium 7.4. Difference of release in two different pH media can be attributed to the difference in swelling behavior of CNF aerogel in two different media. The significant increase in release was observed at pH 7.4 due to the higher swelling index which ultimately leads to higher drug loading.

In-vivo Study

HPLC analysis

HPLC method reported by Xie et al. (18) was used with slight modification to determine the drug concentration in plasma. Figure 4-10 represents the HPLC peak.

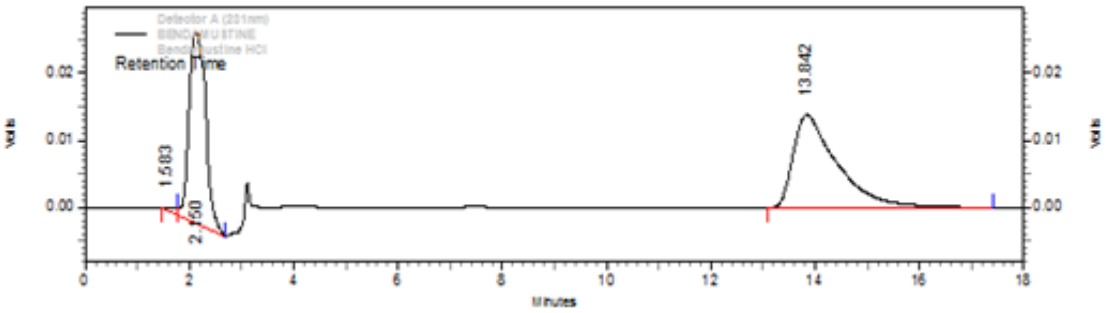

Figure 4-10 HPLC peak of Bendamustine Hydrochloride in rat plasma.

Pharmacokinetic study

The pharmacokinetic studies were performed to evaluate and compare the kinetics as well as the blood levels of drug solution and formulation. The blood samples were collected at various time points, processed and analyzed by HPLC. The retention time was recorded to be 13.842 minutes and R^2 was 0.9961. Concentration of drug at different time intervals for different groups of rats is demonstrated in Figure 4-10(b) and the pharmacokinetic parameters are given in table 4-3.

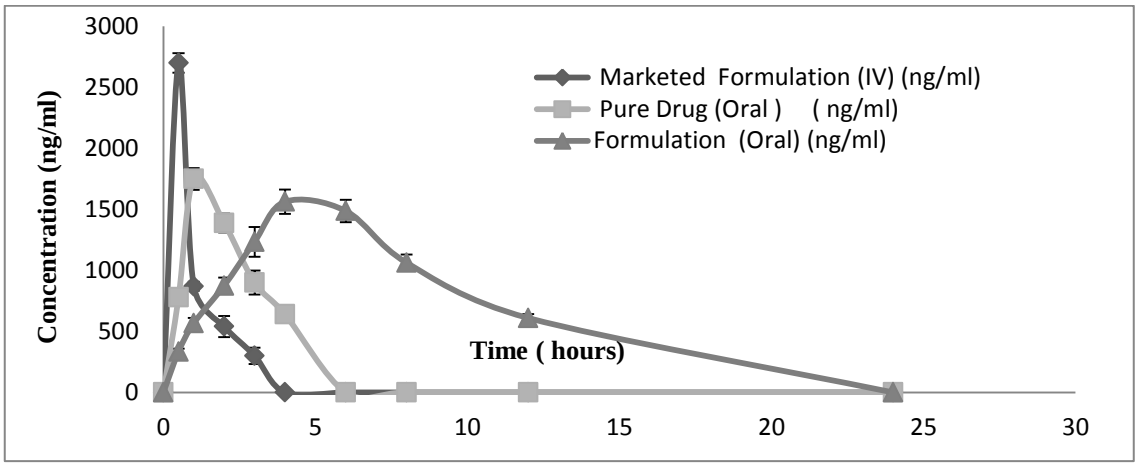

Figure 4-11 Drug concentration in blood vs time.

Table 5-3 Pharmacokinetic parameter results.

	C_{max} (ng/ml)	T_{max} (min.)	Relative BA	Absol. BA	AUC (ng.hr/ml)
Marketed Prepn. (IV)	2700 ±67	30	-		2842.5
Drug Solution (Oral)	1750±43	60	-	1.74	4951.5
Formulation Suspn. (Oral)	1563±58	240	3.25 wrt oral drug soln.	5.66	16089.75

As shown in the Table 4-3, the C_{max} was found to be 2700 ± 67 ng/ml for the marketed drug preparation administered intravenously and 1750 ± 43, 1563 ± 58 ng/ml respectively for the pure drug and drug loaded formulation when given orally. The T_{max} for the marketed drug preparation administered iv was found to be 30minutes while for pure drug solution and DCNF formulation given orally was found to be 1hour and 4 hours respectively. The AUC was found to be 2842.5 ng.hr/ml, 4951.5 ng.hr/ml and 16089.75 ng.hr/ml for marketed formulation administered iv, drug solution given orally and DCNF given orally.

The absolute bioavailability and relative bioavailability of the formulation was found to be increased by 5.66 and 3.25 times as compared to the intravenous and oral bioavailability of the pure drug solution respectively. Hence, it is evident that the formulation is able to enhance the oral bioavailability of the drug by providing controlled drug release.

Conclusion

CNFs are the unique and promising natural material with huge pharmaceutical potential in the biomedicine as drug carrier because of its unique attributes like high surface area per unit mass, extensive porosity, strength with flexibility and economical advantage. They serve as the carrier for the drug delivery like antimicrobials, enzymes, antioxidants, flavors and functional group compounds and also in the anticancer drug delivery in the form of a carrier for targeted delivery. Because of its extremely high surface area, hygroscopic nature and its swelling tendency, it allows the maximum drug loading by physical adsorption method as well as because of its swelling ability, the CNF formulation allows the drug to be released in the controlled manner. Moreover, the floating tendency and the mucoadhesive property of the CNF aerogel present it as a successful gastro retentive drug delivery system. From the results of the study, it can be concluded that the CNFs because of its characteristic features are suitable for loading of water soluble drugs by physical adsorption method. Since the aerogels possess good tensile strength because of the hydrogen bonding between the molecules, it is more suitable for transdermal drug delivery system. Not only tensile strength, its release pattern and its hygroscopic nature present suitability for drug delivery through skin. Thus, it generates a great possibility for implants and transdermal drug delivery systems. Floating tendency is due to the decrease in bulk density of the nanofibres due to entrapment of air in it. Though it floated only for 7 hours and 30 minutes,

modification in cellulose property like making it hydrophobic might help it to float for longer duration of time if it is supposed to be used for oral drug delivery.

REFERENCES

1. Deshpande AA, Rhodes CT, Shah NH, Malick AW. Controlled-Release Drug Delivery Systems for Prolonged Gastric Residence: An Overview. *Drug Development and Industrial Pharmacy*.1996; 22(6): 531-539
2. Silvia M, Kawthar B, Gilles P. Oral delivery of anticancer drugs I: General considerations. *Drug discovery today*. 2012;18(1-2): 25-34.
3. Murphy CS, Pillay V, Choonara YE, Toit LC. Gastroretentive drug delivery systems: current developments in novel system design and evaluation. *Current Drug Delivery*. 2009; 6(5):451-460
4. Abe K, Iwamoto S, Yano H. Obtaining Cellulose Nanofibres with a Uniform Width of 15 nm from Wood. *Biomacromolecules*. 2007;8 (10): 3276-3278.
5. Zhang Y, Lim CT, Ramakrishna S, Huang ZM. Recent development of polymer nanofibres for biomedical and biotechnological applications. *Journal of materials science: material in medicine*. 2005; 16 (10): 933-946.
6. Doshi J, Reneker DH. Electrospinning Process and Applications of Electrospun Fibres. *Journal of Electrostatics*.1995;35(2):151-160.
7. Valo H, Kovalainen M, Laaksonen P, Hakkinen M, Auriola S, Peltonen L. Immobilization of protein-coated drug nanoparticles in nanofibrillar cellulose matrices--enhanced stability and release. Journal of controlled release : official journal of the Controlled Release Society. 2011;156 (3):390-397.
8. Frone AN, Panaitescu DM, Donescu D. Some aspects concerning the isolation of cellulose micro-and nano -fibre. *UPB Scientific Bulletin*. 2011; 73(2):133-152.
9. Jung JY, Khan T, Park JK, Chang HN. Production of bacterial cellulose by Gluconacetobacter hansenii using a novel bioreactor equipped with a spin filter. *Korean Journal of Chemical Engineering*. 2007; 24(2):265-271.
10. CzajaWK, Young DJ, Kawecki M, Brown M. The Future Prospects of Microbial Cellulose in Biomedical Applications. *Bio Macromolecules*. 2007; 8(1):1-12

11. Kolakovic R, Peltonen L, Laukkanen A, Hirvonen J, Laaksonen T. Nanofibrillar cellulose films for controlled drug delivery. *European journal of pharmaceutics and biopharmaceutics*. 2012; 82(2):308-315.
12. Valo H, Arola S, Laaksonen P et al. Drug release from nanoparticles embedded in four different nanofibrillar cellulose aerogels. *European journal of pharmaceutical sciences: official journal of the European Federation for Pharmaceutical Sciences*. 2013; 50(1):69-77
13. Sharma H, Kumar K, Choudhary C, Mishra PK, Vaidya B. Development and characterization of metal oxide nanoparticles for the delivery of anticancer drug. *Artificial cells, Nanomedicine and Biotechnology*. 2016. 44, 672-679.
14. Meng ZX, Xu X, Zheng W, Zhou H, Li L, Zheng Y, Lou X. Preparation and characterization of electrospun PLGA/gelatin nanofibres as a potential drug delivery system. *Colloids Surf B Biointerfaces*. 2011; 84(1):97–102.
15. Thirawong N, Nunthanid J, Puttipipatkhachorn S, Sriamornsak P. Mucoadhesive properties of various pectins on gastrointestinal mucosa: an in vitro evaluation using texture analyzer. *European journal of pharmaceutics and biopharmaceuitics*. 2007; 67(1):132-40
16. Singh H, Sharma R, Joshi M, Garg T, Goyal AK, Rath G. Transmucosal delivery of Docetaxel by mucoadhesive polymeric nanofibres. A*rtificial cells, nanomedicine and biotechnology*. 2015; 43(4):263-269
17. Malik R, Garg T, Goyal AK, Rath G. Diacerein-Loaded novel gastroretentive nanofibre system using PLLA: Development and in vitro characterization. *Artificial Cells, Nanomedicine, and Biotechnology*. 2016; 44(3): 928-936
18. Xie F, Cheng Z, Cheng H, Yu P. Simultaneous determination of bendamustine and its active metabolite, gamma-hydroxy-bendamustine in human plasma and urine using HPLC-fluorescence detector: Application to a pharmacokinetic study in Chinese cancer patients. *Journal of chromatography B*. 2014; 960:98-104
19. Silvestre AJ, Freire CS, Neto CP. Do bacterial cellulose membranes have potential in drug-delivery systems? *Expert opinion on drug delivery*.2014;11(7):1113-1124.
20. Chew SY, Hufnagel TC, Lim CT, Leong KW. Mechanical properties of single electrospun drug-encapsulated nanofibres. *Nanotechnolgy*. 2006;17(5):3880-3891.
21. Haimer E, Wendland M, Schlufter K, Frankenfeld K, Miethe P, Potthast A, RosenauT, Liebner F. Loading of Bacterial Cellulose Aerogels with Bioactive

Compounds by Antisolvent Precipitation with Supercritical Carbon Dioxide. *Macromolecular symposia*. 2010; 294(2): 64-74

22. Colledge, J., 2014. Oral Dosage Forms of Bendamustine. US20140018334 A1.

6. PAPER IV

BIONANOCOMPOSITES: SMART BIODEGRADABLE PACKAGING MATERIAL FOR FOOD PRESERVATION

Sushama Talegaonkar, Harshita Sharma, Pawan Kumar Mishra, Rupert Wimmer

(Accepted Book Chapter- Food Packaging (Elsevier))

ABSTRACT

In this era of increasing demands and consequently improving technology, food packaging is not only aimed to prevent food products from external dust and dirt particles, but also to perform several other functions, such as moisture control, oxygen scavenging, and a number of other actions including antimicrobial activity as well. But, with improving technology, which claims to fulfill most of the consumers' requirements, health, and environmental risks have been a major concern. Biodegradable polymers offer an environmental friendly alternative to this hazardous packaging material. To impart active or smart properties to polymeric packaging films, polymers can be reinforced with nanomaterials. These so formed nanocomposites may exhibit one or more of the above-mentioned properties of an active or smart packaging. This chapter deals with methods of preparation of polymeric nanocomposites, types and properties of nanoreinforcements, and details of few important biodegradable polymers that are commonly used for preparing nanocomposites for food packaging purposes. This chapter also gives an account of commercial active food packaging materials that are currently used in the market.

Keywords: Food packaging, Bionanocomposites, Active packaging, Smart packaging, Cellulose nanocomposites, Starch nanocomposites, Chitosan nanocomposites

INTRODUCTION

Food packaging is generally aimed to prevent the degradation of food by physical or chemical contaminants, microbial contamination, and loss of aroma while retaining the quality of the product during its extended shelf life. To address aforementioned

issues a packaging must act as a gaseous barrier to hinder the exchange of moisture, carbon dioxide, oxygen and aromatics along with acceptable optical, physical and mechanical properties. Classical answer to above-mentioned questions was found in petroleum-based polymers. However, petroleum-based polymers used for food packaging are not biodegradable, non-renewable and non-compostable, therefore presenting a significantly serious environmental and disposal problem and waste generation issues worldwide. According to reports, packaging waste accounted for 71.6 million tons or 29.5% of the total municipal solid waste (MSW) in 2009 in the USA (http://www.epa.gov/osw/nonhaz/ municipal/pubs/msw2009-fs.pdf) and 56.3 million tons or 25% of the Municipal Solid Waste (MSW) in 2006 in Europe [Valdes et al., 2014].

Growing concern over environmental issues and a limited number of disposal methods drive the search for biodegradable polymers (biopolymers) based alternatives to petroleum-based polymers. Biopolymers can be classified based on their origin as natural, synthetic and microbial, as shown in Figure 5-1 [Rhim et al., 2013].

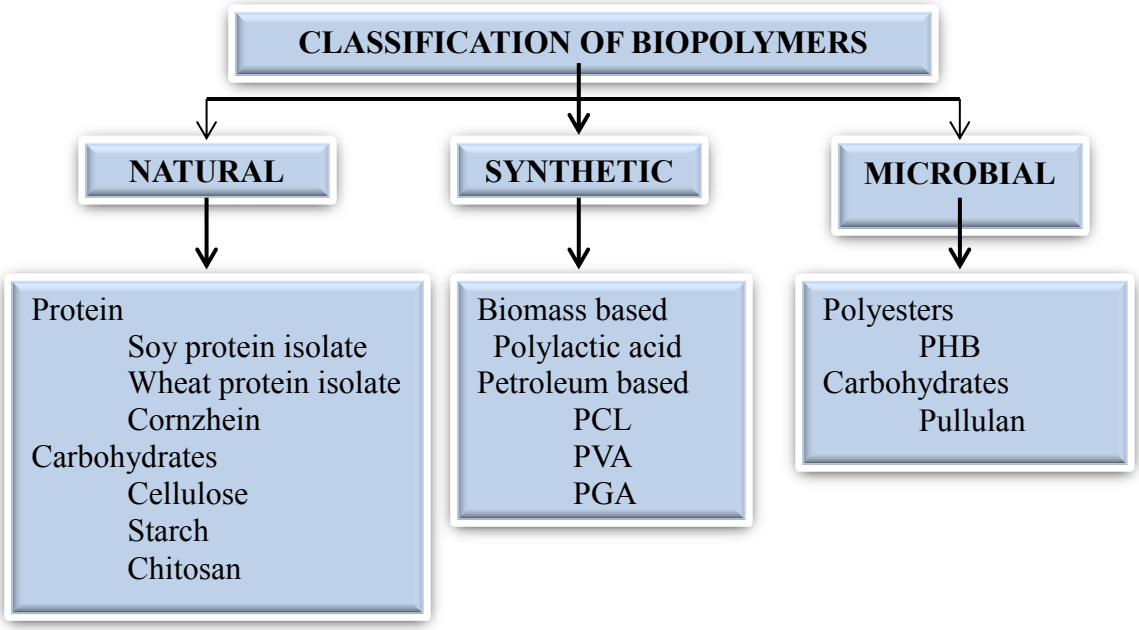

PCL- Polycaprolactone; PVA- Polyvinyl alcohol; PGA- Polyglycolic acid

Figure 5-1 Classification of biopolymers.

Examples of biodegradable polymers include proteins such as soy protein isolate, wheat protein isolate, corn zein, wheat gluten and gelatin etc., whereas carbohydrates include starch cellulose, chitosan, agar etc. Polylactic acid, polycaprolactone, and

polyvinyl alcohol are few examples of synthetic biopolymers. Microbial polyester biopolymers include PHB and carbohydrates include pullulan and curdlan [Rhim et al., 2013].

But polymers, if used alone, have poor tensile, mechanical and barrier properties, which are responsible for them to fail as strong and successful packaging material. Polymers also fail to walk hand in hand with today's increasing demands and expectations of consumers. Thus, to improve their mechanical and barrier properties and to impart them with novel characteristics, polymers are reinforced with nanofillers which interact at various levels. Many terms have been used for advanced multifunctional packaging like the smart, active and intelligent packaging. The idea behind using these terminologies is to explain selective responsiveness of individual packaging when placed in different environments. This responsiveness enables the intelligent packaging to sense changes in certain properties of food product and report it to customer [Robertson, 2006].

Active packaging materials comprising of bionanocomposites play multiple roles, including that of protecting the food item from the external environment, as well as increasing their shelf life by maintaining the quality for a longer period of time. These smart packaging materials prevent oxidation of the food product, thus delaying its deterioration. They may also act as moisture barriers, antimicrobial agents, freshness indicator, etc. (Figure 5-2). There are several reports of active and intelligent packaging

systems that will be dealt in details with individual types of nanocomposites.

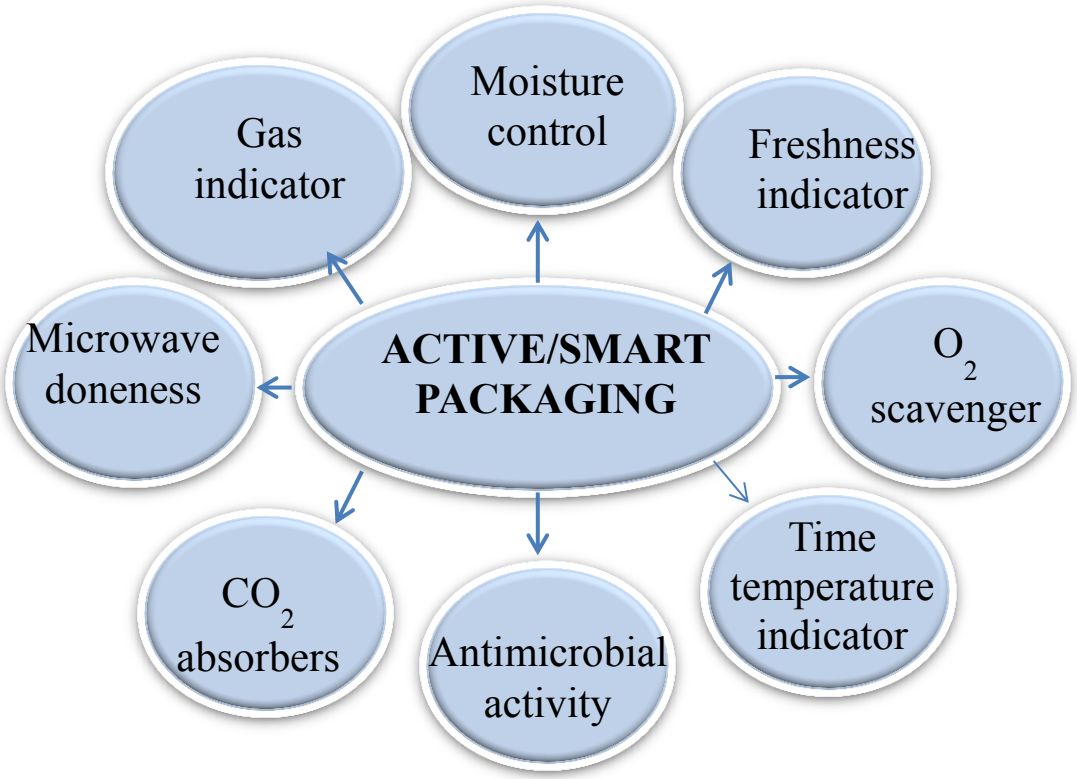

Figure 5-2 Ideal properties of smart packaging.

NANO REINFORCEMENTS

1. Nano clays

Nano clay, also known as layered silicates, is one of the most widely used and studied nano agents that are used to prepare nanocomposites for food packaging. Advantages of nanoclays include their wide availability, easy processability, good performance and lower cost [Ray et al., 2006]. The nanoclays which are used as nanofillers in nanocomposites are usually bidimensional platelets having a length of several micrometres and very minute thickness of around 1 nm [McHugh et al., 2011].

Nanoclays are usually used to prepare nanocomposites of polymeric materials, such as starch. The interaction between nano clays and polymers can produce two types of nanocomposites, first is intercalated nanocomposites, which is formed due to penetration of chains of the polymer into the regions between the layers of the clay, forming an ordered multilayer structure with alternating layers of polymer and clay. The second type of nanocomposite that can be formed is exfoliated nanocomposites, which results from extensive polymer penetration. In this type, clay layers get delaminated and

randomly dispersed in the polymer matrix. Reportedly, exfoliated nanocomposites are known to exhibit the best properties because of the optimal interactions between polymer and clay [McHugh et al., 2011]. Montmorillonite (MMT) is the clay which has been most widely used as Nano filler for preparing nanocomposites for food packaging. Its chemical general formula is Mx(Al4-xMgx) $Si_8O_20(OH)_4$. MMT exhibits excellent reinforcing filler abilities because of its high surface area and large aspect ratio, which ranges between 50 and 1000 [Uyama et al., 2003].

Nielsen [1967] explained the reason behind the success of clay as nanofiller for food packaging materials. According to him, clay, when used as filler, improves barrier properties of nanocomposites, probably by increasing tortuosity of the diffusive path for permeants (such as moisture, oxygen, microbes etc.), presenting a longer path for them to travel to be able to diffuse through the film. This theory is further supported by other authors also [Adame & Beall, 2009; Mirzadeh & Kokabi, 2007]. The mineral clays have also been explored as biocide carriers for inorganic biocides such as silver, zinc, copper, magnesium, etc. [Patakfalvi and Dekany, 2004; Patil et al., 2005]. Nanoclays have also been functionalized to impart antimicrobial properties [Thostenson et al., 2005]. Chandrasekaran et al. [2011] produced aminopropyl functionalized magnesium phillosilicates (AMP clay) by sol–gel synthesis method. This nanocomposite was found to strongly inhibit the growth of microorganisms such as E. coli, S. aureus and Candida albicans [Rhim et al., 2013].

2. Nanocellulose

Nanocellulose is also a suitable candidate to be used as a reinforcement material. It is useful in producing nanocomposites having high strength and low weight. Cellulose is also a low-cost material. Moreover, it is biodegradable, environmental friendly and easy to recycle by combustion [McHugh et al., 2011; Helbert et al. 1996]. Two types of reinforcements can be derived from cellulose, namely microfibrils and whiskers [Azizi Samir et al., 2005]. Microfibrils are the nanofibres which are synthesized from cellulose in plants or animals. Microfibrils are actually the bundles of molecules, elongated and stabilized by hydrogen bonding. The diameters of microfibrils are in nanosize range, around 2–20 nm, and lengths are in the range of micrometer. Each microfibril is made up of two parts: crystalline and amorphous. The crystalline parts of the microfibrils are the whiskers, which are also known as nanocrystals, nanorods, or rodlike cellulose microcrystals. The length of the whiskers ranges from 500 nm to 1–2 μm, and diameter

of 8 nm to 20 nm or less, resulting in high aspect ratios. The whiskers can be isolated from microfibrils by several methods. The most commonly used method is acid hydrolysis. Acid hydrolysis method to separate crystalline part (i.e. whiskers) from microfibrils basically consists of removing the amorphous parts of the fibrils by dissolving them in acid (usually sulphuric acid), leaving the crystalline regions intact [Azeredo, 2009].

Azeredo and group studied the effect of cellulose nanofibres on the physical properties of mango puree edible films and found that cellulose nanofibres when used as filler, effectively increased the tensile strength and young's modulus of the mango puree films [Azeredo et al., 2009]. Helbert et al. [1996] explained this effect of cellulose nanofibres on the modulus. According to them, increase in modulus is not only a result of the geometry and stiffness of the nanofibres but also of the formation of a fibrillar network within the matrix of the polymer. Cellulose nanofibres seem to link through hydrogen bonds.

3. Silicon dioxide (SiO2)

Nanoparticles of silicon dioxide, also known as silica, have been used as nano reinforcements to prepare nanocomposites for food packaging to improve mechanically and/or barrier properties of polymer films [Azeredo, 2009]. In few studies, researchers observed that the presence of grafting polymers on the surface of silicon dioxide improved the tailorability of the composites, which means that presence of different species of grafting monomers effects the tensile properties and interfacial interactions [Zhang & Rong, 2003; Wu et al., 2002]. In the study conducted by Wu et al. [2002], it was observed that silicon dioxide nanoparticles improved tensile properties of the material including strength and modulus as well as elongation when added to polypropylene matrix. Xiong et al. [2008] also obtained similar results where tensile properties including elongation were improved for a starch matrix after addition of silicon dioxide nanoparticles. Water absorption by starch matrix was also found to be decreased. Vladimiriov et al. [2006] incorporated silicon dioxide in an isotactic polypropylene (iPP) matrix using maleic anhydride grafted polypropylene (PP-g-MA) as a compatibilizer. Silicon dioxide was found to increase storage modulus of the iPP matrix, thus making the material stiffer, and also improved the oxygen barrier of the matrix. Jia et al. [2007] prepared nanocomposites of polyvinyl alcohol and silicon dioxide by radical copolymerization of vinyl silicon dioxide nanoparticles and vinyl

acetate. The nanocomposites possessed improved thermal and mechanical properties as compared to the pure polyvinyl alcohol. This was a result of strong interactions between silicon dioxide and the polymer matrix via covalent bonding. Later, Tang et al. [2008] prepared biodegradable films composed of starch, polyvinyl alcohol, and silicon dioxide. As the concentration of silicon dioxide was increased, the tensile properties and water resistance of the films were improved. An increase in the intermolecular hydrogen bonds, as well as formation of C–O–Si groups, between silicon dioxide and starch, or silicon dioxide and polyvinyl alcohol was also observed, which improved the compatibility and miscibility between the components of the film.

4. Carbon nanotubes

Carbon nanotubes are nanoscale tubes which may consist of a one atom thick single wall nanotube, or several concentric tubes known as multi-walled nanotubes [Azeredo, 2009]. Carbon nanotubes possess extraordinarily high aspect ratios and elastic modulus [Zhou et al., 2004]. According to Lau and Hui [2002], carbon nanotubes reportedly have theoretical elastic modulus and tensile strength values as high as 1 TPa and 200 GPa, respectively. In an experiment conducted by Kim and co-workers [2008], carbon nanotubes were modified by introducing carboxylic acid groups on their surfaces with the purpose to enhance intermolecular interactions between the poly(ethylene-2,6-naphtalene) matrix and carbon nanotubes. Carbon nanotubes were found to greatly improve the thermal stability as well as tensile strength and modulus of poly(ethylene-2,6-naphtalene), even at a concentration as low as 0.1 wt.%. Several other experiments have also been conducted to study the effect of carbon nanotubes on polymer films. Polyvinyl alcohol is one such polymer which has been found to have its tensile strength/modulus improved by the addition of carbon nanotubes [Bin et al., 2006; Chen et al., 2005]. Other polymers which have been reinforced with carbon nanotubes to improve their tensile properties include polypropylene [Lopez Manchado et al., 2005] and polyamide [Zeng et al., 2006].

5. Other agents

5.1. Antimicrobial agents

Antimicrobial packaging is a type of active packaging which prevents or retards the growth of microbes in the food products. This is achieved by reinforcing the packaging films with antimicrobial agents. Antimicrobial food packaging materials are expected to extend the lag phase and reduce the growth rate of microorganisms, thus

increasing the shelf life of the food products, while maintaining their quality and safety. Antimicrobial agents are mainly of two types, organic and inorganic. Organic antimicrobial agents are usually less stable, particularly at high temperature and pressure conditions, as compared to inorganic antimicrobial agents. Thus, organic ones are not very suitable and present a major obstacle for the formulation of active or smart packaging films. Consequently, inorganic antimicrobial agents such as metals and metal oxides have gained attention over the recent times. This is because of their ability to withstand harsh process conditions such as high temperatures and pressures [Emamifar, 2011; Zhang et al., 2007].

Direct addition of antimicrobial agents might result in loss of activity due to leaching into the food products and undesirable reactions with food components such as lipids or proteins. Therefore, the packaging films reinforced with antimicrobial agents can prove to be more efficient. This will help in achieving a controlled and sustained migration of the antimicrobial compound into the food, thus allowing for inhibition of microbes, as well as residual activity over time during the transport, storage and shelf-life of the food product [Emamifar, 2011; Mauriello et al., 2005].

5.1.1. Silver Nanoparticles

Silver has been known for its antimicrobial properties since ages and is used for the treatment of burns, wounds and several bacterial infections since ever. It has been used in the form of metallic silver, silver nitrate, silver sulfadiazine, etc. Nanosizing of any metal changes its physical and chemical properties drastically, more often amplifying its therapeutic effects. Silver nanoparticles thus have great potential as an antimicrobial agent. Silver usually shows action against those bacteria also which otherwise have developed resistance against antibiotics [Emamifar, 2011; Rai et al., 2009]. The probable mechanisms of antimicrobial activity of silver nanoparticles include generation of reactive oxygen species (ROS) that induces oxidative stress and causes the degradation of the membrane structure of the cell; and release of ions from the surface of the nanoparticles that may cause death of the microbes due to their binding to cell membrane [Sharma et al. 2015; Emamifar et al., 2011]. Silver ions that are released from the surface of nanoparticles are also reported to interact with thiol groups present in cell proteins inducing bacterial inactivation, condensation of DNA molecules, and loss of their replication ability [Sharma et al. 2015; Emamifar et al., 2010].

5.1.2. Zinc oxide nanoparticles

Few of the ceramic substances, such as zinc oxide (ZnO), calcium oxide (CaO) and magnesium oxide (MgO) are found to show antimicrobial properties and thus can be used to prepare smart packaging systems (Yamamoto, 2001). These ceramic compounds contain minerals which are essentially required by human bodies and they exhibit high potency [Sawai & Yoshikawa, 2004]. Zinc oxide nanoparticles are widely used in a number of applications such as paints, cosmetics, drug delivery system and fillings in medical materials. Zinc oxide is known to exhibit antibacterial activity that increases as the particle size decreases. Antibacterial action of zinc oxide can be stimulated by visible light. Zinc oxide nanoparticles have also been incorporated in various polymers, where they effectively absorb UV light without re-emitting it as heat and therefore improves the stability of polymer composites [Martirosyan and Schneider, 2014]. Also, zinc oxide is recommended as a generally recognized as safe (GRAS) material by FDA. Mechanisms of antimicrobial effect of zinc oxide nanoparticles are similar to that of silver nanoparticles, that is, induction of oxidative stress due to generation of reactive oxygen species which may interact with proteins, DNA, and other components of bacterial cells leading to death; and binding of zinc oxide to the membrane of the microbial cells. Other mechanisms may include disorganization of the cellular membrane due to the accumulation of zinc oxide nanoparticles [Sharma et al., 2015; Emamifar, 2011]. Jin et al., [2009] studied several approaches including film, powder, PVP-capped and coating, for the application of zinc oxide nanoparticles in food systems. They observed that zinc oxide nanoparticles exhibited antimicrobial effects against *L.monocytogenes* and *S.enteritidis* in liquid egg white and in culture media.

5.1.3. Titanium dioxide (TiO2) nanoparticles

Titanium dioxide, also called titania is another non-toxic ceramic compound which can be used as an antimicrobial agent in food packaging materials. Titanium dioxide is approved by the FDA for use in human food, drugs, cosmetics and food contact materials. Cidal effects of titanium dioxide have been reported against *E. coli*, *Salmonella choleraesuis*, *Vibrio parahaemolyticus, Listeria monocytogenes, Pseudomonas aeruginosa, Stayphylococcus aureus*, *Diaporthe actinidiae* and *Penicillium expansum*. The development of TiO2-coated or incorporated food packaging and food preparing equipment has also received attention [Emamifar, 2011].

Chawengkijwanich and Hayata [2008] developed a titania powder coated packaging film and tested its ability to inactivate Escherichia coli both in vitro and in actual tests, using two different particle sizes and two types of illumination at different intensities. The results showed that both ultraviolet A alone and titanium dioxide coated OPP film combined with UVA reduced the number of E. coli cell in vitro, but that the reduction of E. coli cell numbers was greater by titanium dioxide coated OPP film combined with UVA. The antimicrobial effect of titanium dioxide coated film was dependent on the UVA light intensity (0, <0.05 and 1 mW/cm2) and the kind of artificial light (black-light and daylight fluorescent bulbs), but it was independent of the particle size of titanium dioxide coating on the surface of OPP film. And the results of actual tests showed that the titanium dioxide coated film could reduce the microbial contamination on the surface of solid food products and thus reduce the risks of microbial growth.

5.2. Moisture control agents

A certain amount of moisture is essential for most of the food items, but too much of moisture can prove to be detrimental. Also, the complete absence of moisture is vital for dry food products. Too much of moisture can result into caking of powdered products, softening of crispy products such as crackers, and moistening of hygroscopic products such as sweets and candy. Also, excessive moisture loss can lead to desiccation of the food product. Thus, moisture control agents help in overcoming problems caused by the presence of excessive moisture, as well as excessive loss of the moisture from food products. These agents control and regulate moisture activity thereby preventing microbial growth, controlling rate of oxidation and preventing caking and softening of food products [McHugh et al., 2008]. Polyurethane films have been found to show moisture-responsive properties in a number of studies [Huang et al., 2005; Yang et al., 2004]. Sidorenko et al. [2007] used polyglycidyl methacrylate based water responsive hydrogels for constructing a responsive actuator. In another study, the composite films made up of polypyrrole and polyol-borate was found to show fast moisture-responsive properties [Ma et al., 2013]. In a recent study, Zhang et al. [2015] used sustainable cellulose as the starting material to fabricate self-standing moisture responsive films. The cellulose was modified by stearoyl moieties to produce cellulose stearoyl esters (CSEs) which possessed diverse degrees of substitution. The CSE films which had a low degree of substitution of 0.3 (CSE 0.3) showed moisture responsive properties,

while films of CSEs which had higher degrees of substitution of 1.3 or 3 (CSE 1.3 and CSE 3) did not show any moisture responsive property. Also, CSE 0.3 films could be reversibly folded and unfolded in rhythmical bending motions as a result of the absorption and desorption of water molecules over the surface of the film. Moisture responsive films having non-wetting surface were produced by coating the nanoparticles of CSE 3 onto the films of CSE 0.3. These films also possessed the characteristic of performing quick reversible bending movements and shape transition. Moreover, the bilayer films which consisted of a layer of CSE 0.3 at one side and a layer of CSE 3 at the other were found to exhibit the dual character of moisture as well as temperature responsiveness.

5.3. Oxygen Scavengers

The presence of oxygen in any food package can prove to be harmful as oxygen triggers the oxidative reactions and facilitates the growth of certain microbes, all resulting in spoilage or deterioration in the quality of food, foul odors, unacceptable color change, change in flavor, reduction in nutritional values etc. These problems which are caused by the presence of oxygen can be avoided by use of oxygen scavengers. Oxygen scavengers are the agents that reduce the concentration of oxygen by reacting with it, thereby inhibiting various oxidative reactions that could deteriorate the quality of food. Most commonly and widely used oxygen scavenger is a ferrous oxide. Other oxygen scavengers are catechols, ascorbic acid, sulphites, photosensitive dyes, nylons, unsaturated hydrocarbons, enzymes such as glucose oxidase, etc. [McHugh et al., 2008].

SYNTHESIS OF NANOCOMPOSITES

There are various approaches which can be used to synthesize nanocomposites of biopolymers. The preparation method poses a significant effect on the properties of the nanocomposites.

Following are the three major pathways through which nanocomposites may be formed:

1. In situ polymerization: In situ polymerization, also known as an interlamellar method, involves the combination and swelling of fillers by absorption of a liquid monomer, which results in penetration of monomer units in between the layers of filler (e.g. silicates). After penetration of monomer, polymerization is initiated by heat,

radiation, or incorporation of an initiator, which ideally locks the exfoliated filler particles in the resulting polymer matrix.

2. Solvent intercalation/exfoliation method: The solvent intercalation method is used to form both intercalated and exfoliated nanocomposites. In this method, the filler particles are first swollen in a solvent and the polymer (intercalant) is also dissolved in the solvent separately. Next, the filler solution is added to the polymer solution. The polymer chains then intercalate and displace the solvent within the interlayer of the fillers. The solvent is then allowed to evaporate.

3. Melt intercalation/ exfoliation method: In melt intercalation method of nanocomposites formation, the filler and polymer are mixed together at a temperature above the melting point of the polymer. Then they may be kept at that particular temperature for a period of time, put under shear, or other necessary conditions to cause the intercalation and the exfoliation of the filler.

Out of these three commonly used methods for preparation of nanocomposites, the most suitable and appealing method is the melt intercalation/exfoliation method, owing to its versatility, its compatibility with current polymer processing equipment such as extrusion and injection moulding, and its environmentally benign character due to the absence of solvents. Also, the melt intercalation method allows for the use of polymers which are otherwise not suitable for in situ polymerization or solution intercalation method [McHugh et al., 2008; Rhim et al., 2007].

CELLULOSE NANOCOMPOSITES

Cellulose, the main component of plant cell wall is one of the most abundant biopolymers on earth. Cellulose inherently is a hydrophilic polymer of glucose and has been traditionally used in paper industry. Nanocellulose adds a new dimension to the application of cellulose. Nanocellulose can be MFC/NFC/CNF (microfibrillated cellulose/ nanofibrillated cellulose/ cellulose nanofibres), CNC/CNW (cellulose nanocrystals/ cellulose nano-whiskers) and BC (bacterial cellulose). Cellulose nanofibres are prepared mechanically by high-pressure homogenization or milling. They have both amorphous and crystalline regions. Cellulose nanofibres are mainly produced by acid hydrolysis, during which, amorphous regions are dissolved and only crystalline cellulose is left. Bacterial cellulose is a biotechnological product and cellulose fibres are

of bacterial origin (synthesized by bacteria). Due to the nature of their origin, they are of a highest purity and have been widely studied for their biomedical applications.

Nanocellulose has been produced from wide range of lignocellulosic sources that include wood, the lignocellulosic biomass of different origins and even some byproducts of food processing industry. One of the most specific characteristics of cellulose is that each of its glucose unit bears three hydroxyl groups which endows Nanocellulose a reactive surface covered with numerous active hydroxyl groups. The ability of these hydroxyl groups to form hydrogen bonds plays a major role in the formation of fibrillar and semicrystalline packing, which governs the important physical properties of this highly cohesive material. Nanocellulose based composites in comparison to traditional composites show improved and tunable barrier properties while keeping biodegradable nature intact. First, because of the smaller size of nanofibres, surface area to volume ratio is relatively higher than microparticles; and secondly, the nanosize of the fibres improve the barrier properties of the film by forming a dense network in combination with sufficiently strong particle- polymer bonds. The other ways to improve moisture resistance of inherently hydrophilic cellulose can be pretreatment before homogenization, post treatment and chemical grafting [Dufresne, 2013]. Gas permeability can be improved by forming nanocomposites with other fillers (e.g. clay) or chemical modification of cellulose especially for utilization in moist conditions which has been a major limitation of cellulose.

The effect of applying edible coatings to mature-green tomatoes on the survival of *Salmonella montevideo* on the surface and in core tissue was investigated by Zhuang et al. [1996]. A coating of HPMC significantly reduced the number of viable *S. montevideo* cells on the surface of tomatoes. However, only a 2-log-unit reduction was achieved in the core tissue. The addition of citric acid, acetic acid, or sorbic acid at a concentration of 0.2 to 0.4% to HPMC did not significantly improve the bactericidal activity. Concentrations of 72 to 88% ethanol in HPMC were found to be most effective in inactivating *S. montevideo* on the surface of tomatoes. Similar inactivation of *S. montevideo* in the core tissue was achieved by dipping tomatoes in 55 to 88% ethanol solutions. Also, use of HPMC coating retarded the rate of loss of firmness and change in color of tomatoes stored at 20°C for up to 18 days. This study demonstrated the

antimicrobial properties of cellulose and opened up new avenues for further investigation of cellulose in the field of food packaging.

Bruce et al. [2005] used primary cellular material at laboratory scale to develop a method of producing purified cellulose cell wall fragments and cellulose microfibrils. They prepared novel composite materials with a range of matrix binders and determined their tensile properties. Swede root was processed and used to produce fragments of the cell wall. The separation of microfibrils from the cell wall fragments was accomplished using a high-pressure food homogenizer. Four types of composite matrices were prepared from wet state cellulose. Out of the composites that were prepared from fragments of purified cell wall, best strength was found to be possessed by an acrylic matrix (125 MPa) while the composite of purified cell wall fragments and polyvinyl alcohol showed the best stiffness (15.32 GPa). For the composites prepared from fibrilised material of cell wall, polyvinyl alcohol gave the best results in terms of tensile strength (145 MPa) and tensile modulus (8.9 GPa). The composites made up of plant-derived hemicellulose matrix showed a tensile strength value of 100 MPa and tensile modulus value of 6.0 GPa. As all the values obtained were in the acceptable range, the researchers successfully demonstrated the applicability of cellulose in the preparation of composites.

Iwamoto et al. [2005] carried out the fibrillation of pulp fibre by two methods, a high-pressure homogenizer treatment and a grinder treatment. The grinder treatment was found to be a successful method for carrying out fibrillation of wood pulp fibres into nanofibres. The nanofibres demonstrated promising characteristics as reinforcement material for optically transparent composites. Because of the very small size, the nanofibre-reinforced composite retained the transparency of the matrix resin even at high fibre concentration of 70 at %. Since the cellulose nanofibres are an aggregate of semi-crystalline extended cellulose chains, their addition also results into significant improvement in the thermal expansion properties of plastics as well as maintaining the ease of bending.

Ifuku et al. [2007] acetylated the bacterial cellulose nanofibres to enhance the properties of optically transparent composites of acrylic resin reinforced with the bacterial cellulose nanofibres. Due to acetylation, the surface properties of the nanofibres were changed and the moisture content of the composite decreased by approximately 66%

that of unacetylated composite. Also, the acetylation reduced the thermal expansion coefficient of a bacterial cellulose sheet to one third of the initial value.

In an interesting study, all cellulose composite, in which both the fibres and the matrix were cellulose, was prepared by changing the solubility of the matrix cellulose into the solvent from that of the fibres, by pretreatment of matrix cellulose. The tensile strength of uniaxially reinforced all-cellulose composite was found to be 480 MPa at 25 °C, and the dynamic storage modulus was found to be as high as 20 GPa at 300 °C. These values are higher than those of conventional glass-fibre-reinforced composites. In addition, the linear thermal expansion coefficient was about 10^{-7} K^{-1}. This all cellulose composite showed several considerable advantages, including it was composed of sustainable resources; it was biodegradable; there were fewer interfaces between the fibre and the matterix; and it possessed excellent mechanical and thermal performance during use [Nishino et al., 2004].

(Ho et al., 2012)] synthesized nanofibrillated cellulose with cationic functional groups. This trimethylammonium modified nanofibrillated cellulose (TMA-NFC) was used for the preparation of composites with various layered silicates. These belonged to the groups of montmorillonite, kaolin, talc, vermiculite, and mica. The respective composites were prepared by high shear homogenization followed by filtration and hot-pressing. Owing to the electrostatic attraction of cationic cellulose fibrils and anionic silicate layers, the interactions between trimethylammonium modified nanofibrillated cellulose and the layered silicates were very pronounced. This mutual interaction between trimethylammonium modified nanofibrillated cellulose and layered silicate, however, was influenced not only by layered silicate properties but also by the composite preparation method, as the researchers have described in the detailed study.

In another study performed by the same group [(Ho et al., 2012)], composites of trimethylammonium-modified nanofibrillated cellulose and layered silicates were prepared by high shear homogenization followed by pressure filtration and vacuum hot-pressing, which gave rise to the particularly homogeneous dispersion of the silicate particles. Thirteen different clays and micas were employed. Good interactions between trimethylammonium modified nano fibrillated cellulose and layered silicates were obtained due to electrostatic attraction between cationic fibrils and anionic silicate layers, and even favored by high-shear homogenization process. Layered silicates exerted a pronounced influence on the water vapor barrier and mechanical properties.

Importantly, it was found that the insertion of layered silicate particles did not improve automatically the barrier properties as indicated by the commonly used “fibre–brick composite” mode.

Liquid ammonia has been used to treat films of nanofibrillated cellulose, trimethylammonium modified nanofibrillated cellulose, and their composites with vermiculite. Crystal structure, mechanical properties, water vapor permeation and water vapor adsorption of the resulting materials were investigated. With the exception of trimethylammonium modified nanofibrillated cellulose and vermiculite composites, pronounced effects on the addressed mechanical properties arose after exposure of the materials to ammonia. Furthermore, treatment of composite films with ammonia led to a distinct decrease in water vapor permeation. Surprisingly, trimethylammonium modified nanofibrillated cellulose and vermiculite composites films showed the best water vapor barrier properties, highest tensile strength, and highest elastic modulus after treatment with liquid ammonia. This is considered as a consequence of electrostatic attraction between the positively charged ammonium groups in trimethylammonium modified nanofibrillated cellulose and the anionic silicate layers of vermiculite [Ho et al., 2013].

Seydibeyoğlu and Oksman [2008] fibrillated cellulose from micro to nano scale and evaluated how these microfibres and nanofibrils affected the mechanical and thermal properties of thermoplastic polyurethane. They prepared composite materials using compression moulding, by stacking the cellulose fibre mats between polyurethane films. The results showed that both microfibres and nanofibrils reinforced the polyurethane and provided better heat stability. The addition of 16.5 wt% of cellulose nanofibrils to polyurethane increased the strength by approximately 5 times and the stiffness by around 30 times. These results were very promising in terms of obtaining fibrils with a novel processing method and by improving the mechanical and thermal properties of polyurethane. This is also expected to expand the application areas of polyurethanes.

Edible cellulosic films made with hydroxypropylmethylcellulose (HPMC) have proven to be inadequate moisture barriers. To improve its water vapor barrier properties, Coma et al. [2001] incorporated different hydrophobic compounds into the HPMC matrix. They included few fatty acids and derivatives into the film-forming solution prior to film formation. Stearic acid was chosen because of its high capacity to considerably reduce the water vapor transmission rate. Antimicrobial action of edible HPMC film

was obtained by the incorporation of nisin into the film-forming solution. Nisin is an antimicrobial peptide which is effective against gram-positive bacteria. The inhibitory effect of this bacteriocin was tested for inhibition of Listeria innocua and Staphylococcus aureus. The stearic acid was found to reduce the inhibitory effect of active HPMC film against both of the selected strains. The researchers explained this phenomenon by electrostatic interactions between the cationic nisin and the anionic stearic acid. Further studies showed that antimicrobial effect of the films varied with the nature of the hydrophobic compound incorporated; film without lipid exhibited the highest antimicrobial activity, methylstearate film the lower, and stearic acid film the least. This further corroborated the idea of electrostatic interactions.

Very recently, El-Wakil et al. [2015] developed bionanocomposites by casting/evaporation of wheat gluten, cellulose nanocrystals, and titanium dioxide nanoparticles. They studied the effect of the addition of different percentages of cellulose nanocrystals, and titanium dioxide on tensile strength, Young's modulus and water sensitivity. A significant improvement in the studied properties was observed when 7.5% cellulose nanocrystals and 0.6% titanium dioxide were added to wheat gluten. Wheat gluten / cellulose nanocrystals (7.5% / 0.6%) titanium dioxide blend suspension was used to coat commercial packaging unbleached kraft paper sheets via 1, 2 and 3 coating layers. A significant enhancement of 56% and 53% in breaking length and burst index, respectively, was achieved for 3 layers coated paper. The antimicrobial activity of the coated papers, against *Saccharomyces cervisiae*, Gram-negative bacteria *Escherichia coli* and Gram-positive bacteria *Staphylococcus aureus* was investigated and expressed in terms of percent reduction of surviving number of the tested organisms. More than 98.5% reduction of surviving number was observed against the test organisms as compared to titanium dioxide free coated paper.

STARCH NANOCOMPOSITES

Starch has been considered as the most promising and economic member of biodegradable polymers' category. This polymer owe its popularity and wide usage to its several advantages such as wide and easy availability, total compostability without formation of any toxic residues and cost as low as less than 1 euro per kilogram. Another major advantage of starch is its inherent complete biodegradability and it is even known to promote the biodegradability of a nonbiodegradable plastic when

blended [Abreu et al., 2015; Sun et al., 2014; Goyal and Goyal, 2012; Avella et al., 2005].

Starch is a widely available semicrystalline form of carbohydrate, stored in granules as a reserve in most plants, such as potato, rice, corn and cereal grain to name a few. Starch is actually a mixture of two polymers of α-glucose, i.e. linear amylose (poly-a-1,4-Dglucopyranoside) and highly branched amylopectin (poly-a-1,4- D-glucopyranoside and a-1,6-D-glucopyranoside). Amylose molecules consist of 200–20,000 glucose units forming a helix due to the bond angles present among the glucose units. Amylopectin is a highly branched polymer containing short side chains of 30 glucose units attached to every 20–30 glucose units along the chain. Amylopectin molecules may contain up to two million glucose units. The amylose remains linked by a (1,4)-linkages whereas amylopectin has a (1,4)-linked backbone and a (1,6)-linked branches. Amylose forms the amorphous part of the starch, whereas the amylopectin predominantly imparts the crystallinity. The relative amounts of amylose and amylopectin vary with the source of the starch. For example, starch from corn granules contains approximately 30% amylase and 70% amylopectin. The different ratio of amylose to amylopectin imparts very different properties to the materials [Tang et al., 2012; Ren et al., 2009; Avella et al., 2005].

Despite several advantages, starch alone does not make a good candidate for packaging material because of its poor mechanical properties, strong hydrophilic behaviour (thus poor moisture barrier) and crystalline nature leading to poor process capability.

To improve mechanical properties of starch, plasticizers such as glycerol and other low molecular weight polyhydroxy compounds, urea and polyethers are added. Starch exhibits thermoplastic behaviour when a plasticizer is added. Plasticizers efficiently provide stability to starch by reducing the intramolecular hydrogen bonding. Amount of plasticizer and amylase to amylopectin ration can be varied to obtain thermoplastic starch having different water absorbing tendency, water solubility and viscosity. Though plasticizers inmprove the processibility and flexibility of thermoplastic starch, it still is not suitable to be used in food packaging applications because of its poor mechanical properties and sensitivity to moisture [Tang et al., 2012]. Thus, to overcome these problems, preparing nanocomposites of starch is a promising strategy and can be used in order to make it a suitable packaging material having

properties of providing good moisture and oxygen barrier and being mechanically strong along with the inherent advantages that starch already possesses. In recent years, starch nanocomposites have been prepared and have demonstrated their success as a smart packaging material.

Recently, Abreu et al. [2015] prepared nanocomposites of quaternary ammonium salt modified montmorillonite C30B with starch; nanocomposites of silver nanoparticles with starch; and nanocomposites of both silver nanoparticles and C30B with starch. They studied colour and opacity, permeability towards water vapour and oxygen, contact an angle, and dynamic mechanical analysis. Results were correlated to the observations with the incorporation of C30B and silver nanoparticles. Films demonstrated antimicrobial activity against S. aureus, E. coli and C. Albicans without any significant differences between silver nanoparticles concentrations. The presence of silver nanoparticles imparted bacteriostatic effect, as well as also enhanced dispersion of C30B, and changed the surface polarity too. Incorporation of C30B in the starch film was found to improve the mechanical and gas barrier properties. The migration of components from the Nano film of starch was found to be insignificant and within the legal limits. Thus, researchers demonstrated that the starch films incorporated with C30B and silver nanoparticles have potential to be used as a suitable packaging nanostructured material.

Sun et al. [2014] carried out the characterization of edible corn starch films which were impregnated with calcium carbonate nanoparticles. They found that the concentration of calcium carbonate nanoparticles significantly affected the tensile properties of the nanocomposite films. The addition of calcium carbonate nanoparticles to the corn starch films greatly increased tensile strength from 1.40 to 2.24 MPa, elongation from 79.21 to 118.98%, and Young's modulus from 1.82 to 2.41 MPa. The increase in these, mechanical properties of corn starch films with the addition of calcium carbonate nanoparticles indicated that calcium carbonate nanoparticles could be used to improve strength and flexibility of the film to a great extent. The incorporation of calcium carbonate nanoparticles also increased the opacity of films, lowered the degree of water vapour permeability and film solubility value as compared to those of the corn starch films. This suggested that a smooth and compact structure was formed between nanoparticles and corn starch, which could be confirmed by the scanning electron microscopy. The addition of calcium carbonate nanoparticles to corn starch

films also increased the melting temperature of films, as determined by differential scanning calorimetry. Results of this study indicated that the 0.06% concentration of calcium carbonate nanoparticles may serve as the best option for the desirable properties of edible films.

In another experiment, Sadegh-Hassani and Nafchi [2014] used casting method to prepare bionanocomposite films of potato starch reinforced with halloysite nanoclay. The composition included potato starch with 40% (w/w) of a mixture of sorbitol/glycerol (weight ratio of 3 to 1 as plasticizer) with nanoclay (0–5% w/w). Results of the studies performed revealed that mechanical properties of films were improved by increasing the concentration of nanoclay. Tensile strength was found to be increased from 7.33 to 9.82 MPa, and elongation at break decreased from 68.0 to 44.0%. Solubility in water decreased from 35 to 23%, and heat seal strength increased from 375 to 580 N/m. Also, incorporation of clay nanoparticles in the structure of biopolymer decreased the permeability of the gaseous molecules.

Taghizadeh and coworkers [2013] investigated the effect of concentration of sodium montmorillonite clay (MMT-Na) on the physical properties and extent of enzymatic hydrolysis of Polyvinyl Alcohol: Starch: Carboxymethyl Cellulose nanocomposites using enzyme α−amylase. As revealed by the results of this work, the films with montmorillonite clay concentration of 5 wt% exhibited a considerably reduced extent and rate of starch hydrolysis. The authors attributed these results to interactions between Polyvinyl Alcohol: Starch: Carboxymethyl Cellulose and montmorillonite clay that further prevented an enzymatic attack on the remaining starch phases within the blend. The rate of glucose production from each nanocomposite substrates was found to be decreased greatly as the content of montmorillonite clay increased from 0 to 5% (w/w). At this concentration of montmorillonite clay, the films showed the lowest rate of glucose production values. With the increase in the content of montmorillonite clay from 0 to 5%, the strain required to break decreased significantly (from 35.56 to 5.22%).

Fazli et al. recently supported the concept of utilization of the nanomaterials in polymer structure to improve their mechanical and physical properties. He proposed that nano crystalline cellulose has this ability improving mechanical and physical properties of polymeric films. They employed a chemical method to produce nano crystalline cellulose and starch bionanocomposite. X-ray diffraction results of the starch biofilm

showed that crystalline structure of nano crystalline cellulose is maintained [Fazli et al. 2013].

Ren et al. [2009] prepared thermoplastic starch (TPS) and its nanocomposite (TPS/OMMT) with 15% carbamide, 15% ethanolamine and different contents of organic activated montmorillonite (OMMT) by a twin-screw extruder. Results of Fourier transform infrared spectroscopy and wide angle X-ray diffraction showed that the alkylamine in dodecyl benzyl dimethyl ammonium bromide could react with montmorillonite through cation exchange reaction. Scanning electron microscope images revealed that the lower amounts of organic activated montmorillonite were dispersed well in the matrixes of thermoplastic starch. The carbamide, ethanolamine, and the organic activated montmorillonite could destroy the crystallization behaviour of starch, but only the montmorillonite restrained this behaviour which is favorable for long-term storage. Evaluation of mechanical properties revealed that the tensile strength and modulus of thermoplastic starch / montmorillonite nanocomposites were better than those of thermoplastic starch alone, while the elongation at break was decreased with the increasing concentration of organic activated montmorillonite. When the content of montmorillonite was 4%, the tensile strength, and modulus of TPS was improved from 4.2 and 42 MPa to 6.0 and 76 MPa, respectively.

Avella et al. [2005] prepared biodegradable starch / clay nanocomposite films for the purpose of being used as food packaging material. Using polymer melt processing techniques, the films were prepared by homogeneously dispersing the nanoparticles of montmorillonite in various starch based materials. The results of the structural and mechanical characterization of starch and clay nanocomposite films revealed a good intercalation of the polymeric phase into clay interlayer galleries, along with an improvement in mechanical parameters, namely modulus and tensile strength. Migration tests were performed and the films were put in contact with vegetables and stimulants to verify the conformity of prepared samples with actual regulations and European directives on biodegradable materials. Thus, these results demonstrated that biodegradable starch / clay nanocomposite films can be utilized in the food packaging sector owing to their low overall migration limit.

CHITOSAN NANOCOMPOSITES

Chitosan, one of the strongest natural polymers, is the second-most abundant natural polysaccharide. The favorable properties of chitosan which are accountable for its popularity include the ease of obtaining the polymer in different physical forms its non-toxic nature, biocompatibility, biodegradability, and its ability to form films with antibacterial properties [Dias et al. 2014; Mesquita et al., 2010]. Owing to these advantages and its huge abundance, it is extensively used for food packaging, biosensors, water treatment, and biomedical applications such as drug delivery, tissue engineering, wound healing, and for use in antimicrobial strategies [Mesquita et al., 2010].

Chitosan is a partially deacetylated derivative of chitin. It is a linear polysaccharide consisting of β (1,4)-linked D-glucosamine residues (deacetylated unit) with a variable number of randomly located N-acetyl-glucosamine groups (acetylated unit) [Zuo et al., 2013]. The formation of chitosan involves derivatization by the elimination of the acetyl group of chitin, and the final sugar monomer obtained is the N-glucosamine. In its natural form, chitin is predominantly organized in extended chain conformation and assembled in the form of microfibrils. This structural organization is important for the mechanical function of cuticles and exoskeletons of insects and crustaceans. In addition, chitin structures provide support for tissues and organs such as eyes, muscles, throat etc. Chitosan is in nature less common, but is present as a cell wall component in filamentous fungi, where chitosan biosynthesis takes place through deacetylation of chitin [Mushi et al., 2014].

Despite its unique physical and inherent antibacterial properties, chitosan is not found to be suitable enough to satisfy conditions of an ideal packaging material. Chitosan has hydrophilic nature and thus chitosan films exhibit significantly high permeability to water. Its inherent water sensitivity and relatively low mechanical properties, as compared to petroleum-based polymers, restrict the use of chitosan films for food packaging applications. Thus, chitosan needs to be reinforced with nanofillers in order to improve its mechanical and moisture barrier properties, making it a suitable packaging material for food products [Zuo et al., 2013; Mesquita et al., 2010].

In a recent study, an antibacterial and conductive bionanocomposite film consisting of polypyrrole, zinc oxide nanoparticles, and chitosan were electrochemically synthesized on indium tin oxide glass substrate by electrooxidation of 0.1 M pyrrole in

an aqueous solution containing appropriate amounts of zinc oxide nanoparticles uniformly dispersed in chitosan. This method enabled the room temperature electrosynthesis of bionanocomposite film consisting of zinc oxide nanoparticles incorporated within the growing polypyrrole/chitosan composite. The morphology of polypyrrole/ zinc oxide /chitosan bionanocomposite was studied by scanning electron microscopy. Indium tin oxide – Polypyrrole/chitosan and Indium tin oxide – Polypyrrole/ zinc oxide /chitosan bio electrodes were characterized using the Fourier transform infrared technique, X-ray diffraction, and thermogravimetric analysis. The electrical conductivity of nanocomposites was investigated by a four-probe method. The prepared nanocomposites were also analysed for antioxidant activity using the 2,2-diphenyl-1-picrylhydrazyl assay. The results demonstrated that by the addition of zinc oxide nanoparticles, the antioxidant activity of nanocomposites increased significantly. The electrical conductivity of films showed a sudden decrease in lower weight ratios of zinc oxide nanoparticles (5 wt%), while it was increased gradually for higher ratios (10, 15, and 20 wt%). The nanocomposites were analysed for antibacterial activity against Gram-positive and Gram-negative bacteria. The results showed that the synthesized bionanocomposite was effective against all of the studied bacteria, and its effectiveness was higher for *Pseudomonas aeruginosa*. The thermal stability and physical properties of bionanocomposite films were increased by an increase in the weight ratio of zinc oxide nanoparticles, thus promising novel food packaging applications for the electrically conductive polysaccharide-based nanocomposites, particularly owing to their antibacterial properties [Ebrahimiasl et al. 2015].

Dias et al. [2014] developed nanocomposites of chitosan and characterized them using a full factorial design with different levels of montmorillonite and encapsulated tocopherol. Encapsulated tocopherol influenced the intercalation of montmorillonite in the chitosan matrix up to the concentration of 10%, resulting in the formation of the films which had reduced water vapor permeability, increased hydrophobicity, and lower equilibrium moisture content. These observations indicated towards the potential of chitosan: montmorillonite nanocomposites as an active food packaging material. But, agglomeration of encapsulated tocopherol occurred at content more than 10%. Transmission electron microscopy revealed that this agglomeration deteriorated the properties of the prepared films. As the tocopherol content was increased in the films,

the films were found to become slightly more yellow, more irregular and less transparent with a higher haze index.

According to the observation of Mushi et al. [2014], chitosan reinforcement by stiff particles or fibres is usually obtained at the expense of lowered ductility and toughness. Thus, they studied the reinforcement of chitosan film by a new type of native chitin nanofibres. Films were prepared by casting from colloidal suspensions of chitin in dissolved chitosan. The nanocomposite films were actually chitin nanofibre networks in chitosan matrix. The polymer matrix nanocomposites were produced in volume fractions of 8%, 22%, and 56% chitin nanofibres. The results demonstrated favourable chitin-chitosan synergy for colloidal dispersion. Also, the prepared nanocomposites were found to possess lower moisture absorbing tendency, which can probably be due to the favorable chitin-chitosan interface. The highest toughness (area under the stress-strain curve) was observed at 8 vol% chitin content.

In another experiment performed by Zuo and co-workers [2013], free-standing graphene oxide - chitosan (GO-chitosan) nanocomposite films were prepared. It was found that the graphene oxide - chitosan films were biologically compatible and mechanically reinforced. Through the formation of amide linkages between carboxylic acid groups of graphene oxide and amine groups of chitosan, graphene oxide could get evenly dispersed in the chitosan matrix. The tensile strength of graphene oxide - chitosan film was found to be improved by 2.5 folds and Young's modulus was increased by around 4.6 folds, as compared to pristine chitosan film. The glass transition temperature of graphene oxide - chitosan composite film changed from 118°C to 158°C, as compared to the pristine chitosan. This indicated the enhanced thermal stability of the nanocomposite film.

Abdolmohammadi et al. [2012] investigated the effects of calcium carbonate nanoparticles on the mechanical and thermal properties and surface morphology of polycaprolactone/ chitosan nanocomposites. The nanocomposites of polycaprolactone/ chitosan/ calcium carbonate were prepared using a melt blending technique. Results of tensile measurement studies revealed an increase in the tensile modulus after loading of the calcium carbonate nanoparticles. Tensile strength and elongation at break evaluation demonstrated a gradual improvement with the addition of up to 1 wt% of calcium carbonate nanoparticles. But for loading of more than 1 wt% of calcium carbonate nanoparticles, the performance of above-mentioned properties was found to be

decreased. The thermal stability was observed to be most enhanced at a loading of 1 wt% of calcium carbonate nanoparticles. The fractured surface morphology of the polycaprolactone /chitosan blend was found to be more stretched and homogeneous in polycaprolactone /chitosan/ calcium carbonate nanocomposite. Micrograph of transmission electron microscopy displayed good dispersion of calcium carbonate nanoparticles within the matrix of nanocomposite film.

In another experiment, silver nanoparticles of small size were synthesized using the wet chemical reduction method into the lamellar space layer of montmorillonite/ chitosan as an organomodified mineral solid support in the absence of any heat treatment. Silver nitrate, montmorillonite, chitosan, and sodium borohydride were used as the silver precursor, the solid support, the natural polymeric stabilizer, and the chemical reduction agent, respectively. Montmorillonite was suspended in aqueous silver nitrate/ chitosan solution. Silver nanoparticles were formed on the interlayer and external surface of montmorillonite/ chitosan. The antibacterial activity of silver nanoparticles in montmorillonite/ chitosan was investigated against Gram-positive bacteria, ie, *Staphylococcus aureus* and methicillin-resistant *S. aureus* and Gram-negative bacteria, ie, *Escherichia coli*, *E. coli* O157:H7, and *Pseudomonas aeruginosa* by the disc diffusion method using Mueller Hinton agar at different sizes of silver nanoparticles. All of the synthesized silver/ montmorillonite/ chitosan bionanocomposites were found to have high antibacterial activity [Shameli et al., 2011].

A new type of biodegradable nanocomposite was obtained by layer-by-layer (LBL) technique using highly deacetylated chitosan and eucalyptus wood cellulose nanowhiskers. Hydrogen bonds and electrostatic interactions between the negatively charged sulfate groups on the whisker surface and the ammonium groups of chitosan were the responsible factors for the growth of the multilayered films. Images of scanning electron microscopy demonstrated high density and homogeneous distribution of cellulose nanowhiskers adsorbed on all the chitosan layers. Cross-section characterization of the assembled films indicated an average of approximately 7 nm of thickness per bilayer. These results indicated that the methodology used can be extended to different biopolymers for the design of new biobased nanocomposites in a wide range of applications such as food packaging [Mesquita et al., 2010].

Apart from cellulose, starch, and chitosan, there are several other biopolymers which have been explored for the preparation of bionanocomposites for the applications in food packaging. Few of them are enlisted in table 5-1 with examples.

Table 5-1 Other bionanocomposites used for food packaging.

Polymer	Reinforcement	Results	Reference
Wheat gluten	Cellulose nanocrystals; Titanium dioxide nanoparticles	A significant improvement in the tensile strength, Young's modulus, and water sensitivity was observed when 7.5% cellulose nanocrystals and 0.6% titanium dioxide was added to wheat gluten. An enhancement of 56% and 53% in breaking length and burst index, respectively, was achieved when wheat gluten/cellulose nanocrystals 7.5%/0.6% titanium dioxide blend suspension was coated on commercial packaging unbleached kraft paper sheets. Also, the coated packaging paper sheets were found to have significant antimicrobial activity.	El-Wakil et al., 2015
Poly(3-hydroxybutyrate)	Zinc oxide nanoparticles	The Young's modulus, tensile and impact strength of the biopolymer were enhanced by up to 43%, 32% and 26%, respectively. Nanocomposites exhibited reduced water uptake and superior gas and vapor barrier properties. They also showed antibacterial activity against both Gram-positive and Gram-negative bacteria, which was progressively improved upon increasing zinc oxide concentration. The migration levels of composites in both non-polar and polar stimulants also decreased with increasing nanoparticle content.	Díez-Pascual and Díez-Vicente, 2014
Polylactic acid	Montmorillonite	The addition of organoclay (montmorillonite) improved mechanical and biodegradable properties of polylactic acid. Food contact test showed that the nanocomposites are able to be used as food packaging materials.	Pereira et al., 2014
Gelatin	Zinc oxide nanorods	Young's modulus and tensile strength of gelatine films were increased by 42% and 25% respectively with incorporation of 5% zinc oxide nanorods. The surface topography of the gelatin films indicated an Increase in surface roughness with increasing	Rouhi et al., 2013

		concentration of zinc oxide nanorods. The conductivity of the films also significantly increased.	
Polyhydroxy butyrate (PHB)/ Polycaprola ctone (PCL)	Anionic clay Mg-Al layered double hydroxide	Nanocomposite exhibited enhancement of 300% in elongation at break and 66% tensile strength in the presence of 1.0 wt% of the stearate Mg-Al layered double hydroxide. Clay improved compatibility between polymer matrix and the best ratio 80PHB/20PCL/1stearate Mg-Al LDH surface was well dispersed and stretched before it broke.	Liau et al., 2014
Polypropyle ne	Calcium carbonate nanoparticles	Results of mechanical analysis revealed that Young's modulus increased as a function of content of calcium carbonate nanoparticles. Presence of calcium carbonate nanoparticles drastically reduced the permeability of polypropylene to both oxygen and Carbon dioxide.	Avella et al., 2006

COMMERCIAL PRODUCTS IN ACTIVE PACKAGING

Intelligent Packaging Applications are used in tampering detection (breaching of containment), quality indicators, time-temperature indicators (TTIs), gas sensing devices, microbial growth, pathogen detection, traceability devices, radio frequency identification (RFID) labels/ tags/ chips, product authenticity, etc. A brief account of few such commercial examples is given below:

1. Moisture Control Packaging

Dri-loc$^{@}$ absorbant pads from Cryovac$^{@}$, sealed air corporation is based on super-absorbent polymers located between two other plastic layers (http://www.cryovac.com/NA/EN/food-packaging-products/driloc-produce.aspx).

They offer three advantages:

a) Perforated with tiny one-way valves

b) Juices absorbed from the bottom

c) Prevents food from drying

Similar products, Fresh-R-Pax™ Absorbent pads and Fresh-R-Pax™ Absorbent trays are also available from Maxwell Chase Technologies, LLC.

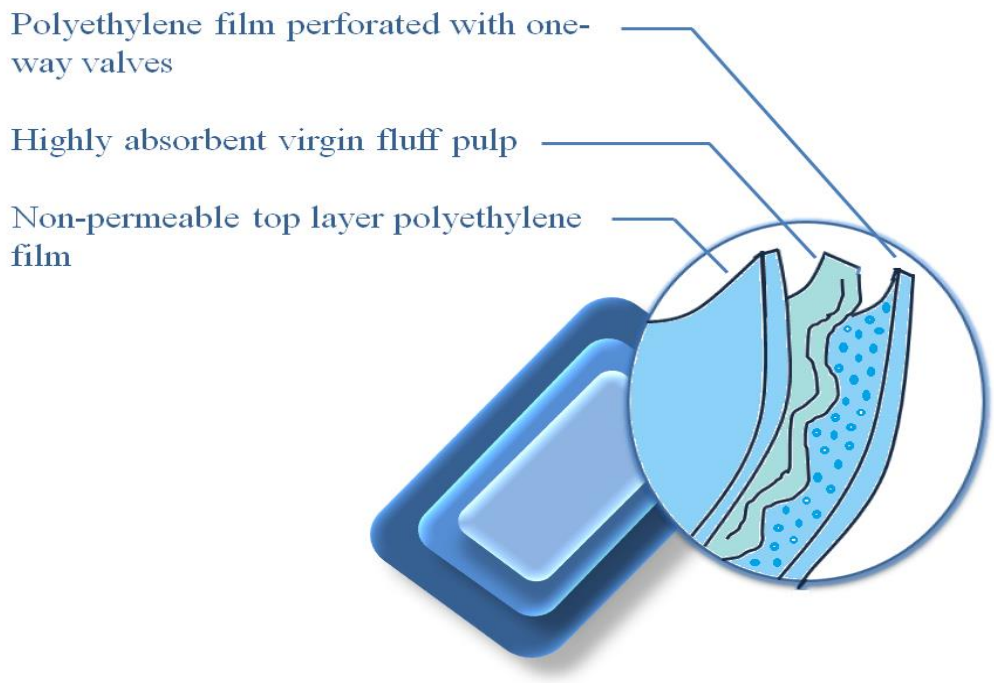

Figure 5-3 Dri-loc@ absorbant pads.

2. Oxygen scavenging packaging

In oxygen scavenging, existing technology is based on: iron powder oxidation, ascorbic acid oxidation, photosensitive dye oxidation, enzymatic oxidation (e.g. glucose oxidase), unsaturated fatty acids, rice extract or immobilised yeast on a solid substrate. They are available as labels, sachets, cards or films which can be incorporated into the packaging film. Majority of commercially available O_2 scavengers are based on the principle of iron oxidation:

$Fe \rightarrow Fe^{2+} + 2e^-$

$½O_2 + H_2O + 2e^- \rightarrow 2OH^-$

$Fe^{2+} + 2OH^- \rightarrow Fe(OH)_2$

$Fe(OH)_2 + ¼O_2 + ½H_2O \rightarrow Fe(OH)_3$

AGELESS OMAC® Oxygen Absorbing Film incorporates oxygen scavenger into a composite film (http://ageless.mgc-a.com/product/ageless-omac/).

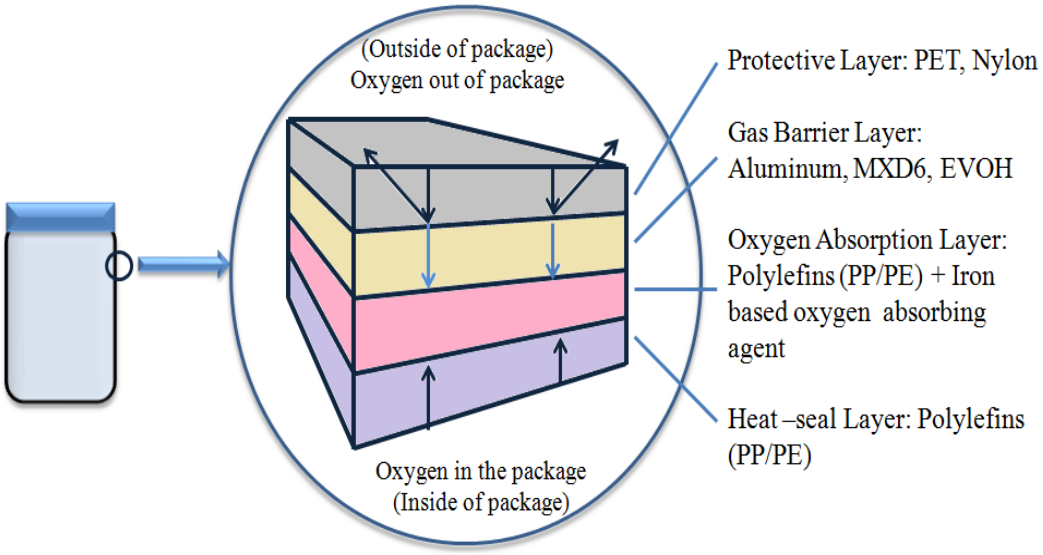

Figure 5-4 Oxygen scavenging Film.

3. Carbon Dioxide Emitters and Scavengers

Function of carbon dioxide is to inhibit microbial growth and extend product shelf-life of the product. Removal of O_2 or dissolution of CO_2 in the product creates a partial vacuum, which may cause collapse of flexible packaging. Dual action CO_2 generators and O_2 scavengers is to work in such a way that package collapsing does not happen.

Verifrais™ package (SARL Codimer) extends shelf-life of fresh red meats. Standard tray with a false, perforated bottom containing sachet of sodium bicarbonate/ascorbate. Juice dripping from the meat onto the sachet results in CO_2 emission. This leads to dual functionalities of replacement of CO_2 absorbed by the meat and prevention of package collapse.

The patented cellulose UltraZap XtendaPak pad from paper Pak industries, packed with super absorbent polymers, effectively wicks juice away from cut tomatoes while generating CO_2 gas to reduce the growth of micro-organisms inside the package (http://paperpakindustries.com/products/ultrazap_xtendapak.php).

4. Oxygen level indicating packaging

The AGELESS EYE®, from mitsubhi gas chemicals is an example of a packaging system which indicates the presence of oxygen. It is an in-package monitor which indicates the presence of oxygen at a glance. The pink color of the indicator indicates

oxygen free packaging (less than 0.1%) whereas blue colour indicates presence of oxygen (0.5% or more) (http://www.mgc.co.jp/eng/products/abc/ageless/eye.html).

CONCLUSION

Food packaging plays role of a physicochemical barrier for the food products in order to maintain their integrity throughout their shelf life. Shortcomings of conventional packaging materials such as poor mechanical strength, low water resistance, inability to prevent degradation and nonbiodegradability can be overcome by use of "bionanocomposites". A bionanocomposite is a nanodimensional multiphase material derived from the combination of two or more natural components. The use of bionanocomposites in food packaging industry is a new strategy to attain markedly improved packaging properties such as increased modulus of strength, decreased gas and water vapour permeability, increased water resistance, improved thermal stability, and barrier properties against the migration of oxygen, carbon dioxide, aroma and flavours. Furthermore, bionanocomposites offer an environmental friendly approach. Biologically active compounds, such as antimicrobials can also be added to impart desired functional properties. Cellulose, starch and chitosan are some of the biopolymers which have been extensively studied and used to prepare bionanocomposites by reinforcing them with ative agents such as nanoclays, silicon dioxide nanoparticles, silver nanoparticles, etc., thus making them suitable to be used as smart packaging material by improving their mechanical properties and imparting "smart" properties such as antimicrobial action. Thus, nanocomposites, when used as or are incorporated in packaging materials, provide "smart" properties to the packaging system, ultimately increasing the shelf life of the product and improving its integrity and quality.

REFERENCES

- Abdolmohammadi, S., Siyamak, S., Ibrahim, N.A., Yunus, W.M.Z.W., M.Z.A.R., Azizi, S., Fatehi, A., 2012. Enhancement of Mechanical and Thermal Properties of Polycaprolactone/Chitosan Blend by Calcium Carbonate Nanoparticles. Int. J. Mol. Sci. 13, 4508-4522.

- Abreua, A.S., Oliveiraa, M., Arsénio de Sáa, Rodriguesb, R.M., Cerqueirab M.A., Vicenteb A.A., Machado, A.V., 2015. Antimicrobial nanostructured starch based films for packaging. Carbohydrate Polymers. 129, 127–134.
- Adame, D., Beall, G.W., 2009. Direct measurement of the constrained polymer region in polyamide/clay nanocomposites and the implications for gas diffusion. Applied Clay Science. 42, 545-552.
- Avella, M., De Vlieger, J.J., Errico M.E., Fischer, S., Vacca, P., Maria Grazia Volpe, M.G., 2005. Biodegradable starch/clay nanocomposite films for food packaging applications. Food Chemistry. 93, 467–474.
- Avella, M., Errico, M.E., Gentile, G., 2006. High performance iPP based nanocomposites for food packaging application. NSTI-Nanotech. 2, 841-844.
- Azeredo, H.M.C., 2009. Nanocomposites for food packaging applications. Food Research International. 42, 1240–1253.
- Azizi Samir, M.A.S., Alloin, F., Dufresne, A., 2005. Review of recent research into cellulosic whiskers, their properties and their application in nanocomposite field. Biomacromolecules. 6, 612-626.
- Bin, Y., Mine, M., Koganemaru, A., Jiang, X., Matsuo, M., 2006. Morphology and mechanical and electrical properties of oriented PVA–VGCF and PVA–MWNT composites. Polymer. 47, 1308–1317.
- Brody, A.L., 2006. Nano and food packaging technologies converge. Food Technology. 60, 92–94.
- Brody, A.L., Bugusu, B., Han, J.H., Sand, C.K., Mchugh, T.H., 2008. Innovative Food Packaging Solutions. Journal of Food Science. 73, R107-R116.
- Bruce, D.M., Hobson, R.N., Farrent, J.W., Hepworth, D.G., 2005. High-performance composites from low-cost plant primary cell walls. Compos. Part Appl. Sci. Manuf. 36, 1486–1493.
- Chandrasekaran, G., Han, H.K., Kim, G.J., Shin, H.J., 2011. Antimicrobial activity of delaminated aminopropyl functionalized magnesium phyllosilicates. Applied Clay Science. 53, 729–36.
- Chawengkijwanich, C., Hayata, Y., 2008. Development of TiO2 powder-coated food packaging film and its ability to inactivate Escherichia coli in vitro and in actual tests. Int J Food Microbiol. 123, 288-92.

- Chen, W., Tao, X., Xue, P., Cheng, X., 2005. Enhanced mechanical properties and morphological characterizations of poly(vinyl alcohol)–carbon nanotube composite films. Applied Surface Science. 252, 1404–1409.
- Coma, V., Sebti, I., Pardon, P., Deschamps, A., Pichavant, F.H., 2001. Antimicrobial edible packaging based on cellulosic ethers, fatty acids, and nisin incorporation to inhibit Listeria innocua and Staphylococcus aureus. J. Food Prot. 64, 470–475.
- Dias, M.V., Azevedo, V.M., Borges, S, V., Soares, N.F.F., Fernandes, R.V.B., Marques, J.J., Medeiros, E.A.A., 2014. Development of chitosan/montmorillonite nanocomposites with encapsulated a-tocopherol. Food Chemistry 165, 323–329.
- Dufresne, A., 2013. Nanocellulose: a new ageless bionanomaterial. Mater. Today 16, 220–227.
- El-Wakil, N.A., Hassan, E.A., Abou-Zeid, R.E., Dufresne, A., 2015. Development of wheat gluten/Nanocellulose/titanium dioxide nanocomposites for active food packaging. Carbohydr. Polym. 124, 337–346.
- Emamifar, A., Kadivar, M., Shahedi, M. Solaimanianzad, S., 2011. Effect of nanocomposite packaging containing Ag and ZnO on inactivation of Lactobacillus plantarum in orange juice. Food Control. 22, 408-413.
- Emamifar, A., Kadivar, M., Shahedi, M., Solaimanianzad, S., 2010. Evaluation of nanocomposite packaging containing Ag and ZnO on the shelf life of fresh orange juice. Innovative Food Science & Emerging Technologies. 11, 742–748.
- Emamifar. A., 2011. Applications of Antimicrobial Polymer Nanocomposites in Food Packaging, Advances in Nanocomposite Technology, Dr. Abbass Hashim (Ed.), ISBN: 978-953-307-347-7, InTech, Available from: http://www.intechopen.com/books/advances-in-nanocomposite-technology/applications-of-antimicrobialpolymer- nanocomposites-in-food-packaging
- Fazli, F.A., Babazadeh, A., Fazli, F.A., 2013. Crystalline Structure of Starch Based Nano Composites. International Journal of Biological, Food, Veterinary and Agricultural Engineering. 7, 725-728.

- Goyal, S., Gyanendra Kumar Goyal, G.K., 2012. Nanotechnology in food packaging – a critical review. Russian Journal of Agricultural and Socio-Economic Sciences. 10, 14-24.
- Helbert, W., Cavaillé, C.Y., Dufresne, A., 1996. Thermoplastic nanocomposites filled with wheat straw cellulose whiskers. Part I: Processing and mechanical behaviour. Polymer Composites. 17, 604-611.
- Henriette Monteiro Cordeiro de Azeredo, Luiz Henrique Capparelli Mattoso and Tara Habig McHugh (2011). Nanocomposites in Food Packaging – A Review, Advances in Diverse Industrial Applications of Nanocomposites, Dr. Boreddy Reddy (Ed.), ISBN: 978-953-307-202-9, InTech, Available from: http://www.intechopen.com/books/advances-in-diverse-industrial-applications-ofnanocomposites/nanocomposites-in-food-packaging-a-review
- Ho a, T.T.T., Ko, Y.S., Zimmermann, T., Geiger, T., Caseri, W., 2012. Processing and characterization of nanofibrillated cellulose/layered silicate systems. J. Mater. Sci. 47, 4370–4382.
- Ho b, T.T.T., Zimmermann, T., Ohr, S., Caseri, W.R., 2012. Composites of Cationic Nanofibrillated Cellulose and Layered Silicates: Water Vapor Barrier and Mechanical Properties. ACS Appl. Mater. Interfaces 4, 4832–4840.
- Ho, T.T.T., Zimmermann, T., Caseri, W.R., Smith, P., 2013. Liquid ammonia treatment of (cationic) nanofibrillated cellulose/vermiculite composites. J. Polym. Sci. Part B Polym. Phys. 51, 638–648.
- Huang, W.M., Yang, B., An, L., Li, C., Chan, Y. S., 2005. Water-driven programmable polyurethane shape memory polymer: Demonstration and mechanism. Appl. Phys. Lett. 86, 114105.
- Ifuku, S., Nogi, M., Abe, K., Handa, K., Nakatsubo, F., Yano, H., 2007. Surface Modification of Bacterial Cellulose Nanofibres for Property Enhancement of Optically Transparent Composites: Dependence on Acetyl-Group DS. Biomacromolecules. 8, 1973–1978.
- Iwamoto, S., Nakagaito, A.N., Yano, H., Nogi, M., 2005. Optically transparent composites reinforced with plant fibre-based nanofibres. Appl. Phys. A 81, 1109–1112.

- Jia, X., Li, Y., Cheng, Q., Zhang, S., Zhang, B., 2007. Preparation and properties of poly(vinyl alcohol)/silica nanocomposites derived from copolymerization of vinyl silica nanoparticles and vinyl acetate. European Polymer Journal. 43, 1123–1131.
- Jin, T., Sun, D., Su, J.Y., Zhang, H., Sue, H.J., 2009. Antimicrobial efficacy of zinc oxide quantum dots against Listeria monocytogenes, Salmonella enteritidis, and Escherichia coli O157:H7. Journal of Food Science. 74, 46-52.
- Kim, J.Y., Han, S.II, Hong, S., 2008. Effect of modified carbon nanotube on the properties of aromatic polyester nanocomposites. Polymer, 49, 3335–3345.
- Lau, K.T., Hui, D., 2002. The revolutionary creation of new advanced Materials – carbon nanotube composites. Composites Part B. 33, 263–277.
- Liau, C.P., Ahmad, M.B., Shameli, K., Yunus, W.M.Z.W., Ibrahim, N.A., Zainuddin, N., Then, Y.Y., 2014. Preparation and Characterization of Polyhydroxybutyrate/Polycaprolactone Nanocomposites. The Scientific World Journal. 2014, 9 pages.
- Lopez Manchado, M.A., Valentini, L., Biagotti, J., Kenny, J.M., 2005. Thermal and mechanical properties of single-walled carbon nanotubes–polypropylene composites prepared by melt processing. Carbon. 43, 1499–1505.
- Ma, M., Guo, L., Anderson, D. G., Langer, R., 2013. Bio-inspired polymer composite actuator and generator driven by water gradients. Science. 339, 186–189.
- Martirosyan, A., Schneider, Y-J., 2014. Engineered Nanomaterials in Food: Implications for Food Safety and Consumer Health. Int. J. Environ. Res. Public Health, 11, 5720-5750.
- Mauriello, G.D.L.E., La Storia, A., Villani, F., Ercolini, D., 2005. Antimicrobial activity of a nisin-activated plastic film for food packaging. Letters in Applied Microbiology. 41, 464–469.
- Mesquita, J.P., Donnici, C.L., Pereira, F.V., 2010. Biobased Nanocomposites from Layer-by-Layer Assembly of Cellulose Nanowhiskers with Chitosan. Biomacromolecules. 11, 473–480.
- Mirzadeh, A., Kokabi, M., 2007. The effect of composition and draw-down ratio on morphology and oxygen permeability of polypropylene nanocomposite blown films. European Polymer Journal. 43, 3757-3765.

- Mushi, N.E., Utsel, S., Berglund, L.A., 2014. Nanostructured biocomposite films of high toughness based on native chitin nanofibres and chitosan. Frontiers in Chemistry. 2.
- Natural additives and agricultural wastes in biopolymer formulations for food packaging Arantzazu Valdés , Ana Cristina Mellinas , Marina Ramos, María Carmen Garrigós and Alfonso Jiménez. Frontiers in Chemistry. February 2014 | Volume 2 | Article 6
- Nielsen, L.E., 1967. Models for the permeability of filled polymer systems. Journal of Macromolecular Science: Part A. 1, 929-942.
- Nishino, T., Matsuda, I., Hirao, K., 2004. All-Cellulose Composite. Macromolecules 37, 7683–7687.
- Özgür Seydibeyoğlu, M., Oksman, K., 2008. Novel nanocomposites based on polyurethane and micro fibrillated cellulose. Compos. Sci. Technol. 68, 908–914.
- Patakfalvi. R., Dékány. I., 2004. Synthesis and intercalation of silver nanoparticles in kaolinite/DMSO complexes. Applied Clay Science. 25, 149–59.
- Patil, A.J., Muthusamy, E., Mann, S., 2005. Fabrication of functional proteinorganoclay lamellar nanocomposites by biomolecule-induced assembly of exfoliated aminopropyl functionalized magnesium phillosilicates. Journal of Materials Chemistry. 15, 3838–43.
- Pereira, M., Abreu, A.S., Oliveira, M., Nobrega, J.M., Machado, A.V., 2014. Biodegradable nanocomposite for food packaging application. XIV SLAP/XII CIP. 4 pages.
- Rai, M., Yadav, A., Gade, A., 2009. Silver nanoparticles as a new generation of antimicrobials. Biotechnology Advances. 27, 76–83.
- Ray, S., Easteal, A., Quek, S.Y., Chen, X.D., 2006. The potential use of polymer-clay nanocomposites in food packaging. International Journal of Food Engineering. 2, 1556-3758.
- Ren, P., Shen, T., Wang, F., Wang, X., Zhang, Z., 2009. Study on Biodegradable Starch/OMMT Nanocomposites for Packaging Applications. J Polym Environ. 17, 203–207.

- Rhim, J.W., Park, H.M., Ha, C.S., 2013. Bio-nanocomposites for food packaging applications. Progress in Polymer Science. 38, 1629– 1652.
- Rhim, J-W., Ng, P.K.W., 2007. Natural Biopolymer-Based Nanocomposite Films for Packaging Applications, Critical Reviews in Food Science and Nutrition. 47, 411-433.
- Robertson G. 2006. Food packaging principles and practices. 2nd ed. Boca Raton, Fla.: Taylor & Francis. 545 p.
- Rouhi, J., Mahmud, S., Naderi, N., Ooi C.R., Mahmood, M.R., 2013. Physical properties of fish gelatin-based bio-nanocomposite films incorporated with ZnO nanorods. Nanoscale Research Letters 2013, 8:364
- Sadegh-Hassani, F., Nafchi, A.M., 2014. Preparation and characterization of bionanocomposite films based on potato starch/halloysite nanoclay International Journal of Biological Macromolecules. 67, 458–462.
- Saeideh Ebrahimiasl, S., Zakaria, A., Kassim, A., Basri, S. N., 2015. Novel conductive polypyrrole/zinc oxide/chitosan bionanocomposite: synthesis, characterization, antioxidant, and antibacterial activities. International Journal of Nanomedicine. 10, 217–227.
- Sawai, J., Yoshikawa, T., 2004. Quantitative evaluation of antifungal activity of metallic oxide powders (MgO, CaO and ZnO) by an indirect conductimetric assay. Journal of Applied Microbiology. 96, 803–809.
- Shameli, K., Ahmad, M.B., Zargar, M., Yunus, W.M.Z.W., Ibrahim, N.A., Shabanzadeh, P., Moghaddam, M. G., 2011. Synthesis and characterization of silver/montmorillonite/chitosan bionanocomposites by chemical reduction method and their antibacterial activity. International Journal of Nanomedicine.6, 271–284.
- Sharma, H., Mishra, P.K., Talegaonkar, S., Vaidya, B., 2015. Metal nanoparticles: a theranostic nanotool against cancer. Drug Discovery Today. [Epub ahead of print].
- Sidorenko, A., Krupenkin, T., Taylor, A., Fratzl, P., Aizenberg, J., 2007. Reversible switching of hydrogel-actuated nanostructures into complex micropatterns. Science 315, 487–490.

- Sun, Q., Xi, T., Li, Y., Xiong, Liu., 2014. Characterization of Corn Starch Films Reinforced with CaCO3 Nanoparticles. PLOS ONE. 9, e106727.
- Taghizadeh, M.T., Sabouri, N., Ghanbarzadeh, B., 2013. Polyvinyl alcohol:starch:carboxymethyl cellulose containing sodium montmorillonite clay blends; mechanical properties and biodegradation behaviour. SpringerPlus. 2, 1-8.
- Tang, S., Zou, P., Xiong, H., Tang, H., 2008. Effect of nano-SiO2 on the performance of starch/polyvinyl alcohol blend films. Carbohydrate Polymers. 72, 521–526.
- Tang, X.Z., Kumar, P., Alavi, S., Sandeep, K.P., 2012. Recent Advances in Biopolymers and Biopolymer-Based Nanocomposites for Food Packaging Materials. Critical Reviews in Food Science and Nutrition. 52, 426-442.
- Thostenson, E.T., Li. C.Y., Chou, T.W., 2005. Nanocomposites in context. Composites Science and Technology. 65, 491–516.
- Uyama, H., Kuwabara, M., Tsujimoto, T., Nakano, M., Usuki, A., Kobayashi, S., 2003. Green nanocomposite from renewable resources: plant oil-clay hybrid materials. Chemistry of Materials. 15, 2492-2494.
- Vladimiriov, V., Betchev, C., Vassiliou, A., Papageorgiou, G., Bikiaris, D., 2006. Dynamic mechanical and morphological studies of isotactic polypropylene/ fumed silica nanocomposites with enhanced gas barrier properties. Composites Science and Technology. 66, 2935–2944.
- Wu, C.L., Zhang, M.Q., Rong, M.Z., Friedrick, K., 2002. Tensile performance improvement of low nanoparticles filled-polypropylene composites. Composites Science and Technology. 62, 1327–1340.
- Xiong, H.G., Tang, S.W., Tang, H.L., Zou, P., 2008. The structure and properties of a starch-based biodegradable film. Carbohydrate Polymers. 71, 263–268.
- Yang, B., Huang, W.M., Li, C., Lee, C.M., Li, L., 2004. On the effects of moisture in a polyurethane shape memory polymer. Smart Mater. Struct. 13, 191–195.
- Zeng, H., Gao, C., Wang, Y., Watts, P.C.P., Kong, H., Cui, X., Yan, D., 2006. In situ polymerization approach to multiwalled carbon nanotubes-reinforced nylon 1010 composites: mechanical properties and crystallization behaviour. Polymer, 47, 113–122.

- Zhang, K., Geissler, A., Standhardt, M., Mehlhase, S., Gallei, M., Chen, L., Thiele, C.M., 2015. Moisture-responsive films of cellulose stearoyl esters showing reversible shape transitions. Scientific Reports. 5, 11011.
- Zhang, L., Jiang, Y., Ding, Y., Povey, M., York, D., 2007. Investigation into the antibacterial behaviour of suspensions of ZnO nanoparticles (ZnO nanofluids). Journal of Nanoparticle Research. 9, 479–489.
- Zhang, M.Q., Rong, M.Z., 2003. Performance improvement of polymers by the addition of grafted nano-inorganic particles. Chinese Journal of Polymer Science. 21, 587–602.
- Zhou, X., Shin, E., Wang, K.W., Bakis, C.E., 2004. Interfacial damping characteristics of carbon nanotube-based composites. Composites Science and Technology. 64, 2425–2437.
- Zhuang, R., Beuchat, L.R., Chinnan, M.S., Shewfelt, R.L., Huang, Y.-W., 1996. Inactivation of Salmonella montevideo on Tomatoes by Applying Cellulose-Based Edible Films. J. Food Prot. 59, 808–812.
- Zuo, P.-P., Feng, H.-F., Xu, Z.-Z., Zhang, L.-F., Zhang, Y.-L., Xia, W., Zhang, W.-Q., 2013. Fabrication of biocompatible and mechanically reinforced graphene oxide-chitosan nanocomposite films. Chemistry Central Journal. 7.

7. PAPER V

Metal Nanoparticles- a theranostic nanotool against cancer

Harshita Sharma[†], Pawan K Mishra[†], Sushama Talegaonkar, Bhuvaneshwar Vaidya

†Equal contribution

(Accepted and printed- Drug Discovery Today)

Teaser: Metal nanoparticles, how promising they are as an advancement towards personalized cancer treatment?

Abstract

Cancer remains to be one of the most deadly diseases worldwide. Conventional anti-cancer therapies come with number of drawbacks. Thus, development of new anti-cancer strategies is the need of the hour. Theranostics is one such novel strategy which combines treatment with diagnosis and monitoring. Metal nanoparticles are reportedly one of the most promising theranostic agents for treatment of cancer. A number of metals like iron, gold, silver, zinc, titanium, etc. hold great potential as anti-cancer agents, either inherently or by surface modifications. Metal nanoparticles, as a functional component of theranostic tools, play a crucial dual-role of a diagnostic as well as an active therapeutic agent for the treatment of cancer.

Key words: Cancer, Theranostic agents, Nanocarriers, Metal nanoparticles, Iron oxide, Zinc oxide, Gold, Silver

Introduction

With over 10 million new cases every year worldwide, cancer remains a difficult disease to treat and a significant cause for morbidity and mortality [1]. It is reported that about half of people receiving treatment for invasive cancer (excluding carcinoma in-situ and non-melanoma skin cancers) die either from cancer or its treatment [2]. It is a well-known fact that cancer is a multifactorial disease caused by a complex combination of genetic and environmental factors. Several studies have been performed on cancer which resulted in better understanding of cancer at genetic, molecular, and cellular levels which opened doors for new targets and strategies for treatment of this deadly disease [3].

Over the last years, several nanocarriers have been explored to increase the effectiveness of chemotherapeutics. Some of these, e.g., Doxil® (PEGylated liposomes of doxorubicin) and Abraxane® (albumin nanoparticles of paclitaxel) are very successful and available in the market. During recent years, so many studies have been reported to develop new tools for diagnostic applications. Advances in cellular and molecular imaging have led to the development of various nanoparticles based imaging agents. Moreover, efforts have also been made to combine both therapy and imaging in single particle to increase the effectiveness of single approach.

The term “theranostics” is fairly new but a revolutionary one in the field of cancer therapy. It is concatenation of two words: therapeutics and diagnostics. There are several definitions of theranostics, but can simply be defined as an integrated therapeutic system, which provides therapy (Rx) as well as aids in diagnosis (Dx) and monitoring of therapy through imaging [4]. Theranostics enables to identify responders and non-responders through imaging of tumor during course of treatment. This helps in determining correct line of treatment for an individual (Figure 6-1). Thus, diagnosis, treatment, and monitoring of the response to the treatment can be achieved through a single agent [5].

Metal nanoparticles have gained significant attention in recent years because of their unique physical (e.g., plasmonic resonance, fluorescent enhancement) and chemical (e.g., catalytic activity enhancement) properties which make them suitable for drug delivery and targeting [6]. Due to larger surface area and area/volume ratio, metal nanoparticles exhibit many physico-chemical properties which are not there in bulk material. These altered properties are lethal to the living cells, making them useful for the treatment of cancer. In addition, inherent properties of metal nanoparticles make them useful for diagnosis and imaging at the same time [7-9]. For example, photoluminescence or superparamagnetic properties of metals are useful for imaging, and their ability to produce reactive oxygen species (ROS) can be used for killing of cancer cells [10, 11]. Therapeutic moieties can also be encapsulated or conjugated with metal nanoparticles. Moreover, surface modifications with antibody or ligand for specific receptor can enhance the targeting ability of metal nanoparticles. Imaging agents can also be attached to nanoparticles which allow them to be used in diagnosis and monitoring [12] (Figure 6-2). Thus metal nanoparticles, as theranostic agents, solve dual purpose of diagnosis, therapy and monitoring, all with one formulation, ultimately

improving the therapeutic outcome of anti-cancer therapy. This also reduces the patient inconvenience and potential unwanted effects. Multifunction metal nanoparticles provide a number of advantages including overcoming stability and solubility problems of drugs, reducing amount of drug to be administered, targeting, fewer side effects, diagnosis, imaging of tumours, and monitoring the success of therapy [13]. However, metal nanoparticles also have some toxicological issues, which should be addressed before their use in clinical applications (Box 1).

General mechanism of cancer cell killing by metal nanoparticles

Following effects produced by metal nanoparticles may lead to killing of cancer cells:

Hyperthermia

Hyperthermia refers to increasing temperature of microenvironment of a tissue to 40-45ºC, in order to initiate a series of subcellular events, which result in cell death. Hyperthermia may cause apoptosis, activation of immunological responses, increasing tumor blood flow and oxygenation, all ultimately leading to cell death [14].

Photothermal Effect

Photothermal effect is produced by a photo thermal agent (photosensitizer) that converts near-infrared (NIR) light into heat. NIR is absorbed by the tissue, where photosensitizer converts it into heat, thereby causing cell death [15].

Generation of Reactive oxygen species (ROS)

ROS include hydroxyl and superoxide radicals, which cause oxidation. Generation of ROS results in elevation of ROS stress level. When ROS stress reaches above cellular tolerance threshold, it exhausts the cellular antioxidant defence system and thus induces cell death [16]. Theranostic Properties of Metal Nanoparticles

Iron/iron oxide nanoparticles

Super-paramagnetic iron oxide nanoparticles (SPION) have been widely used clinically, as contrast agents in magnetic resonance imaging (MRI), for local hyperthermia and as magnetically targetable nano-carriers for several drug delivery systems [7]. SPION exhibit many such properties which are not present in bulk iron. This is because orbital moments in a magnetic substance are much higher at particle surfaces than in bulk. Thus, orbital contribution to total magnetization is much more in nano-dimensional systems due to larger total surface area. Orbital moment is an

important microscopic quantity which determines many macroscopic properties of magnetic substances. [17].

Ferromagnets exhibit a certain value of remnant magnetization even after the removal of external magnetic field. Coercive field is the magnitude of field that must be applied in negative direction to bring magnetization of sample back to zero. Changes in magnetization of a material occur via activation over an energy barrier. If number of atoms per particle is decreasing, interaction energy (exchange energy) could reach values as low as thermal energy at room temperature. This leads to spontaneous random orientation of magnetic spin inside the particles, or in other words, remnant magnetisation as well as coercitivity will be zero. This means no hysteresis and therefore paramagnetic behaviour is exhibited. The super-paramagnetic behaviour is characterised by a certain value of relaxation time (τ), the time which the system needs to achieve zero magnetisation after an external magnetic field is removed. This super-paramagnetic behaviour of iron oxide makes it a useful contrast agent for magnetic resonance imaging (MRI), which in turn makes it an important diagnostic tool.

Therapeutic property of SPION is attributed to energy absorption due to Neel relaxation which results in production of hyperthermia. If particles are exposed to an alternating external magnetic field, the magnetic dipole moments of nanosized particles have to be reoriented very quickly depending on frequency and magnetic strength of applied magnetic field. Power loss of particles in this process releases a considerable amount of heat energy, which is used up in heating of surrounding environment, e.g. a tumor. This heat produced by super-paramagnetic behaviour of iron oxide results in killing of tumor cells due to hyperthermal effect [10].

Zinc oxide nanoparticles

Zinc oxide (ZnO) nanoparticles have received much attention for their implications in cancer therapy. ZnO being a conventional wide band gap semiconductor, has applications in multiple areas of science. Its inherent photoluminescence properties are useful in biosensing applications whereas wide band-gap semiconductor properties are useful in promoting generation of ROS [11]. Bulk ZnO is recognized as a GRAS (Generally Regarded as Safe) substance by Food and Drug Administration (FDA) and ZnO nanoparticles having sizes >100 nm are considered to be relatively biocompatible, which makes them a justified choice for drug delivery. Most important and unique property of ZnO nanoparticles is their inherent preferential cytotoxicity against cancer

cells *in vitro*. This characteristic of ZnO nanoparticles is due to their ability to induce ROS generation, resulting in cell death [18, 19]. The electrons in semiconductors have energies within certain bands (unlike metals which have continuum of electronic states). Band gap (void region extending from top of filled valence band to the bottom of vacant conduction band) for crystalline ZnO is ~3.3 eV. UV rays contain sufficient energy to promote electrons (e^-) to conduction band, leaving behind electron holes (h^+) or unoccupied states in valence band. Electrons and holes can then migrate to the surface of the nanoparticles to react with oxygen and hydroxyl ions, respectively. This results in formation of superoxide and hydroxyl radicals [11]. Various ROS thus produced can then trigger redox-cycling cascades in cells and cause irreparable oxidative damage to cells. For nanosized ZnO, large number of holes and/or electrons is available even in absence of UV light. This is attributed to the fact that nanocrystal quality also decreases with decrease in size of ZnO particles. This results in increased interstitial zinc ions and oxygen vacancies, and donor/acceptor impurities. These crystal defects can generate a large number of electron-hole pairs [20]. This whole phenomenon thus leads to production of ROS, ultimately killing tumor cells.

Gold nanoparticles

Gold (Au) nanoparticles have unique optical properties which make them extremely useful for cancer diagnosis and photothermal therapy. These properties are conferred by interaction of light with electrons present on the surface of Au nanoparticles. Au is a free-electron system which contains equal numbers of positive ions (fixed in position) and conduction electrons (free and highly mobile). Such metals are called plasma. When metal surface is irradiated with an electromagnetic wave, oscillating electric fields of the wave interact with free electrons causing a concerted oscillation of electron charge that is in resonance with frequency of visible light. Free electrons are driven by electric field to oscillate coherently. Quantized plasma oscillations or collective oscillations of free electrons are called plasmons and that of electrons present on surface are called surface plasmons. These surface plasmons interact with visible light in a phenomenon called surface plasmon resonance (SPR) [8, 9]. SPR leads to strong electromagnetic fields on particle surface and consequently enhances all radiative (absorption and scattering) and non-radiative (conversion of absorbed light to heat) properties of Au [21]. Energy loss of electromagnetic wave after passing through metal occurs due to two processes: absorption and scattering. Optical

absorption and scattering mainly depends on size of nanoparticles. For a 20 nm Au nanoparticles, extinction is mainly due to absorption. At 40 nm, scattering starts taking place. At 80 nm, both absorption and scattering contribute to extinction. Thus, ratio of scattering to absorption increases with size of nanoparticles. This fact guides the choice of nanoparticles for biomedical applications. For imaging, larger nanoparticles are preferred because of higher scattering efficiency, whereas smaller nanoparticles are preferred for photothermal therapy, as light is mainly absorbed by nanoparticles and thus efficiently gets converted into heat [22].

Silver nanoparticles

Silver (Ag) nanoparticles are also plasmonic structures which absorb and scatter a portion of impinging light. After their selective uptake into cancer cells, absorbed light can be used for thermal killing, whereas scattered light can be used for imaging. Like Au (and copper), Ag is also a free electron system, containing equal numbers of positive ions and conduction electrons. On irradiation by an electromagnetic wave, free electrons are driven by electric field to oscillate coherently at a plasma frequency. Quantized plasma oscillations (plasmons) interact with visible light, exhibiting surface plasmon resonance [23]. Of the three metals (Ag, Au, Cu) that display plasmon resonance, Ag exhibits highest efficiency of plasmon excitation. Also, Ag is the only material whose plasmon resonance can be tuned to any wavelength in the visible spectrum. [24].

Ag nanoparticles may also affect proteins and enzymes with thiol groups (like glutathione and thioredoxin) by interacting with cells. These proteins and enzymes are responsible for neutralizing ROS which are generated by mitochondrial energy metabolism. Ag nanoparticles thus cause ROS accumulation by depleting antioxidant defense mechanism. ROS accumulation initiates inflammatory response and perturbation and leads to destruction of mitochondria. Apoptogenic factors like cytochrome C are released afterwards which finally results in programmed cell death. [25].

Synthesis of Metal Nanoparticles

Several approaches have been used for the synthesis of metal nanoparticles, which include reduction, sonolysis, hydrothermal synthesis, pyrolysis etc. First and most important requirement for any method is to form particles in nanorange and also impart stability to the produced nanoparticles. Different methods for the production of metal nanoparticles are briefly summarized in Table 6-1.

Applications of Metal Nanoparticles as Theranostic Agents in Cancer Therapy

*Iron nanoparticle*s: Iron is the most explored and widely used metal in the field of cancer therapy. Studies confirmed that iron oxide nanoparticles possess desirable properties to be used as diagnostic and therapeutic agent in cancer management. Ma et al. proposed a new strategy for exploring SPION-based MRI contrast agents with excellent high specificity to cancer cells by conjugating folic acid (FA) at the surface of SPION. These nanoparticles were found to be specific to MCF-7 and SPC-A-1 cells. The r_2/r_1 (transverse vs longitudinal proton relaxation rate) value of SPION was around 40, which is much higher than that of Resovist® (commercial MRI contrast agent consisting of iron oxide nanoparticles coated with carboxydextran) indicating that SPION had stronger T_2 shortening effect, resulting in strong MRI efficacy [26]. Lin et al. used MRI-visible iron oxide nanocomposites as siRNA carriers to overcome multi drug resistance (MDR) through silencing of target messenger RNA and subsequently reducing expression of P-glycoprotein. Nanoparticles led to effective silencing effect comparable to commercial golden standard transfection agent, Lipofectamine 2000. Human breast cancer MCF-7/ADR cells can be vulnerable to doxorubicin treatment after strong down-regulation of P-glycoprotein through siRNA transfection. After transfection, cells also displayed significant contrast enhancement against non-transfected cells under a 3T clinical MRI scanner [27]. A smart magnetic nanoparticle-aptamer probe was developed which could be used for targeted imaging and as a drug carrier for hepatocellular carcinoma treatment. The theranostic nanoprobe combined specific capability of cancer-specific molecule (DNA-based EpCAM aptamer) and imaging capability of magnetic iron oxide nanoparticles [28]. Li et al. constructed nanoparticles comprising a SPIO inner core and a disulfide-containing polyethylenimine outer layer for redox-triggered gene release in response to an intracellular reducing environment. Nanoparticles were also able to deliver siRNA for silencing of human telomerase reverse transcriptase genes in HepG2 cells, causing their apoptosis and growth inhibition. Further, nanoparticles were applicable as T2-negative contrast agents for MRI of a tumor xenograft [29]. Zhou et al. reported PEGylated $Fe@Fe_3O_4$ nanoparticles which possessed triple functional properties: targeting, photothermal therapy (PTT), and imaging. They also showed high magnetization value and transverse relaxivity. In tumour, intensity of MRI signal was ~ three folds and increased temperature was ~ two times than those without magnetic targeting, indicating good

magnetic targeting ability [30]. A hybrid nano-platform with multi-functional characteristics for cancer diagnosis, photodynamic therapy (PDT), radiofrequency thermal therapy (RTT) and magnetic targeting applications was developed via decorating iron oxide nanoparticles onto fullerene (C60). FA was linked for active targeting. C60-IONP-PEG-FA also showed strong photosensitizing and photothermal ablation effect, selectively killing cancer cells via active tumor targeting and magnetic targeting [31]. Wang et al. developed imaging contrast agents using bovine serum albumin capped SPION. The r2/r1 ratio of 13.3 ensured its application as T2-weighted MRI contrast agents. When conjugated with NIR fluorescent dye and monoclonal antibody, these bioconjugates showed excellent targeting capability [32]. Shahbazi-Gahrouei and Abdolahi used SPION attached to C595 mAb that binds to MUC1, to specifically detect ovarian cancer cells. They investigated anticancer effects and MRI parameters of nanoconjugate. Findings of study showed good tumor accumulation and detection, no in-vivo toxicity, and potential selective anti-ovarian cancer activity [33].

Future perspectives: In recent years, SPION have emerged as a new generation of target-specific MRI T2 contrast agents. SPION are efficient relaxation promoters, possess adjustable magnetic properties, and have a long blood retention time and biodegradability. In addition, they cause hyperthermia, resulting in killing of cancer cells and thus are suitable and effective theranostic agent. Since SPION have been used in clinical studies since many years, they hold high potential of being applicable in clinical applications in future. However, issues of potential toxicity, standardization of therapeutic response and stability are still to be addressed [34].

Zinc nanoparticles: During last few years, ZnO nanoparticles have also been considered as a promising theranostic agent for cancer treatment. ZnO nanoparticles exhibit inherent selective antitumor activity. In a recent study, we synthesized doxorubicin (DOX) loaded ZnO nanoparticles to achieve synergistic anti-cancer action. Mixture of ZnO nanoparticles and DOX demonstrated higher cytotoxicity than either of DOX or ZnO nanoparticles alone. However, drug loaded nanoparticles produced even higher cytotoxicity. This proves that the co-administration of DOX and ZnO nanoparticles produces synergistic cytotoxicity and thus higher anti-cancer activity. This might be because of higher cellular uptake of DOX with ZnO nanoparticles and retention of drug loaded nanoparticles in cancerous cells [35]. Imaging ability of zinc

oxide was also studied earlier by Hong et al. They used ZnO nanowires for imaging along with drug delivery. Optical imaging of integrin α(v)β(3) on U87MG human glioblastoma cells with RGD peptide-conjugated green fluorescent ZnO nanowires was achieved [36]. ZnO quantum dots were also investigated for targeting cancer cells (using transferrin). ZnO nanoprobes were selectively bound and internalized through receptor-mediated endocytosis. Time-lapsed photobleaching studies indicated nanoprobes to be resistant to photobleaching, making them suitable for long term imaging purpose [37].

Future perspectives: In several studies performed on ZnO nanoparticles, different mechanisms of ZnO action have been suggested, such as ROS synthesis, photo-oxidation, and release of free metal ions. Since experiments have revealed that ZnO nanoparticles possess huge theranostic utility and are comparatively biocompatible and safer, they hold potential to be successfully used in cancer therapy in future. However, thorough investigation needs to be done to find out actual mode, or most prominent mode of action. Also, the relation of toxicity with decrease in size of the nanoparticles is to be established. [38].

Gold nanoparticles: Au nanoparticles have been extensively explored in recent years for their applications in the field of cancer treatment. Recently, Bogdanov et al. prepared Au nanoparticles with stealth properties by coating with methoxypolyethylene glycol-graft-poly(l-lysine) copolymer. Highly stable radioactive labeling of Au nanoparticles with ^{99m}Tc allowed imaging of particles biodistribution and revealed dose-dependent long circulation in blood. Radiofrequency-mediated heating of nanoparticles solution showed that they exhibited heating behaviour [39]. Au nanoparticles for dual-mode imaging (MRI/CT) and photothermal therapy of hepatocellular carcinoma were developed by Zeng and his co-workers. Imaging ability of nanoparticles was confirmed by enhanced MR and CT imaging showing a shorter T1 relaxation time and higher Hounsfield unit value. Nanoparticles also showed significant photothermal cytotoxicity against liver cancer cells with NIR irradiation due to their strong absorbance between 700 and 850 nm [40]. Chen et al. developed multifunctional nanoparticles which had ability to initiate mitochondria-dependent apoptosis and activate caspase-3 for real-time imaging of progression of apoptosis based on fluorescence resonance energy transfer (FRET) [41]. Core/shell NPs of Au and Prussian blue were prepared as an excellent photoabsorbing agent for both PTT (due to high photostability) and

photoacoustic (PA) imaging (due to high molar extinction coefficient in NIR region). Au core ensured remarkable contrast enhancement for CT imaging. Through one-time treatment of NIR laser irradiation after i.v. injection of nanoparticles, tumors in nude mice could be completely ablated without recurrence [42]. Sahoo et al. reported development of a nanocomposite consisting of highly fluorescent Au nanoclusters and biopolymer chitosan, which could easily be converted into nanoparticles and form a stable polyplex with suicide gene for induction of apoptosis in cervical cancer cells. Simultaneous red, green, and blue fluorescence from nanoclusters provided convenient optical imaging and flow cytometry probes, without having to use additional dyes [43].

Future perspectives: Au nanoparticles are inherently capable of providing useful imaging contrast, as well as killing cancer cells through photothermal effect. They are also explored as successful radiosensitizers, where they increase the vulnerability of cancer cells towards radiations by altering their microenvironment. Where on one hand, Au nanaoparticles have yielded promising results; on the other hand, they suffer with limitations of high cost and longer retention in liver, spleen and other tissues. These issues need to be addressed before using Au nanoparticles clinically [44].

Silver nanoparticles: Studies have also been performed to use Ag nanoparticles as anti-cancer agent and they all have given new hopes in field of anti-cancer therapy. Mukherjee et al. developed Ag nanoparticles using Olaz scadens leaf extracts which showed anti-cancer activity against different cancer cells (A549, B16, MCF7). Nanoparticles also showed bright red fluorescence which could be utilized to detect localization of drug molecules inside cancer cells [45]. Nima et al. presented tunable Ag-Au nanorods with narrow surface-enhanced Raman scattering (SERS) and high photothermal contrast. Ag-Au nanorods were functionalized with four Raman-active molecules and four antibodies specific to breast cancer markers and with leukocyte-specific CD45 marker. More than two orders of magnitude of SERS signal enhancement was observed from these hybrid nanosystems compared to conventional Ag nanorods [46]. Boca-Farcau et al. biocompatilized Ag nanoparticles with chitosan, labeled with para-aminothiophenol Raman reporter molecule, and conjugated with FA. SERS identity of particles was proven to be highly conserved inside cells. Targeted cancer cell treatment conducted by irradiation with NIR laser in resonance with their plasmonic band produced efficient therapeutic response. By integrating advantages of multimodal optical imaging and SERS detection with hyperthermia

capabilities through site specificity, these nanoparticles can represent a real candidate for personalized medicine [47].

Future perspectives: In addition to generation of ROS to kill cancer cells and photoacoustic imaging ability, Ag nanoparticles also offer the advantage of green synthesis. Though Ag nanoparticles have been found to be very promising for theranostic applications in cancer therapy, potential toxicity remains an issue to be addressed. There are a limited number of well-controlled studies on the potential toxicities of Ag nanoparticles. Though risk of toxicity does not ablate their potential applications against cancer, but risk to benefit ratio should be assessed and possibilities must be explored to use Ag nanoparticles in cancer without causing significant toxicity [48].

Applications of other metals, which have also been successfully explored against cancer are compiled in Table 6-2.

Conclusion

Metal nanoparticles have been actively investigated as the next generation of anti-cancer system for more than decades. They overcome many drawbacks of conventional chemotherapy, like unwanted side effects and development of resistance. More importantly, they allow us to diagnose as well as monitor the progress and success of therapy during the course itself. A number of studies confirmed their potential in cancer treatment. Different formulations of metal nanoparticles are already in preclinical and clinical stages. Metal nanoparticles also hold huge research potential and are areas of great interest for scientists. They should be investigated thoroughly to determine their exact mode of action, extent of toxicity risks, and should be worked upon to explore their anti-cancer potential to the fullest, with minimal toxicity.

References

1. Peer, D. et al. (2007) Nanocarriers as an emerging platform for cancer therapy. *Nat Nanotechnol*. 2, 751-761.
2. Jemal, A. et al. (2011) Global cancer statistics. *CA-Cancer J Clin*. 61, 69–90.
3. Conde, J. et al. (2012) Noble metal nanoparticles applications in cancer. *J Drug Deliv.* 2012, 751075.
4. Warner, S. (2004) Diagnostics plus therapy = theranostics. *Scientist*. 18, 38-39.

5. Jeelani, S. et al. (2014) Theranostics: A treasured tailor for tomorrow. *J Pharm Bioallied Sci*. 6, S6-8.
6. Galdiero, S. et al. (2011) Silver nanoparticles as potential antiviral agents. *Molecules.* 16, 8894-8918.
7. Jurgons, R. et al. (2006) Drug loaded magnetic nanoparticles for cancer therapy. *J Phys: Condens. Matter.* 18, S2893–S2902.
8. Khan, M.S. et al. (2013) Gold nanoparticles: A paradigm shift in biomedical applications. *Adv Colloid Interfac*. 199, 44–58.
9. Li, J. et al. (2013) Research perspectives: gold nanoparticles in cancer theranostics. *Quantitative Imaging in Medicine and Surgery.* 3, 284-291.
10. Kleibert, A. et al. (2011) Structure, morphology, and magnetic properties of Fe nanoparticles deposited onto single-crystalline surfaces. *Beilstein J Nanotechnol*. 2, 47–56.
11. Rasmussen, J.W. et al. (2010) Zinc Oxide Nanoparticles for Selective Destruction of Tumor Cells and Potential for Drug Delivery Applications. *Expert Opin Drug Del.* 7, 1063–1077.
12. Lewis, D.J. et al. (2013) Silica nanoparticles for micro-particle imaging velocimetry: fluorosurfactant improves nanoparticle stability and brightness of immobilized iridium(III) complexes. *Langmuir*. 29, 14701-8.
13. Nasongkla, N. et al. (2006) Multifunctional polymeric micelles as cancer-targeted, MRI-ultrasensitive drug delivery systems. *Nano Lett*. 6, 2427–2430.
14. Chatterjee, D. K. et al. (2011) Nanoparticle-mediated hyperthermia in cancer therapy. Ther Deliv. 2, 1001–1014.
15. Zhou, Z. et al. (2014) Tungsten Oxide Nanorods: An Efficient Nanoplatform for Tumor CT Imaging and Photothermal Therapy. Sci Rep. 4, 3653
16. Gupta, S. C. et al. (2012) Upsides and Downsides of Reactive Oxygen Species for Cancer: The Roles of Reactive Oxygen Species in Tumorigenesis, Prevention, and Therapy. Antioxid Redox Signal. 16, 1295–1322
17. Hofmann-Amtenbrink, M. et al. (2009) Superparamagnetic nanoparticles for biomedical applications. In *Nanostructured Materials for Biomedical Applications* (Tan, M.C., eds), pp.119-149, Transworld Research Network
18. Hanley, C. et al. (2008) preferential killing of cancer cells and activated human T cells using ZnO nanoparticles. *Nanotechnology*. 19, 295103.

19. Ryter, S.W. et al. (2007) Mechanisms of cell death in oxidative stress. *Antioxid Redox Signal*. 9, 49–89

20. Sharma, S.K. et al. (2009) Positron annihilation studies in ZnO nanoparticles. *Solid State Commun*. 149, 550

21. Huang, X. and El-Sayed, M.A. (2010) Gold nanoparticles: Optical properties and implementations in cancer diagnosis and photothermal therapy. *Journal of Advanced Research*, 1, 13–28

22. Jain, P.K. et al. (2006) Calculated absorption and scattering properties of gold nanoparticles of different size, shape, and composition: applications in biological imaging and biomedicine. *J Phys Chem B*. 110, 7238–48

23. Sironmani, A. and Daniel, K. (2011) Silver Nanoparticles – Universal Multifunctional Nanoparticles for Bio Sensing, Imaging for Diagnostics and Targeted Drug Delivery for Therapeutic Applications. In *Drug Discovery and Development – Present and Future* (Kapetanovic I.M., eds), pp, 463-488, InTech

24. Evanoff Jr, D.D. and Chumanov, G. (2005) Synthesis and Optical Properties of Silver Nanoparticles and Arrays. *ChemPhysChem.* 6, 1221 – 1231

25. Mohammadzadeh, R. (2012) Hypothesis: Silver Nanoparticles as an Adjuvant for Cancertherapy, *Advanced Pharmaceutical Bulletin*. 2, 133

26. Ma, X. et al. (2014) Exploring a new SPION-based MRI contrast agent with excellent water-dispersibility, high specificity to cancer cells and strong MR imaging efficacy. *Colloids Surf B Biointerfaces.* 126C, 44-49

27. Lin, G. et al. (2014) Delivery of siRNA by MRI-visible nanovehicles to overcome drug resistance in MCF-7/ADR human breast cancer cells. *Biomaterials.* 35, 9495-507

28. Pilapong, C. et al. (2014) Smart magnetic nanoparticle-aptamer probe for targeted imaging and treatment of hepatocellular carcinoma. *Int J Pharm.* 473, 469-74

29. Li, D. et al. (2014) Theranostic nanoparticles based on bioreducible polyethylenimine-coated iron oxide for reduction-responsive gene delivery and magnetic resonance imaging. *Int J Nanomedicine.* 9, 3347-61

30. Zhou, Z. et al. (2014) Iron/iron oxide core/shell nanoparticles for magnetic targeting MRI and near-infrared photothermal therapy. *Biomaterials.* 35, 7470-8

31. Shi, J. et al. (2014) A fullerene-based multi-functional nanoplatform for cancer theranostic applications. *Biomaterials.* 35, 5771-84

32. Wang, X. et al. (2014) Surface engineered antifouling optomagnetic SPIONs for bimodal targeted imaging of pancreatic cancer cells. *Int J Nanomedicine.* 9, 1601-15

33. Shahbazi-Gahrouei, D. and Abdolahi, M. (2013) Detection of MUC1-expressing ovarian cancer by C595 monoclonal antibody-conjugated SPIONs using MR imaging. *Scientific World Journal*. 2013, 609151

34. Peng, X-H. et al. (2008) Targeted magnetic iron oxide nanoparticles for tumor imaging and therapy. *Int J Nanomedicine.* 3, 311–321

35. Sharma, H. et al. (2014) Development and characterization of metal oxide nanoparticles for the delivery of anticancer drug. *Artificial Cells, Nanomedicine, and Biotechnology*, doi:10.3109/21691401.2014.978980 [In press]

36. Hong, H. et al. (2011) Cancer-Targeted Optical Imaging with Fluorescent Zinc Oxide Nanowires. *Nano lett.*11, 3744-3750

37. Sudhagar, S. et al. (2011) Targeting and sensing cancer cells with ZnO nanoprobes in vitro. *Biotechnol Lett.* 33, 1891-6

38. Arooj, S. et al. (2015) Novel ZnO:Ag nanocomposites induce significant oxidative stress in human fibroblast malignant melanoma (Ht144) cells. *Beilstein J Nanotechnol.* 6, 570–582

39. Bogdanov, A.A. Jr. et al. (2015) Gold nanoparticles stabilized with MPEG-Grafted Poly(l-lysine): in vitro and in vivo evaluation of a potential theranostic agent. *Bioconjug Chem.* 26, 39-50.

40. Zeng, Y. et al. (2014) Lipid-AuNPs@PDA nanohybrid for MRI/CT imaging and photothermal therapy of hepatocellular carcinoma. *ACS Appl Mater Interfaces.* 6, 14266-77

41. Chen, W.H. et al. (2014) Cancer-targeted functional gold nanoparticles for apoptosis induction and real-time imaging based on FRET. *Nanoscale*. 6, 9531-5

42. Jing, L. et al. (2014) Prussian blue coated gold nanoparticles for simultaneous photoacoustic/CT bimodal imaging and photothermal ablation of cancer. *Biomaterials.* 35, 5814-21

43. Sahoo, A.K. et al. (2014) Simultaneous RGB emitting Au nanoclusters in chitosan nanoparticles for anticancer gene theranostics. *ACS Appl Mater Interfaces.* 6, 712-24

44. Ngwa, W. et al. (2014) Targeted radiotherapy with gold nanoparticles: current status and future perspectives. *Nanomedicine (Lond).* 9, 1063–1082

45. Mukherjee, S. et al. (2014) Potential theranostics application of bio-synthesized silver nanoparticles (4-in-1 system). *Theranostics*. 4, 316-35.

46. Nima, Z.A. et al. (2014) Circulating tumor cell identification by functionalized silver-gold nanorods with multicolor, super-enhanced SERS and photothermal resonances. *Sci Rep.* 4, 4752

47. Boca-Farcau, S. et al. (2014) Folic acid-conjugated, SERS-labeled silver nanotriangles for multimodal detection and targeted photothermal treatment on human ovarian cancer cells. *Mol Pharm.* 11, 391-9

48. Ge, L. et al. (2014) Nanosilver particles in medical applications: synthesis, performance, and toxicity. Int J *Nanomedicine.* 9, 2399–2407

49. Huang, Y-W. et al. (2010) Toxicity of transition metal oxide nanoparticles: recent insights from in vitro studies. *Materials*. 3, 4842-4859

50. Djuris˘ic´, A.B. et al. (2015) Toxicity of metal oxide nanoparticles: mechanisms, characterization, and avoiding experimental artefacts. *Small*. 11, 26-44

51. Hasany, S.F. et al. (2012) Systematic Review of the Preparation Techniques of Iron Oxide Magnetic Nanoparticles. *Nanoscience and Nanotechnology*. 2, 148-158

52. Wu, W. et al. (2008) Magnetic Iron Oxide Nanoparticles: Synthesis and Surface Functionalization Strategies. *Nanoscale Res Lett.* 3, 397–415

53. Drmota, A. et al. (2012) Microemulsion Method for Synthesis of Magnetic Oxide Nanoparticles. In *Microemulsions - An Introduction to Properties and Applications* (Najjar, R., eds), pp. 191-214, InTech

54. Sabir, S. et al. (2014) Zinc Oxide Nanoparticles for Revolutionizing Agriculture: Synthesis and Applications. *The Scientific World Journal*. 2014, 925494

55. Yadav, A. et al. (2006) Functional finishing in cotton fabrics using zinc oxide nanoparticles. *Bull Mater Sci*. 29, 641-645

56. Wang, Z. et al. (2003) Low-temperature synthesis of ZnO nanoparticles by solid-state pyrolytic reaction. *Nanotechnology.* 14, 11–15

57. Rani, S. et al. (2008) Synthesis of nanocrystalline ZnO powder via sol–gel route for dye-sensitized solar cells. *Sol Energ Mat Sol C.* 92, 1639–1645

58. Turkevich, J. et al. (1951) "A study of the nucleation and growth processes in the synthesis of colloidal gold", Discuss. *Faraday Soc*. 11, 55-75

59. Perrault, S. D. and Chan, W.C.W. (2009) Synthesis and Surface Modification of Highly Monodispersed, Spherical Gold Nanoparticles of 50-200 nm. *J Am Chem Soc.* 131, 17042–17043

60. Sakai, T. and Alexandridis, P. et al. (2005) Mechanism of Gold Metal Ion Reduction, Nanoparticle Growth and Size Control in Aqueous Amphiphilic Block Copolymer Solutions at Ambient Conditions. *J Phys Chem B*. *109*, 7766–7777

61. Brust, M. et al. (1994) Synthesis of Thiol-derivatised Gold Nanoparticles in a Two-phase Liquid-Liquid System. *Chem Commun*. 7, 801–802.

62. Gurunathan, S. et al. (2009) Antiangiogenic properties of silver nanoparticles. *Biomaterials.* 30, 6341–6350

63. Prabhu, S. and Poulose, E. K. (2012) Silver nanoparticles: mechanism of antimicrobial action, synthesis, medical applications, and toxicity effects. *International Nano Letters.* **2**, 32

64. Nazeruddin, G. M. et al. (2014) Extracellular biosynthesis of silver nanoparticle using *Azadirachta indica* leaf extract and its anti-microbial activity. *J Alloy Compd*. 583, 272–277

65. FarrokhTakin, E. et al. (2013) Barium titanate core--gold shell nanoparticles for hyperthermia treatments. *Int J Nanomedicine*. 8, 2319-31

66. Ciofani, G. et al. (2010) Barium Titanate Nanoparticles: Highly Cytocompatible Dispersions in Glycol-chitosan and Doxorubicin Complexes for Cancer Therapy. *Nanoscale Res Lett.* 5, 1093–1101

67. Li, J. et al. (2013) Topological insulator bismuth selenide as a theranostic platform for simultaneous cancer imaging and therapy. *Sci Rep.* 3, 1998

68. Kinsella, J.M. et al. (2011) X-ray computed tomography imaging of breast cancer by using targeted peptide-labeled bismuthsulfide nanoparticles. *Angew Chem Int Ed Engl*. 50, 12308-11

69. Shafiu Kamba A et al. (2013) A pH-sensitive, biobased calcium carbonate aragonite nanocrystal as a novel anticancer delivery system. *Biomed Res Int.* 2013, 587451

70. Altınoˇ glu, E˙.I. et al. (2008) Near-infrared emitting fluorophore-doped calcium phosphate nanoparticles for *in vivo* imaging of human breast cancer. *ACS Nano.* 2, 2075–2084

71. Zhou, Z. et al. (2014) PEGylated nickel carbide nanocrystals as efficient near-infrared laser induced photothermal therapy for treatment of cancer cells in vivo. *Nanoscale*. 6, 12591-600

72. Sankar, R. et al. (2014) Anticancer activity of Ficus religiosa engineered copper oxide nanoparticles. *Mater Sci Eng C Mater Biol Appl*. 44, 234-9

73. Wang, B. et al. (2013) Uniform magnesium silicate hollow spheres as high drug-loading nanocarriers for cancer therapy with low systemic toxicity. *Dalton Trans*. 42, 8918-25

74. Zhou, M. et al. (2014) Theranostic probe for simultaneous in vivo photoacoustic imaging and confined photothermolysis by pulsed laser at 1064 nm in 4T1 breast cancer model. *Nanoscale*. 6, 15228-35

75. Siddiqui, M.A. et al. (2012) Nickel oxide nanoparticles induce cytotoxicity, oxidative stress and apoptosis in cultured human cells that is abrogated by the dietary antioxidant curcumin. *Food Chem Toxicol.* 50, 641-7

76. Wang, Y. et al. (2014) Cytotoxicity, DNA damage, and apoptosis induced by titanium dioxide nanoparticles in human non-small cell lung cancer A549 cells. *Environ Sci Pollut Res Int*. DOI 10.1007/s11356-014-3717-7 [In press]

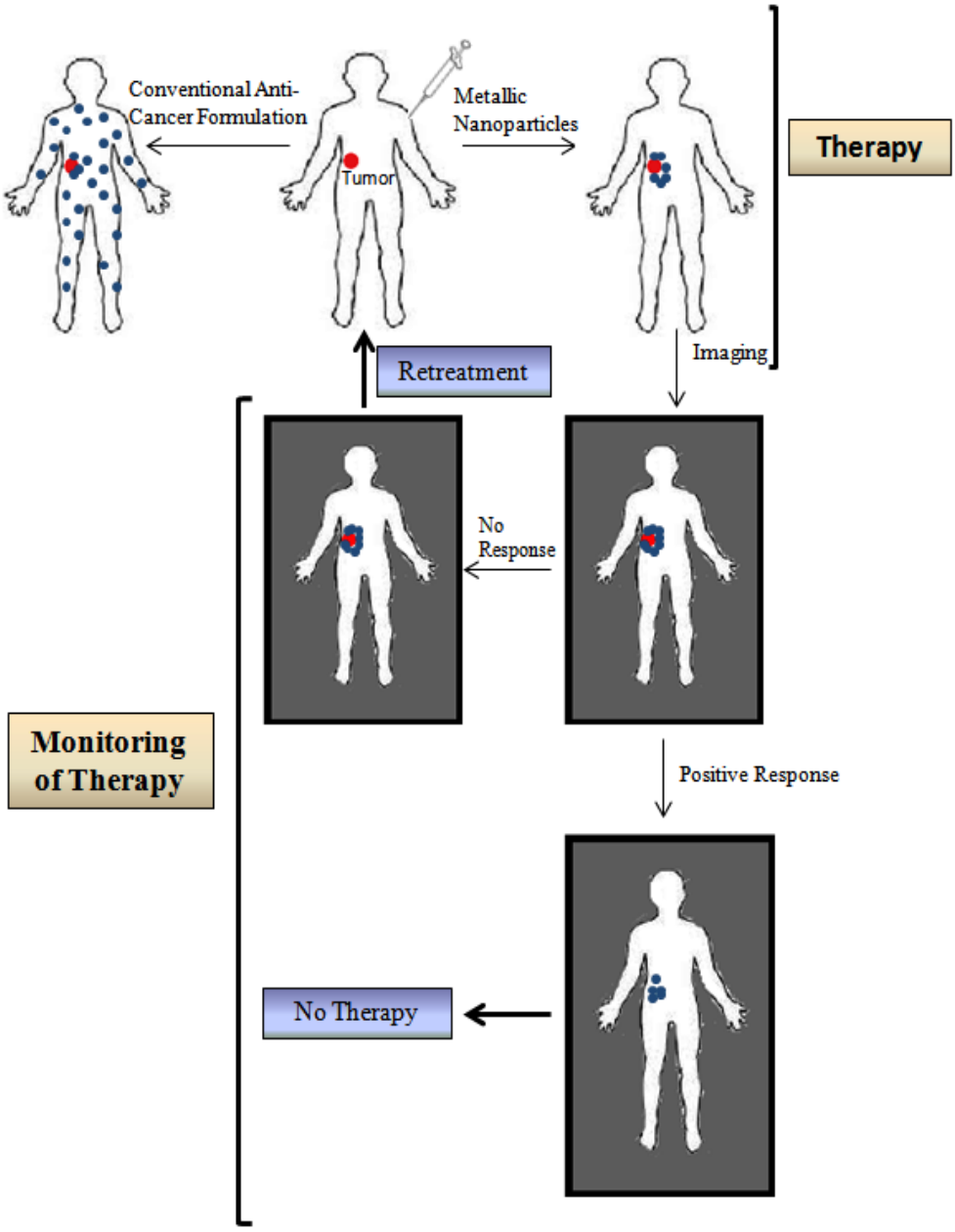

Figure 6-1 Role of theranostics in cancer therapy.

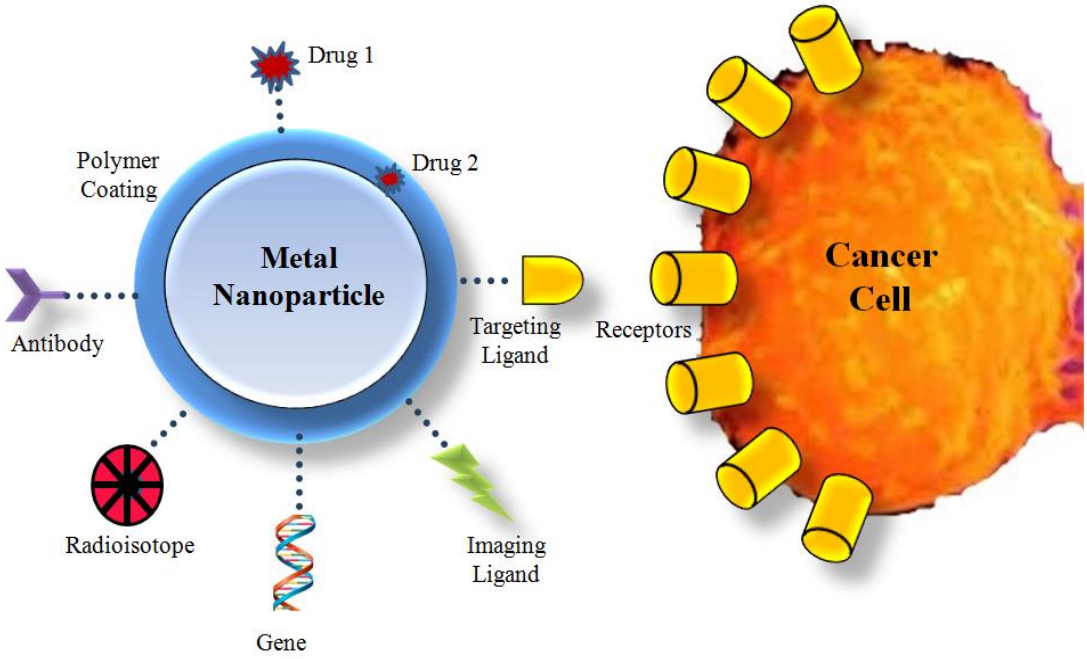

Figure 6-2 Multifunctional metal nanoparticles for cancer therapy.

Box 1: Toxicological Issues of Metal Nanoparticles

Understanding toxicity of metal nanoparticles is essential to determine potential health risks. Normal mode of action of metal nanoparticles is production of ROS. However, excessive oxidative stress can be harmful. Cell may trigger its protective mechanisms in response to elevated oxidative stress, such as enzymatic and non-enzymatic antioxidant defense mechanisms (e.g. glutathione peroxidases, catalases, superoxide dismutases). But when these protective mechanisms fail to restore cellular redox equilibrium, cellular macromolecules such as proteins, lipids, and DNA are damaged. Irreparable damage may then lead to necrosis and/or apoptosis (i.e. cell death). Excess of oxidative stress can also provoke pro-inflammatory responses, such as activation of IL-2, TNF-α etc. Chronic inflammation leads to diseases such as atherosclerosis, pulmonary diseases, and cancer. However, this concept is valid only if ROS production is the dominant mechanism of toxicity [49, 50].

Metal nanoparticles may also disturb the cellular concentration of Ca^{2+} (by increasing Ca^{2+} influx, inhibiting Ca^{2+} sequestration etc.), thereby disturbing and inhibiting the regulatory roles of balanced intracellular Ca^{2+} concentration, such as cellular metabolism, signal transduction, and gene expression [49].

Toxicity of metal nanoparticles can be overcome by passive or active targeting to the specific target site [23, 25, 28, 29, 33, 40, 41]. Other approaches like use of biodegradable polymer as a reducing and functionalizing agent can also reduce toxicity of metal

Table 6-1 Different methods for the preparation of metal nanoparticles.

Metal	Method	Principle	Ref.
Iron	Co-precipitation	Ferric and ferrous ions are mixed in 1:2 molar ratio in highly basic solutions, producing $\mathbf{Fe_3O_4}$. $2\mathbf{Fe^{3+}} + \mathbf{Fe^{2+}} + 8\mathbf{OH^-} \rightarrow \mathbf{Fe_3O_4} + 4\mathbf{H_2O}$	[52, 53]
	Microemulsion method	One microemulsion containing ferric/ferrous ions is mixed with other one containing precipitating agent.	[54]
	Hydrothermal synthesis	Water hydrolyzes and then dehydrates metal salts at high temperatures.	[52]
	Sonochemical synthesis	Sonolysis of iron precursors is done. Sonolysis of aqueous reaction medium (iron precursor + some hydroxide) causes cavitation, which bring chemical changes.	[53]
Zinc	Precipitation	Zinc precursor reacts with precipitating reagent. Precipitated ($Zn(OH)_2$) is calcined to form ZnO nanoparticles.	[55]
	Wet-chemical synthesis	Modification of precipitation method, where starch is used as stabilizing agent that adsorbs at surface of nanoparticles providing stability.	[35, 56]
	Solid-State Pyrolytic Method	Mixture of zinc acetate and sodium bicarbonate is pyrolysis.	[57]
	Sol-gel method	Zinc acetate dehydrate gets solvated and hydrolyzed in a solvent which aids removal of intercalated acetate ions. This leads to formation of colloidal–gel zinc hydroxide. Zinc hydroxide splits into Zn^{2+} and OH^-, followed by polymerization of hydroxyl complex to form ''Zn–O–Zn'' bridges, converting sol into gel. This gel finally gets transformed into Zinc oxide.	[58]
Gold	Turkevich method	Hot chlorauric acid reacts with sodium citrate. Citrate ions reduce Au^{3+} to neutral Au atoms. Gold gradually starts to precipitate from supersaturated solution in form of nanoparticles.	[59]
	Perrault method	Hydroquinone is used to reduce chlorauric acid. Improved monodispersity and shape consistency is achieved as hydroquinone has weak reduction potential.	[60]
	Block Copolymer-mediated synthesis	Au ions are reduced by block copolymer, forming Au clusters. Au ions are further reduced on surfaces of clusters for growth of Au nanoparticles. Nanoparticles are then stabilized by block copolymers.	[61]
	Brust method	Chlorauric acid reacts with tetraoctylammonium bromide (TOAB) and sodium borohydride, where sodium borohydride acts as a reducing agent and TOAB as phase transfer catalyst and stabilizing agent.	[62]
Silver	Chemical reduction	Initially, small Ag nanoparticles are produced using a strong reducing agent. Then particles are enlarged by further reduction with weak reducing agent.	[63]
	Physical synthesis	Silver bulk material is ground into silver target materials. They are vaporized to atomic level followed by condensation in presence of inert gas, and piled up to form Ag nanoparticles.	[64]
	Biological synthesis	Reducing agent is any bio source, e.g. leaf extract of *Azadirachta indica*	[65]

Table 6-2 Other metals explored for the treatment of cancer.

Metal	Formulation	Results	Ref.
Barium	Barium Titanate core-Gold shell Nanoparticles	NIR laser-induced thermoablation experiments revealed ability of nanoshells to produce hyperthermia and destroy human neuroblastoma cells	[66]
	Barium Titanate Nanoparticles	Optimal cytocompatibility of barium titanate nanoparticles was demonstrated based on noncovalent binding to glycol-chitosan. Efficiency of DOX was found to be highly enhanced	[67]
Bismuth	Bismuth Selenide nanoparticles	Nanoparticles absorbed NIR laser light producing irreversible photothermal ablation of tumors. Also exhibited strong X-ray attenuation that can be utilized for X-ray computed tomography imaging	[68]
	Barium Sulphide Nanoparticles	Enhanced visualization of breast cancer using X-ray micro Computed Tomography was achieved using Bi_2S_3 nanoparticles, modified to display a tumor homing peptide (LyP-1, CGNKRTRGC). Accumulation within tumor was increased by 260% over non-labeled nanoparticles	[69]
Calcium	pH-sensitve calcium carbonate Nanocrystals	$CaCO_3$/DOX nanocrystals exhibited high uptake by breast cancer cells, producing greater reduction in growth than free DOX	[70]
	NIR Emitting Fluorophore-Doped Calcium Phosphate Nanoparticles	Nanoparticles accumulated in solid xenograft breast adenocarcinoma tumors *via* EPR. *Ex situ* tissue imaging further verified the facility of the indocyanine green embedded nanoparticles for deep-tissue imaging	[71]
Copper	PEG coated Copper Sulfide Nanoparticles	Nanoparticles could be used both as contrast agent for photoacoustic tomographic imaging of mouse tumor vasculature and for confined photothermolysis of tumor cells	[72]
	Copper oxide Nanoparticles	Apoptotic effect of copper oxide nanoparticles was mediated by ROS generation involving disruption of mitochondrial membrane potential	[73]
Magnesium	Magnesium silicate hollow Nanospheres	Nanoparticles were mostly accumulated in lysosome, which facilitated continual drug release and efficient cancer cell destruction	[74]
Nickel	PEGylated Nickel Carbide Nanocrystals	Nanoparticles exhibited broad absorption from visible to NIR regions and rapid rise in temperature when irradiated by 808 nm laser, damaging cancer cells	[75]
	Nickel Oxide Nanoparticles	NiO nanoparticles reduced cell viability in a dose dependent manner in Hep-2 and MCF-7 cells. Oxidative stress was indicated by depletion of glutathione and induction of ROS and lipid peroxidation. Induction of caspase-3 enzyme activity and DNA fragmentation were also observed	[76]
Titanium	Titanium Dioxide Nanoparticles	Significant induction in DNA damage observed in cells exposed to nanoparticles. Expression of caspase-3 and caspase-9 mRNA was increased	[77]

8. PAPER VI

Ceramic nanoparticles: fabrication methods and applications in drug delivery

Shindu C. Thomas, Harshita, Pawan Kumar Mishra and Sushama Talegaonkar

(Accepted and Printed- Current Pharmaceutical Design)

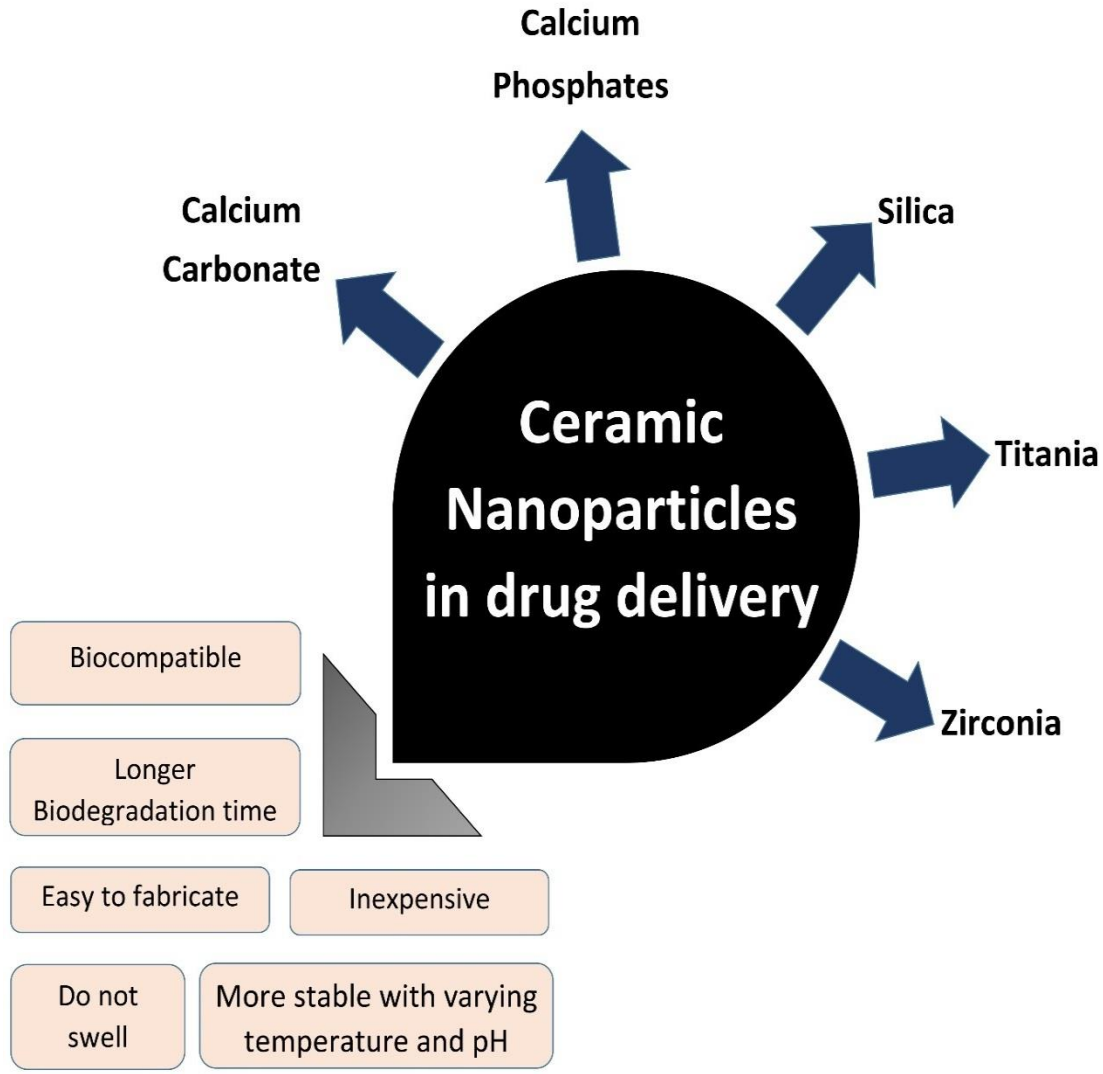

Figure 7-1 Graphical abstract.

Abstract

Ceramic nanoparticles are primarily made up of oxides, carbides, phosphates and carbonates of metals and metalloids such as calcium, titanium, silicon, etc. They have a wide range of applications due to a number of favourable properties, such as high heat resistance and chemical inertness. Out of all the areas of ceramic nanoparticles applications, biomedical field is the most explored one. In the biomedical field, ceramic nanoparticles are considered to be excellent carriers for drugs, genes, proteins, imaging agents etc. To be able to act as a good and successful drug delivery agent, various characteristics of nanoparticles need to be controlled, such as size range, surface properties, porosity, surface area to volume ratio, etc. In achieving these properties on the favourable side, the method of preparation and a good control over process variables play a key role. Choosing a suitable method to prepare nanoparticles, along with loading of significant amount of drug(s) leads to development of effective drug delivery systems which are being explored to a great extent. Ceramic nanoparticles have been successfully used as drug delivery systems against a number of diseases, such as bacterial infections, glaucoma, etc., and most widely, against cancer. This review gives a detailed account of commonly used methods for synthesising nanoparticles of various ceramic materials, along with an overview of their recent research status in the field of drug delivery.

Key Words: Ceramic nanoparticles, hydroxyapatite, calcium carbonate, silica, titania, zirconia, drug delivery, diagnostics, bone repair, bone delivery.

INTRODUCTION

Ceramic nanoparticles are inorganic systems with porous characteristics. Since these particles can be easily engineered with the desired size and porosity, keen interest has recently been shown in utilizing ceramic nanoparticles as drug vehicles. Considerable research has been done exploring typical biocompatible ceramic nanoparticles such as silica, titania, alumina etc. [1,2]. A typical classification of these particles is shown in Figure 7-1. The newly emerging area of utilising inorganic (ceramic) particles with entrapped biomolecules has potential applications in many

frontiers of modern materials science including drug delivery systems. The advantages of ceramic nanoparticles include easy preparation with desired size, shape and porosity, and no effect on swelling or porosity with change in pH [3]. In recent times, the development of new ceramic materials for biomedical applications has hastened. Nanoscale ceramics such as hydroxyapatite (HA), calcium carbonate ($CaCO_3$), zirconia (ZrO_2), silica (SiO_2), titanium oxide (TiO_2), and alumina (Al_2O_3) were made from new synthetic methods to improve their physical-chemical properties seeking to reduce their cytotoxicity in biological systems. The controlled release of drugs is one of the most exploited areas in terms of ceramic nanoparticle application in biomedicine where, the dose and size are important. Also, some features that make these nanoparticles a potential tool in controlling drug delivery are high stability, high loading capacity, easy incorporation of hydrophobic and hydrophilic systems, and different routes of administration (oral, inhalation, etc.). In addition, a variety of organic groups which may be functionalized on their surfaces allow for a directed effect [4,5].

Traditionally, ceramic nanoparticles are prepared by solid state methods, in which hydroxide, oxide, carbonate, nitrate, or sulphate raw materials are physically mixed, and then treated at high temperatures for long periods of time to enable the formation of the nanoparticles. By this method, coarse sized agglomerated particles with low surface area are formed. Use of high temperatures for the formation of solid state compound probably causes abnormal grain growth and lack of control over stoichiometry [6]. Thus, several modified chemical synthesis techniques have been developed to obtain nanoscale ceramic particles with a suitable morphology at a low temperature. The advantages and disadvantages of some common methods of synthesis are given in table 7-1.

Ceramic nanoparticles have attracted attention of researchers from the fields of chemistry, material science, pharmaceutical science and biomedical engineering due to their potential technological importance. The present article provides a comprehensive overview of the various methods of preparing commonly used ceramic nanoparticles and their applications in the field of drug and gene delivery. These ceramic nanoparticles include calcium phosphate, calcium carbonate, silica, titania and zirconia.

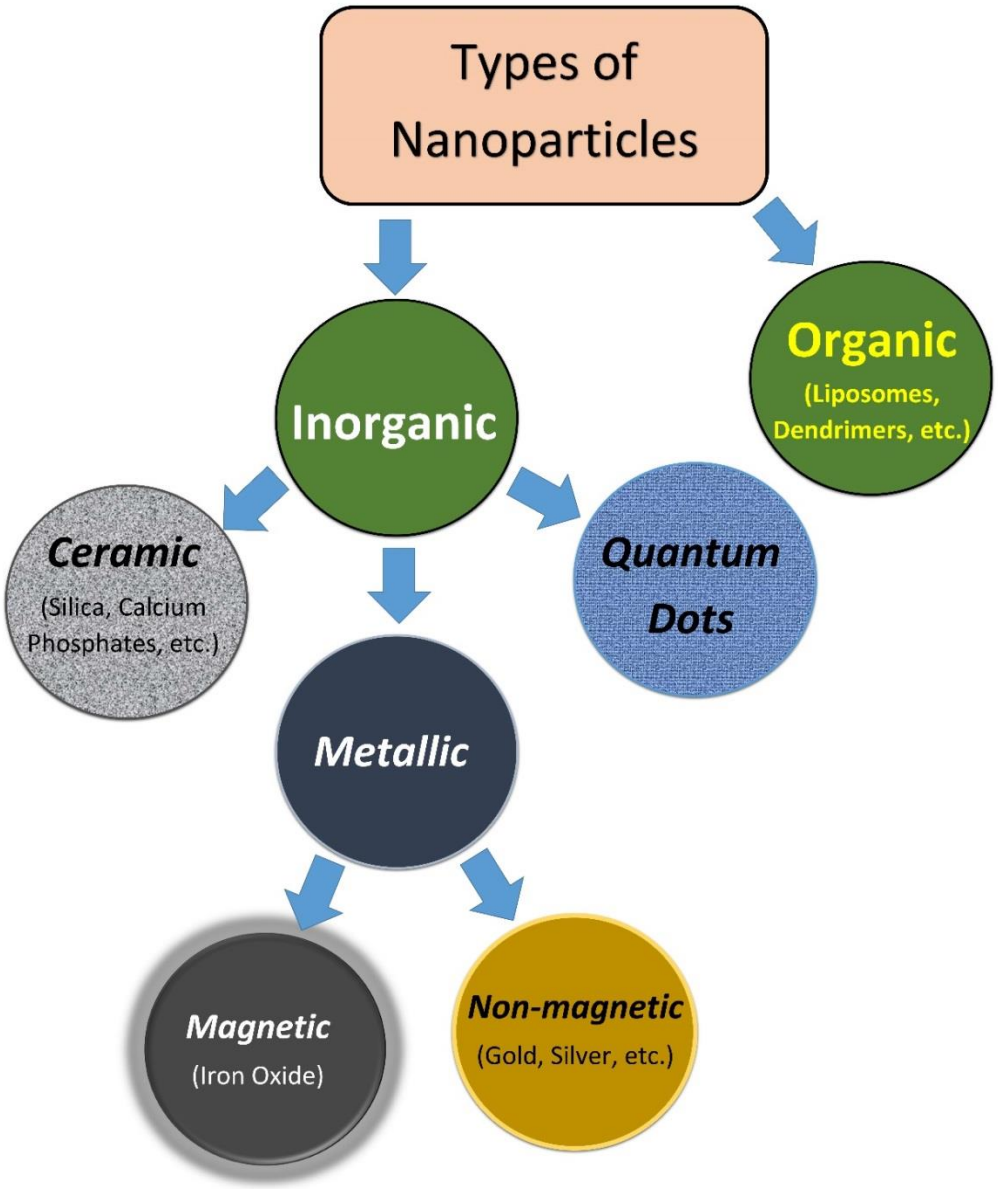

Figure 7-2 Types of inorganic nanoparticles.

Inorganic nanoparticles are made up of materials that do not contain carbon (with a few exceptions such as calcium carbonate). These are further classified into ceramic and metallic nanoparticles. Ceramic nanoparticles are based on materials that have properties lying between metals and non-metals. They usually have low electrical and thermal conductivity, high elastic modulus, high stiffness and are resistant to corrosive environments. The properties are dictated by the type of bonding between their

constituent atoms, which is a combination of ionic and covalent bonds. Metallic nanoparticles are made up of metals that have weaker bonds between the atoms, allowing free movement of electrons; hence they are excellent conductors of heat and electricity. Metals can be easily deformed and are vulnerable to corrosive damage. Metallic nanoparticles can be further classified on the basis of their magnetic properties. Quantum dots are semiconductors, which are made up of metals of group 16 of the periodic table. In terms of rate of degradation inorganic nanoparticles and metallic nanoparticles are less susceptible to degradation than organic nanoparticles [4]. Nanoparticles have also been prepared using a combination of these materials so as to enhance certain properties such as biocompatibility, drug release behaviour, therapeutic effect, etc. Examples of combining different materials to prepare nanoparticles for suitable applications are discussed in later sections of this review.

Table 7-1 Advantages and disadvantages of some common methods for synthesising bioceramic nanoparticles.

Methods	Advantages	Disadvantages
Sol-gel method	• Product synthesized at low temperatures, hence saving energy. • Products formed have better chemical and structural homogeneity and purity than those obtained by conventional methods.	• Raw materials such as metal alkoxides make the process expensive. • Close control over nucleation and growth of particles is required to obtain agglomeration free powder with desired characteristics.
Chemical precipitation method	• Convenient processing. • Large yield; suitable for industrial production. • Use of inexpensive reagents. • Products with variable phase composition can be obtained.	• It is difficult to prepare products with desirable size, high purity and accurate stoichiometry
Reverse microemulsion method	• One of the few techniques to deliver a particle size in the range of nanometres with minimal agglomeration.	• Use of a large amount of oil and surfactant. • Low yield. • Difficulty in removal of surfactants from the final products.

		• High production costs.
Hydrothermal synthesis	• Low temperature alternative to conventional powder synthesis techniques. • Particle size, morphology, structure, phase composition, and chemical properties can be controlled by varying experimental parameters such as temperature, pressure and starting materials.	• Prior knowledge on solubility of starting materials is required. • Hydrothermal slurries are potentially corrosive. • Cannot observe the crystallisation process directly since the process takes place in a hydrothermal reactor.
Mechanochemical method	• Suitable for obtaining large quantities of product. • The process is relatively simple with only a few operational parameters. • Technique is useful in obtaining agglomeration free ultrafine particles.	• Risk of possible contamination by components of the ball mill. • Wear and tear to the components of the ball mill increases the cost of production.
Combustion synthesis	• The process is energy saving, carried out at low temperatures and completes in a short period of time. • Economic advantages such as use of cheap oxide reactants. • Better control of stoichiometry.	• Contamination by carbonaceous residue. • Proper understanding of the reaction mechanism is needed to perform combustion in a controlled manner so as to obtain the desired products. • Careful selection of raw materials is essential for effective combustion reaction.

HYDROXYAPATTITE (CALCIUM PHOSPHATE) NANOPARTICLES

Calcium phosphates are suitable to be used as a carrier for drugs, non-viral gene delivery, antigens, enzymes, and proteins. Calcium phosphate nanoparticles provide the following advantages [7-9]:

- Deliver drugs in minimally invasive manner just as polymeric nanoparticles. Easy to fabricate and inexpensive
- Longer biodegradation time
- Do not swell or change porosity
- Stable upon variation in temperature and pH
- Possess same chemistry, crystalline structure and size as the constituents of targeted tissues
- Fabrication methods enhance their bioavailability and biocompatibility even before releasing drugs

Table 7-2 Different types of calcium phosphates (14-17)

Phase	Chemical formula	Ca/P molar ratio	Density	Crystal Structure	K_{sp} at 37 °C	Melting Point (°C)
Amorphous Calcium Phosphate (ACP)	$Ca_3(PO_4)_2$	1.3–1.5	0.92–1.75	Amorphous	#	Transforms to more stable phase.
Monocalcium Phosphate Monohydrate (MCPM)	$Ca(H_2PO_4)_2 \cdot H_2O$	0.5	2.22	Triclinic	0.14	42
Monocalcium Phosphate Anhydrous (MCPA)	$Ca(H_2PO_4)_2$	0.5	2.546	Triclinic	0.14	109
Dicalcium Phosphate Dihydrate (DCPD)	$CaHPO_4 \cdot 2H_2O$	1	2.32	Monoclinic	0.66	Decomposes and transforms to more stable phase.

Dicalcium Phosphate Anhydrous (DCPA)	$CaHPO_4$	1	2.929	Triclinic	0	Decomposes and transforms to more stable phase.
Calcium Pyrophosphate (β-CPP)	$Ca_2P_2O_7$	1	3.09	Amorphous	4.9	1230
Tricalcium phosphate (α-TCP)	$Ca_3(PO_4)_2$	1.5	2.86	Monoclinic	5.5	1391
Tricalcium phosphate (β-TCP)	$Ca_3(PO_4)_2$	1.5	3.07	Rhombohedral	9.5	Decomposes and transforms to α-TCP
Tetracalcium phosphate (TTCP)	$Ca_4(PO_4)_2O_9$	2	3.05	Monoclinic	7.5	Decomposes and transforms to Hydroxyapatite
Octacalcium Phosphate (OCP)	$Ca_8H_2(PO_4)_6{\cdot}5H_2O$	1.33	2.61	Triclinic	7.4	Decomposes and transforms to Hydroxyapatite
Hydroxyapatite (HAP)	$Ca_{10}(PO_4)_6(OH)_2$	1.67	3.16	Pseudohexagonal	17.3	1670

cannot be determined, since it is unstable in water.

Calcium phosphates are abundant in nature, especially in calcified tissues of vertebrate. The inorganic mineral in bone was determined and clarified as carbonated apatite in early 20^{th} century [10]. The constituting building blocks of bone are composites of biological apatite and molecules of collagen [11, 12]. Hydroxyapatite (HAP) is a type of calcium phosphate that has a similar chemical structure to bone mineral, and hence has excellent biocompatibility, bioactivity, and high affinity to

protein, chemotherapy drugs, and antigens. Apart from hydroxyapatite, other type of calcium phosphates are also used (table 7-2) for e.g.: amorphous calcium phosphate, dicalcium phosphate, etc., which differ chemically on the basis of their calcium to phosphate ratio and hence their physical and mechanical properties also differ. For e.g. Amorphous calcium phosphate is unstable at room temperature and readily transforms to hydroxyapatite. They are also easily hydrolysed to hydroxyapatite when dissolved in water. Tricalcium phosphates are resorbable materials that are also similarly hydrolysed into the more stable hydroxyapatite but at a slower rate. In contrast, hydroxyapatite has strong bioactivity and is able to resist hydrolytic degradation. Thus hydroxyapatite is more stable and is an excellent choice for sustained or controlled delivery of drugs [13].

Methods of preparation

1) Wet chemical deposition

Wet chemical precipitation from a solution is the most common route for synthesising hydroxyapatite which evolves from a chemical reaction between inorganic oxide solutions [18, 19]. Hydroxyapatite nanocrystal suspension was prepared by a wet chemical precipitation reaction as proposed by Bouyer et al, employing the chemical reaction between calcium hydroxide and hydrogen phosphate, yielding nanocrystals of hydroxyapatite.

$$10Ca(OH)_2 + 6H_3PO_4 \rightarrow Ca_{10}(PO_4)_6(OH)_2 + 18H_2O$$

The rate of addition of the reactants, the reaction temperature and pH affect the shape, size and specific surface area of the nanoparticles obtained by this method. The reactant addition rate determines the purity of the synthesized hydroxyapatite and is strongly linked to the pH obtained at the end of the synthesis [7, 18]. The reaction temperature determines whether the crystals are monocrystalline or polycrystalline. Synthesis carried out at low temperatures (lesser than 60°C) will result in monocrystalline nanoparticles. Hydroxyapatite nanocrystals synthesised above this temperature become polycrystalline [18]. Oner and Uysal synthesised HAP particles by wet chemical synthesis under controlled temperature, pH, and atmospheric conditions. The nanoparticles were found to be having particle sizes of less than 100nm [20].

Wet chemical deposition method offers several advantages, such as, simple processing route, large yield, suitability for industrial production, use of inexpensive reagents, and calcium phosphate products with variable phase composition can be obtained. However, multiple process parameters (such as pH of the reaction mixture, reaction temperature, etc.) must be controlled so as to obtain the product with the desired properties [21].

2) Biomimetic deposition

In this method, metastable synthetic body fluids (SBF) are used for preparing hydroxyapatite. These fluids have an inorganic salt composition similar to that of human plasma and facilitate the spontaneous nucleation and growth of a nanosized, carbonated and "bone-like" calcium hydroxyapatite at physiological temperature and pH [22].

SBF prepared according to the chemical analysis of human body fluid, with ion concentrations nearly equal to the inorganic constituent of human blood plasma, were first used by Kokubo et al to prove the similarity between in vitro and in vivo behaviour of certain glass-ceramic compositions [22]. In these studies, the glass-ceramic samples were soaked in SBF solutions and their surfaces coated with a poorly crystallized calcium-deficient and carbonate containing apatite similar to bone apatite [23]. Studies have been conducted in which carbonated and "bone-like" calcium apatite have been spontaneously generated and grown on silica or titania gels, bioglass and titanium samples immersed in synthetic body fluids at physiological pH and temperatures [24-28]. Formation and the presence of such carbonated apatite layer has been proven to promote in vitro cell differentiation in a mineralizing chondrocyte cell culture system [29]. The composition of SBF prepared by Tas et al is similar to the one prepared by Kokubo et al except that $Na_2HPO_4.2H_2O$ has been used instead of $K_2HPO_4.2H_2O$ resulting in an increase in bicarbonate ion concentration(from 4.2mM to 27mM, similar to the plasma bicarbonate concentration) and a decrease in chloride ion concentration to value closer to the plasma chloride ion concentration [30].

Tas et al obtained nanosized and chemically homogenous hydroxyapatite from calcium nitrate tetra hydrate and diammonium hydrogen phosphate salts dissolved in the modified SBF (in comparison to the one prepared by Kokubo et al) at 37 °C and with a pH of 7.4. In addition, these powders contained traces of other inorganic ions provided

and incorporated by the SBF. The average grain sizes of this powder after sintering remained sub-micron [30].

It is a low temperature process applicable to any heat sensitive substrate including polymers [31]. Bone like apatite crystals are formed that have high bioactivity and good resorption characteristics [32]. Apatite is deposited evenly on, or even into porous or complex implant geometrics [28]. It can also incorporate bone-growth-stimulating factors. But the rate of deposition is very slow [33].

3) Surfactant based emulsions (microemulsions) method

A microemulsion is a thermodynamically stable transparent solution of two immiscible liquids such as water and oil stabilized by an amphiphilic surface-active agent or surfactant. Generally, they are prepared by dispersing the water phase (having a high dielectric constant) under agitation into an oil phase (having low dielectric constant). Addition of a surfactant is necessary to control interfacial tension between the two immiscible phases. In the case of a water-in-oil microemulsion, reverse micelles are formed when the aqueous phase is dispersed as microdroplets surrounded by a monolayer of surfactant molecules in the continuous hydrocarbon phase. These microdroplets of water act as microreactors or nanoreactors in which reactions are conducted. These spatially and geometrically restricted, self-assembling media of reverse micelles can be used in the synthesis of nanophase materials without much agglomeration and with high surface area [34].

The aqueous phase contains both the calcium and phosphate precursors as in the method followed by Bose et al [34]. However it is also possible to use an aqueous phase which contains only the calcium precursor while the phosphate precursor is added as an aqueous solution to the prepared emulsion as in the method followed by Lim et al [35]. Bose et al prepared a microemulsion by dispersing aqueous solutions of calcium nitrate and phosphoric acid into the organic phase containing cyclohexane and surfactant. The two phases were mixed to obtain the reverse micelle systems. The emulsion was converted into a transparent gel during mixing and stirring. The emulsion was evaporated. The mass was then dried for several hours to obtain hydroxyapatite precursor powders. They were able to prepare powders with a surface area of 130 m^2/g and particle size between 30 to 50 nm with needle shape and spherical morphology [34].

The composition of the micro emulsion system, pH, aging time and temperature, and the metal ion concentration have a significant effect on the formation of hydroxyapatite nanopowder as well as on their surface area and morphology. For e.g.: the morphology changed from needle shape to nearly spherical when the aqueous/ organic phase volume ratio in the emulsion was decreased [34].

Microemulsion method has been shown to be one of the few techniques which are able to deliver a particle size in the range of nanometres with minimum agglomeration [36-39]. Disadvantages associated with this method are the use of a large amount of oil and surfactant and low yield [40].

4) Sol-Gel process

In this soft chemistry route, the metal alkoxides convert to amorphous gels of metal oxides through hydrolysis and condensation reactions. Liu et al successfully synthesized hydroxyapatite using the sol-gel process at lower temperatures. A two-step procedure was employed. Triethyl phosphite was initially hydrolysed with water, followed by the addition of an aqueous calcium nitrate solution. Subsequently, the amorphous gel transformed into a well crystallized apatite at relatively low temperatures (300-400°C). The calcinated gels showed a nanoscale microstructure, with grains of 20-50 nm diameters. Appropriate heat treatment between 300 and 400 °C resulted in preparation of apatite exhibiting a nanoscale size, low crystallinity, carbonated apatitic structure, resembling that of human bone apatite. The final product and the optimum synthesis conditions such as calcination temperature largely depend on chemical nature of the precursors [41].

The sol–gel materials are transformed to ceramics by heating at relatively low temperatures and have better chemical and structural homogeneity than those obtained by conventional methods [42]. The sol-gel method offers a molecular-level mixing of the calcium and phosphorus precursors, which is capable of improving the chemical homogeneity of the resulting hydroxyapatite to a significant extent. A number of calcium and phosphate precursor combinations have been employed for sol-gel synthesis [7].The major limitation of the sol-gel technique is linked to the possible hydrolysis of phosphates [43].

5) Electrodeposition

Ultrafine-grained hydroxyapatite coatings can be obtained from electrocrystallization of dilute electrolyte solutions containing Calcium and phosphate ions at physiological pH. At these low supersaturations, hydroxyapatite is precipitated without a precursor phase formation.

Shirkhanzadeh along with his co-workers prepared hydroxide nanoparticles through electrodeposition. The electrolyte solution was prepared by dissolving $Ca(NO_3)_2$ and $NH_4H_2PO_4$ in deionized water. $NaNO_3$ was used to improve ionic strength of the electrolyte. The pH of the electrolyte was adjusted such that in all cases electrolyte was saturated with respect to hydroxyapatite. The electrodeposition of calcium phosphate was carried out for 2hr at 85°C. Plate-like crystals of 4-6 μm that deviated markedly from stoichiometric hydroxyapatite were precipitated from the acidic electrolyte and deposited. At very low concentrations of calcium and phosphate ions and physiological pH, nanophase hydroxyapatite is deposited directly on the cathode [44].

The ionic strength and the pH of the electrolyte solution play an important role. The process is carried out at room temperature, and has advantages such as: uniformity of the deposited layer, substrates with different shapes can be used, good control over deposition thickness and quality, and low energy consumption. The main shortcoming of the electrochemical method is that electrolysis of water causes hydrogen bubbles to form on the cathode which obstruct the nucleation and growth of crystals and can also dislodge the crystals already deposited. Hence, dense and adherent coatings are difficult to obtain [45, 46].

6) Mechanochemical synthesis

Mechanochemical synthesis were originally designed for oxide dispersion-strengthened (ODS) alloys [47]. Over the past 20 years, they have grown, diverged and are now used for the fabrication of a wide range of advanced materials, both metallic and non-metallic in composition. Hydroxyapatite has also been synthesized using this method. In this method, chemical reactants react in a ball mill to form the product and size reduction takes place by impact of the balls in the mill.

Yeong et al synthesised hydroxyapatite by using anhydrous calcium hydrogen phosphate and calcium oxide. Appropriate amounts of the two starting materials at a molar ratio of 3:2 were mixed together in a conventional ball mill. The powder mixture was then subjected to mechanical activation carried out in a high-energy shaker mill.

The powder derived from mechanical activation was de-agglomerated in ethanol in order to remove hard agglomerates. The powder was then uniaxially pressed into pellets in a hardened steel die of 10 mm in diameter at a pressure of 25 MPa, followed by isostatic pressing at a pressure of 345 MPa, prior to sintering at 1200°C. Sintered hydroxyapatite pellets were obtained. The resulting hydroxyapatite powder exhibited an average particle size of 25 nm [48]. The nanoparticle properties depend on the amount of reactants in the ball mill and the speed of rotation of the mill. Mechanochemical processing is particularly suitable for obtaining large quantities of product. However, there is a risk of possible contamination by components of the ball mill.

Application of calcium phosphate in Drug Delivery

Calcium phosphate, especially hydroxyapatite has been widely used in treatment of bone diseases such as osteoporosis. These are also being explored as drug carriers for the treatment of cancer and other diseases. The formulated delivery systems were able to prolong drug release due to very low rate of degradation of hydroxyapatite (at neutral or alkaline pH) and possessed excellent biocompatibility [17]. Hydroxyapataite has also been combined with other materials in order to enhance its therapeutic effect and drug release. Sarath et al., 2012 prepared 5- Fluorouracil and Amoxicillin loaded iron doped hydroxyapatite nanoparticles with enhanced bioactivity and prolonged drug release [49]. Superparamagnetic iron-hydroxyapatite nanoparticles were prepared by Panseri et al., 2012. These nanoparticles possessed excellent biocompatibility and also increased osteoblastic cell proliferation on exposure to a static magnetic field [50]. Similar results of accelerated bone tissue formation were observed by using biocompatible super-paramagnetic responsive nanofibrous scaffolds made up of polylactic acid, iron-oxide and hydroxyapatite nanoparticles in rabbits by Meng et al [51]. Nanocomposites prepared by combining hydroxyapatite, magnetite and carbon nanotubes containing clodronate were prepared by Pistone et al and were found to have a durable inhibitory effect on osteoclasts [52]. A pH responsive targeted drug delivery system was prepared by Dalong et al., 2015 by using lactobionic acid-conjugated bovine serum albumin linked to hydroxyapatite via 4-carboxyphenylboronic acid. An enhanced cell uptake in liver carcinoma cells and preferential drug release in acidic conditions was observed [53]. Hydroxyapatite has also been combined with magnetite and silica to develop a pH responsive drug delivery system [54]. Thermal responsive nanoparticles prepared by

grafting poly(N-isopropylacrylamide) via surface initiated atom transfer radical polymerisation were prepared by Wei et al. This thermal responsive system was found to have enhanced bioactivity [55]. Various studies demonstrating their targeting, controlled/sustained drug and gene delivery potential are further summarized in tables 7-3 to 7-7.

Table 7-3 Applications of calcium phosphate nanoparticles in anticancer drug delivery.

Product	Challenge	Inference	Reference
Paclitaxel attached to Hydroxyapatite-PEG-FA	Low water solubility, hypersensitivity reactions and other systemic toxic effects of paclitaxel	Drug release profile showed an initial burst release and a later sustained drug release. These nanoparticles containing folic acid could be used to successfully target tumour cells expressing folate receptors.	[56]
Docetaxel loaded Amorphous Calcium Phosphate porous nanospheres	Systemic toxic effects of Docetaxel.	Prepared porous nanospheres were efficient for anticancer drug-loading and sustained release. The ACP porous nanosphere drug-delivery system showed high ability to damage tumour cells after loading with docetaxel.	[57]
Iron-Doped Nanosize Hydroxyapatite loaded with Amoxicillin and 5-Fluorouracil	Systemic toxic effects of 5-FU	Drug release studies showed that Fe^{3+} doping at a low concentration leads to highly prolonged drug release. Fe^{3+} doping also led to an increase in the bioactivity.	[49]
Celecoxib loaded Hydroxyapatite Chitosan nanocomposites	Poor water solubility, rapid plasma elimination, cardiovascular risk and other toxic effects of celecoxib	Nanoparticles showed high encapsulation efficiency, sustained release patterns, desirable hemocompatibility, enhanced cytotoxicity on HCT 15 colon cancer cells and time dependent cytoplasmic uptake of nanoparticles by HCT 15 and HT 29 cells. In vivo studies proved that drug loaded nanoparticles were more potent in inhibiting tumour growth than free celecoxib with no serious side effects.	[58]
Paclitaxel loaded-aspragalan calcium phosphate nanoparticles	Low water solubility, hypersensitivity reactions and other systemic toxic effects of paclitaxel	Release behaviour of drug showed a biphasic pattern characterised by an initial burst release followed by a slower and continuous release. In-vivo study showed tumour inhibition effect on hepatocarcinoma with few side effects.	[59]
Cisplatin loaded calcium phosphate nanoparticles	Systemic toxic effects of cisplatin	In vitro drug release studies showed sustained release of cisplatin. In vitro cytotoxicity testing showed that the cisplatin released from nanoconjugates retained complete activity during conjugation and release and had comparable cytotoxicity to the free drug.	[60]

Cisplatin, DPM (di(ethylene diamineplatinum) medronate), and Alendronate loaded Hydroxyapatite nanoparticles.	Systemic toxic effects of cisplatin and DPM.	It was found that Hydroxyapatite nanocrystals could be modulated so as to produce HA/biomolecule conjugates suitable for specific therapeutic applications.	[61]

Table 7-4 Applications of calcium phosphate nanoparticles in anticancer drug delivery.

Product	Challenge	Inference	Reference
Methylene blue loaded calcium phosphate nanoparticles.	Rapid enzymatic reduction in body	Methylene blue loaded calcium phosphate nanoparticles prevented enzymatic reduction of the dye. When tested against human breast cancer cells, PDT efficiency was significantly enhanced.	[62]
Calcium phosphate reinforced photosensitizer loaded (Chlorin e6 (Ce6))	Nonspecific cytotoxic action of Ce6	Calcium phosphate mineral layer effectively inhibited Ce6 release from Ce6-loaded mineralized nanoparticles at physiological pH value. At an acidic endosomal pH value of 5.0, Ce6 release was enhanced, owing to rapid dissolution of calcium phosphate minerals. Upon irradiation of Ce6 nanoparticle treated MCF-7 breast-tumour cells, cell viability dramatically decreased with increasing irradiation time. The phototoxicity of Ce6 loaded nanoparticle was much higher than that of free Ce6. Nanoparticles exhibited enhanced tumour specificity compared with free Ce6 and Ce6-loaded nonmineralized polymer nanoparticles.	[63]
Calcium phosphate nanoparticles surface functionalized with poylethylenimine, Methylene blue and 5,10,15,20-tetrakis(3-hydroxyphenyl)-porphyrin (mTHPP)	Nonspecific cytotoxic action of photoactive dye	A high photodynamic activity (killing) together with a very low dark toxicity was observed for HIG-82 and for J774.1 cells at 2 µM dye concentration.	[64]

Table 7-5 Applications of calcium phosphate nanoparticles in bone diseases and bone repair

Product	Challenge	Inference	Reference
Hydroxyapatite-PLGA-PEG nanoparticles of Risedronate	High doses of drug required for therapeutic effect	PEG-PLGA-RIS-HA nanoparticles showed significant enhancement in bone micro-architecture when compared to risendronate monotherapy.	[65]
Nano-hydroxyapatite	Difficulty in delivery of vancomycin to bone	Vancomycin was loaded efficiently on the surface of HAP particles and could be	[66]

particles as carriers for vancomycin hydrochloride	surface	released slowly. Can be utilised in arthroplasty to overcome deep infection in a simple and direct manner.	
Bone morphogenetic protein-2 (BMP-2) loaded hydroxyapatite nanoparticles	Challenging implantation of scaffold for continuous release of repair protein	In both in vitro and in vivo studies, porous scaffold displayed good shape memory recovery from compressed shape with deformed pores of 33 μm diameter to recover its porous shape with original pores of 160 μm diameter. In vitro cytotoxicity study revealed good cytocompatibility. In vivo micro-CT and histomorphometry results demonstrated that the porous scaffold could promote new bone generation in the rabbit mandibular bone defect.	[67]
Clindamycin loaded calcium phosphate nanoparticles	Repetitive administration of antibiotic is required in osteomyelitis	Calcium phosphate nanoparticles enabled localised delivery and sustained release of antibiotic, so as to eliminate the need for repetitive administration of systemically distributed antibiotics and controllably dissolving itself, so as to promote natural remineralisation of the portion of bone lost to osteomyelitis.	[14, 68]
Risedronate absorbed hydroxyapatite nanoparticles	High doses of drug required for therapeutic effect.	Drug loaded nanoparticles have a therapeutic advantage over risendronate administered alone. A significant increase in bone quality and mechanical properties was observed.	[69]
Iron-Doped Nanosize Hydroxyapatite loaded with Amoxicillin and 5-Fluorouracil	Repetitive administration of amoxicillin is required in Osteomyelitis, while 5-FU has systemic toxic effects	Drug release studies showed that Fe^{3+} doping at a low concentration leads to highly prolonged drug release. Fe^{3+} doping also led to an increase in the bioactivity. Antibacterial efficacy as determined against E. coli, S. aureus, and S. epidermidis showed utility in treatment of bone and joint infections.	[49]
Bone Morphogenetic Protein-2 (BMP-2) loaded Hydroxyapatite nanoparticles	During the process of bone formation, continuous release of BMP-2 is extremely important	The release profile showed that the release of BMP-2 could be sustained for over 15 days.	[70]
Cisplatin, DPM (di(ethylene diamineplatinum) medronate), and Alendronate loaded Hydroxyapatite nanoparticles	Systemic toxic effects of cisplatin and DPM; high amounts of alendronate are needed for therapeutic effect	It was found that Hydroxyapatite nanocrystals could be modulated so as to produce HAP/biomolecule conjugates suitable for specific therapeutic applications.	[61]

Table 7-6 Applications of calcium phosphate nanoparticles in delivery of miscellaneous agents.

Product	Challenge	Inference	Reference
Chlorhexidine hexametaphosphate loaded Hydroxyapatite nanoparticles	Unsustained release of chlorhexidine from conventional dosage forms	Chlorhexidine release from nanoparticles was 2-3x greater, and sustained for a longer period of time, in comparison to aqueous solution containing chlorhexidine. Nanoparticles increased both the local dose and duration of chlorhexidine delivery.	[71]
Bovine Serum Albumin loaded Hydroxyapatite nanoparticles.	Higher concentration is required for therapeutic effect	Release of BSA from mesoporous hydroxyapatite nanoparticles was regulated by environmental pH, a faster release was observed in an acidic environment which could be established by osteoclasts.	[72]
Lactose coated calcium phosphate particles for pimozide delivery	Very low aqueous solubility of pimozide	Pimozide loaded aquasomes were prepared consisting of a calcium phosphate core, coated with lactose sugar and the drug was absorbed onto the sugar layer. Release studies showed greater dissolution than that of pure drug.	[73]
Hydroxyapatite nanoparticles added to Calcium hydroxide cements.	Calcium hydroxide cements have disadvantages like high solubility, no adhesive qualities and low mechanical strength.	Addition of Hydroxyapatite nanoparticles improved the mechanical strength of the cement and increased the Ca^{2+} release rate without compromising its antibacterial behaviour.	[74]
Hollow mesoporous Hydroxyapatite nanoparticles loaded with fluorescein isothiocyanate.	Low uptake by breast cancer cells.	The dye loaded nanoparticles were taken up by the cells and remained in the cytoplasm for adequate period of time with high biocompatibility.	[75]
Methazolamide loaded Hydroxyapatite nanoparticles.	Systemic side effects of methazolamide and its insolubility in aqueous tear fluid limiting ocular bioavailability	In-vitro studies showed diffusion controlled release over a period of over 4 hours. In-vivo studies indicated lowering of intra ocular pressure for a period of 18 hours. Formulation was physically stable.	[76]
Insulin loaded PEGylated calcium phosphate nanoparticles	Inconvenience of subcutaneous insulin delivery	PEGylated calcium phosphate nanoparticles were highly compatible with insulin and could deliver insulin in a sustained manner in the physiological pH of the intestine with no degradation or conformational changes of entrapped insulin with no cytotoxicity.	[59]
Hydroxyapatite and Amorphous Calcium Phosphate nanoparticles.	Large sized (more than 100 nm) Hydroxyapatite and Amorphous Calcium Phosphate particle are not useful in enamel repair.	Nanosized Hydroxyapatite and Amorphous calcium phosphate (20-30 nm) were found to be effective anticaries agents.	[77]

Table 7-7 Applications of calcium phosphate nanoparticles in gene delivery.

Product	Inference	Reference
Calcium phosphate nanoparticles loaded with pBI121 harbouring green fluorescent protein.	Nanoparticles successfully delivered pBI121 harbouring GFP driven by 35S promoter-encoding plasmid DNA into tobacco cells. These studies revealed significant efficacy of calcium phosphate nanoparticles in non-viral gene delivery in tobacco plant transformation and proved to be a novel system for plant genetic modification.	[78]
Calcium phosphate nanoparticles loaded with siRNA stabilized by a conjugate of dopa and hyaluronic acid (HA)	Superior ability of Calcium phosphate /siRNA/dopa-HA to maintain integrity of encapsulated siRNA and stability in solution of nanoparticles allow the formulation to achieve improved intratumoural accumulation of siRNA and a high level of target gene silencing in solid tumours after systemic administration.	[79]
hTERT siRNA encapsulated hybrid nanoparticles of PEG-CMCS(carboxy methyl chitosan) and calcium phosphate	After intravenous injection in tumour-bearing BALB/c nude mice, the nanoparticles specifically accumulated into tumour regions by EPR effect, leading to efficient and specific gene silencing sequentially. Nanoparticles inhibited tumour growth significantly via silencing hTERT expression and inducing cell apoptosis in HepG2 tumour xenograft.	[80]
Calcium phosphate nanoparticles loaded with luciferase and lacZ reporter gene	Transfected, transplanted meniscal fibrochondrocytes adhered to meniscal tissue and continued to express the transgene for at least five days following transfection. These results are of value for combining gene therapy and cell transplantation approaches as a means to enhance meniscal repair.	[81]
Calcium phosphate nanocapsule including plasmid DNA complexes as a durable gene transfection system	Nanoparticles degraded slowly, and released DNA complex in body. By this slow-releasing system, significant tumour-growth suppression and, finally, complete tumour disappearance was observed after single intratumoural injection.	[82]
Alginate hydrogels containing preosteoblastic cells and calcium phosphate–DNA nanoparticles	Sustained release of DNA was observed. MC3T3-E1 preosteoblast cells exhibited capability to form bony tissue in as little as two and half weeks when mixed with DNA nanoparticles encoding for BMP-2 into alginate hydrogels and injected subcutaneously in the backs of mice.	[83]
Calcium phosphate nanoparticles combined with suicide genes yCDglyTK	Expression of yCDglyTK was detected in implanted CNE-2 tumours by reverse transcription-polymerase chain reaction (RT-PCR) analysis when CNE-2 tumour was treated with an intratumoural injection of the CPNP-yCDglyTK complex.	[84]
BMP-2 Plasmid DNA/chitosan encapsulated PLGA/Hydroxyapatite scaffolds	The scaffolds were found to have higher cell attachment, cell viability and desirable transfection efficiency of DNA.	[85]
Green fluorescence protein EGFP-N1 plasmid DNA absorbed on Hydroxyapatite nanoparticles.	The DNA–nanoparticle complexes transfected the SGC-79TM. In vivo studies found no acute toxic effect. Biodistribution and expression within the cytoplasm and a little in the nuclei of the liver, kidney and brain tissue cells was also observed.	[86]
Galactopyranoside-tagged calcium pSVbGal plasmid DNA encapsulated in calcium phosphate nanoparticles	Galactopyranoside moiety served as a surface ligand for recognizing asialoglycoprotein receptor on liver cells. Preferential expression of β-Galactosidase was seen more in the liver tissue as compared to lung, spleen and muscle.	[87]

CALCIUM CARBONATE NANOPARTICLES

Calcium carbonate nanoparticles are also found abundantly in nature like calcium phosphates, for e.g. in bones, egg shells, etc. They also possess similar advantages such as biocompatibility, easy fabrication in to nanoparticles, inexpensive, slow biodegradability etc. There are usually three polymorphic forms of calcium carbonate, ranked in order of decreasing thermodynamic stability, calcite, aragonite and vaterite. Calcite is thermodynamically stable under ambient conditions, while aragonite is formed under high pressures and is less stable. Calcite and aragonite are the preferred phases for therapeutic applications. Needle-like aragonite has drawn much attention among material scientists due to its unique properties and potential applications [88, 89].

Methods of preparation

1) Reactive precipitation

Calcium carbonate nanopowder can be precipitated by a chemical reaction between reactants such as calcium chloride and sodium carbonate. There are two basic precipitation methods reported in the literature for synthesising calcium carbonate with the only difference being the chemicals used. The first method consists of bubbling calcium hydroxide ($Ca(OH)_2$) aqueous solutions with CO_2 to form $CaCO_3$.

$$Ca(OH)_2 + CO_2 \rightarrow CaCO_3 + H_2O$$

The alternative method uses a mixture of sodium carbonate (Na_2CO_3)and calcium chloride ($CaCl_2$) or calcium nitrate $Ca(NO)_3$ to synthesise $CaCO_3$ [89].

$$CaCl_2 + Na_2CO_3 \rightarrow CaCO_3 + 2NaCl$$

$$Na_2CO_3 + Ca(NO_3)_2 \rightarrow CaCO_3 + 2NaNO_3$$

Peng et al synthesised calcium carbonate nanoparticles using calcium chloride and sodium bicarbonate as reactants in solution of ethanol and deionised water. Calcium carbonate nanoparticles were formed by the multistage self-assembled strategy in a binary solvent reaction system [90].

The initial supersaturation, pH and temperature of the $Ca(OH)_2$ slurry are possible parameters determining the proportion of calcite, aragonite and vaterite as well as the shape and size of the particles [91]. The crystalline form and the particle size

distribution are affected by the supersaturation level and ionic ratio of Ca^{2+}/CO_3^{2-} in the solution [92, 93].

Among the methods for preparation of calcium carbonate nanoparticles, reactive precipitation is of high industrial interest because of its convenience in processing, low cost, and its ability to produce the product on a large scale. Superfine particles can be easily obtained by this method [89, 94]. But the reaction kinetics greatly affects the quality of the powder formed. Also, multiple process parameters such as temperature, reactant concentration, etc. need to be controlled.

2) The Citrate method (Combustion method)

In usual methods of calcium carbonate nanoparticles synthesis such as the reactive precipitation method, the nanoparticles tend to agglomerate due to their small particle size and high surface energy resulting in a non-steady-state thermodynamics. The strategy of using organic templates and/or additives to control the nucleation, growth, and alignment of inorganic particles has been widely applied to the biomimetic morphogenesis of inorganic materials with complex forms. Using citric acid as an organic additive, the procedure is known as the sol–gel citrate method. In this method, organic additives are used as emulsifiers [95]. The formation of metal carboxylates results from interaction between metal cations and carboxylic acids. When organic additive is used as fuel along with nitrate salt of a cation and heated, the exothermic reaction between nitrate (oxidant reactant) and organates (fuel) leads to formation of corresponding nanocrystalline oxides. The main advantage being that the necessary heat for synthesis is obtained directly from the reaction in which the metal nitrates act both as oxidant and as cation source, while the organic compound functions as the fuel. The combustion method involves the auto ignition of an aqueous solution containing an oxidizer (the corresponding metal nitrates) and an organic fuel, such as citric acid. The combustion reaction is the most vigorous and reaches high temperatures when the fuel/nitrate molar ratio is close to its stoichiometric value, leading to large particles or agglomerates. However, rapid evolution of a large volume of gases during the process cools the product immediately, limits the occurrence of agglomeration, thus leading to nanocrystalline powders [96, 97].

Ghiasi et al prepared calcium carbonate nanoparticles by adding a solution of calcium nitrate to a solution of citric acid in water. The solutions were evaporated at 60

°C. Thus obtained materials were subsequently dried at high temperatures. The materials were completely powdered and calcined at 600 °C to obtain calcium carbonate nanoparticles. It was found that the addition of citric acid at more than a half concentration of calcium nitrate, decreases the particle size of calcium carbonate by about 50% [98].

The amount and nature of fuel added affects the particle size, and so must be carefully selected and used. Advantages of this method include lowering of the calcination temperature and prevention of agglomeration of formed nanoparticles. Disadvantage is the contamination by carbonaceous residue. Proper understanding of the reaction mechanism is needed to perform combustion in a controlled manner so as to obtain the desired products. [95, 98]

3) Reverse microemulsions

The water-in oil (W/O) microemulsion method has been widely used as an ideal method to prepare inorganic nanoparticles, which consists of nanosized water droplets surrounded by surfactants, and are dispersed in the oil phase. The formation of nanoparticles using the microemulsion method is completely governed by the droplet exchange, which provides new reactants in small amounts (few molecules) from other droplets. Since there are many such separate reactors in the system, particles in the size range of nanometres are formed with minimum agglomeration [99, 100].

Ghadam et al prepared calcium carbonate calcite type polymorph nanoparticles using tween 80 and span 80 as surfactants and toluene as the oil phase. They concluded from their studies that by increasing the concentration of surfactants, the water surfactant molar ratio decreases resulting in the decrease of size of the synthesized nanoparticles [101]. In comparison to the other methods, this method produces particles in the size range of nanometres with minimum agglomeration.

4) Mechano-chemical methods

The reactants like $CaCl_2$ and NaCl are milled in a ball mill. As the reactants react, product is formed which is further ground by impact of the balls in the ball mill. A solid-state displacement reaction is induced during mechanical milling of a $CaCl_2$+ Na_2CO_3 powder mixture (containing NaCl as a diluent).

$$CaCl_2 + Na_2CO_3 \rightarrow CaCO_3 + NaCl$$

In the experiment performed by Tsuzuki et al., heat treatment of the milled powder at 350ºC completed the reaction, forming crystalline calcium carbonate nanoparticles. A simple washing process is used to remove the sodium chloride from ultrafine powder. The mean particle size was controlled by changing the volume fraction of $CaCO_3$ in the matrix. Obtained particle size was in the range 80nm-140nm [102].

The product properties are affected by the amount of reactants, and the number and size of the balls in the ball mill. Both the factors are directly related to the collision frequency of the reactants and affect the reaction rate. An optimum speed of rotation of the mill is essential for uniform mixing of the reactants and adequate particle size reduction [103, 104].

Mechanochemical method is particularly suitable for producing large amounts of product. The process is relatively simple with only a few operational parameters. Of significance is the fact that this technique helps in obtaining agglomeration free ultrafine particles. The crystallinity of the nanoparticles can be improved by heat treatment of the powder after milling. The separation of the nanoparticles by a solid salt matrix prevents agglomeration from occurring during heat treatment. Disadvantage of this method is possible contamination by components of the ball mill [105].

5) From biogenic origin

Biological systems are capable of producing inorganic materials such as calcium carbonate with different structures, morphologies, and polymorphs. Such biological systems are observed in numerous marine organisms such as oyster shells, coral, ivory sea urchin, and mollusc shell bivalve nacre, whereby the main components of the shells are calcium carbonate and other organic components, such as anionic protein and glycoprotein [106]. The aragonite polymorph of calcium carbonate is prepared from biogenic materials, cockle shells, and exhibits unique characteristics (i.e., a higher density than that of calcite) which makes it biocompatible [101, 107].

Islam et al synthesised calcium carbonate aragonite type polymorph from cockle shells. A low cost method was used which is easy-to-perform, environment friendly, and involved a simple mechanical stirring of cockle shell powder in presence of BS12 (dodecyl dimethyl betaine), which is a nontoxic and non-hazardous biomineralization catalyst. The size of the nanoparticles lied between 15-25 nm. The method produced very small sized rod shaped aragonite nanoparticles in a reproducible fashion. Only pure

aragonite was produced without any contamination by calcite or vaterite. Hence it is a simple, low cost and an environment friendly method to obtain pure calcium carbonate nanoparticles [108].

Application of Calcium Carbonate in drug delivery

Calcium carbonates like calcium phosphates are found in various natural sources and possess similar advantages such as high biocompatibility and low rate of degradation. Calcium carbonate nanoparticles have been successfully used for the delivery of anti-cancer agents, proteins and other drugs. Like hydroxyapatite, they have also been combined with different materials so as to obtain an enriched therapeutic effect and drug delivery. Liang et al prepared nanoparticles by combining heparin, calcium carbonate and calcium phosphate so as to enhance the sustained release of Doxorubicin. A pH sensitive release can also be obtained since they easily degrade under acidic conditions but remain stable at neutral and basic conditions [63, 109, 110]. pH sensitive nanocomposites have also been prepared by combining different materials. Liang et al., 2014 prepared pH sensitive nanocomposites containing doxorubicin by combining heparin, biotin, calcium carbonate and calcium phosphate [111]. Delivery systems with targeting potential have also been prepared [90]. Their drug and gene applications in cancer and other diseases are summarized in table 7-8 to 7-10.

Table 7-8 Applications of calcium carbonate nanoparticles in anticancer drug delivery.

Product	Challenges	Inference	Reference
Doxorubicin-loaded calcium carbonate hybrid nanoparticles	Therapy and imaging both through same formulation (theranostic approach)	Nanoparticles exhibited strong echogenic signals at tumoural acid pH by producing CO_2 bubbles and showed excellent echo persistence. Nanoparticles could also trigger DOX release simultaneously with CO_2 bubble generation at acidic tumoural environment. Nanoparticles displayed effective antitumor therapeutic activity in tumour-bearing mice.	[63]
Calcium carbonate-mineralized polymer nanoparticles for pH-responsive robust nanocarriers of docetaxel	Systemic toxicity of the drug	The calcium carbonate mineralized micelles were stable towards micelle disrupting surfactants and serums. Docetaxel release was supressed at extracellular pH of 7.4 but was facilitated at an intracellular endosomal pH of 5.0. Thus $CaCO_3$-mineralized polymer micelle can be used as stable and effective nanocarrier system.	[110]

Nanoreactor of amorphous calcium carbonate-doxorubicin@silica	Drug leakage at non target sites	This nanoreactor maintained low drug leakage in physiological and lysosomal/endosomal environments, and responded specifically to pH 6.5 to release drug.	[112]
Inorganic/organic hybrid alginate/calcium carbonate nanoparticles	Difficult co-administration of hydrophilic and lipophilic drugs	In vitro drug release study showed effective sustained release of DOX and paclitaxel. Nanoparticles exhibited significantly enhanced cell uptake and nuclear localization in HeLa and MCF-7/ADR cells, as compared with single drug loaded nanoparticles. Significant enhancement of cell inhibitory activity against drug resistant tumour cells.	[113]
Doxorubicin loaded calcium carbonate nanocrystals	Lack of specificity and selectivity of conventional delivery systems	Nanocrystals significantly inhibited osteosarcoma bone cancer cells with efficient and sustained release of DOX (doxorubicin). A slow release at normal physiological pH 7.4 and a faster release rate in an acidic environment of pH 4.8 was observed.	[109]
Doxorubicin loaded Heparin/$CaCO_3$/ Calcium phosphate	Hydrophilic nature and systemic side effects of DOX	Hybrid nanoparticles with heparin enriched surface layers exhibited a negative surface charge, which ensures good colloidal stability in aqueous media. In vitro drug release showed sustained release of DOX. In vitro cytotoxicity evaluation indicated strong cell inhibition effect.	[114]
Etoposide loaded calcium carbonate nanoparticles	Poor water solubility, metabolic inactivation, side effects on normal tissue, and poor targeting of etoposide	Studies demonstrated pH-sensitive drug release profile and enhanced cytotoxicity by increasing cellular uptake and apoptosis of tumour cell. Cytotoxicity and apoptosis test showed that carrier was almost nontoxic and etoposide nanoparticles were more efficient than free etoposide in antitumor effect.	[90]
Alginate/$CaCO_3$/DNA/Doxorubicin nanoparticles	Hydrophilic drug and systemic side effect of doxorubicin	In vitro cell inhibition evaluation showed that nanoparticles could induce an effective cell inhibition and completely inhibited proliferation of cervical carcinoma cells.	[115]

Table 7-9 Applications of calcium carbonate nanoparticles in delivery of other agents

Product	Challenge	Inference	Reference
Photosens (a photosensitize) loaded calcium carbonate nanoparticles	Nonspecific cytotoxic action of photosens	Vaterite particles were loaded with photosensitizer. Drug release was triggered by $CaCO_3$ crystal phase transitions. Release dynamics were found to be sensitive to environmental pH. This allowed the creation of a controllable photosensitizer delivery system, releasing its payload under acidic conditions.	[116]
Calcium carbonate and calcium citrate nanoparticles.	Large sized calcium carbonate nanoparticles are less effective in preventing osteoporosis because of poor oral	Oral administration of nanocalcium carbonates and nanocalcium citrates enhanced the serum concentration of calcium and maintained the bone density in mice.	[117]

	absorption.		
Acrylic bone cement containing calcium carbonate nanoparticles.	Acrylic bone cements lose their strength with time.	Acrylic cements combined with calcium carbonate showed improved mechanical strength.	[118]
Betamethasone Phosphate and erythropoietin loaded calcium carbonate nanoparticles	Hydrophilic nature and rapid metabolism of betamethasone. Fast degradation of erythropoietin	Subcutaneous injection of nanoparticles resulted in smaller initial increase in plasma concentration and a subsequent sustained release in comparison with betamethasone phosphate solution. In in-vitro releasing test, erythropoietin incorporated in nanocalcium carbonate was chemically stable and released very slowly.	[119]

Table 7-10 Applications of calcium carbonate nanoparticles in gene delivery.

Product	Inference	Reference
Protamine sulphate–calcium carbonate–plasmid DNA (pGL3-Luc and pEGFP-C) ternary nanoparticles	Prepared nanoparticles exhibited significantly enhanced gene delivery due to favourable effect of protamine sulphate on cell uptake and DNA nuclear localization, as well as a decreased particle size and an increased z-potential. Presence of protamine sulphate also improved thermodynamic stability of resultant nanoparticles in aqueous medium.	[120]
Calcium carbonate hybrid nanospheres functionalized with Ca(II)-IP69(inositol hexakisphosphate)- AIB1 siRNA complex	Encapsulated siRNA was well protected from degradation. AIB1 knockdown mediated by nanoparticle-siRNA complexes transfection resulted in cells proliferation inhibition, apoptosis induction and cell cycle arrest in vitro. Nanoparticle-siRNA complexes exhibited good tissue penetrability in localized siRNA delivery. Intratumoural injection of nanoparticle-siRNA complexes could attenuate tumour growth in vivo.	[121]
Alginate/$CaCO_3$/p53 plasmid DNA/doxorubicin nanoparticles	Nanoparticles completely inhibited proliferation of cervical carcinoma cells, indicating that alginate/CaCO3/DNA/DOX nanoparticles could effectively mediate gene transfection and deliver drug to the cells.	[115]
$CaCO_3$–KALA–DNA (p-53 plasmid DNA)-Doxorubicin nanoparticles (KALA is a cationic endosomolytic and fusogenic cell-penetrating peptide)	Nanoparticles exhibited enhanced drug and gene delivery efficiency/gene expression, which led to a stronger inhibition effect on HeLa cells. These results indicated that addition of KALA, which facilitated cellular uptake of various agents, could improve both gene and drug delivery efficiencies.	[122]
Calcium carbonate nanoparticles encapsulating vascular endothelial growth factor-C siRNA	Nanoparticles–DNA complex are capable of transferring DNA into targeted cells with high transfection efficiency while effectively protecting encapsulated DNA from degradation. Transfection of gastric cancer cells with VEGF-C siRNA via calcium carbonate nanoparticle suppressed tumour lymphangiogenesis, tumour growth and regional lymph-node metastasis in subcutaneous xenografts.	[123]

SILICA NANOPARTICLES

Silica is a chemical compound that is an oxide of silicon with the chemical formula SiO_2. Silica is a poor conductor of heat and electrons both, unlike metals [124]. Silica is one of the most valuable materials for biomedical research. It has wide application in the field of drug delivery as nanoparticles. Mesoporous silica nanoparticles (MSNs) which are formed by polymerizing silica in the presence of surfactants offer several advantages such as large surface area and volumes, encapsulation of drugs and other therapeutic molecules, and tunable pore sizes. Furthermore, the surface of silica nanoparticles can be functionalized with a variety of functional groups or ligands which in turn will increase biocompatibility and modify other properties too, such as targeting ability of the nanoparticles. Silica nanoparticles have found applications in controlled delivery systems as it is able to store and gradually release therapeutic agents. Out of several advantages that MSNs offer, the important ones are: automatic release of drugs; ease of dissolution; ease of availability, etc. Also, there are multimodal silica nanoparticles which are applicable as markers in cancer diagnosis and imaging. Silica nanoparticles are also found to significantly reduce cell viability by induction of apoptosis [9]. During last couple of decades, solid silica nanoparticles (SiNPs) and mesoporous silica nanoparticles (MSNs) have been extensively studied and characterized for use in biomedical science. Though SiNPs have been widely used in drug delivery systems and for imaging, the functionalization of SiNPs is limited by their surface. On the other hand, MSNs exhibit a higher surface area and a tunable pore volume, allowing for a higher loading capacity of therapeutic agents [125].

Multimodal silica nanoparticles, are also found to be effective markers in cancer tests. Such nanoparticles are surface functionalized with arginine-glycine-aspartic acid peptide ligands and radioiodine, exhibiting a higher affinity and residence in tumours and peripheral blood fluids. Studies have shown improved selectivity and accumulation of such nanoparticles in xenograft models. Yamashita et al., prepared silica nanoparticles coated with a PEG layer and labelled with amino acid and radioactive peptides. The studies were conducted on various models of nodal metastasis in various mouse tissues at different nanoparticle doses and showed excellent results [126].

However toxicity of these nanoparticles still remains a concern which needs to be addressed before their successful application for human use [127].

Methods of Preparation

1) The sol-gel process

The process includes the hydrolysis and condensation of metal alkoxides ($Si(OR)_4$) such as tetraethylorthosilicate (TEOS, $Si(OC_2H_5)_4$) or inorganic salts such as sodium silicate (Na_2SiO_3) in the presence of a catalyst such as a mineral acid (e.g., HCl) or a base (e.g., NH_3) [128-130]. Stober et al synthesized monodisperse silica particles by hydrolysis and polymerization of tetraalkoxysiliane (TEOS) in a solution containing ammonia, alcohol, and water. The reactions are as follows:

$Si(OC_2H_5)_4+4H_2O \rightarrow Si(OH)_4+4C_2H_5OH$

$Si(OH)_4 \rightarrow SiO_2 + 2\ H_2O$

Silanol groups are formed by the hydrolysis of TEOS molecules. Further the silicate structure is formed by the condensation/ polymerisation in between the silanol groups or between the silanol and the ethoxy groups [130].

The formation of silica particles can be divided into two stages: nucleation and growth. There are two growth mechanisms proposed. The first one is the monomer addition, in which an initial burst of nucleation is followed by particle growth due to the addition of hydrolysed monomers on the (primary) particle surface [131, 132]. While the aggregation model elaborates that the nucleation occurs unceasingly throughout the reaction and the resulting nuclei (primary particles) will aggregate together to form dimmer, trimmer, and larger (secondary) particles [133, 134]. Eddrissi et al prepared silica nanoparticles using an ultrasound assisted sol-gel method. TEOS solution in methanol was mixed with ammonia and water, followed by sonication at different temperatures. The molar concentration of ammonia was found to be the most effective factor on the size of silica nanoparticles. The use of ultrasound in the synthesis process helped to produce 13 nm sized silica nanoparticles with a very narrow size distribution [135].

It had been shown that to synthesize silica with a narrow particle size distribution, the molar ratio of water to TEOS (in ethanol) should be small [136]. Many authors also

agree that particle size increases with increase in concentration of ammonia [134-138]. Presence of anion electrolyte additives such as ammonium salts of bromine, iodine, and chlorine produced monodispersed silica particles ~20nm to ~34nm [139]. Further particle size, mean pore size, and the particle size distribution of the product can be controlled by adjusting the reaction kinetics (by varying the composition of the reaction mixture), the choice of catalyst, gelation and drying temperatures [140, 141].

Sol-gel method has been a method of choice for the preparation of silica nanoparticles, as it offers several advantages such as the possibility of carrying out the synthesis at low temperatures and an appropriate pH, to yield nanoparticles with high purity and homogeneity [135, 140, 141].

2) The Reverse Microemulsion method

In this method spherical micelles of water are formed in oil with the help of a surfactant. Thus these microcavities (also called as reverse micelles) can act as reaction chambers for the formation of silica nanoparticles with diameters ranging from tens to a few hundreds of nanometres.

Finnie et al synthesised silica nanoparticles by using the reverse microemulsion technique. Microemulsions were prepared dissolving the non-ionic surfactant NP-5 (polyoxyethylene (5) nonylphenyl ether) in cyclohexane and adding either dilute nitric acid (pH 1.05) or an ammonia solution (pH 10.85), respectively, in a 6:1 molar ratio of water/surfactant. Tetramethylorthosilicate (TMOS) was then added to the microemulsions with continuous stirring. Carrying out the reaction in an acidic pH (1.05) results in porous nanoparticles particles with an average of 6 nm. However, base synthesis (pH 10.85) resulted in particles with negligible internal porosity and higher particle size (11 nm) [142].

Bagwe et al. and Jin et al. used dye-doped silica NPs with continuously tunable sizes for cellular contrast imaging that obtained by the reverse microemulsion technique [143, 144]. Yoo et al also synthesised fluorescent silica nanoparticles using the reverse microemulsion technique [145]. The addition of silicon alkoxides and catalyst into the medium containing reverse micelles needs to be carefully controlled. Carrying out the reaction in an acidic environment results in porous nanoparticles particles with high surface area. However, synthesis at a higher pH results in lower surface area particles with negligible internal porosity and higher particle size [142].

The advantage of this method is that agglomeration free nanometre sized particles are obtained. The major drawbacks of the reverse microemulsion approach are high cost and difficulties in removal of surfactants in the final products. Additional processing of product is required for surfactant removal. The most common method for surfactant removal is solvent extraction. Solvent extraction is a low temperature process that uses organic solvents such as ethanolic solution of hydrochloric acid, ethanolic solution of ammonium nitrate or methanol solution of Hydrochloric acid, ethanol-acetic acid mixture, etc. for surfactant removal [146-148]. The product is repeatedly washed and centrifuged with the solvents, therefore the method requires large amount of organic solvents. Hence the method is economically expensive and is not suitable for large scale applications. Another disadvantage of this method is the loss of redispersity of the nanoparticles after the process [146, 149]. An alternative method is to use a dialysis membrane for surfactant removal. In this method the dispersity of the nanoparticles is preserved after removal of the surfactant [149]. Other methods of removal include conventional calcination, ozone treatment, supercritical fluid extraction and sulphuric acid treatment [150-153].

3) Flame spray synthesis

Silica nanoparticles can also be produced through high temperature flame decomposition of metal-organic precursors. Silica nanoparticles are produced by reacting a suitable precursor such as tetraethylorthosilicate with oxidants, hydrogen (fuel) and oxygen (oxidant). This process is also referred to as chemical vapour condensation (CVC).

Jang et al used flame spray pyrolysis to produce silica nanoparticles by reacting spray droplets of tetraethylorthosilicate with hydrogen and oxygen. Spherical silica nanoparticles with size ranging from 12 to 47 nm were produced [154]. While Chang et al also used this method to produce 9 to 68 nm sized silica nanoparticles. They produced aggregation-free amorphous silica nanoparticles by rapid cooling of nanoparticles soon after their formation [155].

Flow rate and concentration of precursor solution, H_2 and O_2 gas flow rate are the main factors that affect the particle size. For e.g.: As the TEOS concentration in the flame increased, the particle size also increased as observed by Jang et al [154].

The advantage of the gas phase processes is the production of particles of high purity in large quantities. The associated disadvantage is the difficulty in controlling the particle size, morphology, and phase composition.

Applications of Silica nanoparticles in Drug Delivery

Mesoporous silica nanoparticles are one of the most successful drug delivery agents used in anti-cancer therapy. Unique features such as large surface area, tunable pore diameter, controllable particle size and morphology, excellent biocompatibility, offer great advantages over other materials. Mesoporous silica nanoparticles are capable of delivering hydrophobic and hydrophilic drug molecules for controlled delivery. In addition they have also been used for imaging the delivery site for theranostic applications [156]. Efficient targeting capability has been can be incorporated into these particles by functionalising with molecules such as folic acid, $VEGF_{121}$ or by lactosamination of surface etc. [157-159]. Temperature, pH sensitive and magnetic field sensitive systems for drug delivery have also been prepared by combining silica with thermally responsive polymers. Neetu et al., 2011 used chemically linked polymers (n-isopropylacrylamide, polyethyleneglycol diacrylate and 3-aminopropylaccrylamide) coated onto silica nanoparticles, so as to prepare a temperature and pH responsive system [160]. Temperature and magnetic field responsive silica nanospheres loaded with sophoridine were prepared by Dong et al., 2014 using n-isopropylacrylamide [161]. Glutathione and acidic pH responsive silica nanoparticles loaded with camptothecin and doxorubicin via chemical crosslinking (GSH responsive disulphide and pH responsive hydrazine bonds) were prepared by Zhgang et al [162]. They were successfully able to obtain a controlled release of drug which could be easily modulated with temperature, pH or an external magnetic field. Similar examples and other applications drug and gene delivery are provided in tables 7-11 to 7-13.

Table 7-11 Applications of silica nanoparticles in anticancer drug delivery.

Product	Challenges	Inference	Reference
Avidin capped cisplatin loaded mesoporous silica nanoparticles	Systemic side effects of cisplatin due to untargeted delivery	MMP9-mediated release of cisplatin was achieved, which induced apoptotic cell death only in lung tumour regions. MMP9 responsive nanoparticles also allowed for effective combinatorial drug delivery of cisplatin and proteasome inhibitor bortezomib, which had a synergistic effect on the toxicity.	[163]

Lactosaminated, docetaxel loaded mesoporous silica nanoparticles for asialoglycoprotein receptor targeting.	Systemic toxic effects of drug.	Lactosaminated mesoporous silica nanoparticles loaded with docetaxel were able to inhibit HepG2 and SMMC7721 cells efficiently.	[159]
pH-sensitive multifunctional silica nanoparticles loaded with arsenic trioxide	Poor pharmacokinetic and bioavailability of arsenic trioxide	Acidic stimuli triggered simultaneous release of manganese ions and arsenic trioxide, which dramatically increased T_1 signal and enabled real-time visualization and monitoring of release and delivery. Efficacy of arsenic trioxide was significantly improved which strongly inhibited growth of solid tumours without adverse side effects.	[164]
Folic acid grafted multifunctional Camptothecin loaded mesoporous silica nanoparticles	Uncontrolled and untargeted release of camptothecin	Doping of lanthanide ions, i.e., (europium and gadolinium ions) imparted fluorescence and magnetism that can be used to develop MRI and biological fluorescence tools. Camptothecin, grafted onto the surface through disulphide bonds (cleaved by intracellular glutathione), showed intracellular controlled drug release.	[157]
$VEGF_{121}$ conjugated-sunitinib loaded mesoporous silica nanoparticles	Therapeutic efficacy is limited by insufficient administration of drug.	By efficient targeting higher amount of sunitinib was delivered to U87MG tumour cells.	[158]
Doxorubicin, Layer-by-Layer coated mesoporous silica nanoparticles	Severe side effects of DOX due to non-targeted and uncontrolled delivery	This nanosystem was tuned to respond under specific acidic conditions (endosomal compartments of cancer cells). It possessed excellent biostability, negligible premature drug leakage at pH 7.4, and exceptional stimuli-responsive drug release performance. In vivo experiments demonstrated highly efficient tumour-growth inhibition rate.	[165]
Topotecan, multifunctional enveloped mesoporous silica na noparticles	Toxicity of topotecan due to untargeted delivery	Surface was decorated with mitochondria-targeted therapeutic agent and antibiotic peptide via disulphide linkage, followed by coating with a charge reversal polyanion. Outer shielding layer could be removed at acidic tumour microenvironment and cellular uptake was enhanced. After endocytosis, due to the cleavage of disulphide bonds in the presence of intracellular glutathione (GSH), pharmacological agents could be released.	[166]
6-mercaptopurine loaded redox-responsive colloidal mesoporous silica.	Toxicity of 6-mercaptopurine due to untargeted delivery	Drug was conjugated by cleavable disulphide bonds. Cumulative release of drug was less than 3% in absence of glutathione, and reached 80% in presence of glutathione. Nanoparticles exhibited greater cytotoxicity against HCT-116 cells (CD44 receptors positive) than NIH-3T3 cells due to enhanced cell uptake.	[167]
pH-responsive charge-reversal, polymer-coated doxorubicin loaded	Toxicity of DOX due to untargeted delivery	3-aminopropyl)triethoxysilane was used to synthesize nanocomposites. Nanocomposites effectively delivered and released DOX to the nucleus of HeLa cells.	[168]

mesoporous silica na noparticles.			
Cisplatin, theranostic mesoporous hollow silica nanosp heres	Limited application through conventional dosage form	Exterior surface was acid functionalized and conjugated to cisplatin, folic acid, and rhodamine isothiocyanate. Superparamagnetic $CoFe_2O_4$ nanoparticles and hydrophobic anticancer drug were encapsulated. Nanospheres exhibited enhanced cytotoxicity as compared to individual drugs, as well as MRI contrast properties.	[169]
Hollow mesoporous Bortezomib silica nanospheres	Poor water solubility, low stability, and tumour resistance of bortezomib	In vivo tumour-suppression assay indicated that these nanoparticles showed 1.5 folds stronger anti-tumour activity than free drug. More potent induction of cell cycle arrest and apoptotic cell death, along with promoted activation of Caspase 3 and autophagy was reported.	[170]
Doxorubicin, pH and thermo dual-controllable mesoporous silica nanoparticles	Unmonitored and uncontrolled release of doxorubicin	pH and thermo dual-responsive releasing ability was offered by copolymer-lipid bilayer. Results confirmed that either pH or temperature can trigger drug release. Nanoparticles transported DOX into MCF-7 cells and exhibited pH-sensitive release behaviour.	[171]
Hollow mesoporous silica nanoparticles containing Doxorubicin and siRNA	Multidrug resistance, difficult co-delivery	Electrostatic interactions between PEI-folic acid and siRNA provided pH-controlled release. Studies showed effective targeted delivery to HeLa cells through folic acid receptor meditated cellular endocytosis. pH-responsive intracellular drug/siRNA release greatly minimized pre-release and possible side effects.	[172]

Table 7-12 Applications of silica nanoparticles in gene delivery.

Product	Inference	Reference
Polyethyleneimine coated silica nanoparticles for siRNA delivery	Polyethylene amine was coated onto silica nanoparticles via coordination properties of cerium cation .Cerium dependent gene silencing and cytotoxic activities were observed.	[173]
Mesoporous silica nanoparticles functionalised with polyamidoamine for plasmid DNA delivery.	Polyamidoamine functionalised silica nanoparticles were capable of forming complex with plasmid DNA. The nanoparticles were successfully able to transfect cells.	[174]
Silica nanoparticles functionalised with poly(2-dimethylaminoethl acrylate) for siRNA delivery.	The cationic polymer was bound to gene molecules and underwent a self-catalyzed hydrolysis in water to form a non-toxic anionic polymer poly(acrylic acid), allowing controlled release of siRNA in the cells. The system was successfully able to deliver the siRNA to the cells when tested.	[175]
3-aminopropyltrimethoxysilane functionalised gadolinium doped silica nanoparticles for plasmid DNA delivery and imaging.	Plasmid DNA were firmly bound electrostatically onto the nanoparticle surface and were protected from DNase attack. The system was successfully able to transfect cells. The gadolinium oxide doped silica nanoparticles were paramagnetic as was observed by	[176]

	nuclear magnetic resonance.	
N-trimethoxysilylpropyl-N,N,N-trimethylammonium chloride, (MeO)3Si-PTMA functionalised silica nanoparticles for delivering Granulocyte-macrophage colony-stimulating factor gene.	Granulocyte-macrophage colony-stimulating factor and white blood cell levels were found to increase considerably when tested in animals. No neutralising antibodies were developed against the administered product.	[177]
Poly(L-lysine)-modified silica nanoparticles for the delivery of antisense oligonucleotides.	Nanoparticle surface charge was modified by coating withpoly(l-lysine). The particle surface was successfully able to bind and protect antisense oligonucleotides. Fluorescence microscopy and flow cytometry confirmed the successful delivery of oligonucleotide to cell.	[178]

Table 7-13 Applications of silica nanoparticles in delivery of other agents

Product	Challenge	Inference	Reference
Quercetin containing Modified silica nanoparticles.	Unfavourable loading and release profile of quercetin	Results showed high loading of quercetin and congruence with the physicochemical features determined. Bio-activity profile of quercetin nanoparticles denoted improved specificity of antioxidant activity.	[179]

TITANIUM OXIDE NANOPARTICLES

Titanium dioxide (TiO_2), also called titania, is an important n-type wide band-gap semiconductor with light absorbing, charge transport, and surface adsorption properties. Due to the exclusive properties like photoactivity, photostability, chemical and biological inertness, and high stability, titanium dioxide has found wide variety of applications in various fields [180]. Titanium dioxide nanoparticles have also been widely used as white pigment in paint, UV blocker in cosmetics, welding rod-coating material, disinfectant in environment and wastewater and photosensitizer for the photodynamic therapy [181]. Titanium is widely used in biomedical applications due to its mechanical and photocatalytic properties, and its biocompatibility. It is a well-established and proven fact that titanium dioxide, when photoexcited, exhibits strong oxidizing and reducing ability and also affects cellular functions, thus leading to its applicability in treatment of cancer. According to recent studies, TiO_2 induces death by apoptosis in different types of cells, such as mesenchymal stem cells, osteoblasts, and other cell types. Also, due to its photocatalytic properties, TiO_2 kills cancer cells upon

irradiation with light of wavelength <390 nm via production of reactive oxygen species, which damage cancer cells [182]. Three different crystallite structures of titanium dioxide have been found: brookite, anatase, and rutile. Rutile is a stable phase while anatase and brookite are metastable. Brookite is difficult to synthesise and is seldom studied. Rutile is considered to be more stable but it has lower photolytic activity than anatase [183]

Methods of Preparation

1) Sol-gel method

Sol–gel method is perhaps the most commonly used method to prepare TiO_2 nanoparticles, which is based on hydrolysis of an alkoxide or halide precursor followed by condensation. The formation of TiO_2 from titanium (IV) alkoxide proceeds via acid-catalysed hydrolysis followed by condensation [184]. The precursor undergoes hydrolysis and then polycondensation processes resulting in formation of sol. Gel forms after aging or gelation and then dries off into solid crystals. Bagheri et al. synthesized anatase titanium oxide nanoparticles via sol-gel method by using water-soluble egg white proteins as a gelling agent. The size obtained was in the range of 12 nm, whereas nanoparticles synthesized without using the gelling agent were found to be of 21 nm [185].

Han et al. synthesized monodispersed and highly uniform TiO_2 nanoparticles of size range 10–300 nm using different concentrations of $CaCl_2$ solution. The prepared TiO_2 nanoparticles were calcined at 500 °C for 1 h to yield nanocrystalline anatase TiO_2. They firstly carried out the reaction between different concentrations of $CaCl_2$ solutions and titanium precursor (titanium (IV) isopropoxide), yielding white solutions of different densities depending on the salt concentration. The synthesized TiO_2 nanoparticles were subsequently filtered off and calcined at 500ºC. They concluded that the concentration of $CaCl_2$ solution could be effectively varied as a critical parameter. The ionic strength of the solution, which may affect the nucleation and growth of particles, is directly related to the concentration of salt [186].

Ultrasmall sized titanium dioxide nanoparticles can be obtained by using a suitable gelling agent. The gelling agent helps in controlling the nanoparticles size and dispersion due to expansion during calcination [185]. When salts such as calcium

chloride are used, the ionic strength of solution should be adequately controlled since it affects the particle size as well as the particle size distribution.

Sol-gel method gives a better homogeneity and phase purity in comparison to traditional ceramic methods. But the process could be more expensive when raw materials such as metal alkoxides are used. Also since several steps are involved, close monitoring is required.

2) Hydrolysis method

Hydrolysis method has been used by a number of researchers to prepare TiO_2 nanoparticles. In this method, a suitable Ti precursor, such as titanium tetrachloride ($TiCl_4$), tetra-butyl titanate ($Ti(OC_4H_9)_4$) etc. is hydrolysed using an aqueous solvent such as ammonia solution, hydrochloric acid etc. This results in formation of white precipitate of titanium hydroxide. This titanium hydroxide gets converted into titanium oxide on calcination at high temperature of about 350 ºC [187, 188]. Yue et al. obtained a particle size of approximately 30 nm using hydrolysis method. They hydrolysed $Ti(OC_4H_9)_4$ with distilled water and dried the precipitate at 120 ºC for 20 hours to obtain TiO_2 nanoparticles [188].

Ismagilov prepared 3 series of TiO_2 nanoparticles. For series 1, they hydrolysed $TiCl_4$ with HCl and ammonia solution at specified temperatures of 4, 20 or 70 ºC and pH maintained between 3-4, 6-7 or 9-10. For series 2, $TiCl_4$ was hydrolysed in cold water at 3-4ºC and pH <1. To synthesize series 3 samples, they used a mixture of titanium tetraisopropoxide ($Ti(i\text{-}OC_3H_7)_4$, TIP) and isopropyl alcohol. The mixture was added to aqueous solution of nitric acid. The sol was maintained at temperatures of 20, 50, 70 or 95 ºC.

Radiographic examination of these 3 samples showed that phase state and particle size of TiO_2 depend on conditions of hydrolysis of precursors. For series 1, the dependence of TiO_2 structural modification on pH of the reaction medium was found to be highly pronounced. Neutral or alkaline pH yielded amorphous titanium dioxide. The pH value of 3-4 led to preferential formation of the anatase phase with particle size of 4–6 nm; traces of brookite with particle size less than 3nm were observed. The amount of the brookite phase increased with a decrease in the synthesis temperature. As pH decreased below 1 (series 2), brookite was formed, which turned into rutile upon long-

term heating at 70 ºC. The hydrolysis of $Ti(i\text{-}OC_3H_7)_4$ under varying temperature (series 3) resulted in the formation of anatase phase, whose particle size had a weak tendency to increase with elevating temperature.

The particle size and the phase (anatase, brookite or rutile) formed are affected by the hydrolysis conditions such as pH of the reaction medium, synthesis temperature etc. as examined by Ismagilov et al. [189]. The method has its advantages such as low reaction temperature, low cost and ease of fabrication. Starting materials and reaction conditions need to be chosen carefully for the synthesis of nanosized particles.

3) Hydrothermal synthesis

Hydrothermal synthesis is widely used for the production of very small particles of ceramic materials. It is usually conducted in autoclaves (steel pressure vessels), where the reaction of precursor (e.g. Titanium isopropoxide) and surfactant/stabilizer containing aqueous solutions is carried out under controlled temperature and/or pressure.

Anwar et al. prepared titanium dioxide nanoparticles via hydrothermal processing route, employing sucrose ester as a stabilizing agent. The morphology of the nanoparticles was influenced by reaction temperature and sucrose ester concentration. It was found that degree of crystallinity was improved upon increasing the temperature of hydrothermal reaction. Also, the size of the nanoparticles increased from 5 nm to 20 nm with increasing temperature because of the increasing rate of crystal growth [190].

It is important to select suitable surfactant/stabilizer (e.g. triethanolamine, dodecanediamine, cetylpyridinium chloride, sucrose esters, etc.) that acts as a template or shape controller, directing the formation of the nanosized particles. Besides the surfactant/stabilizer, temperature and pressure are also critical parameters for obtaining particles of the required size. The internal pressure developed can be controlled by the temperature and the amount of solution added to the autoclave. Temperature of the reaction can be increased above the boiling point of the water, reaching the pressure of vapour saturation [184, 190].

Hydrothermal synthesis method provides an easy way to control size, morphology, structure, phase composition, and chemical properties by varying experimental parameters such as temperature and pressure [191].

4) Combustion synthesis

In this method the precursors (e.g. Ti and $NaClO_4$) react to form nanoparticles via gasification in the heating process, nucleation and crystal growth in the cooling sublimation process.

Kitamura et al. obtained TiO_2 nanoparticles sized 100 nm to 1000 nm through gasification, nucleation, and crystal growth from the following reaction:

$Ti + NaClO_4 \rightarrow TiO_2 + NaCl$

They concluded that shape and crystal structure of the obtained nanoparticles depended significantly on the particle size of the titanium raw material, the smaller titanium particles resulted in irregular rutile phase, whereas the larger particles resulted in spherical anatase phase [192].

In combustion synthesis of TiO_2, the size of the raw material is an important operating parameter to control the product size and phase ratio of the product. Combustion synthesis offers a number of benefits such as minimizing energy requirement, good control over reaction stoichiometry and shortening the operation time by use of a sustainable exothermic solid–solid reaction.

Applications of Titania nanoparticles in Drug Delivery

Titania is another ceramic material whose nanoform has been successfully used as drug delivery agent for a number of diseases. Titanium dioxide nanoparticles offer advantages such as high photocatalytic activity and functional surface. On exposure to UV radiations free radicals are generated which can effectively decompose organic compounds present on the surface. A radiation triggered drug release is an interesting feature for designing drug delivery systems [161] [193]. Surface functionalization with ligands such as folic acid is able to impart suitable targeting property [164] [56]. Tables 7-14 and 7-15 summarize the drug delivery applications of titania nanoparticles.

Table 7-14 Potential of titanium dioxide nanoparticles in anticancer drug delivery.

Product	Challenges	Inference	Reference
Paclitaxel loaded multifunctional porous titanium dioxide (TiO_2) nanoparticles modified with polyethylenimine (PEI)	Poor water solubility and unwanted side effects of paclitaxel with non-targeted delivery	Following UV irradiation, PEI molecules on the surface were cut off by the free radicals (OH and O^{2-}) that TiO_2 produced, and drug was released rapidly. Amount of drug released can be regulated by UV irradiation time to further control anti-cancer effect.	[193]
PEG and FA modified hydroxyapatite and	Lower anti-cancer activity and	Nanoparticles have higher anticancer activity than pure paclitaxel, due to	[56]

titanium dioxide nanoparticles loaded with Paclitaxel	systemic toxicity due to non-targeted approaches	targeting of drug to the folate receptor in cancer cells.	
Herceptin modified Silica/titania hollow nanoparticles loaded with camptothecin	Unwanted side effects of herceptin due to non-targeted approaches	Nanoparticles were efficiently internalized owing to their herceptin conjugation and optimized size. Nanoparticles decreased the viability of SK-BR-3 to 60 %.	[194]
pH-responsive titanium dioxide nanoparticles loaded with daunorubicin	Serious side effects of daunorubicin	Drug was released more rapidly at pH 5.0 and 6.0 than at pH 7.4. Nanoparticles increased intracellular concentration of daunorubicin and enhanced its anticancer efficiency by inducing apoptosis in a caspase-dependent manner.	[195]
Doxorubicin loaded titania nanoparticles	Uncontrolled and unmonitored release of DOX	Adsorbed drug was released in a controlled way by external glutathione. Real-time monitoring of drug release was done in the live cell using fluorescence imaging techniques.	[196]
Doxorubicin-titanium dioxide nanocomposites	Serious side effects of DOX	Nanocomposites markedly increased the efficiency of drug per dosage and decreased IC_{50} in human SMMC-7721 hepatocarcinoma cells, resulting in anticancer efficacy enhancement and side effect attenuation. Apoptosis may contribute to the mechanism, due to protein expression of Bcl-2 being downregulated and that of Bax and caspase 3 being upregulated.	[197]

Table 7-15 Application of titania nanoparticles in delivery of miscellaneous agents.

Product	Challenges	Inference	Reference
p-toluene sulfonic acid modified titanium dioxide nanoparticle loaded with Terpinen-4-ol	Uncontrolled release from conventional formulations	Nanoparticles were in hexagonal phase, which allows the controlled release of terpinen-4-ol following zero-order kinetics. Constant concentrations were released per unit time and nanoparticles acted as a transparent inorganic sunscreen.	[198]
Enrofloxacin hydrochloride containing titanium dioxide nanotubes.	Uncontrolled release from conventional formulations	Loading efficiency of drug was increased. Nanotubes provided a better release profile at low temperatures than at high temperatures in PBS solution.	[199]
Protein conjugated titanium oxide nanotubes containing Reprogramming proteins	Difficult and inefficient delivery of proteins	Nanotubes successfully transferred reprogramming factors into differentiated somatic cells. After 3 weeks of treatment, somatic cells adopted an embryonic stem cell-like morphology and expressed activated Oct4-green fluorescent protein, a pluripotency biomarker.	[200]
TiO_2-DB-Haemoglobin hybrid material	Difficult and uncontrolled delivery	Hb can be controlled-released from TiO_2-DB-Hb by switching visible light on/off. Released Hb not only retains its senior structure but also can fulfil the enzymatic bioactivity. Controlled delivery of Hb	[201]

		stems from scission of Ti-O coordination bond with the aid of photo-inducing electron transfer property of titania.	

ZIRCONIA NANOPARTICLES

Zirconia, ZrO_2 is an important ceramic material with applications in the field of structural materials, solid state electrolytes, thermal barrier coatings, electro-optical materials, gas sensing, corrosion resistance, and catalysis. Zirconia exhibits three crystallographic phases with increasing temperature at normal atmospheric pressure: the monoclinic phase (m), from room temperature to 1175 °C; the tetragonal phase (t), from 1175 to 2370 °C; and the cubic phase (c), from 2370 to 2750 °C (melting point). Most of the properties of ZrO_2 depend strongly on its phase formation and transition [202]. The t → m transformation in pure undoped zirconia during cooling is a reversible athermal martensitic transformation, associated with a large temperature hysteresis (around 200 °C for undoped zirconia) and a finite quantity of volume change (4–5%) [203-205].This leads to catastrophic failures of the thermal barrier coating made from pure zirconia. Therefore several dopants (yttria, ceria, calcia, magnesia, etc.) have been frequently added to stabilize the high temperature t and/or c-phase in coated microstructure [206]. Among the three phases, tetragonal zirconia features the highest mechanical stability and is the ideal phase for biomedical applications.

Zirconium oxide presents interesting catalytic properties which are generally attribute to the simultaneous presence of both acidic and basic sites at its surface [207]. For example, it has been reported to selectively produce 1-butene during 2-butanol dehydration [208], in contrast with acidic oxides which are selective for the 2-butenes or produce an equilibrated mixture of the olefins in this reaction. It also displays remarkable selectivity in the hydrogenation of benzoic acid to benzaldehyde [209]. It has also been proven to have activity in the hydrogenation of conjugated dienes [210], in methanol synthesis [211], and as a photocatalyst [212]. When sulphate ion is present at its surface, zirconia is known to behave as a solid superacid [207, 213]. As a catalytic support, it has been proven to be advantageous in several reactions, such as hydrodesulphurization [214], complete oxidation of propane [215], Fischer–Tropsch synthesis [216], and methanol synthesis [217]. Apart from these interesting uses zirconia has also been combined with other nanomaterials for drug delivery. Zirconia

has been used to stabilise Hydroxyapatite. Sintering these composites at low temperatures maintained hydroxyapatite crystallinity, high surface roughness and increased osteoblast adhesion [218]. Mesoporous silica-zirconia oxide matrices have been found to have good stability in biological conditions than pure silica materials [219]. In cell culture experiments zirconia coatings supported cell adhesion and enhanced proliferation [220]. Monoclinic nanograined zirconia coatings obtained by atmospheric plasma spraying exhibited good biocompatibility, bioactivity and high bonding strength and are a promising alternative for coating metallic orthopaedic implants [221]. Combining other nanomaterials with zirconia also allows better tuning of drug release and carrier degradation [222].

Methods of Preparation

1) Combustion synthesis

Combustion synthesis involves the preparation of the precursors by a self-sustaining combustion process using a fuel such as urea, glycine or citric acid followed by exothermic decomposition of precursors at elevated temperatures. The resulting powder is usually in the form of agglomerates having nanoparticles as the building blocks.

For synthesising tetragonal zirconia nanoparticles, Purohit et al mixed pure zirconium oxynitrate and citric acid in a molar ratio of 1:1.5 using required volume of deionized water to obtain a citrate–nitrate solution. Thermal dehydration of the citrate–nitrate solution resulted in a transparent viscous gel. Further heating of the gel to ≈250 °C resulted in blackish brown dry powder with evolution of gaseous products. Further calcination at 600 °C, produced pure well-crystalline ZrO_2 powder. XRD studies showed the presence of predominantly tetragonal phase of zirconia. The agglomerated powder was composed of 10 nm sized spherical nanocrystals [223].

Reddy et al. produced tetragonal nanocrystalline zirconia crystals by the aqueous combustion synthesis method using glycine as a fuel. Glycine was added to the zirconyl nitrate hydrate aqueous solution. The solution was then evaporated in small portions, during which it boils, foams, and undergoes smouldering to produce the corresponding oxides. The fine powders obtained are then calcined at 500 °C. Glycine/Zirconyl nitrate ratio of 0.5 produced particles with the smallest sizes (7-9 nm), a higher ratio produced particles of larger sizes (up to 22 nm). The powders had narrow size limits and

consistent morphology. The tendency of nanocrystallites to form hard agglomerates is observed to be responsible for high temperature tetragonal phase stabilization at room temperature [224].

Phase purity and powder characteristics depend primarily upon the nature and amount of the fuel used in the process, which governs the enthalpy of combustion, amount of gas evolution and rate of combustion [225, 226]. The decomposition rate of the precursor should be fast and enthalpy of combustion should be just sufficient for producing the desired pure single phase nanocrstalline powder without hard agglomerates along with evolution of high volume of gaseous products [223].

The process is energy saving, carried out at low temperatures and completes in a short period of time. It also as economic advantages such as use of cheap oxide reactants instead of expensive elemental reactants.

2) Sol-gel method

The sol-gel process involves the hydrolysis and condensation of molecular precursors such as metal alkoxides or hydroxylated metal ions in aqueous or non-aqueous solution [227]. The chemistry involved in sol-gel reaction can be expressed as follows [228]:

i. Partial hydrolysis of the alkoxide

$$M(OR)_n + xH_2O \rightarrow M(OR)_{n-x}(OH)_x + xROH$$

ii. Polymerisation condensation of the hydroxyloralkoxyl groups

$$M\text{-}OH + HO\text{-}M \rightarrow M\text{-}O\text{-}M + H_2O$$

$$M\text{-}OR + HO\text{-}M \rightarrow M\text{-}O\text{-}M + ROH$$

Beena et al. used zirconium n-propoxide diluted with *n*-propanol as a zirconia precursor. The precursor solution was hydrolysed by aqueous ammonia until the pH of 10-10.5 was reached. After complete hydrolysis, the sol was continuously stirred at ambient temperature to polymerize the gel. The resulting gel was then dried. Thermal drying of zirconium hydroxide gel in an oven resulted in lower crystallite size (11 -13 nm) as compared to drying under vacuum, which shows higher crystallite size (20-21 nm). Sol-gel synthesis was found to stabilize the tetragonal phase at higher temperature and resulted in spherical-shaped particles [229].

The particles are built up by molecule-by-molecule addition. During the process of nanopowder formation, the particles easily adhere and form agglomerates. Therefore

a close control over the nucleation and growth of the particles is required. The gelatinization of the sol followed by thermal treatment are the most important steps that affect the product [230].

The advantages of generating nanoparticles with the combustion method include ease and flexibility in terms of the particle chemical composition. The use of new organic precursors and by careful selection of the processing conditions powders of desired shape and size can be obtained.

3) Hydrothermal synthesis

In this technique, ceramic sols are produced by chemical reactions in an aqueous or organo-aqueous solution under the simultaneous application of heat (>100 °C) and pressure (1 atm) in the presence of an alkali or acid that has a pseudo-catalytic effect upon the reaction [231].

Kanade et al .prepared zirconia nanoparticles by the hydrothermal method. Commercial available zirconia powder was taken in NaOH aqueous solution. The specimen was heated in hydrothermal reactor under pressure at 120°C. The white product obtained was washed and dried. The nanosized zirconia obtained had an average particle size in the range of 24–36 nm. The SEM of nanosized zirconia showed diminutively different morphology than the commercial one [232]. When the process conditions such as solution pH, solute concentration, reaction temperature, reaction time, seed materials, and the type of solvent are carefully controlled, the zirconium oxide particles with desired shape and size can be produced [233, 234].

Hydrothermal synthesis offers the advantage of direct preparation of crystalline ceramic powders with adequate yield and is a low temperature alternative to conventional powder synthesis techniques. This soft chemical route can produce fine, high purity and stoichiometric particles of single and multi-component metal oxides. Prior knowledge on solubility of starting materials is required. Hydrothermal slurries are also potentially corrosive. Further, since the process takes place in a hydrothermal reactor one cannot observe the crystallisation process directly [235].

4) Homogenous precipitation method

Homogeneous precipitation is a simple direct process for synthesis of fine zirconia powders and requires the use of a precipitating agent to precipitate zirconia from a reaction mixture under conditions of elevated temperature and pressure. The

method has been used widely to produce monodispersed metal oxide particles of various shapes and sizes.

Xin et al. synthesised yttria stabilised zirconia by the homogenous precipitation method. Aqueous zirconyl chloride solution was mixed with the yttrium nitrate solution. This solution was added to urea solution, followed by dilution. The solution was autoclaved and heated to generate hydrogel precipitate. The precipitate was calcined at different temperatures (773-1723°K). The nanoparticles obtained by calcination at 773 °K had the size of 7 nm. With increasing calcination temperature of powders, a better crystallization and enhanced crystalline size was reported [236].

Addition of the precipitating agent directly to the reaction mixture results in large and inhomogeneous gradients in solution, allowing only little control of the reaction chemistry. A better control of chemical and morphological characteristics can be achieved if the precipitating ligands are generated simultaneously and uniformly throughout the solution, i.e., by a homogeneous precipitation process. By controlling reaction, it is possible to produce particles with controlled particle size, controlled stoichiometry, and in some cases controlled particle morphology. The elimination of any calcinations step significantly reduces the tendency for agglomeration of the powders [236].

Applications of Zirconia as Drug Delivery agent

Zirconia is a ceramic material holding a great potential in biomedical field as a drug delivery agent, in prosthetics and medical devices [237]. This potential still needs to be explored fully. It has been successfully combined with materials such as titanium dioxide [201] [238]. Zirconia can also be used for preparing pH sensitive drug delivery systems, since it remains stable at neutral or alkaline pH but degrades at acidic pH [203] [239]. It has a fewer number of studies performed as compared to other ceramic materials, which are summarized in table 7-10 to 7-16.

Table 7-16 Application of zirconia nanoparticles in drug delivery.

Product	Challenges	Inference	Reference
Titanium Zirconium Oxide Nanospheres loaded with ibuprofen, dexamethasone, and erythromycin	Co administration of anti-inflammatory, antibiotic and analgesic drugs for rheumatoid arthritis	Nanospheres exhibited a high loading capacity, and sustained release profiles in phosphate buffered saline. Mesoporous nanospheres also exhibited hydrolytic stability, as evidenced by the retention of the integrity of the	[238]

		mesostructures after drug release for 21 days.	
Doxorubicin (DOX) loaded zirconium phosphate nanoplatelets	Hydrophilic nature with systemic side effects.	DOX loaded nanoplatelets had 34.9% (w/w) drug loading. Cellular studies with MCF-7 cells showed higher uptake and cytotoxicity of DOX loaded zirconium phosphate nanoplatelets in comparison to free DOX.	[240]
Doxorubicin loaded hollow mesoporous zirconia nanocapsules	Hydrophilic nature with systemic side effects.	A loading of 102% related to the weight of hollow mesoporous zirconia was achieved. Due to their pH-dependent charge, DOX loaded zirconia nanocapsules exhibited a pH-dependent drug release kinetics, lower pH offering faster drug release. Nanocapsules released more drugs in cancer cells than in normal cells, leading to more cytotoxicity towards tumour cells and less cytotoxicity to healthy cells than free DOX.	[239]

CONCLUSION

The above discussion about the methods of synthesis and applications of inorganic nanoparticles (Ceramic nanoparticles) in the field of drug delivery makes it evident that these nanoparticles hold a great potential as drug carriers to deliver and target the active pharmaceutical ingredient to the desired site in a controlled manner, resulting in achievement of a therapeutic concentration of drug at target site. Ceramic nanoparticles offer a number of technical advantages in terms of drug delivery. Most researched area for the application of ceramic nanoparticles is cancer, where promising results have been obtained. A number of facile methods for preparation of these nanoparticles are available and have been continuously undergoing modifications to achieve better desired characteristics of synthesised nanoparticles. All these favourable facts have resulted in several patents and publications in this area during recent years. Thus, ceramic nanoparticles hold the promise of better, safer and cost effective drug delivery agents in future of biomedical science.

CONFLICT OF INTEREST STATEMENT

The authors have no conflict of interest with any person or party.

References:

1. Yih TC, Al-Fandi M. Engineered nanoparticles as precise drug delivery systems. J Cell Biochem 2006; 97: 1184-1190.
2. Singh S, Pandey VK, Tewari RP, Agarwal V. Nanoparticle Based Drug Delivery System: Advantages and Applications. Indian J Sci Technol 2011; 4: 177-180.
3. Shinde NC, Keskar NJ, Argade PD. Nanoparticles: Advances in drug delivery systems. Res J Pharm Bio Chem Sci 2012; 3: 922-8.
4. Moreno-Vega A-I, Gomez-Quintero T, Nunez-Anita R-E, Acosta-Torres L-S, Castaño V. Polymeric and ceramic nanoparticles in biomedical applications. Journal of Nanotechnology 2012; 2012: 1-10.
5. Fadeel B, Garcia-Bennett AE. Better safe than sorry: Understanding the toxicological properties of inorganic nanoparticles manufactured for biomedical applications. Adv Drug Delivery Rev 2010; 62: 362-374.
6. Zhang L. Preparation of multi-component ceramic nanoparticles. Center for Industrial Sensors and Measurements, Department Materials Science & Engineering Group Inorganic Materials Science. www. mse. eng. ohio-state. edu/fac_staff/faculty/verweij, 2004: 1-29.
7. Ferraz M, Monteiro F, Manuel C. Hydroxyapatite nanoparticles: a review of preparation methodologies. J Appl Biomater Biomech 2004; 2: 74-80.
8. Chen F, Zhu Y, Wu J, Huang P, Cui D. Nanostructured calcium phosphates: preparation and their application in biomedicine. Nano Biomed Eng 2012; 4: 41-49.
9. Yang L, Sheldon BW, Webster TJ. Nanophase ceramics for improved drug delivery. Am Ceram Soc Bull 2010; 89: 24-32.
10. Gassmann T. The preparation of a complex salt corresponding to apatite-typus and its relations to the constitution of bones. H.-SZ Physiol Chem 1913; 83: 403-408.
11. Fratzl P, Gupta H, Paschalis E, Roschger P. Structure and mechanical quality of the collagen–mineral nano-composite in bone. J Mater Chem 2004; 14: 2115-2123.

12. Tzaphlidou M. Bone architecture: collagen structure and calcium/phosphorus maps. J Biol Phys 2008; 34: 39-49.
13. Sitharaman B. Nanobiomaterials handbook. CRC Press 2011.
14. Uskoković V, Desai TA. Phase composition control of calcium phosphate nanoparticles for tunable drug delivery kinetics and treatment of osteomyelitis. I. Preparation and drug release. J Biomed Mater Res, Part A 2013; 101: 1416-1426.
15. Poitout DG. Biomechanics and biomaterials in orthopedics. Springer Science & Business Media 2004.
16. Smith JP, Lehr JR, Brown WE. Crystallography of monocalcium and dicalcium phosphates. Am Mineral 1955; 40: 893-899.
17. Uskoković V, Uskoković DP. Nanosized hydroxyapatite and other calcium phosphates: chemistry of formation and application as drug and gene delivery agents. J Biomed Mater Res, Part B 2011; 96: 152-191.
18. Bouyer E, Gitzhofer F, Boulos M. Morphological study of hydroxyapatite nanocrystal suspension. J Mater Sci Mater Med 2000; 11: 523-531.
19. Hench LL. Introduction to bioceramics. Adv Ser Ceram 1993; 1: 1-24.
20. Öner M, Uysal U. Synthesis of hydroxyapatite crystals using carboxymethyl inulin for use as a delivery of ibuprofen. Mater Sci Eng, C 2013; 33: 482-489.
21. Salma K, Berzina-Cimdina L, Borodajenko N. Calcium phosphate bioceramics prepared from wet chemically precipitated powders. Process Appl Ceram 2010; 4: 45-51.
22. Kokubo T. Surface chemistry of bioactive glass-ceramics. J Non-Cryst Solids 1990; 120: 138-151.
23. Kokubo T. A/W glass-ceramic: processing and properties. Adv Ser Ceram 1993; 1: 75-88.
24. Li P, Nakanishi K, Kokubo T, de Groot K. Induction and morphology of hydroxyapatite, precipitated from metastable simulated body fluids on sol-gel prepared silica. Biomaterials 1993; 14: 963-968.
25. Li P, Kangasniemi I, Groot K, Kokubo T. Bonelike Hydroxyapatite Induction by a Gel-Derived Titania on a Titanium Substrate. J Am Ceram Soc 1994; 77: 1307-1312.

26. Li P, Kangasniemi I, De Groot K, Kokubo T, Yli-Urpo A. Apatite crystallization from metastable calcium phosphate solution on sol-gel-prepared silica. J Non-Cryst Solids 1994; 168: 281-286.
27. Kokubo T, Miyaji F, Kim HM, Nakamura T. Spontaneous formation of bonelike apatite layer on chemically treated titanium metals. J Am Ceram Soc 1996; 79: 1127-1129.
28. Layrolle P, van der Valk C, Dalmeijer R, van Blitterswijk CA, de Groot K. Biomimetic calcium phosphate coatings and their biological performances. Key Eng Mater 2000; 192: 391-394.
29. Loty C, Loty S, Kokubo T, Forest N, Sautier J. Prefabricated biological apatite formation on a bioactive glass-ceramic promotes in vitro differentiation of fetal rat chondrocytes. Bioceramics. Paris: Elsevier Science Publishers, 1997: 219-222.
30. Tas AC. Synthesis of biomimetic Ca-hydroxyapatite powders at 37 C in synthetic body fluids. Biomaterials 2000; 21: 1429-1438.
31. Du C, Klasens P, Haan R, Bezemer J, Cui F, De Groot K, Layrolle P. Biomimetic calcium phosphate coatings on Polyactive® 1000/70/30. J Biomed Mater Res 2002; 59: 535-546.
32. Leeuwenburgh S, Layrolle P, Barrere F, De Bruijn J, Schoonman J, Van Blitterswijk C, De Groot K. Osteoclastic resorption of biomimetic calcium phosphate coatings in vitro. J Biomed Mater Res 2001; 56: 208-215.
33. Nicholson JW. The chemistry of medical and dental materials. Royal Society of Chemistry 2002.
34. Bose S, Saha SK. Synthesis and characterization of hydroxyapatite nanopowders by emulsion technique. Chem Mater 2003; 15: 4464-4469.
35. Lim G, Wang J, Ng S, Gan L. Formation of nanocrystalline hydroxyapatite
36. Pileni MP. Reverse micelles as microreactors. J Phys Chem 1993; 97: 6961-6973.
37. Pileni MP. Nanosized Particles Made in Colloidal Assemblies. Langmuir 1997; 13: 3266-3276.
38. Filankembo A, Pileni MP. Is the Template of Self-Colloidal Assemblies the Only Factor That Controls Nanocrystal Shapes? J Phys Chem B 2000; 104: 5865-5868.

39. Pileni M-P. The role of soft colloidal templates in controlling the size and shape of inorganic nanocrystals. Nat Mater 2003; 2: 145-150.
40. França EL, Honorio-França AC. The Mucosal Immune System: Modulation by Microemulsion. In: Najjar R, ed.^eds., Microemulsions - An Introduction to Properties and Applications. INTECH Open Access Publisher, 2012; pp. 151-158.
41. Liu D-M, Yang Q, Troczynski T, Tseng WJ. Structural evolution of sol–gel-derived hydroxyapatite. Biomaterials 2002; 23: 1679-1687.
42. Layrolle P, Ito A, Tateishi T. Sol-Gel Synthesis of Amorphous Calcium Phosphate and Sintering into Microporous Hydroxyapatite Bioceramics. J Am Ceram Soc 1998; 81: 1421-1428.
43. Liu DM, Chou HM, Wu JD. Plasma-sprayed hydroxyapatite coating: effect of different calcium phosphate ceramics. J Mater Sci Mater Med 1994; 5: 147-153.
44. Shirkhanzadeh M. Direct formation of nanophase hydroxyapatite on cathodically polarized electrodes. J Mater Sci Mater Med 1998; 9: 67-72.
45. Wen C, Guan S, Peng L, Ren C, Wang X, Hu Z. Characterization and degradation behavior of AZ31 alloy surface modified by bone-like hydroxyapatite for implant applications. Appl Surf Sci 2009; 255: 6433-6438.
46. Kuo M, Yen S. The process of electrochemical deposited hydroxyapatite coatings on biomedical titanium at room temperature. Mater Sci Eng, C 2002; 20: 153-160.
47. Gilman P, Benjamin J. Mechanical alloying. Annual Review of Materials Science, 1983; 13: 279-300.
48. Yeong K, Wang J, Ng S. Mechanochemical synthesis of nanocrystalline hydroxyapatite from CaO and CaHPO 4. Biomaterials 2001; 22: 2705-2712.
49. Sarath Chandra V, Baskar G, Suganthi R, Elayaraja K, Ahymah Joshy M, Sofi Beaula W, Mythili R, Venkatraman G, Narayana Kalkura S. Blood compatibility of iron-doped nanosize hydroxyapatite and its drug release. ACS Appl Mater Interfaces 2012; 4: 1200-1210.
50. Panseri S, Cunha C, D'Alessandro T, Sandri M, Giavaresi G, Marcacci M, Hung CT, Tampieri A. Intrinsically superparamagnetic Fe-hydroxyapatite nanoparticles positively influence osteoblast-like cell behaviour. J Nanobiotechnology 2012; 10: 32.

51. Meng J, Xiao B, Zhang Y, Liu J, Xue H, Lei J, Kong H, Huang Y, Jin Z, Gu N. Super-paramagnetic responsive nanofibrous scaffolds under static magnetic field enhance osteogenesis for bone repair in vivo. Sci Rep 2013; 3.
52. Pistone A, Iannazzo D, Panseri S, Montesi M, Tampieri A, Galvagno S. Hydroxyapatite-magnetite-MWCNT nanocomposite as a biocompatible multifunctional drug delivery system for bone tissue engineering. Nanotechnology 2014; 25: 425701.
53. Li D, He J, Huang X, Li J, Tian H, Chen X, Huang Y. Intracellular pH-responsive mesoporous hydroxyapatite nanoparticles for targeted release of anticancer drug. RSC Adv 2015; 5: 30920-30928.
54. Zhao C-X, Yu L, Middelberg AP. Magnetic mesoporous silica nanoparticles end-capped with hydroxyapatite for pH-responsive drug release. J Mater Chem B 2013; 1: 4828-4833.
55. Wei J, He P, Liu A, Chen X, Wang X, Jing X. Surface Modification of Hydroxyapatite Nanoparticles with Thermal-Responsive PNIPAM by ATRP. Macromol Biosci 2009; 9: 1237-1246.
56. Venkatasubbu GD, Ramasamy S, Avadhani G, Ramakrishnan V, Kumar J. Surface modification and paclitaxel drug delivery of folic acid modified polyethylene glycol functionalized hydroxyapatite nanoparticles. Powder Technol 2013; 235: 437-442.
57. Qi C, Zhu YJ, Zhao XY, Lu BQ, Tang QL, Zhao J, Chen F. Highly Stable Amorphous Calcium Phosphate Porous Nanospheres: Microwave-Assisted Rapid Synthesis Using ATP as Phosphorus Source and Stabilizer, and Their Application in Anticancer Drug Delivery. Chem - Eur J 2013; 19: 981-987.
58. Venkatesan P, Puvvada N, Dash R, Kumar BP, Sarkar D, Azab B, Pathak A, Kundu SC, Fisher PB, Mandal M. The potential of celecoxib-loaded hydroxyapatite-chitosan nanocomposite for the treatment of colon cancer. Biomaterials 2011; 32: 3794-3806.
59. Ramachandran R, Paul W, Sharma CP. Synthesis and characterization of PEGylated calcium phosphate nanoparticles for oral insulin delivery. J Biomed Mater Res, Part B 2009; 88: 41-48.

60. Cheng X, Kuhn L. Chemotherapy drug delivery from calcium phosphate nanoparticles. Int J Nanomed 2007; 2: 667-674.
61. Palazzo B, Iafisco M, Laforgia M, Margiotta N, Natile G, Bianchi CL, Walsh D, Mann S, Roveri N. Biomimetic hydroxyapatite–drug nanocrystals as potential bone substitutes with antitumor drug delivery properties. Adv Funct Mater 2007; 17: 2180-2188.
62. Seong D-Y, Kim Y-J. Enhanced photodynamic therapy efficacy of methylene blue-loaded calcium phosphate nanoparticles. J Photochem Photobiol, B 2015; 146: 34-43.
63. Min KH, Min HS, Lee HJ, Park DJ, Yhee JY, Kim K, Kwon IC, Jeong SY, Silvestre OF, Chen X, Hwang Y-S, Kim E-C, Lee SC. pH-Controlled Gas-Generating Mineralized Nanoparticles: A Theranostic Agent for Ultrasound Imaging and Therapy of Cancers. ACS Nano 2015; 9: 134-145.
64. Klesing J, Wiehe A, Gitter B, Gräfe S, Epple M. Positively charged calcium phosphate/polymer nanoparticles for photodynamic therapy. J Mater Sci Mater Med 2010; 21: 887-892.
65. Rawat P, Manglani K, Gupta S, Vohora D, Ahmad FJ, Talegaonkar S. Design and Development of Bioceramic Based Functionalized PLGA Nanoparticles of Risedronate for Bone Targeting: In-vitro Characterization and Pharmacodynamic Evaluation. Pharm Res 2015: 1-10.
66. Yu J, Chu X, Cai Y, Tong P, Yao J. Preparation and characterization of antimicrobial nano-hydroxyapatite composites. Mater Sci Eng, C, 2014; 37: 54-59.
67. Liu X, Zhao K, Gong T, Song J, Bao C, Luo E, Weng J, Zhou S. Delivery of growth factors using a smart porous nanocomposite scaffold to repair a mandibular bone defect. Biomacromolecules 2014; 15: 1019-1030.
68. Uskoković V, Desai TA. Phase composition control of calcium phosphate nanoparticles for tunable drug delivery kinetics and treatment of osteomyelitis. II. Antibacterial and osteoblastic response. J Biomed Mater Res, Part A 2013; 101A: 1427-1436.
69. Sahana H, Khajuria DK, Razdan R, Mahapatra DR, Bhat M, Suresh S, Rao RR, Mariappan L. Improvement in bone properties by using risedronate adsorbed

hydroxyapatite novel nanoparticle based formulation in a rat model of osteoporosis. J Biomed Nanotechnol 2013; 9: 193-201.

70. Xie G, Sun J, Zhong G, Liu C, Wei J. Hydroxyapatite nanoparticles as a controlled-release carrier of BMP-2: absorption and release kinetics in vitro. J Mater Sci Mater Med 2010; 21: 1875-1880.
71. Garner S, Barbour ME. Nanoparticles for controlled delivery and sustained release of chlorhexidine in the oral environment. Oral Dis 2015.
72. Zhang N, Gao T, Wang Y, Wang Z, Zhang P, Liu J. Environmental pH-controlled loading and release of protein on mesoporous hydroxyapatite nanoparticles for bone tissue engineering. Mater Sci Eng, C 2015; 46: 158-165.
73. Vengala P, Dintakurthi S, Subrahmanyam CVS. Lactose coated ceramic nanoparticles for oral drug delivery. J Pharm Res 2013; 7: 540-545.
74. Yasaei M, Zamanian A, Moztarzadeh F, Ghaffari M, Mozafari M. Characteristics improvement of calcium hydroxide dental cement by hydroxyapatite nanoparticles. Part 1: Formulation and microstructure. Biotechnol Appl Biochem 2013; 60: 502-509.
75. C-W Wu K, Yang Y-H, Liang Y-H, Chen H-Y, Sung E, Yamauchi Y, Lin F-H. Facile synthesis of hollow mesoporous hydroxyapatite nanoparticles for intracellular bio-imaging. Curr Nanosci 2011; 7: 926-931.
76. Chen R, Qian Y, Li R, Zhang Q, Liu D, Wang M, Xu Q. Methazolamide calcium phosphate nanoparticles in an ocular delivery system. Yakugaku Zasshi, 2010; 130: 419-424.
77. Li L, Pan H, Tao J, Xu X, Mao C, Gu X, Tang R. Repair of enamel by using hydroxyapatite nanoparticles as the building blocks. J Mater Chem 2008; 18: 4079-4084.
78. Ardekani MRS, Abdin M, Nasrullah N, Samim M. Calcium phosphate nanoparticles a novel non-viral gene delivery system for genetic transformation of tobacco. Int J Pharm Pharm Sci 2014; 6: 605-609.
79. Lee MS, Lee JE, Byun E, Kim NW, Lee K, Lee H, Sim SJ, Lee DS, Jeong JH. Target-specific delivery of siRNA by stabilized calcium phosphate nanoparticles using dopa–hyaluronic acid conjugate. J Controlled Release, 2014; 192: 122-130.

80. Xie Y, Qiao H, Su Z, Chen M, Ping Q, Sun M. PEGylated carboxymethyl chitosan/calcium phosphate hybrid anionic nanoparticles mediated hTERT siRNA delivery for anticancer therapy. Biomaterials 2014; 35: 7978-7991.
81. Lee H-P, Kaul G, Cucchiarini M, Madry H. Nonviral gene transfer to human meniscal cells. Part I: transfection analyses and cell transplantation to meniscus explants. Int Orthop 2014; 38: 1923-1930.
82. Ito T, Koyama Y, Otsuka M. Preparation of Calcium Phosphate Nanocapsule Including Deoxyribonucleic Acid–Polyethyleneimine–Hyaluronic Acid Ternary Complex for Durable Gene Delivery. J Pharm Sci 2014; 103: 179-184.
83. Krebs MD, Salter E, Chen E, Sutter KA, Alsberg E. Calcium phosphate-DNA nanoparticle gene delivery from alginate hydrogels induces in vivo osteogenesis. J Biomed Mater Res, Part A, 2010; 92: 1131-1138.
84. Liu T, Tang A, Zhang G, Chen Y, Zhang J, Peng S, Cai Z. Calcium phosphate nanoparticles as a novel nonviral vector for efficient transfection of DNA in cancer gene therapy. Cancer Biother Radiopharm 2005; 20: 141-149.
85. Nie H, Wang C-H. Fabrication and characterization of PLGA/HAp composite scaffolds for delivery of BMP-2 plasmid DNA. J. Controlled Release 2007; 120: 111-121.
86. Zhu S, Huang B, Zhou K, Huang S, Liu F, Li Y, Xue Z, Long Z. Hydroxyapatite nanoparticles as a novel gene carrier. J Nanopart Res 2004; 6: 307-311.
87. Roy I, Mitra S, Maitra A, Mozumdar S. Calcium phosphate nanoparticles as novel non-viral vectors for targeted gene delivery. Int J Pharm 2003; 250: 25-33.
88. Nagaraja AT, Pradhan S, McShane MJ. Poly (vinylsulfonic acid) assisted synthesis of aqueous solution stable vaterite calcium carbonate nanoparticles. J Colloid Interface Sci 2014; 418: 366-372.
89. Babou-Kammoe R, Hamoudi S, Larachi F, Belkacemi K. Synthesis of CaCO3 nanoparticles by controlled precipitation of saturated carbonate and calcium nitrate aqueous solutions. Can J Chem Eng 2012; 90: 26-33.
90. Peng H, Li K, Wang T, Wang J, Wang J, Zhu R, Sun D, Wang S. Preparation of hierarchical mesoporous CaCO3 by a facile binary solvent approach as anticancer drug carrier for etoposide. Nanoscale Res Lett 2013; 8: 1-11.

91. Reddy MM, Nancollas GH. The crystallization of calcium carbonate: I. Isotopic exchange and kinetics. J Colloid Interface Sci 1971; 36: 166-172.
92. Chakraborty D, Bhatia SK. Formation and aggregation of polymorphs in continuous precipitation. 2. Kinetics of CaCO3 precipitation. Ind Eng Chem Res 1996; 35: 1995-2006.
93. Tai CY, Chen PC. Nucleation, agglomeration and crystal morphology of calcium carbonate. AIChE J 1995; 41: 68-77.
94. Chen J-F, Wang Y-H, Guo F, Wang X-M, Zheng C. Synthesis of nanoparticles with novel technology: high-gravity reactive precipitation. Ind Eng Chem Res 2000; 39: 948-954.
95. Khazaei M, Malekzadeh A, Amini F, Mortazavi Y, Khodadadi A. Effect of citric acid concentration as emulsifier on perovskite phase formation of nano-sized SrMnO3 and SrCoO3 samples. Cryst Res Technol 2010; 45: 1064-1068.
96. Courty P, Ajot H, Marcilly C, Delmon B. Oxydes mixtes ou en solution solide sous forme très divisée obtenus par décomposition thermique de précurseurs amorphes. Powder Technol 1973; 7: 21-38.
97. Zhang H-M, Teraoka Y, Yamazoe N. Preparation of perovskite-type oxides with large surface area by citrate process. Chem Lett 1987; 16: 665-668.
98. Ghiasi M, Malekzadeh A. Synthesis of CaCO3 nanoparticles via citrate method and sequential preparation of CaO and Ca (OH) 2 nanoparticles. Cryst Res Technol 2012; 47: 471-478.
99. Sundar V, Rusin RP, Rutiser CA. Bioceramics: Materials and Applications IV: Proceedings of a symposium to honor Larry Hench at the 105th annual meeting of The American Ceramic Society, April 27-30, 2003, in Nashville, Tennessee, Ceramic Transactions. John Wiley & Sons 2012.
100. Idrees M. Characterization of CaCO3 Nanoparticles Synthesized by Reverse Microemulsion Technique in Different Concentrations of Surfactants. Iran J Chem Chem Eng, 2013; 32: 27-35.
101. Junaidi A, Hazmi A, Zakaria AB, Zuki M, Mohamed Mustapha N, Abu J, Yusof N. Mineral composition of the cockle (Anadara granosa) shells of West Coast of Peninsular Malaysia and it's potential as biomaterial for use in bone repair. J Anim Vet Adv 2007; 6: 591-594.

102. Tsuzuki T, Pethick K, McCormick PG. Synthesis of CaCO3 nanoparticles by mechanochemical processing. J Nanopart Res 2000; 2: 375-380.
103. Mochales C, El Briak-BenAbdeslam H, Ginebra MP, Terol A, Planell JA, Boudeville P. Dry mechanochemical synthesis of hydroxyapatites from DCPD and CaO: influence of instrumental parameters on the reaction kinetics. Biomaterials 2004; 25: 1151-1158.
104. Othman R, Zakaria A. Optimisation of milling parameters during mechanical activation for direct synthesis of hydroxyapatite. ASEAN Engineering Journal 2011; 1: 5-11.
105. Carter CB, Norton MG. Ceramic materials: science and engineering. Springer Science & Business Media 2007.
106. Velázquez-Castillo R, Reyes-Gasga J, Garcia-Gutierrez D, Jose-Yacaman M. Nanoscale characterization of nautilus shell structure: an example of natural self-assembly. J Mater Res 2006; 21: 1484-1489.
107. Mohamed M, Yusup S, Maitra S. Decomposition study of calcium carbonate in cockle shell. J Eng Sci Technol 2012; 7: 1-10.
108. Islam KN, Bakar MZBA, Ali ME, Hussein MZB, Noordin MM, Loqman M, Miah G, Wahid H, Hashim U. A novel method for the synthesis of calcium carbonate (aragonite) nanoparticles from cockle shells. Powder Technol 2013; 235: 70-75.
109. Kamba SA, Ismail M, Hussein-Al-Ali SH, Ibrahim TAT, Zakaria ZAB. In vitro delivery and controlled release of doxorubicin for targeting osteosarcoma bone cancer. Molecules 2013; 18: 10580-10598.
110. Kim B, Min K, Hwang G, Lee H, Jeong S, Kim E-C, Lee S. Calcium carbonate-mineralized polymer nanoparticles for pH-responsive robust nanocarriers of docetaxel. Macromol Res 2015; 23: 111-117.
111. Liang P, Wang CQ, Chen H, Zhuo RX, Cheng SX. Multi-functional heparin–biotin/heparin/calcium carbonate/calcium phosphate nanoparticles for targeted co-delivery of gene and drug. Polym Int 2015; 64: 647-653.
112. Zhao Y, Luo Z, Li M, Qu Q, Ma X, Yu SH, Zhao Y. A Preloaded Amorphous Calcium Carbonate/Doxorubicin@ Silica Nanoreactor for pH-Responsive Delivery of an Anticancer Drug. Angew Chem Int Ed 2015; 54: 919-922.

113. Wu J-L, Wang C-Q, Zhuo R-X, Cheng S-X. Multi-drug delivery system based on alginate/calcium carbonate hybrid nanoparticles for combination chemotherapy. Colloids Surf, B 2014; 123: 498-505.
114. Liang P, Zhao D, Wang C-Q, Zong J-Y, Zhuo R-X, Cheng S-X. Facile preparation of heparin/CaCO 3/CaP hybrid nano-carriers with controllable size for anticancer drug delivery. Colloids Surf, B 2013; 102: 783-788.
115. Zhao D, Liu C-J, Zhuo R-X, Cheng S-X. Alginate/CaCO3 hybrid nanoparticles for efficient codelivery of antitumor gene and drug. Mol Pharm 2012; 9: 2887-2893.
116. Svenskaya Y, Parakhonskiy B, Haase A, Atkin V, Lukyanets E, Gorin D, Antolini R. Anticancer drug delivery system based on calcium carbonate particles loaded with a photosensitizer. Biophys Chem 2013; 182: 11-15.
117. Huang S, Chen JC, Hsu CW, Chang WH. Effects of nano calcium carbonate and nano calcium citrate on toxicity in ICR mice and on bone mineral density in an ovariectomized mice model. Nanotechnology 2009; 20: 375102-375108.
118. Hill J, Orr J, Dunne N. In vitro study investigating the mechanical properties of acrylic bone cement containing calcium carbonate nanoparticles. J Mater Sci Mater Med 2008; 19: 3327-3333.
119. Ueno Y, Futagawa H, Takagi Y, Ueno A, Mizushima Y. Drug-incorporating calcium carbonate nanoparticles for a new delivery system. J Controlled Release 2005; 103: 93-98.
120. Wang C-Q, Wu J-L, Zhuo R-X, Cheng S-X. Protamine sulfate–calcium carbonate–plasmid DNA ternary nanoparticles for efficient gene delivery. Mol BioSyst 2014; 10: 672-678.
121. Wei J, Cheang T, Tang B, Xia H, Xing Z, Chen Z, Fang Y, Chen W, Xu A, Wang S. The inhibition of human bladder cancer growth by calcium carbonate/CaIP6 nanocomposite particles delivering AIB1 siRNA. Biomaterials 2013; 34: 1246-1254.
122. Zhao D, Zhuo R-X, Cheng S-X. Modification of calcium carbonate based gene and drug delivery systems by a cell-penetrating peptide. Mol BioSyst 2012; 8: 3288-3294.

123. He X, Liu T, Chen Y, Cheng D, Li X, Xiao Y, Feng Y. Calcium carbonate nanoparticle delivering vascular endothelial growth factor-C siRNA effectively inhibits lymphangiogenesis and growth of gastric cancer in vivo. Cancer Gene Ther 2008; 15: 193-202.
124. Boysen E, Muir NC, Dudley D. Nanotechnology for dummies. John Wiley & Sons 2011.
125. Chen Y-C, Huang X-C, Luo Y-L, Chang Y-C, Hsieh Y-Z, Hsu H-Y. Non-metallic nanomaterials in cancer theranostics: a review of silica-and carbon-based drug delivery systems. Sci Technol Adv Mater 2013; 14: 044407-044429.
126. Yamashita K, Yoshioka Y, Higashisaka K, Mimura K, Morishita Y, Nozaki M, Yoshida T, Ogura T, Nabeshi H, Nagano K. Silica and titanium dioxide nanoparticles cause pregnancy complications in mice. Nat Nanotechnol 2011; 6: 321-328.
127. Benezra M, Penate-Medina O, Zanzonico PB, Schaer D, Ow H, Burns A, DeStanchina E, Longo V, Herz E, Iyer S. Multimodal silica nanoparticles are effective cancer-targeted probes in a model of human melanoma. J Clinical Invest 2011; 121: 2768.
128. Klabunde KJ, Stark J, Koper O, Mohs C, Park DG, Decker S, Jiang Y, Lagadic I, Zhang D. Nanocrystals as stoichiometric reagents with unique surface chemistry. J Phys Chem 1996; 100: 12142-12153.
129. Hench LL, West JK. The sol-gel process. Chem Rev 1990; 90: 33-72.
130. Stöber W, Fink A, Bohn E. Controlled growth of monodisperse silica spheres in the micron size range. J Colloid Interface Sci 1968; 26: 62-69.
131. Matsoukas T, Gulari E. Dynamics of growth of silica particles from ammonia-catalyzed hydrolysis of tetra-ethyl-orthosilicate. J Colloid Interface Sci 1988; 124: 252-261.
132. Matsoukas T, Gulari E. Monomer-addition growth with a slow initiation step: a growth model for silica particles from alkoxides. J Colloid Interface Sci 1989; 132: 13-21.
133. Bogush G, Tracy M, Zukoski C. Preparation of monodisperse silica particles: control of size and mass fraction. J Non-Cryst Solids 1988; 104: 95-106.

134. Bogush G, Zukoski C. Studies of the kinetics of the precipitation of uniform silica particles through the hydrolysis and condensation of silicon alkoxides. J Colloid Interface Sci 1991; 142: 1-18.
135. Edrissi M, Soleymani M, Adinehnia M. Synthesis of Silica Nanoparticles by Ultrasound-Assisted Sol-Gel Method: Optimized by Taguchi Robust Design. Chem Eng Technol 2011; 34: 1813-1819.
136. Park SK, Do Kim K, Kim HT. Preparation of silica nanoparticles: determination of the optimal synthesis conditions for small and uniform particles. Colloids Surf, A 2002; 197: 7-17.
137. Bailey J, Mecartney M. Formation of colloidal silica particles from alkoxides. Colloids Surf 1992; 63: 151-161.
138. Rao KS, El-Hami K, Kodaki T, Matsushige K, Makino K. A novel method for synthesis of silica nanoparticles. J Colloid Interface Sci 2005; 289: 125-131.
139. Rahman I, Vejayakumaran P, Sipaut C, Ismail J, Bakar MA, Adnan R, Chee C. Effect of anion electrolytes on the formation of silica nanoparticles via the sol–gel process. Ceram Int 2006; 32: 691-699.
140. Brinker CJ, Scherer GW. Sol-gel science: the physics and chemistry of sol-gel processing. Academic press 2013.
141. Fardad M. Catalysts and the structure of SiO2 sol-gel films. J Mater Sci 2000; 35: 1835-1841.
142. Finnie KS, Bartlett JR, Barbé CJ, Kong L. Formation of silica nanoparticles in microemulsions. Langmuir 2007; 23: 3017-3024.
143. Bagwe RP, Yang C, Hilliard LR, Tan W. Optimization of dye-doped silica nanoparticles prepared using a reverse microemulsion method. Langmuir 2004; 20: 8336-8342.
144. Jin Y, Lohstreter S, Pierce DT, Parisien J, Wu M, Hall Iii C, Zhao JX. Silica nanoparticles with continuously tunable sizes: synthesis and size effects on cellular contrast imaging. Chem Mater 2008; 20: 4411-4419.
145. Yoo H, Pak J. Synthesis of highly fluorescent silica nanoparticles in a reverse microemulsion through double-layered doping of organic fluorophores. J Nanopart Res 2013; 15: 1-10.

146. Kumar R, Chen H-T, Escoto JL, Lin VS-Y, Pruski M. Template removal and thermal stability of organically functionalized mesoporous silica nanoparticles. Chem Mater 2006; 18: 4319-4327.
147. Suteewong T, Sai H, Lee J, Bradbury M, Hyeon T, Gruner SM, Wiesner U. Ordered mesoporous silica nanoparticles with and without embedded iron oxide nanoparticles: structure evolution during synthesis. J Mater Chem 2010; 20: 7807-7814.
148. Kobler J, Möller K, Bein T. Colloidal suspensions of functionalized mesoporous silica nanoparticles. Acs Nano 2008; 2: 791-799.
149. Baù L, Bártová B, Arduini M, Mancin F. Surfactant-free synthesis of mesoporous and hollow silica nanoparticles with an inorganic template. Chem Commun 2009: 7584-7586.
150. Yanagisawa T, Shimizu T, Kuroda K, Kato C. The preparation of alkyltriinethylaininonium–kaneinite complexes and their conversion to microporous materials. Bull Chem Soc Jpn 1990; 63: 988-992.
151. Keene MT, Denoyel R, Llewellyn PL. Ozone treatment for the removal of surfactant to form MCM-41 type materials. Chemical Commun 1998: 2203-2204.
152. Kawi S, Lai M. Supercritical fluid extraction of surfactant from Si-MCM-41. AIChE J 2002; 48: 1572-1580.
153. Yang C-M, Zibrowius B, Schmidt W, Schüth F. Stepwise removal of the copolymer template from mesopores and micropores in SBA-15. Chem Mater 2004; 16: 2918-2925.
154. Jang HD, Chang H, Suh Y, Okuyama K. Synthesis of SiO 2 nanoparticles from sprayed droplets of tetraethylorthosilicate by the flame spray pyrolysis. Curr Appl Phys 2006; 6: e110-e113.
155. Chang H, Park J-H, Jang HD. Flame synthesis of silica nanoparticles by adopting two-fluid nozzle spray. Colloids and Surfaces A: Physicochemical and Engineering Aspects, 2008; 313: 140-144.
156. Mai WX, Meng H. Mesoporous silica nanoparticles: a multifunctional nano therapeutic system. Integr Biol 2013; 5: 19-28.

157. Chan M-H, Lin H-M. Preparation and identification of multifunctional mesoporous silica nanoparticles for in vitro and in vivo dual-mode imaging, theranostics, and targeted tracking. Biomaterials 2015; 46: 149-158.
158. Goel S, Chen F, Hong H, Valdovinos HF, Hernandez R, Shi S, Barnhart TE, Cai W. VEGF121-Conjugated Mesoporous Silica Nanoparticle: A Tumor Targeted Drug Delivery System. ACS Appl Mater Interfaces 2014; 6: 21677-21685.
159. Quan G, Pan X, Wang Z, Wu Q, Li G, Dian L, Chen B, Wu C. Lactosaminated mesoporous silica nanoparticles for asialoglycoprotein receptor targeted anticancer drug delivery. J Nanobiotechnol 2015; 13: 1-12.
160. Singh N, Karambelkar A, Gu L, Lin K, Miller JS, Chen CS, Sailor MJ, Bhatia SN. Bioresponsive mesoporous silica nanoparticles for triggered drug release. J Am Chem Soc 2011; 133: 19582-19585.
161. Dong L, Peng H, Wang S, Zhang Z, Li J, Ai F, Zhao Q, Luo M, Xiong H, Chen L. Thermally and magnetically dual-responsive mesoporous silica nanospheres: preparation, characterization, and properties for the controlled release of sophoridine. J Appl Polym Sci 2014; 131: 40477.
162. Xu Z, Liu S, Kang Y, Wang M. Glutathione-and pH-responsive nonporous silica prodrug nanoparticles for controlled release and cancer therapy. Nanoscale 2015; 7: 5859-5868.
163. Van Rijt SH, Bölükbas DA, Argyo C, Datz S, Lindner M, Eickelberg O, Königshoff M, Bein T, Meiners S. Protease Mediated Release of Chemotherapeutics From Mesoporous Silica Nanoparticles to Ex Vivo Human and Mouse Lung Tumors. ACS Nano 2015; 9: 2377-2389.
164. Zhao Z, Wang X, Zhang Z, Zhang H, Liu H, Zhu X, Li H, Chi X, Yin Z, Gao J. Real-Time Monitoring of Arsenic Trioxide Release and Delivery by Activatable T1 Imaging. ACS Nano 2015; 9: 2749-2759.
165. Li Q-L, Sun Y, Sun Y-L, Wen J, Zhou Y, Bing Q-M, Isaacs LD, Jin Y, Gao H, Yang Y-W. Mesoporous Silica Nanoparticles Coated by Layer-by-Layer Self-assembly Using Cucurbit [7] uril for in Vitro and in Vivo Anticancer Drug Release. Chem Mater 2014; 26: 6418-6431.

166. Luo G-F, Chen W-H, Liu Y, Lei Q, Zhuo R-X, Zhang X-Z. Multifunctional Enveloped Mesoporous Silica Nanoparticles for Subcellular Co-delivery of Drug and Therapeutic Peptide. Sci Rep 2014; 4: 1-10.
167. Zhao Q, Geng H, Wang Y, Gao Y, Huang J, Wang Y, Zhang J, Wang S. Hyaluronic Acid Oligosaccharide Modified Redox-Responsive Mesoporous Silica Nanoparticles for Targeted Drug Delivery. ACS Appl Mater Interfaces 2014; 6: 20290-20299.
168. Zhang P, Wu T, Kong J-L. In Situ Monitoring of Intracellular Controlled Drug Release from Mesoporous Silica Nanoparticles Coated with pH-Responsive Charge-Reversal Polymer. ACS Appl Mater Interfaces 2014; 6: 17446-17453.
169. Mohapatra S, Rout SR, Narayan R, Maiti TK. Multifunctional mesoporous hollow silica nanocapsules for targeted co-delivery of cisplatin-pemetrexed and MR imaging. Dalton Trans 2014; 43: 15841-15850.
170. Shen J, Song G, An M, Li X, Wu N, Ruan K, Hu J, Hu R. The use of hollow mesoporous silica nanospheres to encapsulate bortezomib and improve efficacy for non-small cell lung cancer therapy. Biomaterials 2014; 35: 316-326.
171. Wu X, Wang Z, Zhu D, Zong S, Yang L, Zhong Y, Cui Y. pH and Thermo Dual-Stimuli-Responsive Drug Carrier Based on Mesoporous Silica Nanoparticles Encapsulated in a Copolymer–Lipid Bilayer. ACS Appl Mater Interfaces 2013; 5: 10895-10903.
172. Ma X, Zhao Y, Ng KW, Zhao Y. Integrated Hollow Mesoporous Silica Nanoparticles for Target Drug/siRNA Co-Delivery. Chem - Eur J 2013; 19: 15593-15603.
173. Kapilov-Buchman Y, Lellouche E, Michaeli S, Lellouche J-P. Unique Surface Modification of Silica Nanoparticles with Polyethylenimine (PEI) for siRNA Delivery Using Cerium Cation Coordination Chemistry. Bioconjug Chem 2015; 26: 880-889.
174. Lin J-T, Wang C, Zhao Y, Wang G-H. Mesoporous silica nanoparticles with controlled loading of cationic dendrimer for gene delivery. Mater Res Express 2014; 1: 035403.

175. Hartono SB, Phuoc NT, Yu M, Jia Z, Monteiro MJ, Qiao S, Yu C. Functionalized large pore mesoporous silica nanoparticles for gene delivery featuring controlled release and co-delivery. J Mater Chem B 2014; 2: 718-726.
176. Bhakta G, Sharma RK, Gupta N, Cool S, Nurcombe V, Maitra A. Multifunctional silica nanoparticles with potentials of imaging and gene delivery. Nanomedicine: Nanotechnology, Biology and Medicine, 2011; 7: 472-479.
177. Choi EW, Koo HC, Shin IS, Chae YJ, Lee JH, Han SM, Lee SJ, Bhang DH, Park YH, Lee CW. Preventive and therapeutic effects of gene therapy using silica nanoparticles–binding of GM-CSF gene on white blood cell production in dogs with leukopenia. Exp Hematol 2008; 36: 1091-1097.
178. Zhu SG, Xiang JJ, Li XL, Shen SR, Lu Hb, Zhou J, Xiong W, Zhang BC, Nie XM, Zhou M. Poly (l-lysine)-modified silica nanoparticles for the delivery of antisense oligonucleotides. Biotechnol Appl Biochem 2004; 39: 179-187.
179. Nday CM, Halevas E, Jackson GE, Salifoglou A. Quercetin Encapsulation in Modified Silica Nanoparticles. Potential Use Against Cu (II)-Induced Oxidative Stress in Neurodegeneration. J Inorg Biochem 2015; 145: 51-64.
180. Ramimoghadam D, Bagheri S, Abd Hamid SB. Biotemplated synthesis of anatase titanium dioxide nanoparticles via lignocellulosic waste material. BioMed Res Int, 2014; 2014: 1-7.
181. Choi J, Kim H, Choi J, Oh SM, Park J, Park K. Skin corrosion and irritation test of sunscreen nanoparticles using reconstructed 3D human skin model. Environ Health Toxicol 2014; 29: 1-10.
182. Lagopati N, Tsilibary E-P, Falaras P, Papazafiri P, Pavlatou EA, Kotsopoulou E, Kitsiou P. Effect of nanostructured TiO2 crystal phase on photoinduced apoptosis of breast cancer epithelial cells. Int J Nanomed 2014; 9: 3219-3230.
183. Hanaor DA, Sorrell CC. Review of the anatase to rutile phase transformation. J Mater Sci 2011; 46: 855-874.
184. Chen X, Mao SS. Synthesis of titanium dioxide (TiO2) nanomaterials. J Nanosci Nanotechnol 2006; 6: 906-925.
185. Bagheri S, Shameli K, Abd Hamid SB. Synthesis and characterization of anatase titanium dioxide nanoparticles using egg white solution via Sol-Gel method. J Chem 2013; 2013: 1-5.

186. Han C, Luque R, Dionysiou DD. Facile preparation of controllable size monodisperse anatase titania nanoparticles. Chem Commun 2012; 48: 1860-1862.
187. Wang Y, Yu X, Sun D. Synthesis, characterization, and photocatalytic activity of TiO 2− x N x nanocatalyst. J Hazard Mater 2007; 144: 328-333.
188. Yue J, Chen Z, Yifeng E, Chen L, Zhang J, Song Y, Zhai Y. Preparation TiO2 core-shell nanospheres and application as efficiency drug detection sensor. Nanoscale Res Lett 2014; 9: 1-6.
189. Ismagilov Z, Shikina N, Mazurkova N, Tsikoza L, Tuzikov F, Ushakov V, Ishchenko A, Rudina N, Korneev D, Ryabchikova E. Synthesis of Nanoscale T i O 2 and Study of the Effect of Their Crystal Structure on Single Cell Response. Sci World J 2012; 2012: 1-14.
190. Anwar NS, Kassim A, Lim HN, Zakarya S, Huang NM. Synthesis of titanium dioxide nanoparticles via sucrose ester micelle-mediated hydrothermal processing route. Sains Malays 2010; 39: 261-265.
191. Chang BYS, Huang NM, An'amt MN, Marlinda AR, Norazriena Y, Muhamad MR, Harrison I, Lim HN, Chia CH. Facile hydrothermal preparation of titanium dioxide decorated reduced graphene oxide nanocomposite. Int J Nanomed 2012; 7: 3379-3387.
192. Kitamura Y, Okinaka N, Shibayama T, Mahaney OOP, Kusano D, Ohtani B, Akiyama T. Combustion synthesis of TiO2 nanoparticles as photocatalyst. Powder Technol 2007; 176: 93-98.
193. Wang T, Jiang H, Wan L, Zhao Q, Jiang T, Wang B, Wang S. Potential application of functional porous TiO2 nanoparticles in light-controlled drug release and targeted drug delivery. Acta Biomater 2015; 13: 354-363.
194. Kim C, Kim S, Oh WK, Choi M, Jang J. Efficient intracellular delivery of camptothecin by silica/titania hollow nanoparticles. Chem - Eur J, 2012; 18: 4902-4908.
195. Zhang H, Wang C, Chen B, Wang X. Daunorubicin-TiO2 nanocomposites as a "smart" pH-responsive drug delivery system. Int J Nanomed 2012; 7: 235-242.

196. Kim M, Seo JH, Jeon WI, Kim M-Y, Cho K, Lee SY, Joo S-W. Real-time monitoring of anticancer drug release in vitro and in vivo on titania nanoparticles triggered by external glutathione. Talanta 2012; 88: 631-637.
197. Chen Y, Wan Y, Wang Y, Zhang H, Jiao Z. Anticancer efficacy enhancement and attenuation of side effects of doxorubicin with titanium dioxide nanoparticles. Int J Nanomed 2011; 6: 2321-2326.
198. Manaia EB, Kaminski RCK, de Oliveira AG, Corrêa MA, Chiavacci LA. Multifunction hexagonal liquid-crystal containing modified surface TiO2 nanoparticles and terpinen-4-ol for controlled release. Int J Nanomed 2015; 10: 811-819.
199. Lai S, Zhang W, Liu F, Wu C, Zeng D, Sun Y, Xu Y, Fang Y, Zhou W. TiO2 nanotubes as animal drug delivery system and in vitro controlled release. J Nanosci Nanotechnol 2013; 13: 91-97.
200. Cho SJ, Choi HW, Cho J, Jung S, Seo HG, Do JT. Activation of pluripotency genes by a nanotube-mediated protein delivery system. Mol Reprod Dev 2013; 80: 1000-1008.
201. Luo L, Guo Y, Yang J, Liu Y, Chu S, Kong F, Wang Y, Zou Z. An efficient visible light controlled protein delivery system. Chem Commun 2011; 47: 11243-11245.
202. Lin C, Zhang C, Lin J. Phase transformation and photoluminescence properties of nanocrystalline ZrO2 powders prepared via the pechini-type sol-gel process. J Phys Chem C, 2007; 111: 3300-3307.
203. Rühle M, Evans AG. High toughness ceramics and ceramic composites. Prog Mater Sci 1989; 33: 85-167.
204. Kisi EH, Howard C. Crystal structures of zirconia phases and their inter-relation. Key Eng Mater 1998; 153: 1-36.
205. Hannink RH, Kelly PM, Muddle BC. Transformation toughening in zirconia-containing ceramics. J Am Ceram Soc 2000; 83: 461-487.
206. Hajizadeh-Oghaz M, Razavi RS, Estarki ML. Large-scale synthesis of YSZ nanopowder by Pechini method. Bull Mater Sci 2014; 37: 969-973.
207. Yamaguchi T. Application of ZrO2 as a catalyst and a catalyst support. Catal Today 1994; 20: 199-217.

208. Tanabe K, Yamaguchi T. Acid-base bifunctional catalysis by ZrO2 and its mixed oxides. Catal Today 1994; 20: 185-197.
209. Yokoyama T, Setoyama T, Fujita N, Nakajima M, Maki T, Fujii K. Novel direct hydrogenation process of aromatic carboxylic acids to the corresponding aldehydes with zirconia catalyst. Appl Catal, A 1992; 88: 149-161.
210. Nakano Y, Yamaguchi T, Tanabe K. Hydrogenation of conjugated dienes over ZrO2 by H2 and cyclohexadiene. J Catal 1983; 80: 307-314.
211. Silver RG, Hou CJ, Ekerdt JG. The role of lattice anion vacancies in the activation of CO and as the catalytic site for methanol synthesis over zirconium dioxide and yttria-doped zirconium dioxide. J Catal 1989; 118: 400-416.
212. Colón G, Hidalgo M, Navio J. Influence of carboxylic acid on the photocatalytic reduction of Cr (VI) using commercial TiO2. Langmuir 2001; 17: 7174-7177.
213. Chokkaram S, Davis BH. Dehydration of 2-octanol over zirconia catalysts: Influence of crystal structure, sulfate addition and pretreatment. J Mol Catal A: Chem 1997; 118: 89-99.
214. Vrinat M, Breysse M, Geantet C, Ramirez J, Massoth F. Effect of MoS2 morphology on the HDS activity of hydrotreating catalysts. Catal Lett 1994; 26: 25-35.
215. Fujii H, Mizuno N, Misono M. Pronounced catalytic activity of la 1− x Sr x CoO 3 highly dispersed on ZrO 2 for complete oxidation of propane. Chem Lett 1987; 16: 2147-2150.
216. Bruce L, Mathews J. The fischer-tropsch activity of nickel-zirconia. Appl Catal 1982; 4: 353-369.
217. Fisher IA, Bell AT. In situ infrared study of methanol synthesis from H 2/CO over Cu/SiO 2 and Cu/ZrO 2/SiO 2. J Catal 1998; 178: 153-173.
218. Evis Z, Sato M, Webster TJ. Increased osteoblast adhesion on nanograined hydroxyapatite and partially stabilized zirconia composites. J Biomed Mater Res, Part A 2006; 78: 500-507.
219. Bass JD, Grosso D, Boissiere C, Belamie E, Coradin T, Sanchez C. Stability of mesoporous oxide and mixed metal oxide materials under biologically relevant conditions. Chem Mater 2007; 19: 4349-4356.

220. Racek O, Berndt CC, Guru D, Heberlein J. Nanostructured and conventional YSZ coatings deposited using APS and TTPR techniques. Surf Coat Technol 2006; 201: 338-346.
221. Wang G, Meng F, Ding C, Chu PK, Liu X. Microstructure, bioactivity and osteoblast behavior of monoclinic zirconia coating with nanostructured surface. Acta Biomater 2010; 6: 990-1000.
222. Colilla M, Manzano M, Izquierdo-Barba I, Vallet-Regí Ma, Boissiére C, Sanchez C. Advanced drug delivery vectors with tailored surface properties made of mesoporous binary oxides submicronic spheres. Chem Mater 2009; 22: 1821-1830.
223. Purohit R, Saha S, Tyagi A. Combustion synthesis of nanocrystalline ZrO 2 powder: XRD, Raman spectroscopy and TEM studies. Mater Sci Eng, B 2006; 130: 57-60.
224. Reddy B, Mal I, Tewari S, Das K, Das S. Aqueous combustion synthesis and characterization of nanosized tetragonal zirconia single crystals. Metall Mater Trans A 2007; 38: 1786-1793.
225. Purohit R, Sharma B, Pillai K, Tyagi A. Ultrafine ceria powders via glycine-nitrate combustion. Mater Res Bull 2001; 36: 2711-2721.
226. Purohit RD, Tyagi AK. Auto-ignition synthesis of nanocrystalline BaTi 4 O 9 powder. J Mater Chem 2002; 12: 312-316.
227. Livage J, Beteille F, Roux C, Chatry M, Davidson P. Sol–gel synthesis of oxide materials. Acta Mater 1998; 46: 743-750.
228. Jaenicke S, Chuah G, Raju V, Nie Y. Structural and morphological control in the preparation of high surface area zirconia. Catal Surv Asia 2008; 12: 153-169.
229. Tyagi B, Sidhpuria K, Shaik B, Jasra RV. Synthesis of nanocrystalline zirconia using sol-gel and precipitation techniques. Ind Eng Chem Res 2006; 45: 8643-8650.
230. Suciu C, Gagea L, Hoffmann A, Mocean M. Sol–gel production of zirconia nanoparticles with a new organic precursor. Chem Eng Sci 2006; 61: 7831-7835.
231. Kaya C, He J, Gu X, Butler E. Nanostructured ceramic powders by hydrothermal synthesis and their applications. Microporous and Mesoporous Mater 2002; 54: 37-49.

232. Kanade K, Baeg J, Apte S, Prakash T, Kale B. Synthesis and characterization of nanocrystallined zirconia by hydrothermal method. Mater Res Bull 2008; 43: 723-729.
233. Bae D-S, Han K-S, Cho S-B, Choi S-H. Synthesis and characterization of the ultrafine ZnFe2O4 powder by glycothermal [J]. Kor Assoi Crys Grow 1997; 1: 167-173.
234. Piticescu R, Monty C, Millers D. Hydrothermal synthesis of nanostructured zirconia materials: Present state and future prospects. Sens Actuators, B 2005; 109: 102-106.
235. Byrappa K, Yoshimura M. Handbook of hydrothermal technology. William Andrew 2012.
236. Xin X, Lü Z, Ding Z, Huang X, Liu Z, Sha X, Zhang Y, Su W. Synthesis and characteristics of nanocrystalline YSZ by homogeneous precipitation and its electrical properties. J Alloys Compd 2006; 425: 69-75.
237. Hisbergues M, Vendeville S, Vendeville P. Zirconia: Established facts and perspectives for a biomaterial in dental implantology. J Biomed Mater Res, Part B 2009; 88: 519-529.
238. Wang X, Chen D, Cao L, Li Y, Boyd BJ, Caruso RA. Mesoporous titanium zirconium oxide nanospheres with potential for drug delivery applications. ACS Appl Mater Interfaces 2013; 5: 10926-10932.
239. Tang S, Huang X, Chen X, Zheng N. Hollow Mesoporous Zirconia Nanocapsules for Drug Delivery. Adv Funct Mater 2010; 20: 2442-2447.
240. Díaz A, Saxena V, González J, David A, Casañas B, Carpenter C, Batteas JD, Colón JL, Clearfield A, Hussain MD. Zirconium phosphate nano-platelets: a novel platform for drug delivery in cancer therapy. Chem Commun 2012; 48: 1754-1756.

9. CONCLUSIONS

The presented doctoral thesis summarizes the research in the field of Lignocellulosic nanomaterials and presents the research-review results focused on preparation, characterisation, and their interdisciplinary application. Results of scientific papers published in peer review journals can be concluded as follows:

- A multistep process to obtain value-added products was proposed and established. Cellulose nano-fibrils were successfully prepared as one of the products of a multistep process to obtain value-added products from brewer's spent grain. Obtained results can contribute to the techno-economical analysis of utilization of brewer's spent grains in the Czech Republic.

- Lignin colloid particles were synthesized without any pre-chemical modification and the stable aqueous suspension was obtained in alkaline pH (10.5). In particle formation, peripheral and volumetric precipitation was observed to be the dominant mechanism at low concentration and high concentrations respectively.Lignin colloids were successfully used in six layered coating by layer by layer deposition on quartz slide with the aid of polyelectrolyte PDADMAC (negligible UV absorbance) and increase in absorbance with an increase in a number of layers was observed. Thus, this work presented a unique and novel method for preparation of hollow/ solid lignin colloids which is supposed to be a better technique than other existing methods in terms of control of structure (solid/ hollow), pre-functionalization of lignin and use of electrostatic stabilization.

- Cellulose nanofibres are the unique and promising natural material with huge pharmaceutical potential in the biomedicine as drug carrier and drug delivery because of its unique attributes like high surface area per unit mass, extensive porosity, strength with flexibility and economical

advantage. They serve as the carrier for the drug delivery like antimicrobials, enzymes, other drugs, antioxidants, flavours and functional group compounds and also in the anticancer drug delivery in the form of mat for targeted delivery. Because of its extremely high surface area, hygroscopic nature and its swelling tendency, it allows the maximum drug loading by physical adsorption method as well as because of its swelling ability, the cellulose nanofibre formulation allows for the drug to be released in the controlled manner. Moreover, the floating tendency and the mucoadhesive property of the cellulose nanofibre aerogel present it as a successful gastro retentive drug delivery system. From the results of the study, it can be concluded that the cellulose nanofibres because of its characteristic features are suitable for loading water soluble drugs by physical adsorption method. Since the aerogels possess good tensile strength because of the hydrogen bonding between the molecules, it is more suitable for transdermal drug delivery system. Not only tensile strength, its release pattern and its hygroscopic nature present suitability for drug delivery through skin. Thus, it generates a great possibility for implants and transdermal drug delivery systems. Floating tendency is due to the decrease in bulk density of the nanofibres due to entrapment of air in it. Though it floated only for 7 hours and 30 minutes, modification in cellulose property like making it hydrophobic might help it to float for longer duration of time if it is supposed to be used for oral drug delivery.

- Food packaging plays role of a physicochemical barrier for the food products in order to maintain their integrity throughout their shelf life. Shortcomings of conventional packaging materials such as poor mechanical strength, low water resistance, inability to prevent degradation and nonbiodegradability can be overcome by use of “bionanocomposites”. A bionanocomposite is a nanodimensional multiphase material derived from the combination of two or more natural components. The use of bionanocomposites in food packaging industry is a new strategy to attain markedly improved packaging properties such as increased modulus of strength, decreased gas and water vapour permeability, increased water resistance, improved thermal stability, and barrier properties against the

migration of oxygen, carbon dioxide, aroma and flavours. Furthermore, bionanocomposites offer an environmental friendly approach. Biologically active compounds, such as antimicrobials can also be added to impart desired functional properties. Cellulose, starch and chitosan are some of the biopolymers which have been extensively studied and used to prepare bionanocomposites by reinforcing them with active agents such as nanoclays, silicon dioxide nanoparticles, silver nanoparticles, etc., thus making them suitable to be used as smart packaging material by improving their mechanical properties and imparting "smart" properties such as antimicrobial action. Thus, nanocomposites, when used as or are incorporated in packaging materials, provide "smart" properties to the packaging system, ultimately increasing the shelf life of the product and improving its integrity and quality.

- Metal nanoparticles have been actively investigated as the next generation of anti-cancer system for more than decades. They overcome many drawbacks of conventional chemotherapy, like unwanted side effects and development of resistance. More importantly, they allow us to diagnose as well as monitor the progress and success of therapy during the course itself. A number of studies confirmed their potential in cancer treatment. Different formulations of metal nanoparticles are already in preclinical and clinical stages. Metal nanoparticles also hold huge research potential and are areas of great interest for scientists. They should be investigated thoroughly to determine their exact mode of action, extent of toxicity risks, and should be worked upon to explore their anti-cancer potential to the fullest, with minimal toxicity.
- The discussion about the methods of synthesis and applications of inorganic nanoparticles (Ceramic nanoparticles) in the field of drug delivery makes it evident that these nanoparticles hold a great potential as drug carriers to deliver and target the active pharmaceutical ingredient to the desired site in a controlled manner, resulting in achievement of a therapeutic concentration of drug at target site. Ceramic nanoparticles offer a number of technical advantages in terms of drug delivery. Most researched area for the application of ceramic nanoparticles is cancer,

where promising results have been obtained. A number of facile methods for preparation of these nanoparticles are available and have been continuously undergoing modifications to achieve better desired characteristic of synthesised nanoparticles. All these favourable facts have resulted in several patents and publications in this area during recent years. Thus, ceramic nanoparticles hold the promise of better, safer and cost effective drug delivery agents in future of biomedical science.

Results of this doctoral thesis show that Lignocellulosic nanomaterial has potential in high end applications like drug delivery and smart packaging. Considering growing interest in nanomaterials and their unique properties, they can offer a viable and sustainable alternate to traditional materials. The investigation on novel and facile methods (lignin nanoparticles) and new source (for nanocellulose) can provide a starting ground for Lignocellulosic nanomaterial research at Mendel University in Brno. As Lignin nanoparticles is new field of research, its application in wood science and other fields' needs to be explored. Similarly, some inputs for techno-economic analysis of BSG utilization (for upscaling and commercialization) can be taken from the obtained results.

10.REFERENCES

- Abdul Khalil, H.P.S., Davoudpour, Y., Islam, M.N., Mustapha, A., Sudesh, K., Dungani, R., Jawaid, M., 2014. Production and modification of nanofibrillated cellulose using various mechanical processes: A review. Carbohydr. Polym. 99, 649–665. doi:10.1016/j.carbpol.2013.08.069
- Achyuthan, K.E., Achyuthan, A.M., Adams, P.D., Dirk, S.M., Harper, J.C., Simmons, B.A., Singh, A.K., 2010. Supramolecular Self-Assembled Chaos: Polyphenolic Lignin's Barrier to Cost-Effective Lignocellulosic Biofuels. Molecules 15, 8641–8688. doi:10.3390/molecules15118641
- Agarwal, V., Mishra, B., 1999. Design, Development, and Biopharmaceutical Properties of Buccoadhesive Compacts of Pentazocine. Drug Dev. Ind. Pharm. 25, 701–709. doi:10.1081/DDC-100102229
- Awungacha Lekelefac, C., Hild, J., Czermak, P., Herrenbauer, M., 2014. Photocatalytic Active Coatings for Lignin Degradation in a Continuous Packed Bed Reactor. Int. J. Photoenergy 2014, e502326. doi:10.1155/2014/502326
- Babeł, K., Jurewicz, K., 2008. KOH activated lignin based nanostructured carbon exhibiting high hydrogen electrosorption. Carbon 46, 1948–1956. doi:10.1016/j.carbon.2008.08.005
- Belgacem, M.N., Gandini, A., 2011. Monomers, Polymers and Composites from Renewable Resources. Elsevier.
- Bentivenga, G., Bonini, C., D'Auria, M., De Bona, A., 2003. Degradation of steam-exploded lignin from beech by using Fenton's reagent. Biomass Bioenergy 24, 233–238. doi:10.1016/S0961-9534(02)00135-6
- Bruce, D.M., Hobson, R.N., Farrent, J.W., Hepworth, D.G., 2005. High-performance composites from low-cost plant primary cell walls. Compos. Part Appl. Sci. Manuf. 36, 1486–1493. doi:10.1016/j.compositesa.2005.03.008
- Chandra, R.P., Bura, R., Mabee, W.E., Berlin, A., Pan, X., Saddler, J.N., 2007. Substrate pretreatment: the key to effective enzymatic hydrolysis of lignocellulosics? Adv. Biochem. Eng. Biotechnol. 108, 67–93. doi:10.1007/10_2007_064

- Cheng, G., Varanasi, P., Li, C., Liu, H., Melnichenko, Y.B., Simmons, B.A., Kent, M.S., Singh, S., 2011. Transition of Cellulose Crystalline Structure and Surface Morphology of Biomass as a Function of Ionic Liquid Pretreatment and Its Relation to Enzymatic Hydrolysis. Biomacromolecules 12, 933–941. doi:10.1021/bm101240z
- Coccia, F., Tonucci, L., d'Alessandro, N., D'Ambrosio, P., Bressan, M., 2013. Palladium nanoparticles, stabilized by lignin, as catalyst for cross-coupling reactions in water. Inorganica Chim. Acta 399, 12–18. doi:10.1016/j.ica.2012.12.035
- Colledge, J., 2014. Oral Dosage Forms of Bendamustine. US20140018334 A1.
- De Jong, W.H., Borm, P.J., 2008. Drug delivery and nanoparticles: Applications and hazards. Int. J. Nanomedicine 3, 133–149.
- Dufresne, A., 2013. Nanocellulose: a new ageless bionanomaterial. Mater. Today 16, 220–227. doi:10.1016/j.mattod.2013.06.004
- Engelhardt, J., Kosan, B., Kruger, C.M., Meister, F., Nachtkamp, K., Schaller, J., 2010. Production of cellulose nanoparticles. US20100272819 A1.
- Fan, J., Zhan, H., 2008. Optimization of Synthesis of Spherical Lignosulphonate Resin and Its Structure Characterization* *Supported by the Ph.D. Programs Foundation of Ministry of Education of China (20020561001). Chin. J. Chem. Eng. 16, 407–410. doi:10.1016/S1004-9541(08)60097-X
- Ferrer, A., Quintana, E., Filpponen, I., Solala, I., Vidal, T., Rodríguez, A., Laine, J., Rojas, O.J., 2012. Effect of residual lignin and heteropolysaccharides in nanofibrillar cellulose and nanopaper from wood fibres. Cellulose 19, 2179–2193. doi:10.1007/s10570-012-9788-z
- Frangville, C., Rutkevičius, M., Richter, A.P., Velev, O.D., Stoyanov, S.D., Paunov, V.N., 2012. Fabrication of Environmentally Biodegradable Lignin Nanoparticles. ChemPhysChem 13, 4235–4243. doi:10.1002/cphc.201200537
- Frei, M., Frei, M., 2013. Lignin: Characterization of a Multifaceted Crop Component, Lignin: Characterization of a Multifaceted Crop Component. Sci. World J. Sci. World J. 2013, 2013, e436517. doi:10.1155/2013/436517, 10.1155/2013/436517

- Frey, M., Joo, Y., 2005. Cellulose solution in novel solvent and electrospinning thereof. US20050247236 A1.
- Frone, A.N., Panaitescu, D.M., Donescu, D., Spataru, C.I., Radovici, C., Trusca, R., Somoghi, R., 2011. Preparation and characterization of pva composites with cellulose nanofibres obtained by ultrasonication. BioResources 6, 487–512. doi:10.15376/biores.6.1.487-512
- Garrido-Herrera, F.J., Daza-Fernández, I., González-Pradas, E., Fernández-Pérez, M., 2009. Lignin-based formulations to prevent pesticides pollution. J. Hazard. Mater. 168, 220–225. doi:10.1016/j.jhazmat.2009.02.019
- Gilca, I.A., Pupa, V.I., Crestini, C., 2015. Obtaining lignin nanoparticles by sonication. Ultrason. Sonochem. 23, 369–375. doi:10.1016/j.ultsonch.2014.08.021
- Guerra, A., Gaspar, A.R., Contreras, S., Lucia, L.A., Crestini, C., Argyropoulos, D.S., 2007. On the propensity of lignin to associate: A size exclusion chromatography study with lignin derivatives isolated from different plant species. Phytochemistry 68, 2570–2583. doi:10.1016/j.phytochem.2007.05.026
- Ho, T.T.T., Ko, Y.S., Zimmermann, T., Geiger, T., Caseri, W., 2012. Processing and characterization of nanofibrillated cellulose/layered silicate systems. J. Mater. Sci. 47, 4370–4382. doi:10.1007/s10853-012-6291-8
- Iwamoto, S., Nakagaito, A.N., Yano, H., Nogi, M., 2005. Optically transparent composites reinforced with plant fibre-based nanofibres. Appl. Phys. A 81, 1109–1112. doi:10.1007/s00339-005-3316-z
- Kamel, S., Ali, N., Jahangir, K., Shah, S., El-Gendy, A., 2008. Pharmaceutical significance of cellulose: a review. Express Polym Lett 2, 758–778.
- Kirillov, A.D., Serkov, A.T., Shevchenko, A.S., Berestyuk, G.I., 1987. Mechanism of the development of nonuniformity in properties of yarn prepared by the centrifugal method. Fibre Chem. 19, 47–49. doi:10.1007/BF00544618
- Klemm, D., Heublein, B., Fink, H.-P., Bohn, A., 2005. Cellulose: Fascinating Biopolymer and Sustainable Raw Material. Angew. Chem. Int. Ed. 44, 3358–3393. doi:10.1002/anie.200460587

- Lang, R.J., 1962. Ultrasonic Atomization of Liquids. J. Acoust. Soc. Am. 34, 6–8. doi:10.1121/1.1909020
- Leitner, J., Hinterstoisser, B., Wastyn, M., Keckes, J., Gindl, W., 2007. Sugar beet cellulose nanofibril-reinforced composites. Cellulose 14, 419–425. doi:10.1007/s10570-007-9131-2
- Lievonen, M., Valle-Delgado, J.J., Mattinen, M.-L., Hult, E.-L., Lintinen, K., Kostiainen, M.A., Paananen, A., Szilvay, G.R., Setälä, H., Österberg, M., 2016. A simple process for lignin nanoparticle preparation. Green Chem. 18, 1416–1422. doi:10.1039/C5GC01436K
- Lin, X., Zhou, M., Wang, S., Lou, H., Yang, D., Qiu, X., 2014. Synthesis, Structure, and Dispersion Property of a Novel Lignin-Based Polyoxyethylene Ether from Kraft Lignin and Poly(ethylene glycol). ACS Sustain. Chem. Eng. 2, 1902–1909. doi:10.1021/sc500241g
- Miyawaki, S., Katsukawa, S., Abe, H., Iijima, Y., Isogai, A., 2009. Process for production of cellulose nanofibre, catalyst for oxidation of cellulose, and method for oxidation of cellulose. WO2009084566 A1.
- Nechyporchuk, O., Belgacem, M.N., Pignon, F., 2014. Rheological properties of micro-/nanofibrillated cellulose suspensions: Wall-slip and shear banding phenomena. Carbohydr. Polym. 112, 432–439. doi:10.1016/j.carbpol.2014.05.092
- Nypeloe, T.E., Carrillo, C.A., Rojas, O.J., 2015. Lignin supracolloids synthesized from (W/O) microemulsions: use in the interfacial stabilization of Pickering systems and organic carriers for silver metal. Soft Matter 11, 2046–2054. doi:10.1039/c4sm02851a
- Ohnishi, H., Matsumura, M., Tsubomura, H., Iwasaki, M., 1989. Bleaching of lignin solution by a photocatalyzed reaction on semiconductor photocatalysts. Ind. Eng. Chem. Res. 28, 719–724. doi:10.1021/ie00090a012
- Özgür Seydibeyoğlu, M., Oksman, K., 2008. Novel nanocomposites based on polyurethane and micro fibrillated cellulose. Compos. Sci. Technol. 68, 908–914. doi:10.1016/j.compscitech.2007.08.008
- Purkiss, B., n.d. Pure Lignin Environmental Technology » Lignin.

- Qian, Y., Deng, Y., Qiu, X., Li, H., Yang, D., 2014a. Formation of uniform colloidal spheres from lignin, a renewable resource recovered from pulping spent liquor. Green Chem. 16, 2156–2163. doi:10.1039/C3GC42131G
- Qian, Y., Qiu, X., Zhu, S., 2014b. Lignin: a nature-inspired sun blocker for broad-spectrum sunscreens. Green Chem. 17, 320–324. doi:10.1039/C4GC01333F
- Qian, Y., Zhang, Q., Qiu, X., Zhu, S., 2014c. CO_2 -responsive diethylaminoethyl-modified lignin nanoparticles and their application as surfactants for CO_2 /N_2 -switchable Pickering emulsions. Green Chem 16, 4963–4968. doi:10.1039/C4GC01242A
- Rajan, R., Pandit, A.B., 2001. Correlations to predict droplet size in ultrasonic atomisation. Ultrasonics 39, 235–255. doi:10.1016/S0041-624X(01)00054-3
- Snowdon, M.R., Mohanty, A.K., Misra, M., 2014. A Study of Carbonized Lignin as an Alternative to Carbon Black. ACS Sustain. Chem. Eng. 2, 1257–1263. doi:10.1021/sc500086v
- Spence, K.L., Venditti, R.A., Rojas, O.J., Pawlak, J.J., Hubbe, M.A., 2011. Water vapor barrier properties of coated and filled microfibrillated cellulose composite films. BioResources 6, 4370–4388. doi:10.15376/biores.6.4.4370-4388
- Tejado, A., Peña, C., Labidi, J., Echeverria, J.M., Mondragon, I., 2007. Physico-chemical characterization of lignins from different sources for use in phenol–formaldehyde resin synthesis. Bioresour. Technol. 98, 1655–1663. doi:10.1016/j.biortech.2006.05.042
- Ten, E., Vermerris, W., 2015. Recent developments in polymers derived from industrial lignin. J. Appl. Polym. Sci. 132, n/a-n/a. doi:10.1002/app.42069
- Thao Ho, T.T., Zimmermann, T., Caseri, W.R., Smith, P., 2013. Liquid ammonia treatment of (cationic) nanofibrillated cellulose/vermiculite composites. J. Polym. Sci. Part B Polym. Phys. 51, 638–648. doi:10.1002/polb.23241
- Tonucci, L., Coccia, F., Bressan, M., d'Alessandro, N., 2011. Mild Photocatalysed and Catalysed Green Oxidation of Lignin: A Useful Pathway to

Low-Molecular-Weight Derivatives. Waste Biomass Valorization 3, 165–174. doi:10.1007/s12649-011-9102-6

- Upton, B.M., Kasko, A.M., 2016. Strategies for the Conversion of Lignin to High-Value Polymeric Materials: Review and Perspective. Chem. Rev. 116, 2275–2306. doi:10.1021/acs.chemrev.5b00345
- Willför, S., Pranovich, A., Tamminen, T., Puls, J., Laine, C., Suurnäkki, A., Saake, B., Uotila, K., Simolin, H., Hemming, J., Holmbom, B., 2009. Carbohydrate analysis of plant materials with uronic acid-containing polysaccharides–A comparison between different hydrolysis and subsequent chromatographic analytical techniques. Ind. Crops Prod. 29, 571–580. doi:10.1016/j.indcrop.2008.11.003
- Xu, F., Sun, J.-X., Sun, R., Fowler, P., Baird, M.S., 2006. Comparative study of organosolv lignins from wheat straw. Ind. Crops Prod. 23, 180–193. doi:10.1016/j.indcrop.2005.05.008